

Performance Evaluation of Damage-Integrated Composite Steel Girder Highway Bridges

A Dissertation

Presented to
the faculty of the School of Engineering and Applied Science
University of Virginia

in partial fulfillment
of the requirements for the degree

Doctor of Philosophy

by

Amir Gheitasi

August

2014

APPROVAL SHEET

The dissertation
is submitted in partial fulfillment of the requirements
for the degree of
Doctor of Philosophy

AUTHOR

The dissertation has been read and approved by the examining committee:

Devin K Harris

Advisor

Osman E. Ozbulut

Thomas T. Baber

John R. Scully

Theresa M. Ahlborn

Accepted for the School of Engineering and Applied Science:



Dean, School of Engineering and Applied Science

August
2014

Dedicated to the memory of my mother

Acknowledgement

First and foremost, I would like to express my most sincere thanks and appreciation to Dr. Devin K. Harris for his years of advice on this dissertation and his continuous support during my time at Michigan Tech. and University of Virginia. More than all the scientific knowledge and experience with regards to my research, you have helped me tremendously with the career pursuit and at the same time allowed me to flourish on my own. All the classroom experiences I have gained during these four years would have not been possible without your trust and help. I will be forever grateful for your guidance and wisdom, which I believe will continue to prove invaluable to me throughout my future career.

My dissertation committee, Dr. Theresa M. Ahlborn, Dr. Thomas T. Baber, Dr. Osman E. Ozbulut, and Dr. John R. Scully, your guidance, assistant, and time are much appreciated. Your experience and insight have given me the opportunity to visualize concepts from different perspectives which I believe helped me significantly to improve the research work done.

I would also like to express my appreciation to my research sponsor; Mid-Atlantic Universities Transportation Centers (MAUTC) for providing support and interest for this project.

I am also thankful to the Department of Civil and Environmental Engineering at the University of Virginia for their financial support that enabled me to attend several national conferences and annual meetings during my PhD, and for the unique opportunity to teach my own class on “Bridge Engineering and Design”.

I would also like to thank Dr. Brown, Dr. Chase, Dr. Kassner for providing structural details and plans of the selected in-service structures within the Commonwealth of Virginia; and Mr. Prasad Nallapaneni from Virginia Department of Transportation (VDOT) for his help on providing details on the selected damage scenarios.

Finally and most importantly, I would like to thank my family’s generous love and support during my academic life especially my PhD program. My heartfelt gratitude goes to my father, wife, family, and decent friends in Charlottesville for providing the support during this time. Without your support, encouragement, and love, none of this would have been possible.

Amir Gheitasi
Charlottesville, VA

Abstract

The safety and condition of transportation infrastructure has been at the forefront of national debates in recent times due to the catastrophic bridge failures occurred in the United States, but the issue has been a longstanding challenge for transportation agencies for many years as resources continue to diminish. The performance of this infrastructure has a direct influence on the lives of most of citizens in developed regions by providing a critical lifeline between communities and the transportation of goods and services, and as a critical component of the transportation network, bridges have received a lot of attention regarding condition assessment and maintenance practices. To date, several inspection methods and monitoring techniques have been developed and used by the bridge owners to monitor the in-service behavior and detect different sourced of damage and deterioration in bridge structures. Despite successful implementation of these methods, what is still lacking is a fundamental understanding of the system behavior in the presence of deteriorating conditions that can be used to estimate the remaining service life of the structure and facilitate the preservation decision-making process.

This research project aims to present a performance-based numerical modeling framework that can be used to characterize the behavior of in-service bridge superstructures under the impact of common deteriorating mechanisms. Representative numerical models were generated based on available experimental data in literature, ranging from basic levels of intact bridge components to more complicated levels of bridge superstructural systems with both intact and damaged configurations. Both material and geometric non-linearities were included in the corresponding computational analyses to describe the behavior and failure characteristics of the simulated structures and their sub-components. Critical to this modeling approach is the strategy to leverage simulation techniques and appropriately integrate the effects of existing deteriorating conditions into the measure of system performance. The validity and accuracy of the proposed modeling approach were evaluated through comparisons of the numerical results to those obtained from the corresponding experimental investigations.

Upon validation, the methodology was extended to study the impact of corrosion in steel girders and subsurface delamination in reinforced concrete decks on the ultimate capacity, redundancy, and operational safety of representative in-service composite steel girder bridges. Results from this investigation demonstrated that corrosion in steel girder may significantly influence the capacity and performance of the composite steel bridge superstructures; while

subsurface delamination would reduce the overall system ductility due to local premature failure mechanisms associated with the reinforced concrete decks. It should be noted that although this investigation is limited to composite stringer bridges, the proposed approach is generic and can be extrapolated to assess the functionality of other types of structures under various in-service conditions. It is expected that the proposed framework for evaluating system behavior will provide a critical first step for establishing a critical linkage between design, maintenance, and rehabilitation of highway bridges, which are uncoupled in current infrastructure decision-making practices.

Keywords

Composite steel girder bridges; Ultimate capacity; System-level redundancy; System ductility; Operational safety; In-service conditions; Deck deterioration; Girder corrosion; Model updating; Non-linear finite element analysis (NLFEA)

Table of Contents

List of Figures	x
List of Tables	xvi
List of Symbols	xvii
Research Objective and Dissertation Outline	1
Introduction	1
Common Deteriorations in Highway Bridges	2
Problem to Address	4
Challenges for Evaluating Bridge System Performance	5
Modeling assumptions and simulation techniques	6
Constitutive material models	7
Understanding system-level behavior	7
Damage modeling and integration	8
Investigation Approach	8
Dissertation outline	10
Chapter 1: Implementation of an Energy-Based Stiffened Plate Formulation for Lateral Load	
Distribution Characteristics of Girder-Type Bridges	12
Summary	12
Introduction	12
Lateral Load Distribution	14
AASHTO Specifications	15
Investigation Approach	16
Stiffened Plate Model	16
Method of Solution	17
Relationships, Challenges and Assumptions	20
Representative Bridges for Validation	21
Stanley Bridge	22
Description	22
Testing Program	23
Huron Bridge	24
Description	24

Testing Program.....	24
Shenley Bridge.....	25
Description.....	25
Testing Program.....	27
Results.....	28
Deflection response.....	28
Lateral Load Distribution Behavior.....	31
Stanley Bridge.....	32
Huron Bridge	33
Shenley Bridge.....	33
Discussion and Conclusions	35
Chapter 2: Case Study: Failure Characteristics and Ultimate Load-Carrying Capacity of Redundant Composite Steel Girder Bridges	37
Summary	37
Introduction.....	37
State of Practice	37
Background and Research Significance.....	39
Case Studies.....	40
Nebraska Laboratory Test.....	41
Bridge Description	41
Test Setup and Experimental Results	42
Tennessee Field Test.....	42
Bridge Description	42
Test Setup and Experimental Results	42
FE Simulation and Analysis.....	43
Element Types	43
Section Properties	44
Material Models	45
Loading and Boundary Conditions	45
Analysis.....	47
Discussion of Results.....	47

Validation.....	47
Nebraska Laboratory Test.....	47
Tennessee Field Test.....	49
Behavioral Stages.....	51
Crack Initiation in Concrete Deck (Stage A).....	51
First Yield in Steel Girders (Stage B).....	51
Formation of Plastic Hinge in Steel Girders (Stage C).....	51
Failure of the system (Stage D)	52
Nominal Design Capacity – AASHTO LRFD.....	53
Generic Non-Local Failure Criterion.....	54
Sensitivity Study	55
Conclusions and Path Forward	61
Chapter 3: Overload Flexural Distribution Behavior in Composite Steel Girder Bridges	63
Summary	63
Introduction.....	63
Research Significance.....	65
AASHTO LRFD Distribution Factors	66
Method of Study	66
Numerical Modeling and Validation	66
Representative Bridges	68
Stanley Bridge.....	68
Huron Bridge	69
Investigative Approach	70
Discussion of Results.....	71
Linear-Elastic Behavior	71
Nonlinear Characteristics.....	72
Effect of Boundary Conditions	72
Effect of Loading Position	76
Effect of Truck Configuration	80
Comparison of FE results with AASHTO	83
Conclusions.....	84

Chapter 4: Redundancy and Operational Safety of Composite Stringer Bridges with Deteriorated

Girders.....	87
Summary	87
Introduction.....	88
State of Practice	88
Deteriorations in Highway Bridges	88
Background of Study	89
Research Significance.....	91
Investigation Approach.....	91
Phase I: Intact Element-Level Validation	93
Phase II: Intact System-Level Validation	94
Phase III: Damaged Element-Level Validation	96
Phase IV: System-Level Damage Integration.....	97
System Safety Assessment.....	97
Methodology – NCHRP Approach.....	98
Member failure.....	98
Ultimate Limit State.....	99
Functionality Limit State	99
Damaged Condition Limit State	100
Redundancy Factors.....	101
Application to In-service Structures	102
Selected Structures.....	103
Damage Scenarios.....	104
Model Development and Updating	105
Results and Discussion	107
Conclusions.....	109

Chapter 5: Performance Assessment of Steel-Concrete Composite Bridges with Subsurface Deck

Delamination	111
Summary	111
Introduction.....	111
State of Practice	111

Challenges for Composite Steel Girder Bridges	112
Delamination in Reinforced Concrete Decks	113
Background	114
Method of Study	115
FE Modeling and Analysis.....	116
Modeling of Bridge Superstructure – System Behavior	116
Damage Modeling – Element Behavior.....	118
Damage Integration – Damaged System Behavior	120
Sensitivity Analysis	122
Area of Delamination.....	122
Fracture Plane/ Depth of Delamination	123
Steel Reduction	123
Steel Material Degradation	124
Concrete Material Degradation.....	124
Bond Deterioration.....	125
4.7. Crack Width / Opening	126
Results and Discussion	126
Deck Behavior and Design	129
Application to In-service Structures	131
Conclusions.....	134
Chapter 6: Summary and Future Work.....	136
Appendices.....	139
Appendix A: Numerical Analysis of a Simply Supported Concrete Beam	140
A.1. Experimental Investigation	140
A.2. Finite Element Characterization.....	141
A.3. Modeling	148
A.4. Analysis.....	149
A.5. Discussion of Results	150
Appendix B: Numerical Analysis of a Corner Supported Two-Way Concrete Slab.....	156
B.1. Experimental Investigation	156
B.2. Finite Element Characterization.....	156

B.3. Modeling	158
B.4. Analysis	159
B.5. Discussion of Results	159
Appendix C: Numerical Analysis of a Simply Supported Steel Plate Girder.....	165
C.1. Experimental Investigation	165
C.2. Finite Element Characterization.....	165
C.3. Modeling	167
C.4. Analysis.....	169
C.5. Discussion of Results	169
Appendix D: Numerical Analysis of a Full Scale Composite Bridge	172
D.1. Experimental Investigation	172
D.2. Finite Element Characterization.....	173
D.3. Modeling	178
D.4. Analysis.....	179
D.5. Discussion of Results	180
References.....	186

List of Figures

Fig. I-1: Recent bridge collapses in the U.S.: (a) I-35, Minnesota (NTSB 2008), (b) I-5, Washington (NTSB 2013a), (c) M bridge, Missouri (NTSB 2013b)	1
Fig. I-2: Commonly recognized damage mechanism in steel girder bridges: (a) steel corrosion, (b) section loss, (c) fatigue cracks, (d) rebar corrosion, (e) delamination, (f) spalling, (g) bridge settlement, (h) frozen bearing, (i) lateral impact.....	3
Fig. I-3: Schematic representation of the proposed framework.....	9
Fig. 1-1: Physical representation of lateral load distribution.....	13
Fig. 1-2: Representation of beam-line analysis.....	14
Fig. 1-3: Representation of a slab-girder bridge as an equivalent stiffened plate.....	17
Fig. 1-4: Composite cross-section vs. equivalently stiffened plate section	21
Fig. 1-5: Stanley Bridge: (a) plan diagram (second span only), (b) cross-section diagram	23
Fig. 1-6: Stanley Bridge live load test vehicle axle and loading configuration: (a) Truck 1 (660 kN, 11 axles, 15.67m wheelbase), (b) Truck 2 (657 kN, 11 axles, 15.55m wheelbase).....	24
Fig. 1-7: Huron Bridge: (a) plan diagram, (b) cross-section diagram	25
Fig. 1-8: Huron Bridge live load test vehicle axle and loading configuration: (a) Truck 1 (666 kN, 11 axles, 17.66m wheelbase), (b) Truck 2 (652 kN, 11 axles, 17.76m wheelbase).....	25
Fig. 1-9: Shenley Bridge: (a) plan diagram, (b) cross-section diagram.....	26
Fig. 1-10. Layered sandwich plate transformation to equivalent homogeneous plate.....	27
Fig. 1-11. Shenley Bridge live load test: (a) Truck (434.6 kN, 3 axles, 5.5m wheelbase), (b) Transverse Loading Positions from curb	28
Fig. 1-12: Influence of Secondary Members on the Stiffened Plate Behavior in Stanley Bridge	30
Fig. 1-13. Stanley Bridge Load Distribution Behavior.....	32
Fig. 1-14. Huron Bridge Load Distribution Behavior.....	33
Fig. 1-15. Shenley Bridge Load Distribution Behavior: (a) load case A, (b) load case E.....	34
Fig. 2-1: Nebraska laboratory test: (a) cross section, (b) loading configuration	41
Fig. 2-2: Tennessee field test: (a) cross section, (b) loading configuration.....	43
Fig. 2-3: Generated FE model: (a) Nebraska bridge, (b) Tennessee bridge	44
Fig. 2-4: Deck reinforcement details: (a) Tennessee bridge, (b, c) Nebraska bridge (cantilever, non-cantilever)	45
Fig. 2-5: Material failure surfaces and stress-strain relationships of proposed FE models	46

Fig. 2-6: Assumed boundary conditions for the continuous bridge model - Tennessee field test	47
Fig. 2-7: FE model validation - Nebraska lab test: (a) interior girder deflection, (b) exterior girder separation	48
Fig. 2-8: Exterior girder separation: (a) Nebraska lab test postulation, (b) numerical results.....	49
Fig. 2-9: FE model validation - Tennessee field test: (a) centerline deflection, (b) deflection profile	50
Fig. 2-10: Behavioral stages: (a) Nebraska lab test, (b) Tennessee field test	52
Fig. 2-11: Relative variations in structural stiffness: (a) Nebraska lab test, (b) Tennessee field test	54
Fig. 2-12: Analysis cases for sensitivity study on the Tennessee bridge.....	57
Fig. 2-13: Behavioral stages in the refined models of the Tennessee bridge	58
Fig. 3-1: Nebraska laboratory test (a) FE model, (b) validation	67
Fig. 3-2: Stanley bridge: (a) plan view of tested span, (b) cross section, (c) deck reinforcement, (d) CF1, (e) CF2, (f) girder elevation, (g) truck S1, (660kN-15.67m wheelbase), (h) truck S2 (657kN-15.55m wheelbase)	69
Fig. 3-3: Huron bridge: (a) plan view, (b) cross section (non-skewed), (c) CF2, (d) CF, (e) deck reinforcement, (f) girder elevation, (g) truck H1, (666 kN-17.66 m wheelbase), (h) truck H2 (652 kN-17.76 m wheelbase)	69
Fig. 3-4: Assumed material properties.....	70
Fig. 3-5: Transverse loading positions: (a) Position 1, one-lane loaded close to the curb; (b) Position 2, one-lane loaded; (c) Position 3, two-lane loaded	71
Fig. 3-6: Linear elastic analysis: (a) position 1; (b) position 2; (c) position 3	72
Fig. 3-7: Effect of boundary conditions on nonlinear behavior – position3: (a) Stanley Bridge, (b) Huron bridge	73
Fig. 3-8: Evolution of distributing behavior throughout loading history of the selected bridges loaded with oversized trucks in position 3: (a) PR, (b) PF, (c) PP	74
Fig. 3-9: Variation of distributing behavior over cross section of the selected bridges loaded with oversized trucks in position 3: (a) PR, (b) PF, (c) PP	75
Fig. 3-10: Effect of loading positions on nonlinear behavior with PR boundary conditions: (a) Stanley Bridge, (b) Huron bridge.....	77

Fig. 3-11: Evolution of distributing behavior throughout loading history of the selected bridges with PR boundary conditions: (a) position 1, (b) position 2	78
Fig. 3-12: Variation of distributing behavior over cross section of the selected bridges with PR boundary conditions: (a) position 1, (b) position 2	79
Fig. 3-13: Variation of distributing behavior over cross section of the selected bridges with PP boundary conditions - position 2: (a) Stanley Bridge, (b) Huron bridge	80
Fig. 3-14: Effect of truck configuration on nonlinear behavior with PR boundary conditions: (a) Stanley Bridge, (b) Huron bridge.....	81
Fig. 3-15: Variation of distributing behavior over cross section of the selected bridges loaded with HS20 trucks with PR boundary conditions: (a) position 2, (b) position 3	82
Fig. 4-1: Corrosion-induced damage scenarios	90
Fig. 4-2: Schematic representation of the proposed framework	92
Fig. 4-3: Intact element-level FE model development (a) concrete slab, (b) plate girder	93
Fig. 4-4: Intact element-level validation (a) concrete slab (b) steel girder	94
Fig. 4-5: Intact system-level simulation (a) FE model development (b) validation	95
Fig. 4-6: Damaged element-level simulation (a) FE model development (b) validation	96
Fig. 4-7: Measure of system performance	100
Fig. 4-8: Geometrical characteristics of the selected bridges	104
Fig. 4-9: Selected damage scenarios.....	105
Fig. 4-10: Developed FE models with integrated damage for the selected structures.....	106
Fig. 5-1: Corrosion-induced damage scenarios	113
Fig. 5-2: Nebraska laboratory test (a) bridge cross section, (b) bridge plan, (c) proposed FE model.....	117
Fig. 5-3: Assumed material behavior and corresponding failure criteria: (a) concrete, (b) steel	117
Fig. 5-4: FE model validation - Nebraska lab test	118
Fig. 5-5: Reinforced concrete slab with overlay: (a) elevation, (b) plan, (c) proposed FE model	119
Fig. 5-6: Contact/target element behavior	120
Fig. 5-7: FE model validation - UCSD lab test.....	120
Fig. 5-8: Effects of deck delamination on material properties and geometrical characteristics .	121
Fig. 5-9: Integrated delamination patterns	123

Fig. 5-10: Effect of damage on system behavior: (a) measured behavior (b) damage pattern, (c) fracture plane, (d) damage depth,(e) steel material degradation (f) concrete material degradation.....	127
Fig. 5-11: Lateral load distribution mechanism.....	129
Fig. 5-12: Refined model for deck (no girders).....	130
Fig. 5-13: Impact of damage on deck behavior: (a) damage pattern, (b) damage depth, (c) fracture plane.....	131
Fig. 5-14: Selected in-service bridge: (a) superstructure geometry, (b) generated FE model....	132
Fig. 5-15: Damage integration: (a-c) damage scenarios, (d) measured behavior, (e) impact on system behavior, (f) Impact on deck behavior.....	133
Fig. A.1: Experimental setup, Buckhouse (Buckhouse 1977).....	140
Fig. A.2: Reinforcing details for tested beam, Buckhouse (1977).....	141
Fig. A.3: Application of symmetry in FE modeling.....	141
Fig. A.4: Implemented volumetric elements: (a) Solid65, (b) Solid 185	142
Fig. A.5: Link180 element.....	142
Fig. A.6: Modeling techniques for reinforcing bars: (a) discrete, (b) embedded, (c) Smeared model.....	143
Fig. A.7: Actual uniaxial stress-strain curve for concrete both in tension and compression.....	145
Fig. A.8: Idealized uniaxial stress-strain curve for concrete in compression: (a) model C1, (b) model C2	146
Fig. A.9: William and Warnke failure surface: (a) 3D representation, (b) 2D representation ...	146
Fig. A.10: Idealized uniaxial stress-strain curve for steel in tension/compression: (a) model S1, (b) model S2.....	147
Fig. A.11: Von-Mises failure surface: (a) 3D representation, (b) 2D representation	148
Fig. A.12: FE modeling of reinforced concrete beam	148
Fig. A.13: Load deflection curves at the midspan of the beam	151
Fig. A.14: Longitudinal stress distribution in concrete at bifurcation: (a) analysis case 1, (b) analysis case 2.....	152
Fig. A.15: Longitudinal stress distribution in concrete at bifurcation: (a) analysis case 1, (b) analysis case 2.....	152
Fig. A.16: Behavioral stages throughout the loading history	153

Fig. A.17: Cracking pattern at different stages of loading: (a) first crack in concrete, (b) crack propagation, (c) first yield in rebars, (d) crushing in concrete.....	154
Fig. A.18: Axial strain distribution in concrete body at different stages of loading: (a) first crack in concrete, (b) crack propagation, (c) first yield in rebars, (d) crushing in concrete.....	155
Fig. B.1: Configuration of two-way slab tested by McNeice (1967).....	156
Fig. B.2: Application of symmetry in FE modeling	157
Fig. B.3: FE modeling of reinforced concrete slab.....	159
Fig. B.4: Deflection pattern of the proposed FE model: (a) top view, (b) bottom view.....	160
Fig. B.5: Load deflection curves at: (a) point "a", (b) point "b", (c) point "c", (d) point "d"	161
Fig. B.6: Cracking pattern at different stages of loading: (a) first crack in concrete, (b) crack propagation, (c) first yield in rebars, (d) crushing in concrete.....	162
Fig. B.7: Strain distribution (along x direction) in concrete body at different stages of loading: (a) first crack in concrete, (b) crack propagation, (c) first yield in rebars, (d) crushing in concrete.	163
Fig. C.1: Geometrical configuration of selected plate girder for validation study	165
Fig. C.2: Shell181 element.....	166
Fig. C.3: FE modeling of steel plate girder and applied boundary conditions	168
Fig. C.4: Geometrical imperfection applied to FE model of plate girder	168
Fig. C.5: Nonlinear response of slender plate girder subjected to patch loading	169
Fig. C.6: Behavioral stages and state of stresses in simulated plate girder	170
Fig. D.1: Cross section of Tennessee 4-span continuous bridge	172
Fig. D.2: Loading configuration of a 4-span continuous bridge.....	173
Fig. D.3: Implemented elements in numerical simulation: (a) Beam188, (b) MPC184 rigid beam	174
Fig. D.4: FE model for a 4-span continuous bridge superstructure (only end span of model shown): (a) 3D representation of mesh generation, (b) concrete deck elements, (c) reinforcing rebar elements, (d) Steel girders and cross frame (bracing) elements.	178
Fig. D.5: Deflection in the proposed FE model of composite bridge.....	180
Fig. D.6: Comparison of load-deflection responses: (a) ANSYS, University of Virginia, (b) ABAQUS, West Virginia University.....	181
Fig. D.7: Structural behavior at different stages of loading.....	182

Fig. D.8: Cracking pattern in concrete deck of the loaded span, at different stages of loading: (a) first crack in deck, (b) first yield in girder, (c) plastic hinge in girder, (d) ultimate capacity	182
Fig. D.9: Longitudinal strain distribution in concrete deck of the loaded span, at different stages of loading: (a) first crack in deck, (b) first yield in girder, (c) plastic hinge in girder, (d) ultimate capacity	184
Fig. D.10: Distribution of Von-Mises stresses in steel girders of the loaded span, at different stages of loading: (a) first crack in deck, (b) first yield in girder, (c) plastic hinge in girder, (d) ultimate capacity	185

List of Tables

Table 1-1: Summary of AASHTO LRFD moment distribution factors for slab on girder bridges	15
Table 1-2: Displacement Comparison Summary	29
Table 1-3: Summary of distribution factors	31
Table 2-1: Section properties of proposed FE models	44
Table 2-2: Material properties of proposed FE models	46
Table 2-3: Ultimate capacities of the simulated bridges	56
Table 2-4: Failure characteristics (Tennessee bridge)	60
Table 2-5: Behavioral stages of the refined models (Tennessee bridge)	60
Table 3-1: Comparison between distribution factors, FE results vs. AASHTO-LRFD	84
Table 4-1: Redundancy ratios for the Aylett bridge	108
Table 4-2: Redundancy ratios for the Creek bridge	108
Table 4-3: Redundancy factors for the selected structures	109
Table 5-1: Effect of material and geometrical refinements on the behavior of damaged models	128
Table 5-2: Impact of delamination on the behavior of the selected in-service structure	134
Table A.1: Real constants for proposed FE model of concrete beam	144
Table A.2: Load steps for the FE analysis: (a) analysis case 1, (b) analysis case 2	150
Table A.3: Comparison of the results	155
Table B.1: Real constants for proposed FE model of concrete slab	157
Table B.2: Material properties for FE model of reinforced concrete slab	158
Table B.3: Load steps for the FE analysis of concrete slab	160
Table C.1: Material properties for FE model of steel plate girder	167
Table C.2: Comparison of the results	171
Table D.1: Real constants for FE model of girder type bridge superstructure	175
Table D.2: Cross sections for FE model of girder type bridge superstructure	176
Table D.3: Material properties for FE model of girder type bridge superstructure	177
Table D.4: Load steps for the FE analysis of composite girder type bridge	180

List of Symbols

a, b	Length and width of equivalent stiffened plate system
\bar{A}_b, \bar{A}_d	Cross sectional area of girder and deck in non-composite section
A_{mn}	A series of unknown coefficients for deflection shape function
A_{pit}	Area of the pit in corroded rebar
A_{stnom}	Nominal cross section area of the intact rebar
A_x	Shear area of stiffening elements
d_b, d_d	Distance between the center of gravity of girder and deck, with respect to the composite neutral axis
d_e	Horizontal distance from the centerline of the exterior web of exterior girder at deck level to the interior edge of curb or traffic barrier
D, D_{eq}	Flexural rigidity of regular/equivalent deck system
e	Exterior girder correction factor
$f_m(x), f_n(y)$	Deflection functions of equivalent stiffened plate system in longitudinal and transverse directions
E	Elastic Modulus
E_c, E_p	Elastic modulus of central core and steel plates in composite deck system
E_x, E_y	Elastic modulus of stiffening elements
f'_c	Compressive strength of concrete (intact)
$f_c'^D$	Compressive strength of concrete (damaged)
f_t	Tensile strength of concrete
f_y	Yield stress of steel (intact)
f_y^D	Yield stress of steel (damaged)
f_u	Ultimate strength of steel
g, DF, GDF	Girder distribution factor
G_x	Shear modulus of stiffening elements
\bar{I}_b, \bar{I}_d	Moment of inertia of girder and deck in non-composite section

I_x, I_y	Effective moment of inertia of stiffening elements
J_x	Torsional rigidity of stiffening elements
K_i	Initial stiffness of the bridge superstructural system
K_g	Longitudinal stiffness parameter
K_t	Tangential (instantaneous) stiffness of the bridge superstructural system
L	Span Length
LF_1	Load factor for nominal member failure
$LF_{1,required}$	Load factor required member capacity
LF_d	Load factor for damaged condition limit state
LF_f	Load factor for functionality limit state
LF_u	Load factor for ultimate capacity limit state
m, n	Number of half waves in longitudinal and transverse directions
$M_{bx}(x)$	Flexural moment in stiffening element
N_b	Number of girders
N_{trucks}	Number of trucks
N_x, N_y	Number of stiffening elements
$p(x, y)$	Loading function
P_u	Ultimate capacity of the bridge system
r_1	Member reserve ratio
r_d	Redundancy ratio for damaged condition limit state
R_d	System reserve ratio for damaged condition limit state
r_f	Redundancy ratio for functionality limit state
R_f	System reserve ratio for functionality limit state
$R_{\max i}$	Maximum response in ith girder
$R_{provided}$	Nominal capacity of the bridge component
$R_{required}$	Required capacity of the bridge component based on design specifications

r_u	Redundancy ratio for ultimate capacity limit state
R_u	System reserve ratio for ultimate capacity limit state
S	Girder spacing
t_p, t_c	Thickness of steel plate and central core in composite deck system
t_s	Deck thickness
U_{bx}, U_{by}	Strain energy of stiffening elements
U_s	Strain energy of deck plate
U_t	Total potential energy of the system
$w, w(x, y)$	Out-of-plane deflection
x_k, y_k	Location of stiffening elements
$\Delta_{\max i}$	Maximum defection in ith girder
ε_0	Concrete strain at the peak strength (intact)
ε_1	Corrosion-induced tensile strain in transverse direction
$\varepsilon_{\max i}$	Maximum strain in ith girder
ϕ_{bx}	Elastic curvature of stiffening elements
ϕ_{red}	System redundancy factor
ν	Poisson's ratio
ν_s, ν_{eq}	Poisson's ratio of regular/equivalent deck system
ν_c, ν_p	Poisson's ratio of central core and steel plates in composite deck system
ζ, η	Central coordinate of loading patch area in longitudinal and transverse directions
μ, ν	Length and width of the loading patch area

Research Objective and Dissertation Outline

Introduction

The national highway system is recognized as one of the greatest engineering achievements of the 20th century by the National Academy of Engineering, rivaling achievements such as electrification, the Internet, the airplane, and the spacecraft (Constable and Somerville 2000). An efficient and well maintained transportation infrastructure system not only serves as a core component to the economic health of the United States by providing a corridor for the transportation of goods and people (CSI 2008, Kavinsky 2007), but also provides a coast to coast and border to border passageway for the nation's military (GAO 2008). Historically the highway system, which includes both roads and bridges, has flown underneath the radar of the public opinion when compared to other engineering marvels, but is easily recognized as a critical component in the everyday lives of most people. However, tragic events such as the I-35W bridge collapse in August 2007 (Minnesota) and the more recent I-5 (Washington) and Highway M bridge (Missouri) collapses in May 2013 have brought the challenges associated with an aging infrastructure to the forefront of public scrutiny (see Fig. I-1). The cause of this scrutiny can be attributed to the fact that these failures often result in loss of human life and significant economic hardship to the surrounding communities. However, this attention is often compounded by the media's tendency to overstate and dramatize the current state of safety of bridges, which stems from being somewhat misinformed.

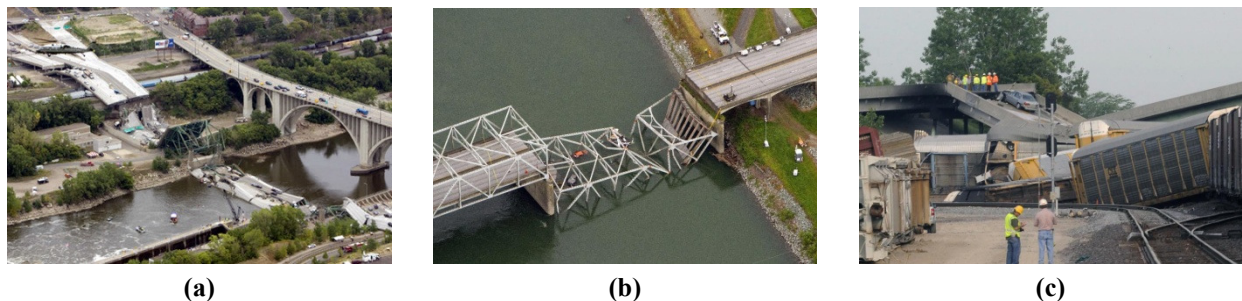


Fig. I-1: Recent bridge collapses in the U.S.: (a) I-35, Minnesota (NTSB 2008), (b) I-5, Washington (NTSB 2013a), (c) M bridge, Missouri (NTSB 2013b)

A review over the recent bridge failures in the United States during last few decades found that these failures are often attributed to unforeseen events and manmade hazards such as impact, fires, or flooding and are not exclusively related to the existing conditions (Kumalasari 2003).

Nevertheless, it is the condition states associated with deterioration that represents the greatest challenges for transportation agencies across the country. According to the latest report of the National Bridge Inventory (FHWA 2013), 24% of over 600,000 bridges are classified as structurally deficient (10%) or functionally obsolete (14%). This illustrates that strategies and resources for maintenance is an ongoing challenge for federal, state and local governments, especially considering that many bridges are reaching or exceeding their design service lives of 50 years. A recent estimate provided by the Federal Highway Administration suggested that a \$20.5B annual investment in infrastructure (bridges would be needed) to eliminate the deficient backlog by the year 2028, in light of the fact that only \$12.8B is spend annually (AASHTO 2008). While it is not feasible to immediately repair all of the deficient bridges, this deteriorating condition does underscore the importance of quality inspection and assessment mechanisms to prioritize these repair efforts. What is needed is a rational comprehensive preservation framework that uses a fundamental understanding of the system behavior under the impact of existing in-service conditions and facilitates the decision-making process to optimize the current maintenance and repair efforts.

Common Deteriorations in Highway Bridges

Within the selected genre of the bridges of this study (i.e. composite steel girder bridges), there are certain similarities in materials, geometry, and configuration, which make them serve common functionalities such as overpasses and modest water crossing. Under the premise of a rational structural design, the service lives of these bridges are governed by the operating environment, load effects and history, and maintenance and preservation practices; with really only the last factor being under the owner's influence. Successful maintenance practices require knowledge of condition state of the bridge system and also an understanding of the impacts of all possible damage and deterioration mechanisms on the overall system performance and serviceability.

The main types of deterioration that composite steel girder bridges experience have been well documented in recent years (FHWA 2012), as illustrated in Fig. I-2. Much of the degradation often manifests in the steel girders as corrosion and section loss, which are most commonly caused by the wet-dry cycles of exposed steel or the leaking expansion joints. When deicing chemicals are present, the effect of corrosion is accelerated. Fatigue cracks are the other type of degradation common in steel girder bridges which can lead to sudden and catastrophic failure.

This type of cracking occurs at a stress level below the yield stress of the girder's material due to repeated traffic loading. The development of fatigue cracks is mainly influenced by the frequency of moving traffic, age or load history of the bridge, magnitude of stress range, material fracture toughness, and temperature.

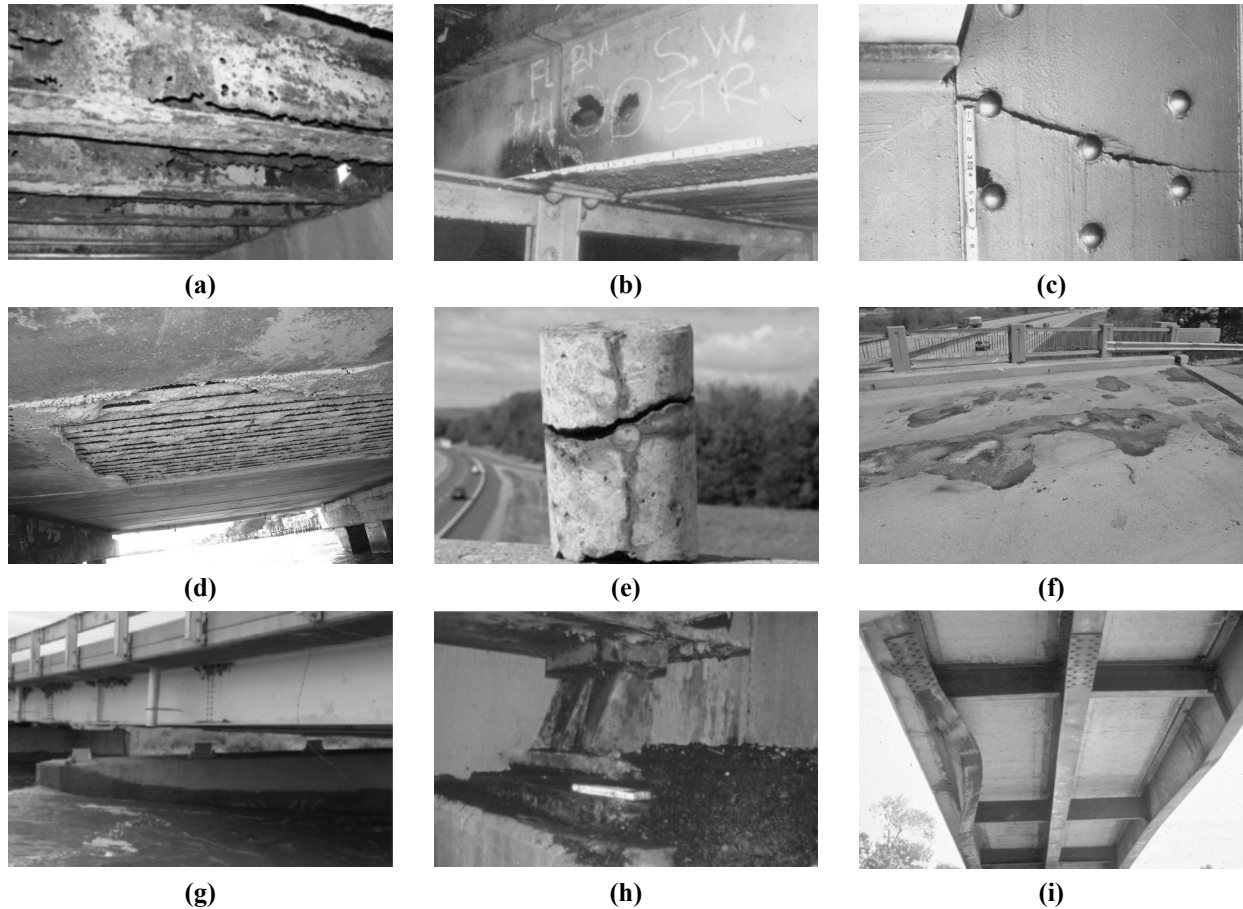


Fig. I-2: Commonly recognized damage mechanism in steel girder bridges: (a) steel corrosion, (b) section loss, (c) fatigue cracks, (d) rebar corrosion, (e) delamination, (f) spalling, (g) bridge settlement, (h) frozen bearing, (i) lateral impact

Reinforced concrete slabs usually suffer from cracking due to low tensile resistance of the concrete material. Concrete cracks could be categorized into structural and non-structural cracks. Structural cracks are caused by dead and live load stresses (flexure and shear), while non-structural cracks result from internal stresses due to dimensional changes which are divided into temperature, shrinkage, and mass concrete cracks. However, corrosion in reinforcing rebars as a result of chloride penetration through the concrete cracks is the most well-known sources of degradation associated with the concrete decks. The corrosion product (rust) can occupy up to 10

times the volume of the corroded steel that it replaces. This expansive action creates internal pressures up to 20.7 MPa (3000 psi) resulting in wider cracks, delaminations, and spalls (FHWA 2012). Delamination occurs when layers of concrete separate at or near the outermost layer of reinforcing steel. Besides, spalls result from the separation and removal of a portion of the surface concrete, revealing a fracture roughly parallel to the surface. Delamination and spalling could happen in both surface and subsurface of an operating reinforced concrete slab. In addition to the corrosion-induced damage mechanisms, concrete decks also suffer from scaling, which is a gradual and continuing loss of surface mortar and aggregate over an area due to the chemical breakdown of the cement bond.

Other mechanisms such as bridge settlement, bridge movement, frozen bearings and expansion joints, and high load impacts which address the overall system behavior are also common in this type of bridge superstructure systems. Differential settlement or movement of bridge substructure may cause excessive cracks in the structural members of the bridge superstructure, producing serious distress depending on span length and bridge structural system. Frozen bearings and expansion joints can occur when deterioration and accumulated debris cause the bearing to bind up, thereby preventing free movement, improper alignment of load-carrying members, and cracks in the bearing or bearing seats. Components and structural members of a bridge system that are adjacent to a roadway or waterway are also susceptible to impact damage. Indications of impact damage include dislocation or distortion in the structural members.

Problem to Address

Over the past few years, a number of research efforts have concentrated on developing an applicable mechanism to qualitatively and quantitatively characterize the main sources of deterioration and damage associated with transportation infrastructure, especially bridges. The concept of structural health monitoring (SHM), which can be described as a system performance evaluation strategy for in-service structures, has come to the forefront of the research community as a mean to mitigate the challenges associated with aging highway infrastructure. Implementing this concept has the potential to characterize the behavior of the investigated structures and provide indications of damage and even forewarning of impending failure. To date, a significant amount of research has been performed on structural health monitoring of bridges with advances in novel technologies, but a comprehensive solution to the challenges described also requires integrated strategies for routine inspection, data management, result interpretation and decision

support to make SHM an ongoing framework in progress. On the other hand, with the sheer volume of bridges in the United States, transportation officials seek a “one-size fits all” solution for preservation, which is a daunting task considering the wide variety of structure types, component materials, existing conditions, and operational environments under which bridges can be categorized.

In recent years, the industry has attempted to integrate some of the research findings in the area of SHM into practice by developing long-term bridge monitoring systems. Most of these applications have been deployed on high profile structures; however, these applications have been met with skepticism by transportation agencies which are notoriously slow to adopt innovation. At the core of the skepticism is the cost of the systems relative to the inventory of bridges, the potential for large amounts of data and the manpower and skills required to interpret the results, and long-term durability and power requirements of installed sensors. For SHM to gain traction within the transportation community a number of questions still need to be answered including: 1) what does the data collected mean?; 2) how can the data be used for decision making?; 3) what impact does damage and deterioration have on performance?; and 4) how can this data be effectively managed over the structure’s lifetime?.

Successful implementation of the SHM framework to evaluate the operational safety of routine bridges with common functionalities not only requires knowledge of the current condition state, but also an understanding of the impact of specific deterioration mechanisms on the overall system performance. Recent advances in non-destructive evaluation (NDE) have furthered the science of assessment, allowing for more accurate quantification of visible deteriorations and improved confidence in locating internal deterioration mechanisms. Even within the spectrum of these assessment methods, there exists a divide between metrics for structural response at the global level and material distress at the local level. What is lacking within the current framework is an integrated approach that considers the existing system-level condition driven structural performance as part of the maintenance and preservation decision-making process.

Challenges for Evaluating Bridge System Performance

Similar to the concept of immediate depreciation of a new vehicle purchase, bridge superstructures begin to degrade after they are placed in service, albeit at much slower rate. Current practices for evaluating system performance use results from the various inspection

methods to monitor degradation over time and help provide guidance on maintenance/rehabilitation schedules. However, they rely primarily on human evaluation, which creates the subjectivity. With a lack of fundamental understanding of the influence of the existing damage mechanisms on the overall system performance, bridge engineers are tasked with making a subjective judgment on the implications without the science to support their decision.

In order to accurately evaluate the system-level behavior, an ideal approach would be the implementation of full scale field tests on a series of representative bridges; however, this approach is neither feasible nor cost-effective. Laboratory testing can also be considered as an alternative approach, but challenges with dimensional scaling and simulation of exact boundary conditions are considered as limitations of this method, in addition to associated costs. With today's computational resources and capabilities, the development of an analytical model to study the performance of intact or damaged bridge systems could be best handled numerically, using a tool such as the Finite Element Method (FEM). While FEM provides an efficient mechanism to simulate the bridge system behavior, there are certain challenges that must be properly treated to yield representative results. These challenges are summarized in the following sub-sections.

Modeling assumptions and simulation techniques

The level of accuracy provided by Finite Element analysis is known to be significantly influenced by modeling assumptions such as mesh generation, element selection, assumed loading/boundary conditions. As an example, representation of the internal reinforcement in concrete members or enforcement of composite action between structural members, are the examples of simulation techniques requiring proper treatment in the numerical analysis of composite structures. These features have been handled numerically using a variety of methods such as discrete, embedded, or smeared models for the concrete reinforcement (Tavarez 2001) or multi point constraint (MPC) or contact elements for to provide composite action between structural components (Barth and Wu 2006). However, selection of an appropriate simulation technique and the corresponding modeling assumptions require a comprehensive understanding of the actual behavior of the structural system.

Constitutive material models

Implementation of reasonable and appropriate material properties to each of the structural components in a bridge model is also essential from the modeling perspective to accurately capture system failure characteristics. Considering concrete and steel as the primary materials being used in bridge constructions, their elastic and inelastic properties including features such as cracking/crushing and plastic deformations may dictate the ultimate capacity and even failure mode of the system. With concrete, the primary challenges in modeling are its non-homogeneity and brittle nature, making the mechanical response highly complex. Numerous models have been proposed in the literature to accurately predict material characteristics of concrete. Among those are the empirical models developed under different loading conditions, including uniaxial (Wang et al. 1978, Tsai 1988), biaxial (Taylor et al. 1972, Gerstle 1981), and triaxial (Bazant and Oh 1982, Domingo et al. 2002). Moreover, theoretical models associated with suitable failure criteria such as Mohr-Coulomb (1776), Drucker and Prager (1952) and Willam and Warnke (1974) were introduced to represent material non-linearity and describe ultimate strength of the material. In contrast, constitutive material relationships for structural steel are normally less complex, most of which exhibit elastic-plastic behavior with potential strain-hardening near failure associated with the Von-Mises (1913) yield criterion. However, to capture the system response under cyclic loading, the assignment of specific hardening rules (isotropic, kinematic, or mixed) based on material characteristics is necessary.

Understanding system-level behavior

From a historical perspective, the complex interaction between structural components, which causes inherent structural redundancy in bridge superstructures, is critical to the understanding of bridge life-cycle performance and behavior. Current design specifications generally simplify this interaction and deal with individual components; thus provide a vague and noncommittal description of the system redundancy. The concept of redundancy, which can be defined as “exceeding what is necessary or normal” or alternatively “superfluous” is easily understood from its common definition, but when applied to bridges and other complex structures the quantification of the amount or degree of redundancy is not well understood.

The bridge system redundancy can be exclusively defined as the capability of the bridge superstructure to redistribute and carry loads beyond the design capacity. For bridges in service, the existence of damage and deteriorating conditions affects the system-level behavior and

makes it more complicated to interpret the redundancy of the system. As a result, for a true measure of system performance, there exists a need to develop a robust definition of bridge redundancy, one that is capable of integrating the effects of different damage scenarios and correlate the element-level behavior to the system-level response. This would require deep understanding of actual system-level behavior including non-linear characteristics of the system.

Damage modeling and integration

While the constitutive relationships for the intact material models are generally well understood from a macro-scale perspective, a significant degree of complexity is introduced into the numerical models of the bridge structures in the presence of different damage scenarios. Regardless of the source, cause, and initiating mechanism, the degradation usually progresses and causes additional mechanisms to form or progressive failure. As a result, several analytical studies were conducted to integrate the effects of different damage mechanisms into numerical models (Dagher and Kulendran 1992, Coronelli 2002, Zhou 2005, Van de Lindt and Ahlborn 2005); nevertheless, these studies have been mostly limited to the element-level behavior. What is still lacking for the bridge community is a practical approach to integrate common damage mechanisms and their coupled effects into the system-level bridge models, which is the impetus for this research project. It is this challenge that describes the core focus of the proposed research, which aims to create a mechanism for integrating damage into a measure of system performance and correlate impacts of damage on the redundancy, ductility and remaining service life of the in-service bridge superstructures.

Investigation Approach

For a robust system-level evaluation framework, it is necessary for constitutive material models, damage models, and element-level and system-level behavior to be integrated into a composite model that describes their interaction. With the goal of establishing a performance-based framework to evaluate the behavior of in-service bridge superstructures, the investigation approach of this study has been categorized into four different phases to accomplish this goal. Fig. I-3 illustrates the schematic of the proposed framework that can be applied to any type of bridge superstructure. As illustrated, the first phase focuses on the development of undamaged element-level numerical models representing the main structural components of the desired bridge system. Extensive experimental data in the literature along with rational assumptions on

material constitutive relationships are available to validate the accuracy and consistency of the developed models. This phase aims to characterize the behavior and failure modes of the intact bridge sub-components, with consideration of both material and geometric non-linearities.

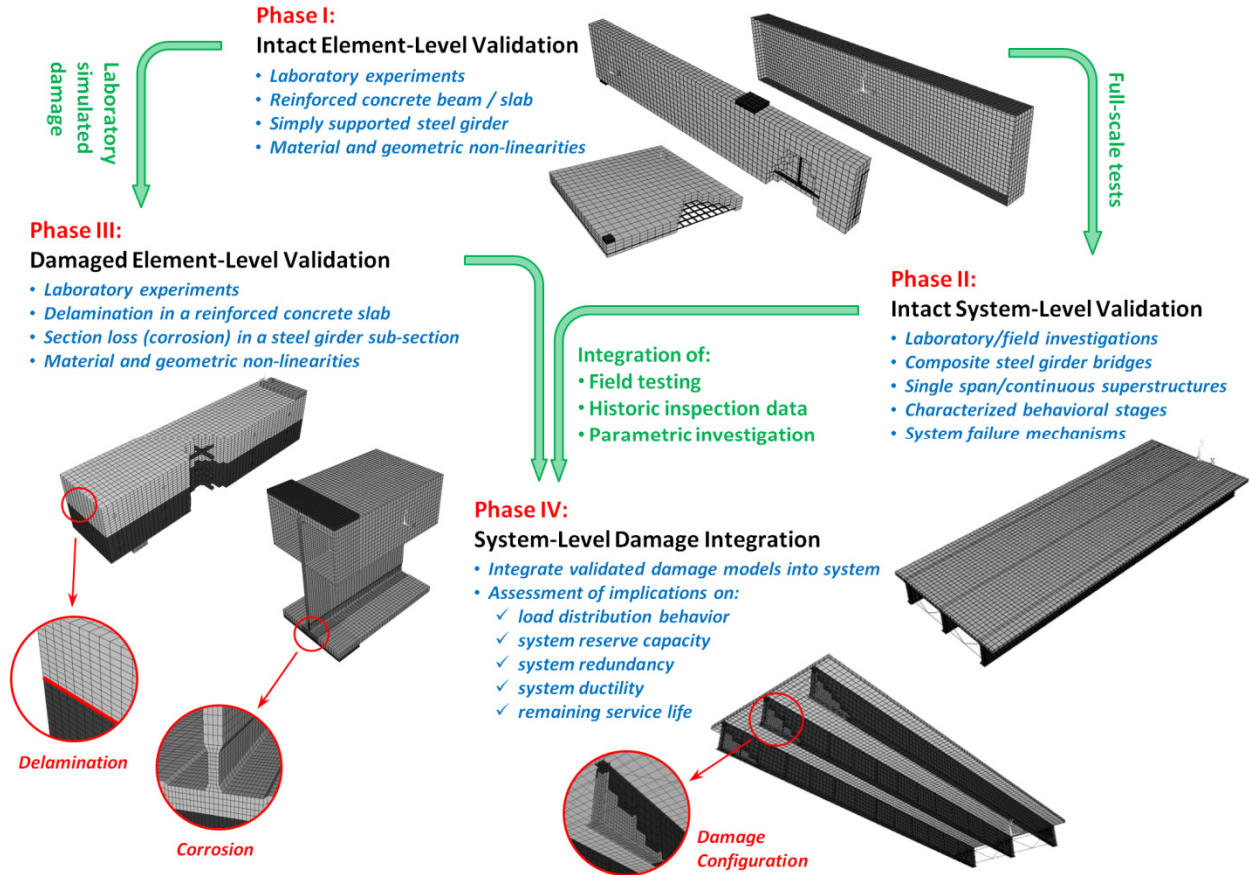


Fig. I-3: Schematic representation of the proposed framework

Following validation of the intact models within the element domain, phase two focuses on the development of system-level numerical models representing ideal intact bridge superstructures. These models can be loaded to their system-level ultimate capacity to define their full non-linear system behavior. Evaluation of the non-linear system behavior highlights the critical behavioral stages inherent to a particular bridge system and also allows for correlation with the expected element-level response. Ideally complete experimental data of newly constructed bridges tested to failure is needed to validate, update, and/or refine the established system-level models; however, the primary challenge associated with model validation of bridges is the lack of complete datasets, especially those for full non-linear behavior characterization (Burdette et al. 1971, Kathol et al. 1995). The limited pool of data that exists in

the literature is used in this study to develop the skeleton of the proposed framework. It is envisioned that this skeleton framework could be supplemented in the future with focused full-scale lab or field investigations to fill the void of available experimental data. The outcome of this phase will be a mechanism to describe the behavior of bridge systems based on their inherent level of system redundancy that are expected to be unique to each bridge superstructure type and design characteristics. This component will be essential to the latter stages of the investigation as it provides a baseline for as-designed behavior from which actual in-service behavior can be referenced to define the influence of damage and deterioration (phase IV).

Following the first two phases, the purpose of the third phase of the proposed framework is to establish an effective constitutive behavior of the individual bridge components that are affected by common damage and deteriorating mechanisms. Despite the variety of sources that may cause each damage scenario, from a mechanics perspective it is their influence on the structural behavior that is of primary concern. Critical to this phase is the strategy to leverage modeling techniques appropriate for each damage mechanism considered. Validation of the damage-integrated elements through available experimental data is essential to the last phase of this investigation. Upon completion of the damaged element-level validation, the damage modeling strategies will be integrated into the system-level models to investigate their influence on system behavior. Parametric investigations can then be performed to quantify the influence of damage mechanisms on the system-level behavioral stages defined in Phase II and establish a measure of remaining life and susceptibility to failure.

Dissertation outline

In pursuit of the main goal of this research project in establishing a comprehensive performance-based framework for maintenance and preservation of national bridge infrastructure, the technical contents of this dissertation were organized in such manner as to accomplish three objectives that will serve as the foundation to: 1) characterize the system-level intact behavior of non-complex bridges subjected to mechanical loading; 2) quantify the influence of existing damage and deteriorating mechanisms on the overall bridge performance; and 3) formulate a performance-based framework for maintenance and preservation of in-service bridges.

As a starting point, the first chapter will focus on understanding the system-level response of the beam-slab type of bridges within the elastic range of behavior. An analytical approach was

presented to investigate the lateral load distribution behavior in the selected type of bridges using the classical plate theory and traditional finite element modeling. Successful completion of this section provides a foundation to extend the numerical analyses to study the non-nonlinear characteristics of the non-complex bridge superstructures, as they approach their ultimate capacity. As a result, Chapter 2 presents an approach for capturing the full system-based behavior and stages to failure in the subset of composite steel girder bridges. This chapter is essential to understanding the concept of redundancy in bridge system and how the redundant structures would behave in the presence of coupled and uncoupled damage and deteriorating conditions. Chapter 3 extends the investigation on the non-linear characteristics of concrete-steel composite bridges by studying the evolution of the live load distributing mechanism in the presence of high material non-linearities and oversized loading scenarios.

With the knowledge obtained from the first three chapters regarding the behavioral characteristics of intact steel stringer bridges, the last two chapters build on this foundation and focus on characterizing the impact of damage scenarios on the performance of in-service bridge superstructures. Corrosion in steel girders and subsurface delamination in reinforced concrete slabs are the most common types of deteriorating conditions associated with the selected genre of the structures. Chapter 4 presents a numerical modeling framework which exclusively focuses on evaluating the impact of corrosion in steel members on the ultimate capacity, redundancy and operational safety of representative composite girder bridges. Moreover, Chapter 5 will assess the sensitivity of the bridge system performance to the corrosion-induced deck deteriorations. It should be noted that dynamic effects and the cycling nature of the moving trucks as well as the fatigue damage scenario were not considered in this study. With the ability to integrate existing observable deteriorations using the proposed numerical model approach, an in-service performance baseline can be established and coupled with SHM strategies to redefine current condition assessment and maintenance practices of transportation agencies.

The contents of the described chapters were exactly adopted based on five individual manuscripts, which either were already published or are currently under peer review process. Nevertheless, the formats of these manuscripts were visually updated to be consistent and follow the style of this dissertation. It should also be noted that the intermediate work and validation that were performed as preliminary investigations are not included in the main body of this dissertation, but rather presented as supplemental information in the appendices.

Chapter 1:

Implementation of an Energy-Based Stiffened Plate Formulation for Lateral Load Distribution Characteristics of Girder-Type Bridges

(Elsevier, Engineering Structures, Volume 54, September 2013, Pages 168-179)

Summary

Although the calculation of lateral load distribution behavior of girder type bridges is widely discussed in AASHTO LRFD based on semi-empirical formulations, the range of applicability is still considered as a restriction for applying the corresponding equations to complex bridge superstructures. In this study, an analytical approach is presented for determining lateral load distribution characteristics of beam-slab type bridges, using classical plate theory. In addition, finite element simulations along with field investigation of three different bridges were implemented to examine the accuracy and validity of the proposed methodology. While the classical plate model is capable enough of predicting the load sharing behavior of the bridge system, it often yields more flexible response of the system in comparison to the upper bound of finite element (FE) results. Moreover, the use of the proposed approach allows for the evaluation of bridge systems outside of the current limits of applicability, such as new composite systems or non-conventional designs, without significant deviations from current practice.

Introduction

Highway bridges represent a critical component within the North American infrastructure system. While high profile bridges such as the I-35W in Minnesota and the Bay Bridge in California often receive a great deal of attention, the majority of bridges in-service are typical short and medium span beam-slab or stringer bridges (FHWA 2013). These bridges are often comprised of a cast in place (C.I.P) or precast reinforced concrete deck supported by steel or prestressed concrete girders; however, in recent years numerous composite deck systems have been utilized as potential alternatives in both new and rehabilitation operations.

While the bridge community has successfully designed bridges of these types for several years, many components of the design approach are based on methods without a firm foundation in mechanics and are prescriptive in nature. Although these processes work well for common

design scenarios, they are often restricted for cases violating the limits of applicability of the design provisions (e.g. new materials). This characteristic is particularly true for lateral load distribution, which is a phenomenon that describes how live loads are distributed through the bridge deck into the primary load carrying members, ideally girders. In beam-slab bridges, distribution factors define a fraction of the load applied to the driving surface, for which the girders or stringers must be designed. (see Fig. 1-1). Within the AASHTO bridge design provisions (AASHTO 2012), distribution factors are used to translate a three-dimensional analysis of the entire bridge structure into a one-dimensional member analysis (see Fig. 1-2). Current design provisions, developed through research studies, have demonstrated that lateral load distribution is primarily a function of transverse girder spacing with additional influence from factors such as span length, girder stiffness, deck thickness/stiffness, skew, continuity, and stiffness of secondary members, (i.e. lateral bracings and diaphragms) (Zokaie 2000). However, the approach within the current AASHTO LRFD Bridge Design Specifications is empirical and only considered applicable to a limited range of bridge, those most prevalent in practice.

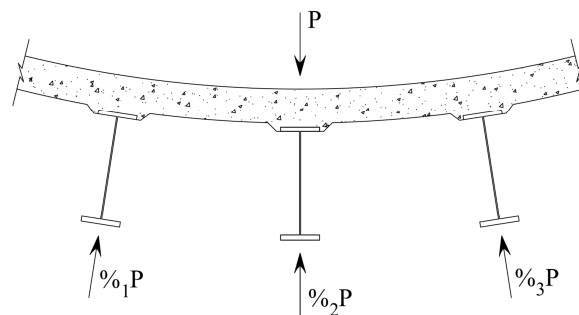


Fig. 1-1: Physical representation of lateral load distribution

As new design approaches evolve and new materials are introduced, there is a need for alternative methods of analysis. This paper presents an analytical approach for determining lateral load distribution characteristics of beam-slab type bridges using classical plate theory. A key attribute of the proposed method is that it is adaptable to scenarios outside the range of applicability of current design provisions and provides a physical representation to the problem. Included in this investigation are the results from the analytical-based approach as well as finite element (FE) numerical analysis outcomes, derived for three bridge scenarios including two steel girder bridges supporting concrete decks, with and without skew, and a steel girder bridge with a composite deck system. For validation purposes, the results are then compared to the

corresponding values obtained from field-test investigations (Eom and Nowak 2001, Harris et al. 2008, Nowak and Eom 2001). The author recognizes that for widespread adoption of the proposed approach, a more comprehensive parametric study, similar to the NCHRP 12-26 investigations (Zokaie et al. 1991), would be required; however, while the scenarios are non-exhaustive, they are sufficiently representative to illustrate the feasibility of the plate approach described.

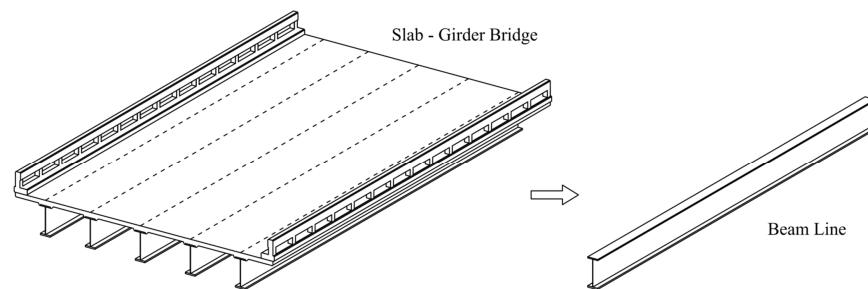


Fig. 1-2: Representation of beam-line analysis

Lateral Load Distribution

Currently, bridges in the United States receiving federal funding must be designed according to the design provisions of the AASHTO LRFD (2012). Lateral load distribution has been a major topic of debate in the bridge community for a number of years, especially since the AASHTO adoption of the semi-empirical approach developed as part of the NCHRP project 12-26 (Zokaie et al. 1991). This approach replaced the simple “S-over” method (AASHTO 2002), having been utilized by designers as a simple ratio method, which can be traced back to early research by Westergaard (1930) and Newmark (1948). As a result, this method has received a fair amount of attention due to the increased complexity of bridge structural systems and lack of familiarity by designers. Common concerns with the empirical method in the AASHTO LRFD (2012) include the iteration required for the calculation of stiffness parameter (K_g), limits of applicability, and the uncertainty in validity for alternative bridge systems such as composites, and implications for overload vehicles. In response, researchers have explored alternative approaches to predict the lateral load distribution characteristics, capable of providing significant accuracy without unnecessary complexity inherent to the current AASHTO LRFD method. These research efforts have included further investigations of the variables and new material

properties that influence lateral load distribution, in order to develop new equations for prediction (Cai 2005, Sotelino et al. 2004). The work presented herein follows suit, but differs by presenting a basic analytical approach for determining lateral load distribution characteristics using classical plate theory, with modification for a stiffened plate, that can be applied to a wide variety of scenarios.

AASHTO Specifications

While the AASHTO LRFD Bridge Design Specification is intended to cover most generic bridge types, the majority of bridges in-service are beam-type such as steel girders, prestressed girders, and box-beam girders with reinforced concrete decks (AASHTO 2012). For this reason, only beam-type bridges are considered herein.

For beam-type bridges the AASHTO LRFD provides guidance for both approximate and refined methods of analysis. For lateral load distribution, these approximate methods of analysis are in the form of empirical equations specific to the bridge cross-section type. Table 1-1 provides a summary of the empirical relationships applicable to both steel and concrete girders supporting a reinforced concrete deck. As highlighted, the relationships include equations for interior and exterior girders under both single and multiple lane loading scenarios and are primarily a function of girder spacing, span length, deck thickness, and longitudinal stiffness parameter. Furthermore, only moment distribution factors are considered in this study, albeit relationships exist for shear as well.

Table 1-1: Summary of AASHTO LRFD moment distribution factors for slab on girder bridges

Interior Girder	Applicability	Exterior Girder	Applicability
One design lane loaded			
$g = 0.06 + \left(\frac{S}{4300}\right)^{0.4} \left(\frac{S}{L}\right)^{0.3} \left(\frac{K_g}{Lt_s^3}\right)^{0.1}$	$1100 \leq S \leq 4900$ $110 \leq t_s \leq 300$ $6000 \leq L \leq 73000$ $N_b \geq 4$ $4 \times 10^9 \leq K_g \leq 3 \times 10^{12}$	Lever rule (static distribution)	Does not include multiple presence factor
Two or more design lanes loaded			
$g = 0.075 + \left(\frac{S}{2900}\right)^{0.6} \left(\frac{S}{L}\right)^{0.2} \left(\frac{K_g}{Lt_s^3}\right)^{0.1}$	$1100 \leq S \leq 4900$ $110 \leq t_s \leq 300$ $6000 \leq L \leq 73000$ $N_b \geq 4$ $4 \times 10^9 \leq K_g \leq 3 \times 10^{12}$	$g = e \cdot g_{interior}$ $e = 0.77 + \frac{d_e}{2800}$	$-300 \leq d_e \leq 1700$

All units are in (mm)

In addition to the approximate methods, the AASHTO LRFD (2012) allows for alternative methods of analysis that satisfy the requirements of equilibrium and compatibility; whilst utilizing appropriate stress-strain relationships for the materials considered. The use of a plate theory formulation allows for both of these requirements to be satisfied and thus is acceptable as a refined method; however, the proposed approach utilizes a variational formulation and should be categorized as an approximate solution.

Investigation Approach

Stiffened Plate Model

The approach proposed herein seeks to provide a basic methodology that can be applied to characterize lateral load distribution behavior using a classical plate approach. Eqn. 1-1 represents the basic differential equation for an ideal plate system resisting the out-of-plane loads in a flexural manner. In a girder bridge superstructure, the deck system can be idealized as a plate structure and the existence of girders and lateral bracings in longitudinal and transverse directions, respectively, provide stiffening contributions to the flexural rigidity of the simulated deck plate. As a result, the application of classical plate theory in analyzing girder bridge systems requires some modifications to the corresponding methodology for consideration of the effect of stiffening elements (e.g. girders and lateral bracing).

$$\nabla^4 w(x, y) = \frac{d^4 w(x, y)}{dx^4} + 2 \frac{d^4 w(x, y)}{dx^2 dy^2} + \frac{d^4 w(x, y)}{dy^4} = \frac{p(x, y)}{D} \quad (1-1)$$

Researchers in other fields such as aerospace engineering have studied similar structures that include a plate supported by elastic beams; which are typically referred to as a stiffened plate structures. A few researchers have even developed solutions for bridge structures, but these solutions are often tailored for a specific case (Kukreti and Cheraghi 1993, Kukreti and Rajapaksa 1990, Sapountzakis EJ, Katsikadelis 2000 and 2002). Presented herein is a method applicable to slab-girder bridges, which simulates the deck system as a plate element stiffened by longitudinal and transverse members representative of the girders, diaphragms, and bracing (see Fig. 1-3), to characterize lateral load distribution behavior of a beam-type bridge. The proposed approach represents a departure from the norm, where traditionally the bridge system is simplified down to a single beam element; with this approach, the bridge is simplified into a

plate system with stiffened regions representing the superstructure elements and lateral bracing. A primary advantage of this approach is that the lateral load distribution behavior of the bridge system is described with a mechanical-based formulation that accounts for the complex two-way behavior of the system and can be solved with relatively basic mathematical software or even a spreadsheet.

Method of Solution

The Ritz energy method, a solution procedure based on minimizing the system potential energy, was used in this study to solve the stiffened plate differential equation for a bridge system, deflected under external applied loading. Details on the Ritz method can be found in most textbooks on Plates and Shell Theory (Timoshenko and Woinowsky, 1959, Ugural 1999), but the basic solution requires the selection of a suitable shape function to satisfy the differential plate equation (Eqn. 1-1). In addition, the shape function must also satisfy the geometric boundary conditions (as illustrated in Fig. 1-3), but need not satisfy static or force boundary conditions exactly. For a single span bridge with simply supported boundary conditions at the ends and two lateral free edges, the out-of-plane deflection can be expressed in the format of infinite series, as given in Eqn. 1-2:

$$w(x, y) = \sum_{m=1}^{\infty} \sum_{n=1}^{\infty} A_{mn} f_m(x) f_n(y) \quad (1-2)$$

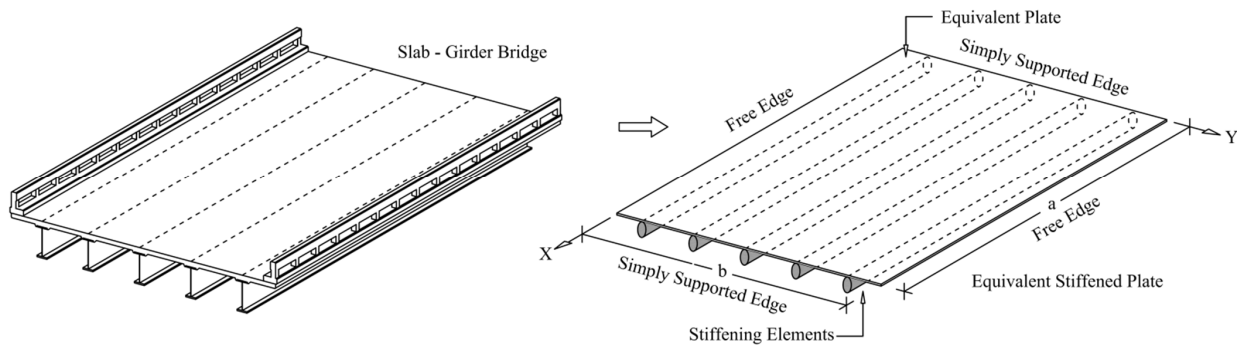


Fig. 1-3: Representation of a slab-girder bridge as an equivalent stiffened plate

Where A_{mn} is a series of unknown coefficients to be defined, while $f_m(x)$ and $f_n(y)$ are the functions that represent the deflection pattern of the system in x and y directions (see Fig. 1-3). These functions should be selected in a way that satisfies the boundary conditions of the bridge

system. At simply supported edges, both the deflection and in-plane bending moment are zero, therefore:

$$w|_{x=0,a} = 0 \quad (1-3)$$

$$\frac{\partial^2 w}{\partial x^2}|_{x=0,a} = 0 \quad (1-4)$$

For free lateral edges, on the other hand, the in-plane bending moment and shear force are zero:

$$\left(\frac{\partial^2 w}{\partial y^2} - \nu_s \frac{\partial^2 w}{\partial x^2} \right) \Big|_{y=0,b} = 0 \quad (1-5)$$

$$\left(\frac{\partial^3 w}{\partial y^3} - (2 - \nu_s) \frac{\partial^2 w}{\partial x^2 \partial y} \right) \Big|_{y=0,b} = 0 \quad (1-6)$$

Considering the assumed boundary condition for a single span bridge, an appropriate shape function was selected based on work by Kukreti and Cheraghi (1993) and presented in Eqn. 1-7.

$$w(x, y) = \sum_{m=1}^{\infty} \sum_{n=1}^{\infty} A_{mn} \frac{y^{n-1}}{b^{n-1}} \sin\left(\frac{m\pi x}{2}\right) \quad (1-7)$$

A solution for the unknown coefficients (A_{mn}) of the selected shape function was achieved by minimizing the potential energy of the system. A sensitivity analysis has also been done to demonstrate that implementing 6 terms for m and n ($m, n = 1...6$) adequately ensures the convergence of the solution.

The expression of the total potential energy in a stiffened plate system was derived from the investigation performed by Rajapaksa (1985). According to this study, it was assumed that the in-plane deflections are negligible in comparison to the out-of-plane deformations. Moreover, the connections between the concrete deck and steel girders were also assumed to be rigid enough to transfer the torsion and shear effects. Considering elastic, homogeneous and isotropic material

properties for the equivalent stiffened model of the bridge system, the total strain energy stored in the slab (plate) can be written as:

$$U_s = \int_0^b \int_0^a \frac{D}{2} \left\{ \left(\frac{\partial^2 w}{\partial x^2} + \frac{\partial^2 w}{\partial y^2} \right)^2 - 2(1-\nu_s) \left(\frac{\partial^2 w}{\partial x^2} \frac{\partial^2 w}{\partial y^2} - \left(\frac{\partial^2 w}{\partial x \partial y} \right)^2 \right) \right\} dx dy \quad (1-8)$$

The total energy in longitudinal girders can be attributed to the deformations that arise from flexure, torsion, and shear effects, and given by Eqn. 1-9:

$$U_{bx} = \sum_{i=1}^{N_{bx}} \left(\underbrace{\int_0^a \frac{E_x I_x}{2} \left(\frac{\partial^2 w}{\partial x^2} \right)^2_{y=y_k} dx}_{\text{Flexural Contribution}} + \underbrace{\int_0^a \frac{G_x J_x}{2} \left(\frac{\partial^2 w}{\partial x \partial y} \right)^2_{y=y_k} dx}_{\text{Torsional Contribution}} + \underbrace{\int_0^a \frac{(E_x I_x)^2}{2G_x A_x} \left(\frac{\partial^3 w}{\partial x^3} \right)^2_{y=y_k} dx}_{\text{Shear Contribution}} \right) \quad (1-9)$$

In transverse direction where the bracing elements act like stiffening member, the total energy can be expressed in a similar form as the longitudinal girders (Eqn. 1-9), but these members are typically flexible truss members so it was assumed that the flexural contribution dominates the behavior and the total energy only included the flexural contribution (Eqn. 1-10).

$$U_{by} = \sum_{i=1}^{N_{by}} \left(\int_0^b \frac{E_y I_y}{2} \left(\frac{\partial^2 w}{\partial y^2} \right)^2_{x=x_k} dy \right) \quad (1-10)$$

By adding up the energies stored in each main structural components together with the work done by the external loads, the total potential energy of the system can be written as follows:

$$U_t = U_s + U_{bx} + U_{by} + \underbrace{\int_{\zeta - \frac{\mu}{2}}^{\zeta + \frac{\mu}{2}} \int_{\eta - \frac{\nu}{2}}^{\eta + \frac{\nu}{2}} p(x, y) \cdot w dx dy}_{\text{Work Done by External Load}} \quad (1-11)$$

Once the unknown coefficients of selected shape function are derived, additional system response of the equivalent plate such as rotation, shear, and moment can be derived from the equation of the deflected shape, using traditional plate strain-displacement relationships (see Eqn. 1-12); however, in this study only the deflections along the stiffened locations were considered since the focus was concentrated on lateral load distribution rather than deck response. The deflections at midspan were then used to determine fractions of the total load resisted by each of the main stiffening elements (girders) based on Eqn. 1-13, which is common practice for assessing lateral load distribution behavior from field testing (Harris, et al. 2008 and 2010, Nowak, et al. 1999, Waldron, et al. 2005).

$$\frac{d^2w}{dx^2} = \phi_{bx} = \frac{M_{bx}(x)}{E_x I_x} \quad (1-12)$$

$$GDF_i = \frac{R_{\max i}}{\sum_{i=1}^{N_b} R_{\max i}} \cdot N_{trucks} = \frac{\Delta_{\max i}}{\sum_{i=1}^{N_b} \Delta_{\max i}} \cdot N_{trucks} = \frac{\varepsilon_{\max i}}{\sum_{i=1}^{N_b} \varepsilon_{\max i}} \cdot N_{trucks} \quad (1-13)$$

Relationships, Challenges and Assumptions

The treatment of the bridge system as an equivalent stiffened plate presents a few challenges related to boundary restraint and equivalent mechanical properties of the stiffening elements. With the proposed approach, concentric boundary conditions at the mid-plane of the plate are dramatically different than those of in-service bridges. This difference has been shown to induce errors in member response in finite element analyses of bridges with similar idealizations (Chan and Chan 1999). However, this effect does not influence the load sharing or load distribution behavior inherent to the system performance, indicating minimal impact on lateral load distribution behavior.

In a typical bridge, composite action between the deck and girder constrains the analysis to the neutral axis of the composite section, but for the case of the equivalent stiffened plate the analysis is about the mid-plane of the plate. For a consistent equivalent plate analysis, it is necessary to include the contribution of composite action which results in a stiffening of the plate at the locations of stiffening elements, provided by the non-composite stiffness of the longitudinal and transverse elements. Considering that the plate stiffness is accounted for in the

flexural rigidity (D) term of the plate analysis, these additional stiffening effects ($\bar{A}_b d_b^2$ and $\bar{A}_d d_d^2$ as depicted in Fig. 1-4) were included in to generate the effective bending stiffness term in the beam strain energy components of the stiffened plate energy relationship (Eqns. 1-9 and 1-10). Similarly, the stiffening effects from the transverse members (bracing and diaphragms) were also accommodated by considering only the bending component of the strain energy and the non-composite member section properties. Overall the effects of these factors are expected to be minimal on the load distribution behavior because it is primarily influenced by girder spacing and to a lesser extent, girder stiffness and boundary restraint (Zokaie 1992 and 2000).

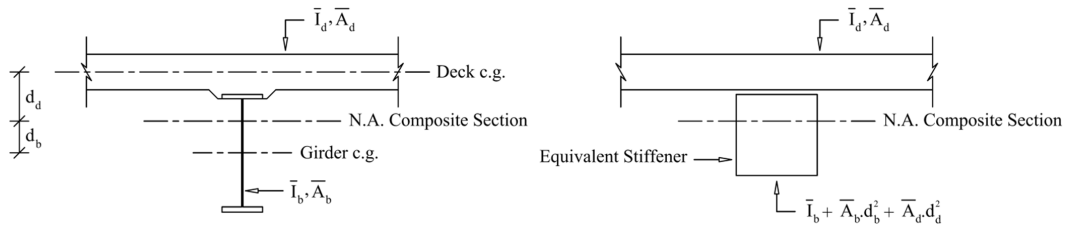


Fig. 1-4: Composite cross-section vs. equivalently stiffened plate section

Representative Bridges for Validation

To evaluate the performance and validity of the proposed approach, the load distribution behavior of three bridges were investigated. The bridges studied included were designated as Stanley Bridge, Huron Bridge, and Shenley Bridge. These bridges were selected primarily due to the availability of data from performed live load tests (sufficient structural member details, load magnitude and configuration, and measured data) and their appropriateness to the proposed approach (simple spans, composite behavior between deck and girder, limited skew), but were considered sufficiently representative to demonstrate the feasibility of the proposed approach. The selected bridges each maintain unique features that allow for validation of the proposed stiffened plate approach with a wider population spectrum. Field test data, including both strain and displacement measurements at midspan, were used to determine lateral load distribution characteristics, based on Eqn. 1-13 for the respective loading configuration. This field test data served as the metric for comparison of the proposed stiffened plate approach.

In addition to the stiffened plate models developed for these bridges, finite element models were also created to provide additional comparison and congruence with the field test results.

Each of the models were developed based on the geometric details included in the construction plans with loading conditions corresponding to testing program performed by Harris et al. (2008) and Nowak and Eom (2001). All models were developed using the commercial finite element software ANSYS (2011) with an eccentric plate formulation proposed by Chung and Sotelino (2006) or solid element system models (Nowak and Eon 2001, Nowak et al. 1999). A validation of the eccentric plate formulation is presented in another work by Harris (2010) along with additional details on the model development. The solid element system models developed in this investigation were validated using a similar approach. Each evaluated bridge was tested in the field under a series of loading configurations; however only representative test scenarios from each bridge are included in the comparisons. For the bridges tested by Nowak and Eom (2001), the choice of test scenarios was governed primarily by available results from the testing program and sufficiency of details on the loading configuration. In this testing program, only strain measurements were recorded and as a result, all distribution factors from field tests are derived from these values. For the bridge tested by Harris et al. (2008), both displacements and strains were measured and distribution factors presented in this paper are derived from the displacement measurements. It should be noted that an investigation by Harris (2010) demonstrated that distribution factor results from both of these measurement types are equivalent.

Stanley Bridge

Description

The bridge on Stanley Road over I-75 (S11-25032) in Flint, Michigan (Nowak and Eom 2001, Nowak et al. 1999) is a three span structure with simple supports and a total length of 86.8 m. Seven steel plate girders with a transverse spacing of 2.21 m support a 203 mm reinforced concrete deck. Only the second span of the structure was selected for validation and is 41.1 m long with a clear span of 38.4 m between pin and hanger connections. Michigan Department of Transportation (MDOT) plans indicated that Grade A concrete with a compressive strength of 20.7 MPa and A36 steel with an allowable stress of 137.9 MPa were used in the construction. This bridge is referred to herein as the Stanley Bridge, (see Fig. 1-5).

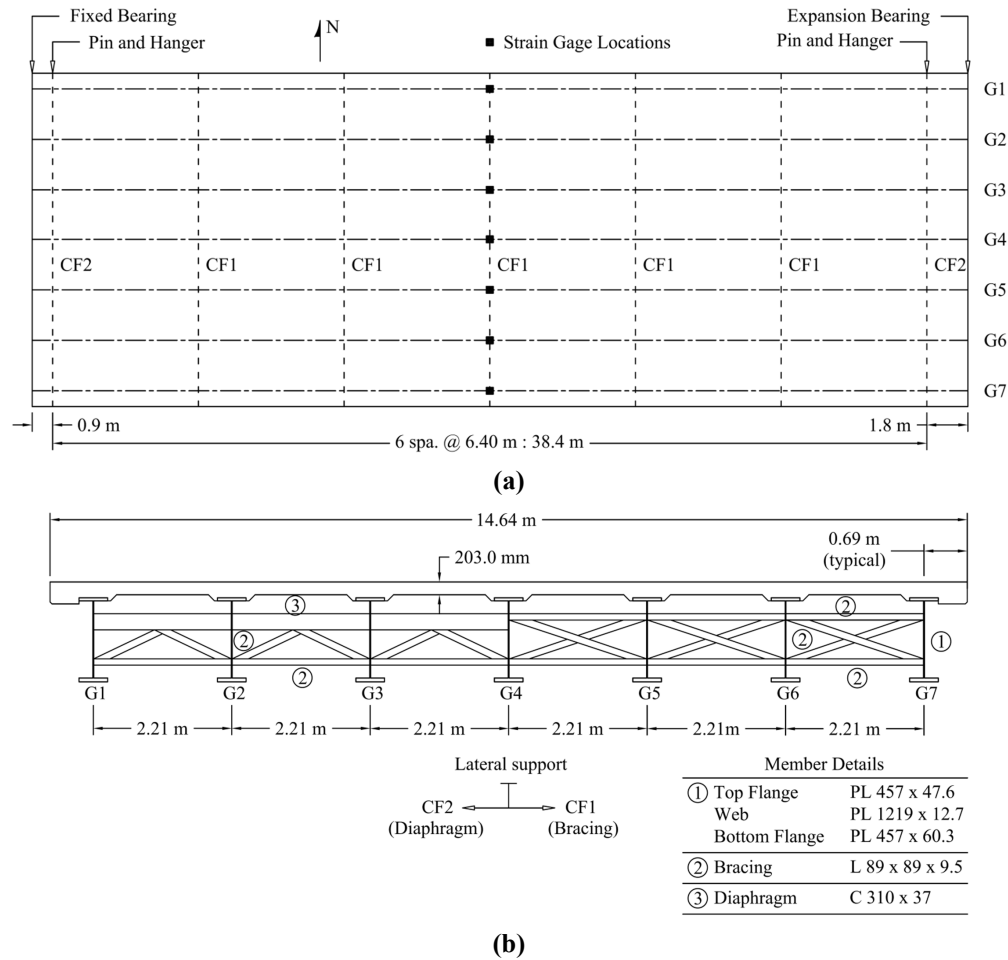


Fig. 1-5: Stanley Bridge: (a) plan diagram (second span only), (b) cross-section diagram

Testing Program

The live load testing was performed with two eleven-axle trucks, common to the state of Michigan, as illustrated in Fig. 1-6, centered within the 3.7 m lanes. Additional loading scenarios were evaluated in the testing program, but only the two truck-loading center of lane scenario (Run #13) was considered in this investigation (Nowak and Eom 2001, Nowak et al. 1999). Strains were measured at midspan on the extreme tension face of the bottom flange of the girders and used to calibrate finite element models of the bridge. Results from both the field testing and finite element models were used to determine distribution factors for the loading scenario. Additional details of the live load testing and finite element model validation are presented elsewhere (Harris 2010).

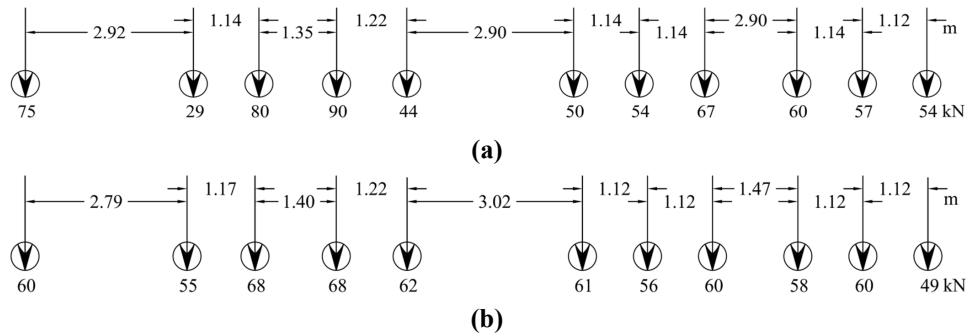


Fig. 1-6: Stanley Bridge live load test vehicle axle and loading configuration: (a) Truck 1 (660 kN, 11 axles, 15.67m wheelbase), (b) Truck 2 (657 kN, 11 axles, 15.55m wheelbase)

Huron Bridge

Description

The bridge on M-36 over the Huron River (B01-47041) in Livingston County, Michigan (Nowak and Eom 2001, Nowak et al. 1999) is a single span, 15° skew, simply supported bridge. The 42.6 m long bridge consists of six steel girders spaced at 2.85 m supporting a 229 mm reinforced concrete deck with a transverse width of 15.62 m. MDOT plans indicated that Grade 35T concrete with a compressive strength of 20.7 MPa and ASTM A572 Gr. 50 steel with an allowable stress of 137.9 MPa was used in the construction. This bridge is referred to herein as the Huron Bridge, as illustrated in Fig. 1-7.

Testing Program

Similar to the Stanley Bridge testing program, the live load testing was performed with two eleven-axle truck trucks, common to the state of Michigan, as given in Fig. 1-8, centered within the 3.7 m lanes. Additional loading scenarios were evaluated in the testing program, but only the two side by side truck-loading center of lane scenario (Run #5) was considered in this investigation (Nowak and Eom 2001, Nowak et al. 1999). Strains were measured at midspan on the extreme tension face of the bottom flange of the girders and used to calibrate finite element models of the bridge. Results from both the field-testing and finite element models were used to determine distribution factors for the loading scenario. Additional details of the live load testing are presented elsewhere (Nowak and Eom 2001, Nowak et al. 1999).

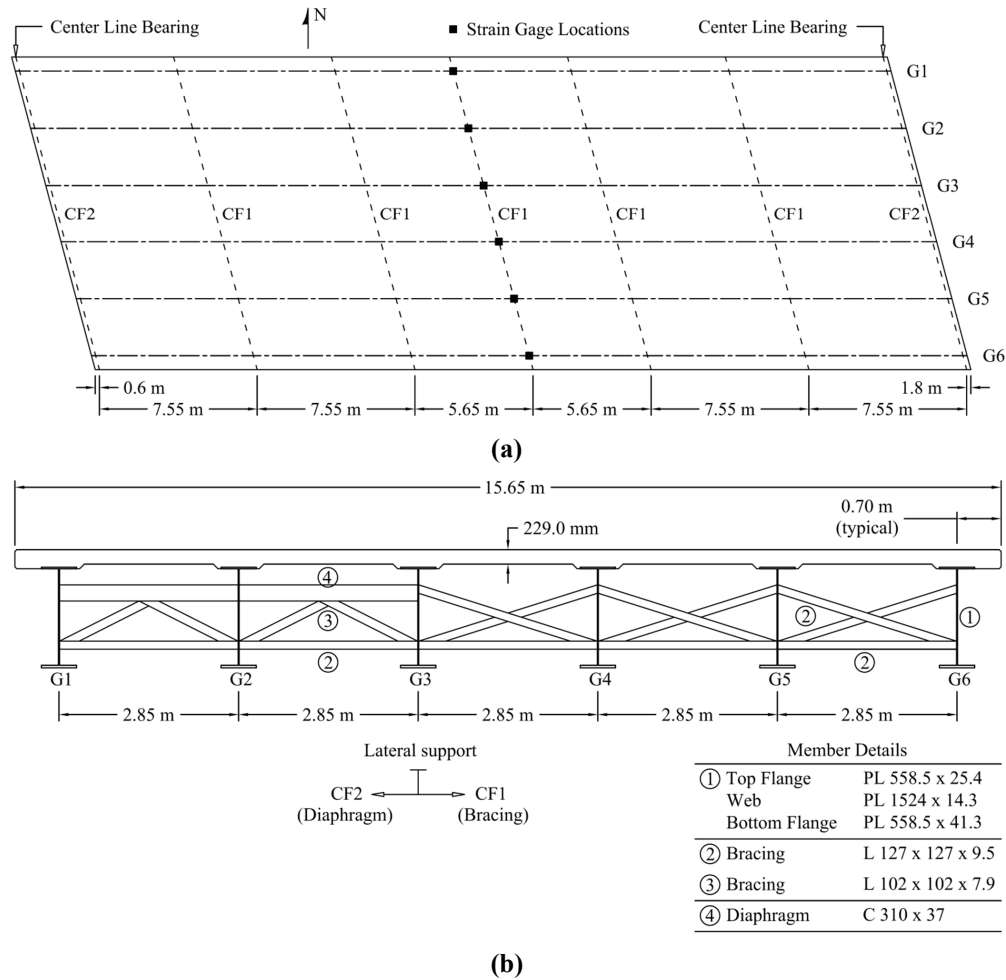


Fig. 1-7: Huron Bridge: (a) plan diagram, (b) cross-section diagram

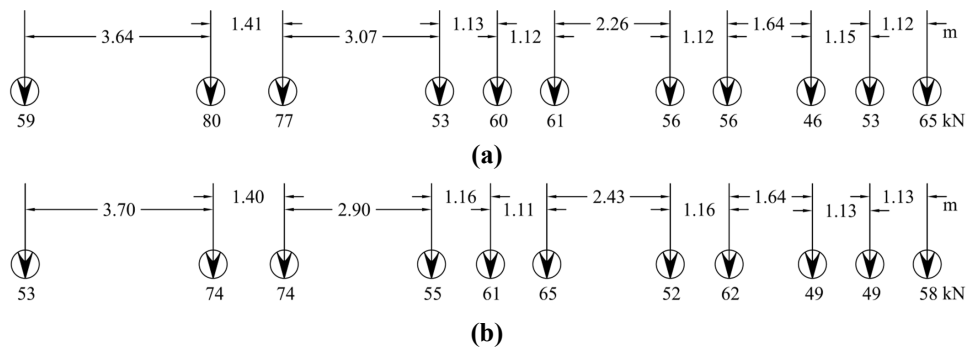


Fig. 1-8: Huron Bridge live load test vehicle axle and loading configuration: (a) Truck 1 (666 kN, 11 axles, 17.66m wheelbase), (b) Truck 2 (652 kN, 11 axles, 17.76m wheelbase)

Shenley Bridge

Description

The Shenley Bridge is a simple span bridge, located in St. Martin, Quebec. The bridge has a

22.5 m span, a transverse width of 7.1 m, and utilizes a composite sandwich deck system known as the Sandwich Plate System (SPS). The deck was fabricated from a series of ten panel sections with identical cross sectional configurations with a designation of 6.4-38-6.4, representing the steel plate, polymer core, and steel plate thicknesses in millimeters. The deck panels are supported by three identical longitudinal plate girders, which are laterally braced along the span. The bridge system is considered fully composite based on field test results. Plans indicated that ASTM A572 Gr. 50 (weathering) steel was used in the construction of the plate girders with CAN/CSA-G40.21 steel used for the steel faceplates of the deck. The polymer core was rigid polyurethane foam with an elastic modulus of 750 MPa. This bridge is referred to herein as the Shenley Bridge, as depicted in Fig. 1-9.

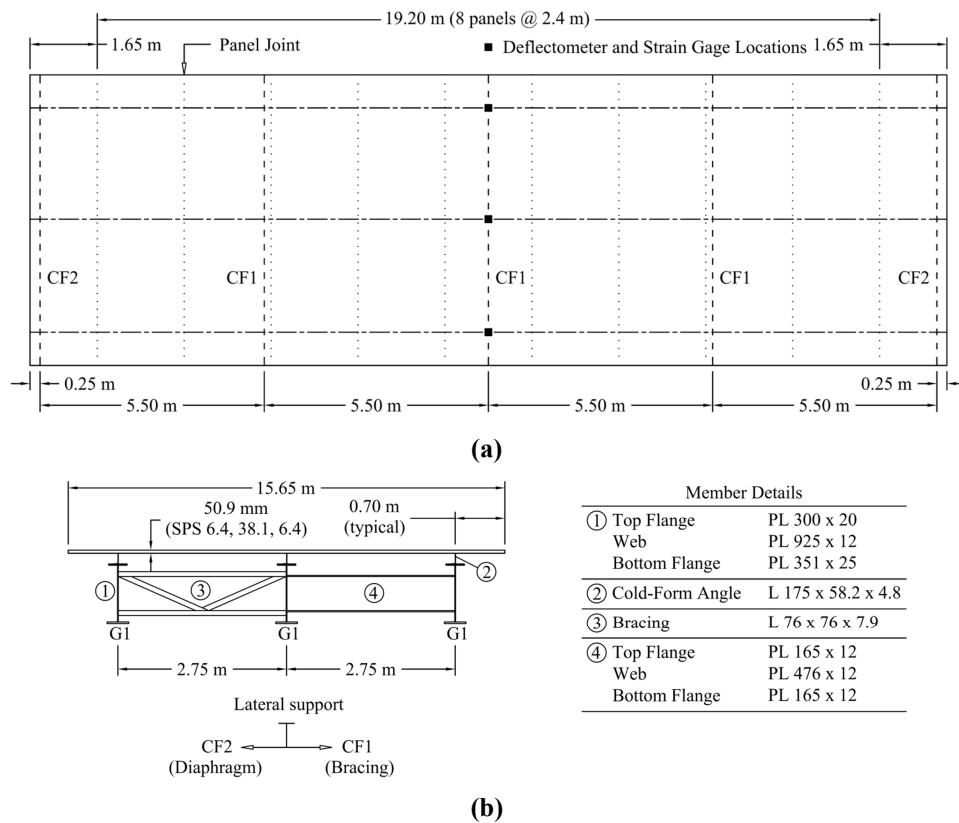


Fig. 1-9: Shenley Bridge: (a) plan diagram, (b) cross-section diagram

While classical plate theory is typical for homogeneous plates, in this study the approach was extended to the case of a layered plate system (see Fig. 1-10) using the equivalent cross-sectional relationships. The corresponding formulations for equivalent flexural rigidity and Poisson's ratio

are given in Eqn. 1-14 and Eqn. 1-15, respectively (Ugural 1999, Ventsel and Krauthammer 2001, Vinson 1999). These equivalent cross-sectional/material properties were then implemented in updating the strain energy of the deck plate, utilizing Eqn. 1-11.

$$D_{eq} = \frac{2}{3} \left(E_p \frac{\left(\frac{t_c}{2} + t_p \right)^3 - \left(\frac{t_c}{2} \right)^3}{1 - \nu_p^2} + E_c \frac{\left(\frac{t_c}{2} \right)^3}{1 - \nu_c^2} \right) \quad (1-14)$$

$$\nu_{eq} = \frac{2}{3 D_{eq}} \left(E_p \nu_p \frac{\left(\frac{t_c}{2} + t_p \right)^3 - \left(\frac{t_c}{2} \right)^3}{1 - \nu_p^2} + E_c \nu_c \frac{\left(\frac{t_c}{2} \right)^3}{1 - \nu_c^2} \right) \quad (1-15)$$

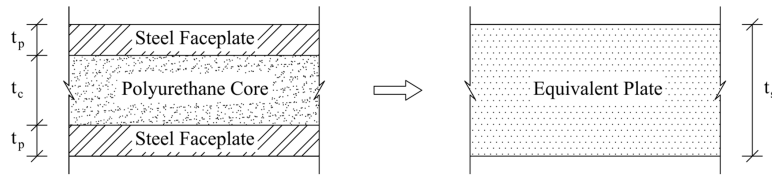


Fig. 1-10. Layered sandwich plate transformation to equivalent homogeneous plate

Testing Program

The live load testing was performed with a three-axle dump truck crept along the bridge span. Multiple loading scenarios were evaluated in the testing program, but only load cases A and E as depicted in Fig. 1-11, were considered in this investigation to illustrate the influence of load position (Harris et al. 2008). Displacement and strains were measured at midspan on the extreme tension face of the bottom flange of the girders, but only displacements are used in the comparisons. Results from both the field testing and finite element models were used to determine distribution factors for the loading scenarios using the load fraction approach described in a previous section. Additional details of the live load testing and finite element model validation are presented elsewhere (Harris et al. 2006 and 2008).



Fig. 1-11. Shenley Bridge live load test: (a) Truck (434.6 kN, 3 axles, 5.5m wheelbase), (b) Transverse Loading Positions from curb

Results

The corresponding stiffened plate models for the reference bridges, were analyzed using the commercial software Mathematica (2008). In this approach, the coefficients of the deflected shape function, described in Eqn. 1-7, have been determined by numerically minimizing the equation of the total potential energy for the system (Eqn. 1-11). The derived shape function was then used to calculate the deflections at midspan, which corresponded with the measurement locations in the field tests, for the three reference bridges. Finally distribution factors were determined using the load fraction relationship (Eqn. 1-13) typical to field-testing. It should be stressed that strain response from the stiffened plate models were deemed inappropriate for evaluation of lateral load distribution behavior because these strains are located at the mid-plane of the plate; while the response of interest would correspond to the neutral axis of the composite girder (Harris 2010).

Deflection response

Comparisons of the deflections for each of the bridges are presented in Table 1-2. Due to the limited data available from the field-testing programs, measured deflection data is limited to the Shenley Bridge. However, results from finite element models, which have been validated with measured strain data, are included for the bridges tested by Nowak et al. (2006 and 1999). The finite element model results represent upper and lower bounds on the support restraint by considering pin-roller (PR) and pin-pin (PP) support conditions. Nowak (2006) also presented a calibrated restraint model, which included modified restraint conditions to better mimic field test results; however, a similar model was not developed for this study, because the objective of the current investigation was to evaluate the ability of the basic stiffened plate approach to characterize the load distribution response of beam-slab bridges.

For the Stanley and Huron Bridges, the stiffened plate model exhibited larger deflections at the interior girders and smaller deflections for the exterior girders when compared to the upper bound results of the finite element models. On the other hand for the Shenley Bridge, there is no specific correlation between the results obtained for the load Case A. Moreover, negative deflection of the exterior girder opposite to the location applied load, indicates uplift in the system, which was not previously observed in the field investigations. However, the load Case E yielded larger deflections for both interior and exterior girders when compared to both finite element and field measurements.

Table 1-2: Displacement Comparison Summary

Girder Number	Displacements (mm)			
	Measured	Stiffened Plate	FEA (PP)	FEA (PR)
Stanley Bridge				
G1	-	17	9	22
G2	-	26	12	26
G3	-	32	15	30
G4	-	33	16	31
G5	-	30	15	30
G6	-	23	12	26
G7	-	14	9	22
Huron Bridge				
G1	-	15	10	24
G2	-	30	14	29
G3	-	40	17	32
G4	-	40	17	32
G5	-	30	14	29
G6	-	14	10	25
Shenley Bridge, Load Case A				
G1	16	18	NA	15
G2	8	7	NA	6
G3	1	-2	NA	-1
Shenley Bridge, Load Case E				
G1	7	7	NA	6
G2	8	10	NA	9
G3	6	7	NA	6

From a qualitative perspective, it appears that the stiffened plate model is unable to accurately simulate the deflection response with a high level of accuracy. However, it should be emphasized that the response from the finite element models compared to field test results exhibited similar characteristics for the upper and lower bound restraint conditions previously described and only a refinement of the restraint conditions improved this agreement. This characteristic is expected from any numerical representation of a physical system such as a bridge superstructure, which is highly dependent on loading and boundary conditions as well as model simplifications. It should also be stressed that features such as the barriers and parapets, which are known to influence the stiffness of the system, were not included in the stiffened plate approach. For the Stanley Bridge, a comparison of the deflection with the effects of parapets and bracing demonstrated that the global behavior of the bridge system is influenced by both of these features, but the impact of the bracing is more significant, resulting in a large stiffening effect of the overall system, as illustrated in Fig. 1-12. While the stiffened plate approach appears to have limitations in estimating deflection, it is clear that the methodology provides a reasonable measure of the relative system behavior, which is essential for evaluating load sharing or load distribution.

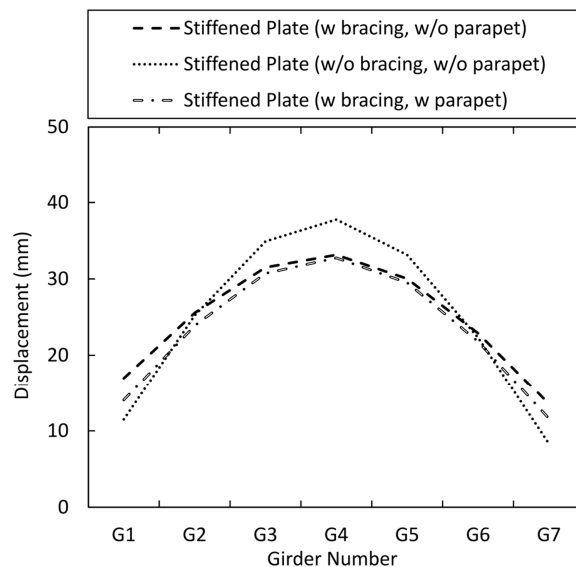


Fig. 1-12: Influence of Secondary Members on the Stiffened Plate Behavior in Stanley Bridge

Lateral Load Distribution Behavior

Similar to the deflection response, comparisons of lateral load distribution factors for each of the reference bridges, derived from stiffened plate and FE numerical methods as well as field-test investigations, are presented in Table 1-3 and Figs. 1-13 to 1-16. Also included in Table 1-3 for comparison, are the calculated distribution factors for design without multiple presence factors, which are generally considered conservative when applicable.

Table 1-3: Summary of distribution factors

Girder Number	Displacements (mm)				
	Measured	Stiffened Plate	FEA (PP)	FEA (PR)	AASHTO
Stanley Bridge					
G1	0.17*	0.20	0.20	0.23	0.48
G2	0.29*	0.29	0.27	0.28	0.59
G3	0.35*	0.36	0.35	0.32	0.59
G4	0.39*	0.38	0.37	0.34	0.59
G5	0.36*	0.35	0.35	0.32	0.59
G6	0.27*	0.26	0.27	0.28	0.59
G7	0.17*	0.16	0.20	0.24	0.48
Huron Bridge					
G1	0.21*	0.17	0.25	0.28	0.57
G2	0.36*	0.36	0.34	0.34	0.68
G3	0.42*	0.47	0.41	0.37	0.68
G4	0.44*	0.47	0.41	0.37	0.68
G5	0.34*	0.35	0.34	0.34	0.68
G6	0.23*	0.17	0.25	0.29	0.57
Shenley Bridge, Load Case A					
G1	0.65**	0.77	-	0.73	NA
G2	0.32**	0.31	-	0.31	NA
G3	0.02**	-0.08	-	-0.04	NA
Shenley Bridge, Load Case E					
G1	0.33**	0.32	-	0.31	NA
G2	0.38**	0.40	-	0.42	NA
G3	0.29**	0.28	-	0.27	NA

* Measured strains

** Measured deflections

Because the deck system of the Shenley bridge is outside the limits of applicability of the AASHTO LRFD design specifications, the distribution factors cannot be calculated based on the empirical equations mentioned in Table 1-1. When comparing load distribution behavior, features such as boundary restraint and secondary member contributions are minimized. From these comparisons it becomes evident that the proposed approach is able to simulate the system behavior and relative load sharing better than local response and also yields less conservative estimates of distribution behavior when compared to design distribution factors without multiple presence factors, see Table 1-3.

Stanley Bridge

The lateral load distribution response from the stiffened plate methodology for the Stanley Bridge provided good agreement with both the finite element model results and the distribution response derived from measured strain data from the field test (see Fig. 1-13). The flexibility observed in the displacement comparison is not present in this relative load sharing system response. This characteristic is also true for the finite element model results where the effects of boundary restraint (pin-pin vs. pin-roller) are negated. Compared to the field test results, the stiffened plate methodology results in less load being supported by girders 4-7 and a greater load being supported by girders 1-3. These differences can be attributed to the simplifications in the modeling approach such as neglecting parapets and simplification of the bracing contribution.

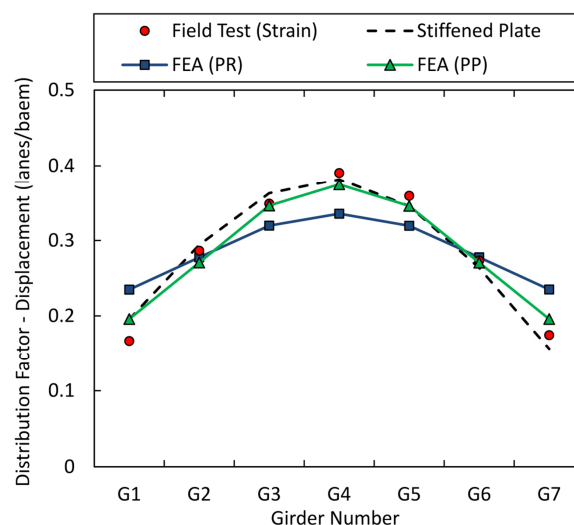


Fig. 1-13. Stanley Bridge Load Distribution Behavior

Huron Bridge

The lateral load distribution response of the Huron Bridge exhibited more transverse flexibility than the Stanley Bridge, with the interior girders resisting a greater fraction of the total load than the exterior girders, as depicted in Fig. 1-14. This trend was observed in both the finite element model and field test results, but was more pronounced in the results from the stiffened plate methodology. It might be expected that this difference could be attributed to the impact of the skew, where in practice, the presence of skew would be expected to increase the load resistance for exterior girders and decrease that for interior girders. This effect is not obvious from the results presented herein without a companion non-skewed for comparison, but past research has indicated that the effects of skew are not significant for small skew angles (less than 30 degrees according to the AASHTO LRFD) and the influence is primarily associated with shear distribution behavior which would be exhibited at the supports rather than moment distribution behavior near midspan (Barr and Amin 2006, Ebeido and Kennedy 1995 and 1996, Huang et al. 2004). The increased flexibility is more likely associated with the wider girder spacing, simplification of the bracing contribution, and the exclusion of the parapets (type 4), which were more rigid than those of the Stanley Bridge, in the stiffened plate model.

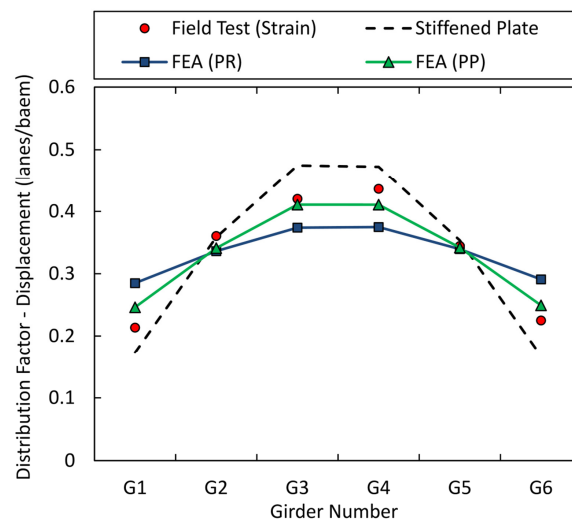


Fig. 1-14. Huron Bridge Load Distribution Behavior

Shenley Bridge

The geometry of the Shenley Bridge allowed for consideration of deck flexibility as well as

the effect of new composite material properties in lateral load distribution behavior, due to the thin composite bridge deck and relatively wide girder spacing as compared to the Stanley and Huron Bridges. The loading scenarios also allowed for consideration of the effects of load eccentricity (i.e. exterior versus interior girder response). For both load cases, distribution factors determined using the stiffened plate approach were within 20% of the distribution factors determined from measured data without the inclusion of parapets, refinement of boundary condition restraints, and consideration of lateral bracing (see Fig. 1-15). Better agreement was observed for loading scenario E, where the stiffened plate results were within 10% of those determined from measured data. This trend was not observed for G3 in loading scenario A because the experimental measured response for this girder was nearly zero, indicating minimal load sharing to the opposite side of the bridge when the other side is loaded. The inclusion of parapets and refinement of the bracing contributions would reduce this effect, but it should be noted that a similar response was observed in the finite element model results. However, both the FE and stiffened plate models predicted that G3 was lifted up in this loading scenario (A) as demonstrated by the negative deflections and distribution factors.

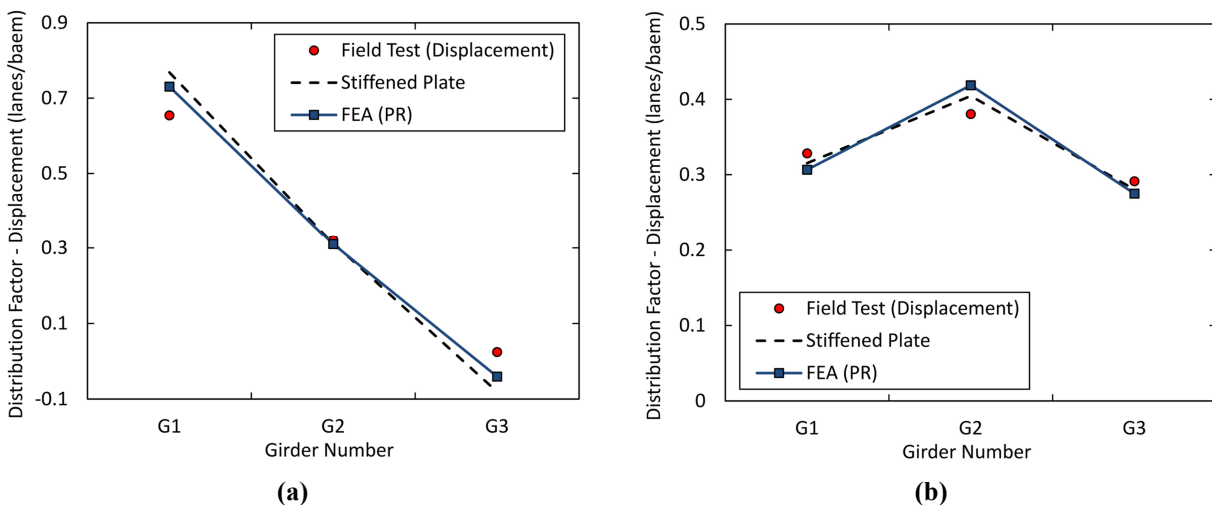


Fig. 1-15. Shenley Bridge Load Distribution Behavior: (a) load case A, (b) load case E

The apparent transverse flexibility of the Shenley Bridge lead to the conclusion that this type of system can be better represented as a stiffened plate than the more conventional design, utilizing stiff reinforced concrete decks and tighter girder spacings. In fact, the new composite material used for the deck with the wide-spaced girders cause more flexibility in the Shenley

bridge superstructure system, which actually justifies that the general plate theory is more capable in predicting the load distribution characteristics for these type of bridges, in comparison to the codified empirical design equations.

Discussion and Conclusions

Included in this study is the presentation of a stiffened plate methodology for evaluating the bridge system behavior, specifically load sharing or lateral load distribution behavior. The proposed methodology represents a departure from common practice where a complex bridge system is reduced down to a single beam, by representing the bridge system as a plate with discrete stiffening elements representing the girders and secondary members. The importance of such a methodology is that it can be applied to a variety of bridge systems that are outside the range of applicability of existing design specifications without the need to develop highly sophisticated finite element models. The simplicity would also allow rapid evaluation of distribution characteristics of in-service bridges based solely on design or as-built details, with potential to include additional complexity such as parapets, toppings, and even damage. A key feature of the proposed method is that it can be employed with relatively low computational demand, using basic numerical software without the need for specialized finite element analysis software.

The proposed stiffened plate methodology was evaluated for its ability to predict lateral load distribution characteristics of simple span bridges. Moreover, this study assessed the performance of the stiffened plate methodology against field test and finite element results of three bridges with varying geometries, constituent materials, and loading configurations. From this investigation, the following conclusions were observed regarding the proposed methodology:

- The methodology was generally able to simulate the deflection response of the three bridges considered, but the stiffened plate model often yielded a more flexible system response when compared to upper bound finite element model results. The deflection response was in better agreement with the measured and finite element model results for the Shenley Bridge, which can most likely be attributed to the flexibility of this bridge relative to the Stanley and Huron Bridges. The Shenley Bridge was constructed with a thin (~50 mm) composite deck system with relatively wide girder spacings as compared

to the Stanley and Huron Bridges, which were constructed with concrete decks and moderate girder spacings.

- When comparing lateral load distribution, which is a measure of relative load sharing behavior, the stiffened plate methodology correlated well with both field measured and finite element results. The methodology also provided a less conservative estimate of the load sharing characteristics when compared to AASHTO design equations.
- For the Stanley and Huron Bridges, the distribution factors from the stiffened plate methodology were within 30% of the measured distribution factors, but the majority of the results were within 15%. For these bridges the exterior girder regions exhibited less contribution to the load sharing response than the actual system, which is attributed the exclusion of the stiffening contribution from secondary elements such as the parapets and simplification of the bracing and diaphragm details.
- The distribution factors from the stiffened plate methodology for the Shenley Bridge agreed well and were consistently within 20% of the measured response with the exception of the exterior girder in the unloaded region of the bridge for load case A. In this case, the load sharing contribution observed from the field testing is essentially zero for this exterior girder with the load on the opposite side of the bridge, but the stiffened plate methodology indicated negative deflection for this load case. Similar to the Stanley and Huron Bridges, this deviation can also be attributed to the exclusion and simplification of secondary member contributions, but is more related to sensitivity of the measured data.

Chapter 2:

Case Study: Failure Characteristics and Ultimate Load-Carrying Capacity of Redundant Composite Steel Girder Bridges

(ASCE, Journal of Bridge Engineering, in press, 2014)

Summary

With the existence of aging highway bridges within the US transportation network, federal and local agencies typically encounter a wide assortment of maintenance issues ranging from cracking, spalls, delaminations and corrosion to high load impacts and fire damage. This paper presents an approach for capturing the full system-level behavior and stages of failure in the composite bridge superstructures as they approach ultimate capacity. This step is instrumental to the understanding of how redundant bridges behave in the presence of coupled and uncoupled damage and deteriorations. The investigation includes a comprehensive nonlinear finite element analysis of two representative intact composite steel girder bridges that were tested to failure and provided sufficient details for model validation. Results demonstrate the high degree of additional reserve capacity, inherent to redundant superstructures, over the theoretical nominal design capacity. A rational approach was established to describe the actual system-level ultimate capacity, which is not explicitly considered in the current design methodology. In addition, a limited sensitivity study was performed on one of the selected representative bridges to investigate the sensitivity of the characterized failure stages to variations in the geometrical parameters and material properties of the bridge system.

Introduction

State of Practice

To ensure a robust and sustainable infrastructure network, in-service superstructures including composite steel girder bridges, are routinely monitored and periodically inspected for the existence of any probable damage or deteriorating conditions. In the United States, these inspections occur on a biennial basis using routine visual assessments (FHWA 2001, 2006) and non-destructive evaluation techniques (SHRP2 2012) to accurately monitor degradation over time and provide guidance on maintenance and rehabilitation schedules. However, there is a

lack of knowledge regarding the actual structural response, including the nonlinear behavior and ultimate capacity of the inspected bridges, under the effect of existing deterioration conditions. From a historical perspective, the complex interaction between structural components which causes inherent structural redundancy in bridge superstructures, is overly simplified in the design process and even further so in the maintenance and rating processes. These simplifications result in a critical missing link in the understanding of bridge system behavior and life-cycle performance.

The performance and serviceability of a bridge structural system can be significantly affected not only by the specific type of incorporated damage, but also by its location, extent and coupling with other damage or degradation scenarios. As a result, it is essential to quantify the impacts of different probable damage mechanisms on the overall system behavior and accurately characterize the ultimate capacity of the degraded bridges to ensure continued safe operation. This phenomenon represents an area of critical need with an aging and deteriorating bridge infrastructure network that has experienced prominent bridge failures such as the I-35W in Minnesota (NTSB 2008), I-5 in Washington and Scout city roadway in Missouri (NTSB 2013a and 2013b). While these failures were not attributed to deterioration, they do highlight the importance of system redundancy and the relationships with safety and maintenance.

To evaluate these characteristics, an ideal approach would be the implementation of full-scale destructive field tests on a series of representative bridges; however, this approach is neither feasible nor cost-effective. Laboratory testing can also be considered as an alternative approach, but challenges with dimensional scaling and simulation of representative boundary conditions are considered as limitations of this method, in addition to associated costs. With today's computational resources and capabilities, the development of an analytical model to study the performance of intact or damaged bridge systems could be best handled numerically, using a tool such as the Finite Element Method (FEM). While FEM provides an efficient mechanism to simulate the system interaction, a proper treatment of boundary conditions, the use of accurate material constitutive relationships, and system-level failure criteria remain as the main challenges with this numerical modeling approach and must be properly treated to yield accurate results.

Background and Research Significance

During the last few decades, several researchers have utilized FE method to carry out nonlinear analyses on steel-concrete composite girders. In these studies, numerous efforts were concentrated towards modeling the composite action between the steel girders and reinforced concrete deck. Yam and Chapman (1968, 1972) performed a series of numerical analyses on simply-supported and continuous composite beams, in which the inelasticity of steel, concrete, and shear connections were taken into account. Thevendran et al. (1999) used rigid connection beam elements to model shear studs in their FE analysis to study nonlinear behavior and ultimate load-carrying capacity of steel-concrete composite beams curved in plan. Baskar et al. (2002) used a surface interaction technique to model slab-girder connection in composite plate girders, which allowed slip and predefined tensile and frictional stresses. Queiroz et al. (2006) performed an extensive parametric study on composite beams to evaluate the effect of full and partial shear connection that were modeled using non-linear spring elements.

Refined FE analyses (one- and two-dimensional models) were also performed by Queiroz et al. (2009) and Zona et al. (2011) to evaluate the nonlinear behavior of composite beams in which the load-slip characteristics of shear connectors were taken into account. In a series of recent studies (Ellobody and Young 2006, Qureshi et al. 2011, Tahmasebinia et al. 2013), three-dimensional FE models were proposed to assess the nonlinear behavioral characteristics of composite steel-concrete floors consisting of concrete slabs cast on steel profiled sheeting and connected to steel beams by means of shear connectors. In these models, nonlinear constitutive material behavior was considered for 3D modeled shear studs. A surface-to-surface contact algorithm was also implemented to simulate the interface condition between concrete and steel elements.

The three-dimensional finite element modeling technique was also implemented by several researchers to investigate the overall flexural behavior of composite slab on steel stringer bridge superstructures under different load conditions (e.g. Hall and Kostem 1981, Razaqpur and Nofal 1990, Lin et al. 1991, Sebastian et al. 2000, Fu and Lu 2003, Chung and Sotelino 2005, Barth et al. 2006, and Bechtel et al. 2011). Included in their studies were detailed discussions on selection of appropriate constitutive material models representing cracking/crushing in concrete and yielding/strain hardening in steel, together with arguments on different element types used for numerical modeling of concrete decks, steel girders, reinforcing rebars, and providing the

composite action between the concrete slab and steel girders. The accuracy of the proposed models was verified against the results obtained from different full-scale laboratory experiments on model bridges or field tests on actual structures. While previous studies using nonlinear finite element analysis have proven successful, these investigations on composite steel girder bridges have typically been limited to achieve an appropriate correlation between the numerical results and the existing experimental data. In fact, their investigations were limited to the study the global behavior of bridge superstructures, with less focus on the critical behavioral stages of the bridge system.

This paper builds from this foundation of research with an objective of providing a comprehensive characterization of the nonlinear behavior and stages to failure of two representative intact composite steel girder bridges. The goal of this study is to provide a formal relationship between their ultimate capacity and system redundancy, based on the results of three-dimensional nonlinear FE analysis. Novel to this investigation is the classification of system response into different behavioral stages and the development of a generic failure criterion to predict the overall system capacity of the composite steel girder bridges irrespective of local failure effects. The proposed generic failure criterion not only provides a mechanism to describe system-level structural capacity, but also a rational foundation for understanding the impact of damage and deteriorating conditions on the system-level behavior. In addition, a sensitivity study was performed on one of the selected representative structures to evaluate the effects of variations in different geometrical and material properties on the overall system behavior and the characterized stages of failure. As this concept advances and the bridge community develops a better understanding of these behavioral characteristics, it is expected that this system-level treatment will help guide both maintenance and rating decisions. While the analyses and result are limited to the selected bridges, the methodology is generic and the rationale can also be extended to other types of bridge superstructures to help provide a measure of remaining capacity that can be used to prevent future failures.

Case Studies

A full-scale laboratory investigation on a simply-supported steel girder bridge (Kathol et al. 1995) and a field test on a four-span continuous composite girder bridge (Burdette et al. 1971) are the two case studies that have been evaluated using the proposed approach. These structures were selected due to availability of the well-documented reports containing detailed information

on the testing procedures, data acquisitions, loading conditions and obtained results. It should be noted that very few documented full-scale ultimate capacity tests are available in the literature, but these cases provide a number of features that allow for the modeling approaches to be extrapolated to alternative scenarios, considering different structural types, geometric properties, and loading conditions.

Nebraska Laboratory Test

Bridge Description

In the study by Kathol et al. (1995), a full-scale simply-supported steel girder bridge with the span length of 21.34 m (70 ft) and uniform cross section having a 7.92 m (26 ft) width, was tested under controlled laboratory conditions. The bridge superstructure consisted of a 190.5 mm (7.5 in) thick reinforced concrete deck, supported by three steel plate girders spaced at 3.05 m (10 ft), as shown in Fig. 2-1a. The model bridge was designed using the Load Factor Design (LFD) approach of the 15th edition of the AASHTO Standard Specifications for Highway Bridges (AASHTO 1992). However, it should be noted that the deck itself was designed based on the empirical design approach proposed in the draft of the AASHTO LRFD Bridge Design Specification (1992).

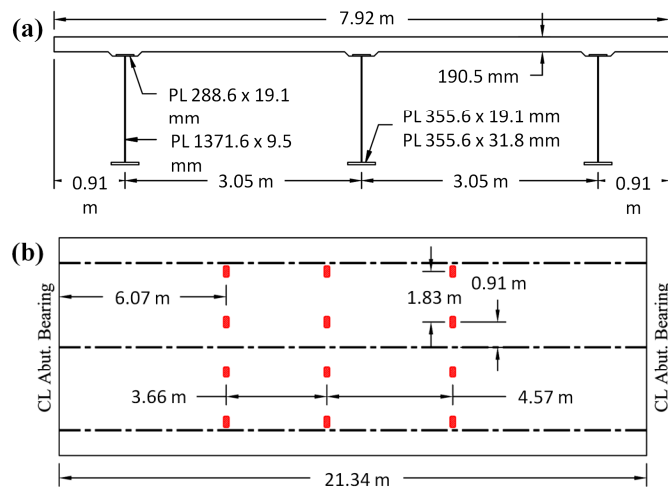


Fig. 2-1: Nebraska laboratory test: (a) cross section, (b) loading configuration

Test Setup and Experimental Results

An ultimate load test was conducted on the model bridge to evaluate the load carrying capacity of this superstructure. In this test, vertical concentrated loads were applied to the system by twelve post-tensioned rods to simulate two side-by-side HS-20 trucks with modified axle spacing, see Fig. 2-1b. The rods were fastened to twelve steel plates with dimensions of 500 x 200 x 50 mm on the top surface of the bridge deck and passed through the floor of the structural lab, individually connected to twelve 1780-kN (400-kip) hydraulic rams. Under the application of increasing loads, the bridge system remained almost elastic until material yielding initiated on the bottom flanges of both interior and exterior girders at mid-span. The ultimate test was terminated due to a local punching shear failure that occurred in the concrete slab.

Tennessee Field Test

Bridge Description

The four-span continuous steel girder bridge was one of the four selected highway bridges in the state of Tennessee that was part of an experimental research project by Burdette et al. (1971) to evaluate its ultimate strength and failure mode. This bridge had a total length of 97.54 m (320 ft) with two exterior and interior spans, having lengths of 21.34 m (70 ft) and 27.43 m (90 ft), respectively. The driving surface was provided by a 177.8 mm (7 in) reinforced concrete deck made composite with four identical steel girders uniformly spaced at 2.54m (8 ft - 4 in), as depicted in Fig. 2-2a.

Test Setup and Experimental Results

In a static test to failure, eight identical concentrated loads were applied on one of the interior spans of this continuous bridge, at specific longitudinal positions to create the maximum positive moment approximately near the midspan (see Fig. 2-2b). The spacing and magnitude of the applied loads were chosen to mimic the rear wheels of regular HS-20 trucks in each lane. These point loads were applied on the system through a series of steel bars anchored to the limestone rock under the bridge, while extended on the other end through a 1000-kN (225-kips) capacity center-hole jack resting on a bearing grill. Under the applied loads, the bridge behaved almost linearly elastic until yielding occurred in steel girders. Shortly after yielding began, the bridge lifted up at the abutment adjacent to the loaded span, followed by large deflections and the formation of plastic hinges in the steel girders. The test was terminated due to a compression

failure that occurred in one of the curbs at the location of maximum moment after the formation of the hinges in the girders.

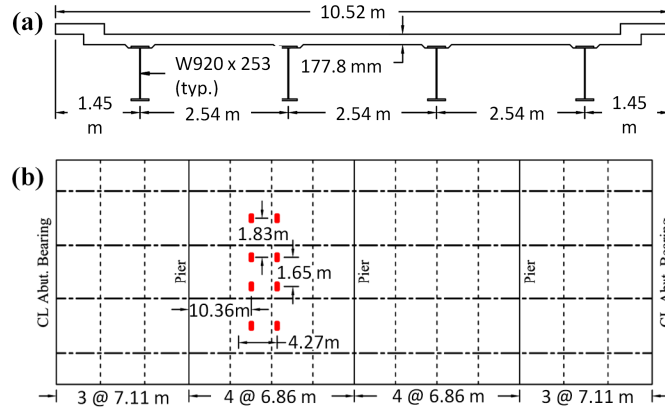


Fig. 2-2: Tennessee field test: (a) cross section, (b) loading configuration

FE Simulation and Analysis

ANSYS (2011), a commercial finite element program, was used in this study to validate the nonlinear response of the selected bridges systems. A detailed summary of the simulation process is provided in the following subsections.

Element Types

As illustrated in Fig. 2-3, an 8-node full integration solid element, Solid65, with embedded features such as cracking, crushing, and plastic deformations was used to model the concrete deck. The internal reinforcement of the deck system was discretely modeled (Tavarez 2001) using uniaxial tension-compression spar elements, Link180. For the steel girders, a 4-node reduced integration shell element, Shell181, was used to model the flanges and web, while lateral bracing were provided by cross-frames modeled with linear 2-node beam elements, Beam188. The girders are assumed to be in full composite action with the concrete deck during the nonlinear analysis, since no evidence of loss in the composite behavior was observed in corresponding failure tests of the selected bridges. However, the implemented simulation approach has the ability to integrate features such as bond-slip and nonlinear behavior of shear studs (Fu and Lu 2003) into the proposed numerical models to account for potential failure characteristics associated with the girder-deck connection.

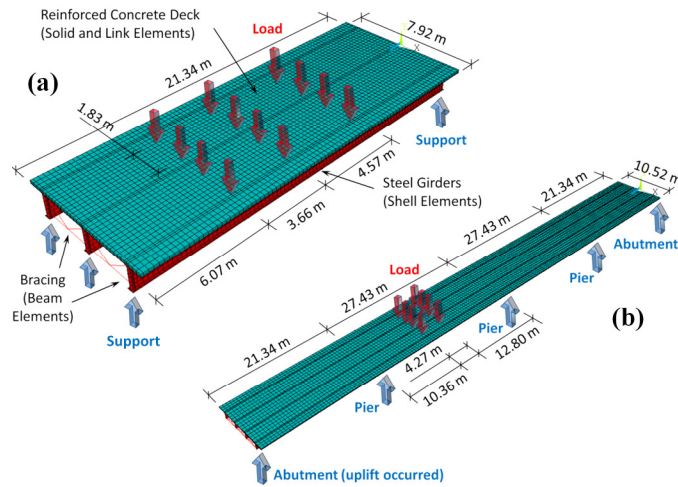


Fig. 2-3: Generated FE model: (a) Nebraska bridge, (b) Tennessee bridge

Section Properties

Section properties of steel members in the proposed FE models as well as deck reinforcement details are summarized in Table 2-1 and Fig. 2-4, respectively. Due to limited information provided on the details of reinforcement in the four-span continuous bridge, assumptions were made in this study based on practical design values previously proposed by Barth et al. (2006). For the simply-supported bridge, however, flexural reinforcement was separately specified for cantilever and non-cantilever portions of the deck.

Table 2-1: Section properties of proposed FE models

Simply supported bridge (Nebraska lab test)			Four-span continuous bridge (Tennessee field test)		
Member	Component	Dimensions (mm)	Member	Component	Dimensions (mm)
Girder	Top flange	PL 228.6 x 19.1	Girder	Top flange	PL 304.8 x 27.9
	Web plate	PL 1371.6 x 9.5		Web plate	PL 863.6 x 17.3
	Bot. flange	PL 355.6 x 31.8 (19.1)		Bot. flange	PL 304.8 x 27.9
K-frame	Angle	L 75 x 75 x 9.5	X-frame	Angle	L 100 x 100 x 12.5
	Wide T	WT 100 x 13.3			
Stiffener	End	PL 177.8 x 15.9			
	Bracing	PL 177.8 x 9.5			
	Intermediate	PL 101.6 x 7.9			

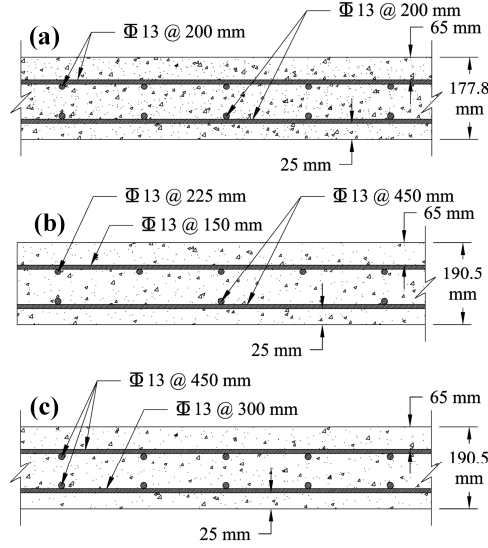


Fig. 2-4: Deck reinforcement details: (a) Tennessee bridge, (b, c) Nebraska bridge (cantilever, non-cantilever)

Material Models

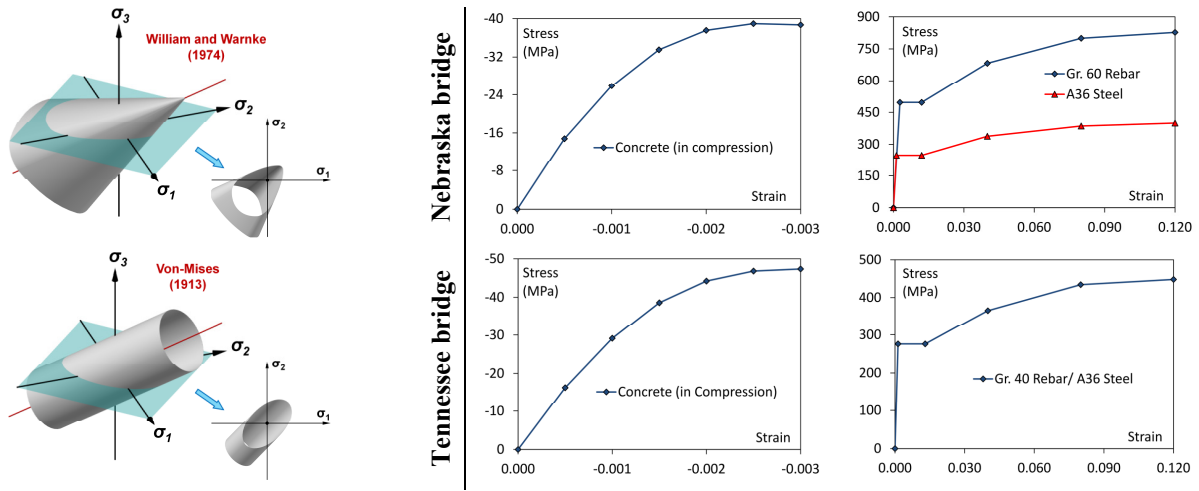
Detailed material properties, derived from the described experimental programs, were included in the validation study of these intact systems. As given in Table 2-2 and Fig. 2-5, a multi-linear stress-strain relationship was introduced to simulate nonlinear behavior of concrete in compression. In tension, the concrete was assumed to have linear elastic behavior prior to cracking with tensile stress relaxation beyond the cracking limit. Shear transfer coefficients were set to 0.3 and 1 for open and closed cracks, respectively. The Willam and Warnke (1974) model was also used in the analysis to define a triaxial failure surface of the concrete (see Fig. 2-5). Nonlinear behavior of steel components, including reinforcing steel, steel girders, and lateral bracings was defined using multi-linear isotropic material model associated with Von-Mises (1913) yield criterion, as depicted in Fig. 2-5.

Loading and Boundary Conditions

Based on the loading configurations illustrated in Figs. 2-1b and 2-2b, each numerical model was loaded with a series of point loads applied over a patch area independent of the generated mesh patterns (Harris 2010). The loading patch for the simply-supported bridge was assumed to have the same dimensions as the steel plates used in the lab test; while for the continuous bridge, an ideal tire patch area of 500 x 250 mm was assumed in the analysis to simplify the complex configuration of the bearing grills used in the field test.

Table 2-2: Material properties of proposed FE models

Simply supported bridge (Nebraska lab test)				Four-span continuous bridge (Tennessee field test)		
	Deck	Reinforcement	Girders/Frames	Deck	Reinforcement	Girders/Frames
E:	29564 (MPa)	200000 (MPa)	200000 (MPa)	32574 (MPa)	200000 (MPa)	212000 (MPa)
ν :	0.18	0.30	0.30	0.18	0.30	0.30
f'_c :	39.0 (MPa)	-	-	47.4 (MPa)	-	-
f_t :	2.3 (MPa)	-	-	2.1 (MPa)	-	-
f_y :	-	496.4 (MPa)	248.2 (MPa)	-	275.8 (MPa)	275.8 (MPa)
f_u :	-	827.4 (MPa)	400.0 (MPa)	-	475.7 (MPa)	448.2 (MPa)

**Fig. 2-5: Material failure surfaces and stress-strain relationships of proposed FE models**

The numerical model of the simple span bridge was restrained with hinge and roller supports at both ends. In the continuous bridge, however, no information was provided on the actual support conditions of the system, especially for the abutment at which the uplift occurred. Although the experimental results of this specific bridge superstructure have been widely used in the literature (Razaqpur and Nofal 1990, Barth 2006) to validate the corresponding modeling approaches, less attention was attributed to capture the uplift phenomenon in the developed models. This study aims to fill this gap and extend the previous modeling efforts on this bridge superstructure by considering three different boundary conditions in the proposed numerical model. As depicted in Fig. 2-6, the critical abutment was fully restrained in case (I) while it was free to move upward in case (II). This abutment was restrained in case (III) with an ideal rigid-perfectly plastic nonlinear spring, the stiffness of which reduces to zero once uplift occurs.

Additional boundary constraints were also provided as a horizontal line of restraint on the bottom flanges of girders, at the locations of intermediate piers as well as the other end of the bridge.

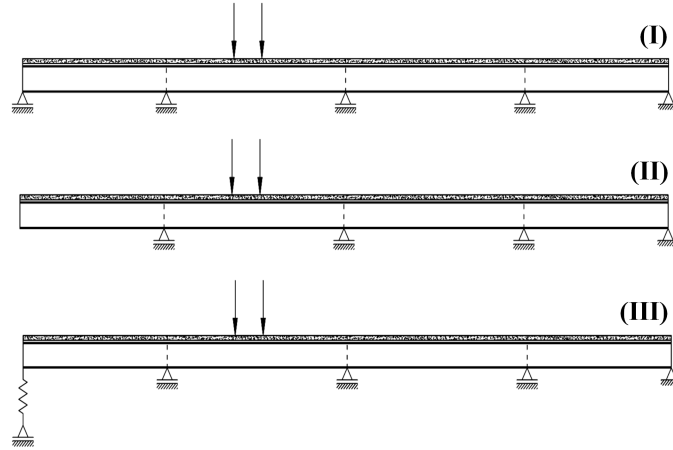


Fig. 2-6: Assumed boundary conditions for the continuous bridge model - Tennessee field test

Analysis

Static analyses with small displacements were selected in this study for the numerical investigation of composite girder bridges, with the Newton-Raphson method chosen as the nonlinear solver. Loads were applied incrementally using automatic time stepping. Due to convergence failure of the force criterion upon cracking in concrete elements (Wolanski 2004), only displacement criterion, with reference and tolerance values of 5 and 0.05 respectively, was implemented in this study to control convergence at the end of each substep.

Discussion of Results

With the modeling approach proposed, the following sections describe the system behavior observed in the analysis. These characteristics are critical for understanding the anticipated response of the composite steel girder bridges beyond the service region, specifically for future integration of damage mechanisms.

Validation

Nebraska Laboratory Test

Among all results obtained in the failure test, interior girder deflection and exterior girder separation at mid-span of the bridge superstructure are presented in this study as a measure to validate the proposed numerical model. As illustrated in Fig. 2-7, results obtained via nonlinear

FE analysis correlate well with the actual response of the system recorded in the laboratory experiment within the elastic limit of the behavior. As the material nonlinearities initiate and propagate throughout the structure, numerical results start to deviate from experimental data. The discrepancy between the results (8% at most) can likely be attributed to the residual stresses that exist in the steel plate girders, which could potentially promote the early onset of material plasticity in the girders. However, the residual stresses were not included in the proposed numerical model given the insufficient information provided in the test report.

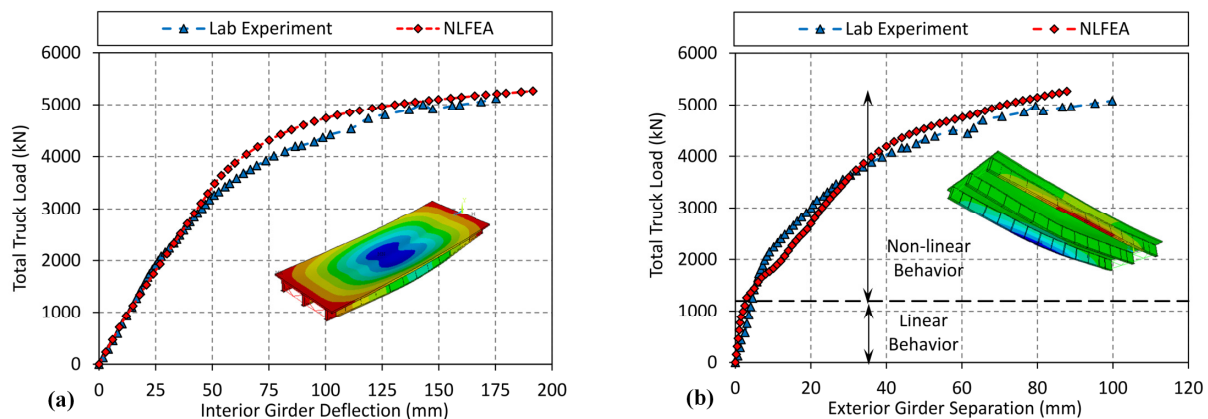


Fig. 2-7: FE model validation - Nebraska lab test: (a) interior girder deflection, (b) exterior girder separation

The exterior girder separation herein describes the increase in the spacing between bottom flanges of exterior and interior girders. Kathol et al. (1995) previously hypothesized that any nonlinear characteristic in the concrete deck dictates nonlinearity in the girder separation behavior. As depicted in Fig. 2-8a, the lack of interior bracing in the ultimate capacity evaluation of this bridge system allows girders to deflect laterally without any restraint. In order to represent the effect of deck nonlinearity on the girder separation behavior, crack propagation in the concrete deck at the very first stages of material nonlinearity in the system was derived from numerical analysis and depicted in Fig. 2-8b. Cracked regions are defined by areas in which tensile strains exceed the cracking limit of the concrete in the transverse direction. As illustrated, tensile cracks propagate not only on the bottom surface of the slab between the girders, but also on the top surface of the slab right above the interior girder. This specific cracking pattern produces a mechanism causing the exterior girder to rotate with the slab and deform laterally, which in turn can strongly support the previous girder separation hypothesis postulated by Kathol et al. (1995). However in practice, separation of the exterior girders could also happen

due to elastic deformation of the deck under the regular traffic loads, which is considered as the main cause of the fatigue cracking in exterior girders of in-service bridges (FHWA 2011). This feature highlights the additional complexity that exists in steel girder bridges when considering a large variation in design choices, and the potential influence of secondary members during latter stages of the load-deflection response.

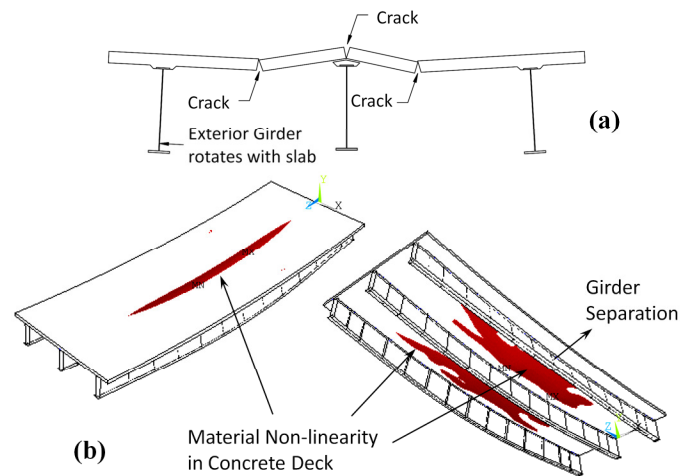


Fig. 2-8: Exterior girder separation: (a) Nebraska lab test postulation, (b) numerical results

Tennessee Field Test

For validation of the FE model, the total applied load versus centerline deflection of the loaded-span at center of the roadway, was derived from nonlinear FE analysis for all assumed boundary conditions and compared to the corresponding results reported by Burdette et al. (1971). As it is demonstrated in Fig. 2-9a, the structural behavior of the system is highly sensitive to the boundary conditions applied at the critical abutment which experienced uplift during testing. In case (I), the abutment was assumed to be fully restrained with no uplift occurring during the analysis. The applied ideal roller support contributes to the load bearing mechanism of the bridge by producing an anchorage system for the loaded span. This would increase the structural stiffness of the system and provides higher capacity for the bridge superstructure. On the other hand, the system capacity was considerably decreased in case (II), where no vertical restraint was provided on the critical abutment and it was free to uplift from very first stages of loading. Numerical results obtained from these two cases provide upper and

lower bounds on the actual response of the bridge superstructure; albeit, they were not able to capture the true behavior of the system.

As observed in the field investigations (Burdette et al. 1971), the uplift occurred shortly after yielding was initiated in the girders at centerline of the loaded span. This means that the actual support condition at this abutment is neither fully restrained nor free. In fact, there was a definite amount of tensile fixity at this support which was diminished after the applied loads reached a certain level. In order to simulate the effect of uplift in the system, the boundary condition at this abutment was refined using an ideal nonlinear spring with rigid-perfectly plastic behavior, (see case III in Fig. 2-6). In this model, the implemented spring has infinite stiffness providing initial full restraint at the abutment. Once yielding occurred in the steel girders, the spring stiffness reduces to zero which allows uplift to occur under higher levels of the applied loads. Results obtained from the numerical model with this refined boundary condition yielded better correlation with the actual response of the system; as depicted in Fig. 2-9a.

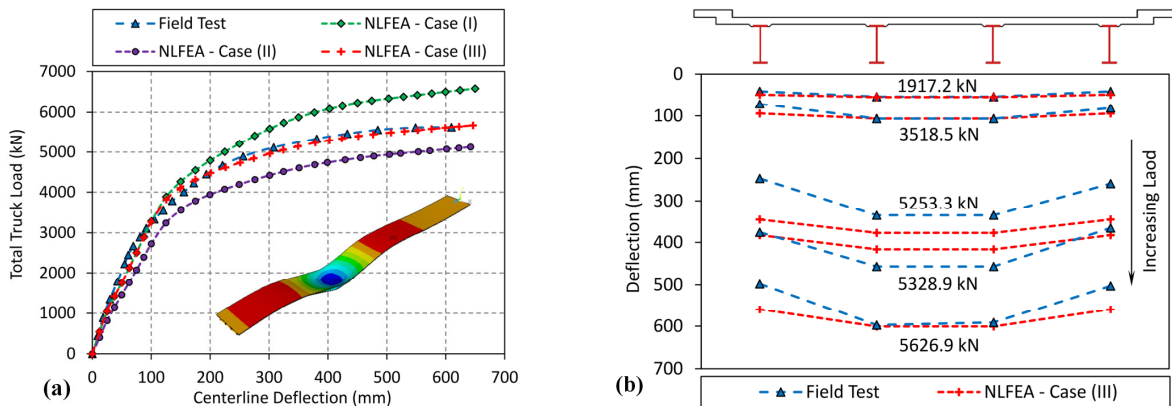


Fig. 2-9: FE model validation - Tennessee field test: (a) centerline deflection, (b) deflection profile

Moreover, Fig. 2-9b demonstrates variations in the profile of this continuous bridge superstructure with increasing load at the centerline of the loaded-span, obtained from both field investigations and numerical analysis with refined boundary conditions (case III). As illustrated, the results are generally in good agreement with each other, indicating a uniform growth in the deflection profile of the system with increasing load. In comparison to the test results, however, the bridge FE model experiences higher levels of deflection in the exterior girders. This can be attributed to the existence of parapets in the bridge system which were not included in the FE model. A recent investigation by Harris and Gheitasi (2013) demonstrated that the global

behavior of the bridge systems is influenced by non-structural features such as parapets and bracings. While the FE results appears to have some discrepancies with the experimental outcomes due to limited information provided on the bridge configuration and boundary conditions, it is clear that the methodology provides a rational measure of the relative system behavior which is deemed adequate for the objective of this study.

Behavioral Stages

Fig. 2-10 demonstrates different behavioral stages observed throughout the loading history of simulated composite girder bridges. Based on the results obtained via nonlinear FE analysis, the response of these systems can be generally classified into the following four stages.

Crack Initiation in Concrete Deck (Stage A)

Both of the simulated bridge superstructures behave linearly elastic prior to formation of the first flexural cracks in the concrete deck. Cracking occurs in concrete elements when the principal tensile stresses fall outside of the William and Warnke (1974) failure surface (Fig. 2-5), and can propagate in any principal direction under excessive loading. The slope of the load-deflection curve within the elastic region is referred to herein as initial stiffness of the structural system (K_i), which is fairly constant prior to the formation of the first flexural cracks. All other components of the bridge superstructures, including the steel girders remain elastic through this stage of loading.

First Yield in Steel Girders (Stage B)

By increasing the external applied load beyond first cracking point, flexural cracks propagate in all directions over the concrete deck. After cracking, concrete elements at the cracked integration points undergo stress relaxation in the direction perpendicular to the crack surface and parallel to the principal tensile stress exceeding the limit of failure surface. Therefore, the global structural stiffness decreases slightly and the slope of the response curves also drops off. However, the bridge superstructure system continues to carry loads with a constant sloped load-deflection curve, due to linear elastic behavior of steel girders prior to their first yield point.

Formation of Plastic Hinge in Steel Girders (Stage C)

Once the steel girders yield under increasing load, the global structural stiffness of the system decreases significantly. At this point, the load-deflection curves start to deviate from their previous steady states, due to the considerable amount of material nonlinearity, especially

plasticity in steel members. However, the load bearing capacity of the bridge superstructure continues until plastic hinges form in the girders. In the current numerical analysis, the formation of plastic hinges was recognized by the yielded area propagating throughout the depth of the girder web plate. Meanwhile, flexural cracks dominate most parts of the deck in the loaded span.

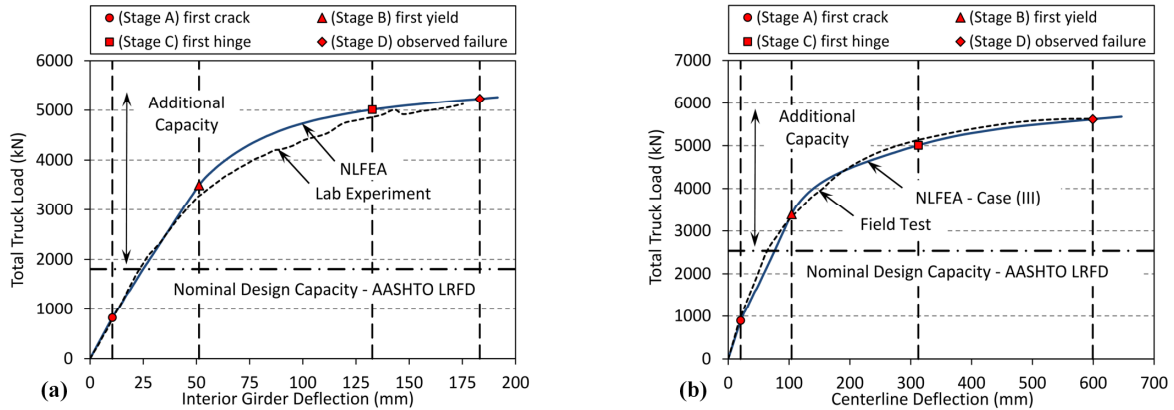


Fig. 2-10: Behavioral stages: (a) Nebraska lab test, (b) Tennessee field test

Failure of the system (Stage D)

Upon further application of external loading, the ultimate capacity tests of these bridge superstructures were terminated due to local failures that occurred in the structural components. Punching shear in the concrete slab governed the failure mode of the single span bridge tested in the lab; while the field test on continuous bridge was terminated due to compression failure (crushing) in one of the curbs. In this study, the observed failure mechanisms were identified in the results obtained via numerical analysis to assess the ability of the proposed FE models to predict the actual response of the simulated bridges. For the single span bridge, the local failure mechanism was characterized at the level of applied load which corresponds to the maximum nominal punching shear resistance of the concrete slab, calculated based on AASHTO LRFD (2012) design specification. On the other hand, the observed failure mechanism in the numerical model of the continuous bridge system was captured once crushing occurred in concrete elements close to the curb at the location of maximum positive moment. As demonstrated in Fig. 2-10, the proposed FE models are able to accurately predict not only the overall behavior of the simulated bridge systems, but also accommodate the presence of the local failure mechanisms observed in the corresponding experimental investigations.

Nominal Design Capacity – AASHTO LRFD

According to the AASHTO specification, bridge superstructures are implicitly designed on a component basis. In this approach, the bridge superstructure system is broken down into a series of sub-elements which are analyzed and designed individually to determine the required section sizes and material characteristics. For composite steel girder bridges, the critical sub-element is comprised of an effective portion of the concrete deck supported by a steel girder. This element-level evaluation is an approximate representation of the actual system-level behavior, which does not consider the complex interaction between the bridge components. As a result, this conservative design approach could significantly underestimate the actual reserve capacity of the bridge system.

In this study, the theoretical nominal design capacities of both investigated bridges, under the applied loading configurations, were calculated based on AASHTO LRFD (2010) specification and compared to the actual capacity of the bridge systems defined in experimental and numerical investigations. As illustrated in Fig. 2-10, both bridge systems provide a significant amount of additional reserve capacity over the theoretical nominal design capacity, up to 120% and 185% for the simply-supported and continuous bridges, respectively. This reserve capacity demonstrates the high level of system-level interaction that produces the inherent redundancy in the representative steel I-girder bridges, and also illustrates that this complex phenomena cannot be easily described using the current element-level design methodology.

However, the amount of additional reserve capacity of the intact system over the element-level design capacity does not solely provide a quantitative measure of the system redundancy. As specified in the NCHRP Report 406 (Ghosn and Moses 1997), the bridge redundancy is the capability of the bridge superstructure to continue to perform its design functions after the damage or failure of one of its structural members. In order to assess whether or not a given bridge superstructure has adequate level of system redundancy and safety, the system reserve capacity shall also be evaluated at the functionality and damaged limit states (Ghosn and Moses 1997). It is expected that the level of system redundancy for each bridge superstructure highly depends on the bridge type (material, design, geometry), but also on the existing condition states which generally include different damage scenarios such as corrosion, delamination, fire, truck/ship collision, or even complete loss of the load-carrying capacity of a main structural member.

Generic Non-Local Failure Criterion

Due to redundancy and complex interaction that exists among the structural components, local failure mechanisms may or may not limit the actual capacity of composite girder bridges. As a result, there is a pressing need to define a criterion, based on which the reserve capacity of the bridge system can be evaluated numerically, especially for those bridges that have not been tested to failure. Theoretically, an ideal structural system reaches its ultimate capacity when it goes through large deformations with an infinitesimal increment in the applied loads. In other words, the global structural stiffness of the system approaches zero at the moment of failure. Implementing this concept, a generic non-local failure criterion is introduced in this study to estimate the actual capacity of in-service bridges, based on relative variation in structural stiffness. The relative variation in structural stiffness can be defined as the ratio of instantaneous slope, K_t (also known as tangential stiffness) of the load-deflection curves to the initial stiffness of the system, K_i .

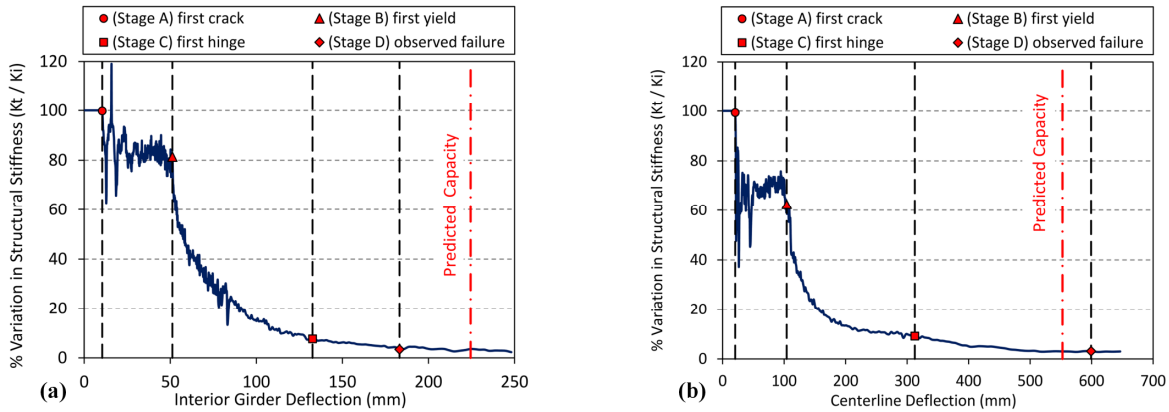


Fig. 2-11: Relative variations in structural stiffness: (a) Nebraska lab test, (b) Tennessee field test

Fig. 2-11 illustrates the relative variations in structural stiffness for both investigated bridges, which correspond to the numerical results depicted in Fig. 2-10. Despite the perturbations included in the results due to nonlinear solver iterations, the general trend indicates a global reduction in structural stiffness as the bridge superstructure experiences higher loads. As demonstrated, there is no reduction in the structural stiffness prior to the formation of the first flexural cracks in concrete deck (stage A), which would confirm the state of linear elastic behavior of the system. With additional external loading applied, first yield occurs in steel

girders (stage B) and the bridge superstructure loses its initial stiffness. The reduction in structural stiffness continues at an increasing rate as the structure tolerates more loads. This behavior would be expected intuitively, but the results illustrate this phenomenon as the system goes through the various stages of loading. The ultimate capacity of the system is finally characterized at the moment in which the reduction in structural stiffness reaches a constant rate and almost plateaus.

The single span bridge appears to have an additional capacity beyond the observed failure of the system, as the relative variation in structural stiffness continues to decrease (Fig. 2-11a). Therefore, additional loading was applied on the numerical model of this bridge to quantify the actual system capacity irrespective of the local failure effects. The bridge system continues to tolerate additional loads beyond the level where the laboratory experimentation was terminated. Using the proposed failure criterion, the ultimate capacity of the system was predicted as illustrated in Fig. 2-11a. In comparison to experimental investigation, the interior girder of this bridge superstructure experiences almost 30% increase in the vertical deflection at the predicted capacity. For the continuous bridge superstructure, however, the ultimate capacity can be clearly distinguished based on the stiffness reduction behavior in the numerical model with refined boundary conditions, see Fig. 2-11b.

The system reserve capacities of both investigated bridges, defined based on the proposed generic failure criterion, are summarized in Table 2-3 and compared to the observed failure loads obtained in experimental and numerical investigations. The single span bridge appears to have additional capacity beyond the failure load observed in the lab test. It can be concluded that the punching shear dictates a premature failure mechanism of the system, which in turn reduces the system-level capacity as well as overall ductility. For the continuous bridge, on the other hand, the predicted capacity is much closer (98.7%) to the failure load of the system recorded in the field-test experimentation. This would suggest that effects such as plastic hinging in the girders and crushing in the concrete deck can be identified as the primary failure mechanism associated with composite steel girder bridges, a finding which was also recognized previously in a comprehensive investigation by Ghosn and Moses (1997).

Sensitivity Study

The stages of failure introduced in this study were characterized based on the behavior of the selected representative bridges. The occurrence and sequence of these identified stages are

subjected to change for any given bridge superstructure as a function of the bridge geometrical characteristics, material properties, as well as loading and boundary conditions. In order to investigate the sensitivity of the system failure characteristics to variations in the geometrical and material properties, a limited sensitivity study was conducted on the 4-span continuous bridge superstructure. This structure was selected for the sensitivity study as it represents an actual in-service bridge system and has all the structural features which are common in practice (e.g. intermediate bracings). The geometrical and material parameters selected for the sensitivity study were assumed to be representative scenarios describing the effect of different damage and deteriorating mechanisms on the bridge superstructure. Due to additional reserve capacity of the structure over the design level, all of the selected parameters were reduced to define their impact on the capacity of the system.

Table 2-3: Ultimate capacities of the simulated bridges

Simply supported bridge (Nebraska lab test)		
Experimental evaluation (kN)	NLFEA	
	Observed failure (kN) ^a	Predicted capacity (kN)
5124	5235	5348
Four-span continuous bridge (Tennessee field test)		
Experimental evaluation (kN)	NLFEA - case (c)	
	Observed failure (kN) ^b	Predicted capacity (kN)
5627	5614	5553

^a punching shear

^b curb crushing/ plastic hinging in girders

Figure 2-12 illustrates different analysis cases considered in this study. In case (1), one of the interior girders was removed while the others were reconfigured to maintain the symmetric configuration within the cross section of the structure. Case (2) represents the condition where the overhangs on the both sides of the deck were reduced in length. In case (3) all the intermediate bracings were removed from the structure, except for the ones at either end of the bridge and the locations of the piers. For the analysis cases (4) and (5), the deck thickness and depth of the girders were reduced 30% and 25 %, respectively, while the amount of deck reinforcement was reduced by 25% in case (6). Material properties are the main parameters which were subjected to change in cases (7) and (8), where the compressive strength of the

concrete and the yield stress of the girders were reduced by 30%, respectively. Nevertheless, span length, number of spans, and deck reinforcement pattern remained unchanged.

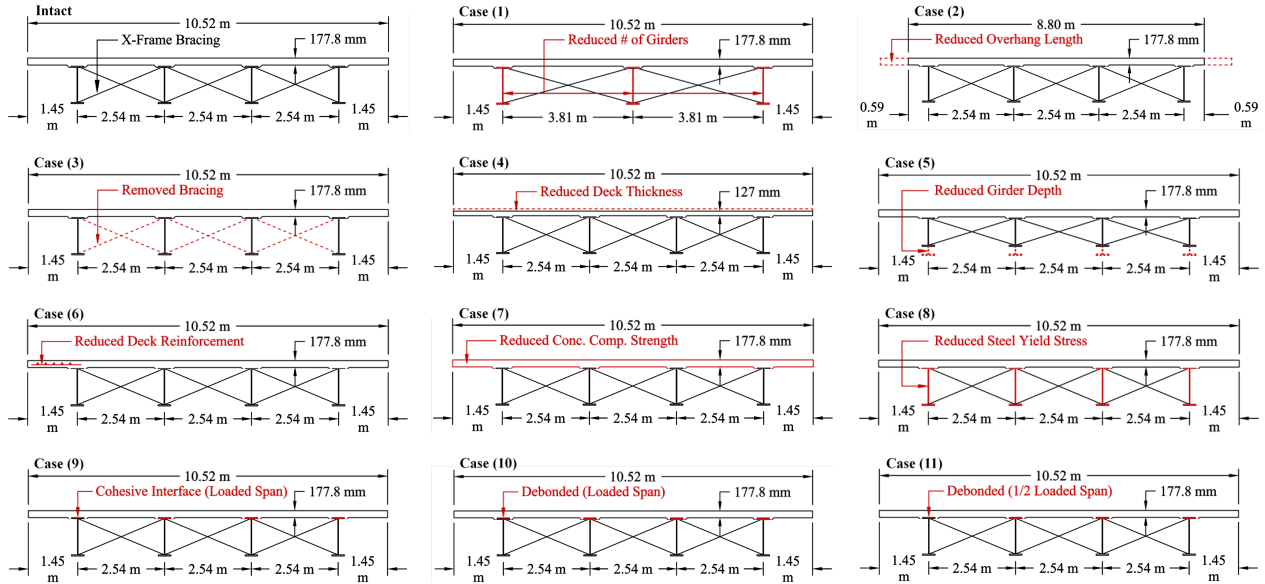


Fig. 2-12: Analysis cases for sensitivity study on the Tennessee bridge

In the analysis of the corresponding intact system, the girders were assumed to be in full composite action with the deck while the connection was modeled using MPC rigid elements. However, with respect to damaged state of the structure, any defect in girder-deck connection would influence the nonlinear behavior of the system. In order to investigate the potential impact of the girder-deck bond deterioration on the ultimate capacity and ductility of the system, the intact bridge model was updated in three cases (9-11). Among all available techniques that exist in the literature, surface-to-surface contact algorithm was selected to simulate interface connection between the top flange of the girder and the bottom surface of the deck in the loaded span. The properties of the implemented contact elements were defined such that the compressive stresses can be fully transferred between the surfaces, while the amount of shear stresses that is being transferred was defined based on the Coulomb friction model. In case (9), the coefficient of friction was assumed to be 0.7 based on the design recommendation provided by ACI 318 (2011). The ideal state of debonding was also included in the sensitivity analysis by eliminating the shear transferring mechanism along the full and half length of the loaded span (case 10 and 11, respectively). These cases would represent the worst case scenarios with respect to the magnitude of bond deterioration that can occur in actual practices. Under the same loading

and boundary condition for all variations, the revised models were analyzed. Results of the nonlinear analysis as well as the stages to failure for each case are demonstrated in Fig. 2-13.

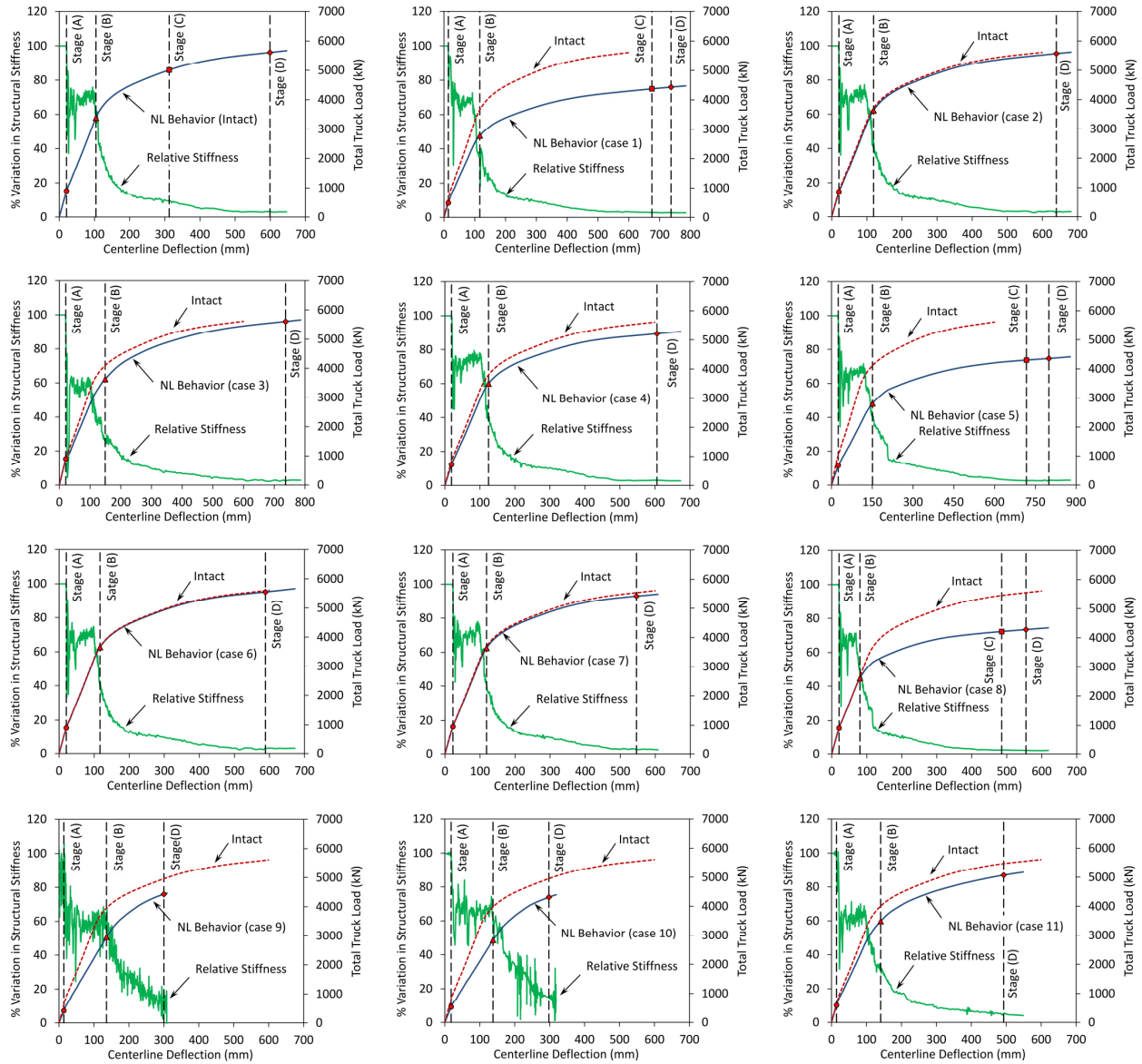


Fig. 2-13: Behavioral stages in the refined models of the Tennessee bridge

The ultimate capacities of the parametrically refined structures were also defined using the proposed generic failure criterion. As illustrated in Fig.2-13, reductions in the overhang length, deck reinforcement amount, and concrete compressive strength (cases 2, 6, and 7) have the lowest impacts on the nonlinear behavior and ultimate capacity of the structure. However, the behavioral stages were affected so that no plastic hinges were completely formed in the girders.

On the other hand, variations in intermediate bracings and deck thickness (cases 3 and 4) have moderate impact on both the behavior (no plastic hinge) and ultimate capacity of the structure. Any variations in the girders' properties including their number (spacing), depth, and material characteristics (cases 1, 5, and 8) imposed significant influences on the capacity of the structure, while the behavioral stages developed completely in these cases. This would highlight the fact that the behavior of the girder-type bridge superstructures (i.e. steel bridges) is generally governed by the behavior of the main load-carrying elements.

In cases (9-11), bond deterioration reduces the cracking capacity of the deck and causes the girders to experience lateral instability on their top flanges. Moreover, loss in the composite action results in premature crushing on the top surface of the deck which dominates the failure of the system with major reduction in both capacity and ductility. However, the reduction in the overall system ductility was less severe in case (11) where the deterioration in the girder-deck connection was limited to the half of the loaded span. In all last three cases, material plasticity in the girders initiates on both flanges and propagate towards the centerline of the girders, as opposed to other damage scenarios where the yielding started from the bottom flange and propagated upwards through the depth of the girder cross section. However, complete plastic hinges were not formed in any of these three cases. It can be concluded that the formation of full plastic hinges highly depends on the geometrical characteristics of the bridge cross section and usually occurs relatively close to the failure of the system.

Table 2-4 provides a summary on the observed behavioral stages as well as the corresponding failure characteristics for all of the refined models. As tabulated, the ultimate capacity of the system is reduced in all analysis cases. System ductility, which can be defined as the ratio of maximum measure deflection to the deflection at the moment of first yield in the girders, is increased in cases 1 and 8 while reduced in all other cases. Table 2-5 summarizes the loads and corresponding deflections at the identified behavioral stages for each of the analysis cases. The percentages represent the relative ratios of the loads and deflections defined at each stage with respect to the maximum measured values. In all cases, the formation of first crack in concrete deck and first yield in steel girders had limited variations relative to the capacity of the system. Concrete cracking occurs at 9% to 21% of the maximum applied load, while plasticity in girders initiates at 60% to 69% of the system capacity. The same trend was observed in the deflection behavior of the structure in cases (1-8) with relatively lower ratios when comparing to

the maximum measured deflection (2% to 4% for the first crack, 15% to 21% for the first yield). In cases (9-11), however, results demonstrate higher relative ratios for deflection at first yield in the girders, which highlights the significant reduction in the overall system ductility.

Table 2-4: Failure characteristics (Tennessee bridge)

Analysis Cases	Behavioral stages				Observed phenomena at failure
	(A)	(B)	(C)	(D)	
Case (1)	Y	Y	Y	Y	Reduced capacity/increased ductility
Case (2)	Y	Y	N	Y	Reduced capacity/reduced ductility
Case (3)	Y	Y	N	Y	Reduced capacity/reduced ductility
Case (4)	Y	Y	N	Y	Reduced capacity/reduced ductility
Case (5)	Y	Y	Y	Y	Reduced capacity/reduced ductility
Case (6)	Y	Y	N	Y	Reduced capacity/reduced ductility
Case (7)	Y	Y	N	Y	Reduced capacity/reduced ductility
Case (8)	Y	Y	Y	Y	Reduced capacity/increased ductility
Case (9)	Y	Y	N	Y	Reduced capacity/reduced ductility
Case (10)	Y	Y	N	Y	Reduced capacity/reduced ductility
Case (11)	Y	Y	N	Y	Reduced capacity/reduced ductility

Table 2-5: Behavioral stages of the refined models (Tennessee bridge)

Analysis Cases	Load at different behavioral stages (kN (%))				Deflection at different behavioral stages (mm (%))			
	(A)	(B)	(C)	(D)	(A)	(B)	(C)	(D)
Intact	895 (16%)	3390 (60%)	5009 (89%)	5614 (100%)	20 (3%)	104 (17%)	312 (52%)	599 (100%)
Case (1)	486 (11%)	2778 (63%)	4372 (99%)	4429 (100%)	14 (2%)	116 (16%)	675 (92%)	737 (100%)
Case (2)	857 (15%)	3632 (65%)	-	5573 (100%)	20 (3%)	119 (19%)	-	640 (100%)
Case (3)	899 (16%)	3632 (65%)	-	5607 (100%)	21 (3%)	149 (20%)	-	737 (100%)
Case (4)	714 (14%)	3504 (67%)	-	5212 (100%)	19 (3%)	125 (21%)	-	606 (100%)
Case (5)	672 (15%)	2807 (64%)	4301 (99%)	4357 (100%)	25 (3%)	151 (19%)	717 (90%)	800 (100%)
Case (6)	899 (16%)	3661 (66%)	-	5554 (100%)	21 (3%)	117 (20%)	-	588 (100%)
Case (7)	956 (18%)	3647 (67%)	-	5426 (100%)	23 (4%)	119 (21%)	-	546 (100%)
Case (8)	914 (21%)	2607 (61%)	4216 (98%)	4283 (100%)	21 (4%)	80 (15%)	486 (87%)	555 (100%)
Case (9)	415 (9%)	2953 (67%)	-	4428 (100%)	14 (5%)	136 (45%)	-	300 (100%)
Case (10)	529 (12%)	2835 (66%)	-	4312 (100%)	18 (6%)	138 (46%)	-	298 (100%)
Case (11)	586 (12%)	3490 (69%)	-	5068 (100%)	14 (3%)	141 (29%)	-	493 (100%)

Conclusions and Path Forward

Bridge superstructures play a key role in the national transportation network and recent bridge failures only highlight the need to understand the actual response of the in-service bridges and estimate their remaining service life under the effect of different deteriorating conditions. In this study, the structural performances of two intact composite steel girder bridges were investigated using nonlinear finite element analysis. In comprehensive experimental programs (Kathol et al. 1995, Burdette et al. 1971), these bridges were previously tested to failure with detailed information collected on the testing procedures and data acquisitions. On the basis of the results obtained via numerical analysis of the selected representative bridges, the following observations can be highlighted:

- The general behavior of the investigated bridges was classified into four different behavioral stages. Accordingly, these bridges behave linearly elastic prior to formation of first flexural cracks in the concrete deck (stage A). Beyond first cracking point, they continue to carry more loads until plasticity initiates in steel girders (stage B). With further increment in the external loading, the structural stiffness drops off significantly and plastic hinges are formed in steel girders at the location of maximum moment (stage C). Eventually, the proposed FE models capture the local failure mechanisms in the system that terminated the corresponding experimental investigations (stage D).
- Local effects such as punching shear may not define the actual capacity of girder-type bridge superstructures, due to system redundancy and complex interaction which exists between structural components. These effects may also impose a premature failure mechanism to the bridge superstructure, beyond which the system is expected to have additional capacity. As a result, a generic non-local failure criterion was proposed in this study to predict the actual reserve capacity of composite girder bridges based on relative variations in structural stiffness.
- The limited sensitivity analysis performed in this study demonstrated that the identified behavioral stages and corresponding failure characteristics in composite steel-concrete bridge superstructures are highly dependent on the geometrical characteristics, material properties, boundary conditions, girder-deck bond properties, and even loading scenarios and are subject to change for each and every bridge system.

- Both investigated bridges demonstrated additional reserve capacity over the theoretical nominal capacity obtained using the AASHTO LRFD design methodology. This would indicate that the element-level representative behavior, used in the current design practices, is an overly conservative approximation of the actual system-level behavior for composite steel girder bridges. While this finding is based on a limited population, the implications have the potential to influence both design and preservation practices and warrants further investigation.
- The proposed analysis method can be implemented for future integration of damage mechanisms in composite steel girder bridges, by incorporating data from routine field inspections of in-service bridge superstructures to estimate their remaining service life and schedule future maintenance practices (Gheitasi and Harris 2014a, b).

Chapter 3:

Overload Flexural Distribution Behavior in Composite Steel Girder Bridges

(ASCE, Journal of Bridge Engineering, in press, 2014)

Summary

Using equations proposed by the AASHTO LRFD specifications, live load distribution factors in bridge superstructures are calculated based on the linear elastic behavior of the system. In this study, the applicability of these equations in predicting the girder distribution behavior in the presence of high material nonlinearity and oversized loading scenarios has been investigated. Two representative composite steel girder bridge superstructures, which are in service in the State of Michigan and have previously been subjected to a live load testing program, were selected in this study. Sixteen cases were analyzed to study the effect of boundary conditions, loading position, and load configuration on the girder distribution behavior of the selected bridges as they approach their ultimate capacities. Comparing the results obtained from nonlinear finite element analysis with those proposed by AASHTO LRFD specification demonstrated that the code-specified values for the distribution factors are overly conservative. Much of the variation in distribution behavior occurs when plasticity propagates in steel girders, while initiation of material nonlinearity in concrete deck (cracking) has a negligible effect on the evolution of distribution behavior. Results from this investigation also highlight the importance of accurate modeling and analysis in the load rating practices of existing in-service bridge superstructures.

Introduction

The semi-empirical equations of the AASHTO LRFD (1994) bridge specifications are widely being used to calculate live load distribution factors in design and load rating practices of all federally funded bridges. The developed relationships within the AASHTO LRFD were formulated based on a parametric investigation of several hundred bridges from National Bridge Inventory by Zokaie et al. (1991) under the National Cooperative Highway Research Program (NCHRP) 12-26 project. These equations replaced the traditional “S-over” method from the

standard specifications (1992). Since the introduction of the new design equations, there has been a significant amount of skepticism regarding adoption. Research efforts have focused on evaluating their range of applicability and assessing the influence of various parameters, such as parapets and railings (Mabsout et al. 1997, Corner and Huo 2006), bracing and secondary members (Green et al. 2004, Chung et al. 2006), skewed configuration (Bishara et al. 1993, Khaloo and Mirzabozorg 2003), continuity (Mabsout et al. 1998, Zokaei 2000), and special applications and non-traditional designs (Moses et al. 2006, Harris et al. 2008), on the load distribution behavior of bridge superstructures.

The majority of previous studies, predicting load distribution characteristics, considered linear elastic behavior of the bridge system. This assumption conflicts with the LRFD methodology in design and rating of bridge superstructures, where inelastic behavior of the material is being considered. A number of research studies were performed to investigate the inelastic distribution behavior in bridge superstructures as they approach their ultimate capacities. The results of early works demonstrated a significant redistribution of loads in the transverse direction from the elastic to inelastic behavior of girder-type bridges (Heins et al. 1975, Cheung et al. 1986). In an experimental study, Bakht and Jaeger (1992) performed a failure test on a short-span simply supported girder bridge to study the load distribution pattern at the bridge ultimate capacity. It was reported that the inelastic distribution behavior at the ultimate stage was not even close to uniform pattern. In a recent study, Razaqpur et al. (2012) performed nonlinear finite element analyses on a series of hypothetical composite steel girder bridges designed according to CSA 2000, to study the effects of key geometric parameters on the inelastic load distribution characteristics. They concluded that no single adjustment factor can be applied to the elastic distribution factors to make them applicable for the ultimate limit state.

On the other hand, the ever-increasing demands for moving goods and services have resulted in a great deal of pressure on transportation officials over the years, as truck sizes and weights continue to grow and exceed legal limits (Robitaille et al. 2013). Several research studies have been conducted to evaluate the distribution behavior in bridge structures under the effect of irregular loading scenarios. Fu and Hag-Elsafi (1996a and b) proposed a permit checking procedure in the form of load and resistance factors to evaluate the reliability of highway bridges. Many other researchers focused their investigations on adjusting the current design specifications and proposing modification factors to better accommodate the effect of oversized

overweight trucks have on the lateral load distribution behavior in girder-type bridge superstructures (Hays 1984; Tabsh and Tabatabai 2001; Bae and Oliva 2012).

However, in practice, applying weight restrictions and forcing oversized vehicles to take secondary routes have proven ineffective for solving this issue completely as they cause several other economical concerns including higher operation costs, greater expenses for the detour route, and longer travel time. As a result, bridge engineers are tasked with assessing the safety of in-service highway bridges subjected to the ever increasing demands. Although, it is recognized that girder-type bridge superstructures tend to have a great amount of additional reserve capacity over the design level due to inherent redundancy and system-level interaction (Kathol et al. 1995; Ghosn and Moses 1997; Gheitasi and Harris 2014a, c), the question that still needs to be answered is the reliability of in-service structures to provide service for unusual operating loads in terms of magnitude and configuration.

Research Significance

The potential impact of material nonlinearity on the load distribution mechanism of the bridge superstructures could be even more significant in the presence of irregular loading scenarios. Although there are legal restrictions to prevent oversized trucks from violating the federal and state weight limits, bridges owners are hesitant to impede commerce and as a result there is a pressing need to understand the effects of irregular loading configurations on the load distribution behavior, especially when the bridge system approaches its ultimate capacity.

The present study aims to expand the recent investigation performed by Razaqpur et al. (2012), by evaluating the effect of three other parameters including support conditions, loading position and load configuration on the inelastic distribution behavior. In contrast to the idealized bridges evaluated by Razaqpur et al., two in-service bridges from the State of Michigan were selected for evaluation. These particular structures were selected as they are representative of typical girder-type construction and also have available field test data using non-standard truck loadings (MDOT 2013), which allow for comparison of numerical and experimental results (Nowak and Eom 2001). The results of this investigation highlight the need for a refined method of analysis to accurately predict the lateral distribution behavior in the load rating practices and performance evaluation of in-service multi-girder bridge superstructures. It should be noted that the study presented herein is not exhaustive and limited to the selected composite steel girder

bridges, but the implemented approach can be extended to other bridge superstructures with different design categories.

AASHTO LRFD Distribution Factors

AASHTO LRFD provides a series of empirical equations to determine the live load distribution factors for different bridge superstructural systems. In addition to the equations, AASHTO also allows for alternative methods of analysis in calculating the distribution factors that satisfy the requirements of equilibrium and compatibility; whilst making reasonable assumptions regarding material properties and realistic boundary conditions.

The distribution factor can be defined using various analytical approaches, but a commonly recognized definition is the beam-line method (Barker and Puckett 2007), which can be defined as the ratio of maximum load effect in a single member defined from a system analysis ($F_{refined}$), to the maximum load effect in that member obtained from an influence-line analysis (F_{beam}), see Eqn. 1. However, the load fraction definition is not directly applicable to the evaluation of in-service bridges because the load effects cannot be measured in the field, whereas the member response can (i.e. deflection and strain). As a result, the distribution factor can alternatively be determined by taking the ratio of response in a given member to the summation of all primary load-carrying member responses and multiplying by the number of trucks applied on the bridge, see Eqn. 2. These methods have been demonstrated to be analogous in a previous study by Harris (2010).

$$g = \frac{F_{refined}}{F_{beam}} \quad (1)$$

$$g_i = \frac{R_{max,i}}{\sum_{i=1}^{#girders} R_{max,i}} \cdot N_{trucks} = \frac{\Delta_{max,i}}{\sum_{i=1}^{#girders} \Delta_{max,i}} \cdot N_{trucks} = \frac{\epsilon_{max,i}}{\sum_{i=1}^{#girders} \epsilon_{max,i}} \cdot N_{trucks} \quad (2)$$

Method of Study

Numerical Modeling and Validation

The commercial Finite Element computer package, ANSYS (2011), was implemented in this study to evaluate the inelastic load distribution behavior of the selected bridges. The primary

challenge associated with model validation of bridges is the lack of complete datasets, especially those for full non-linear behavior characterization. In this study, results from a full-scale ultimate load test on a simply supported model bridge, performed at the University of Nebraska (Kathol et al. 1995) was selected to validate the nonlinear (inelastic) modeling approach. In the model, the concrete slab was simulated using solid elements and discretely reinforced by link elements in two layers. Shell elements were used to model the steel girders, which were laterally braced with beam elements at the supports. With no evidence of loss in the composite behavior observed during the test, the girders were assumed to be in full composite action with the concrete deck. All sources of material nonlinearities including cracking/crushing and inelastic deformations in the concrete and plasticity in the steel components were included in the model.

The model was restrained with hinge and roller supports at the ends and loaded with a series of concentrated loads applied on the bridge deck to mimic two side-by-side HS20 trucks with modified axle spacing (see Fig. 3-1a). Interior girder deflection at mid-span of the bridge was selected to validate the proposed numerical modeling approach. As illustrated in Fig. 3-1b, result obtained via nonlinear FE analysis correlates well with experimental outcome within both elastic and inelastic ranges of the behavior.

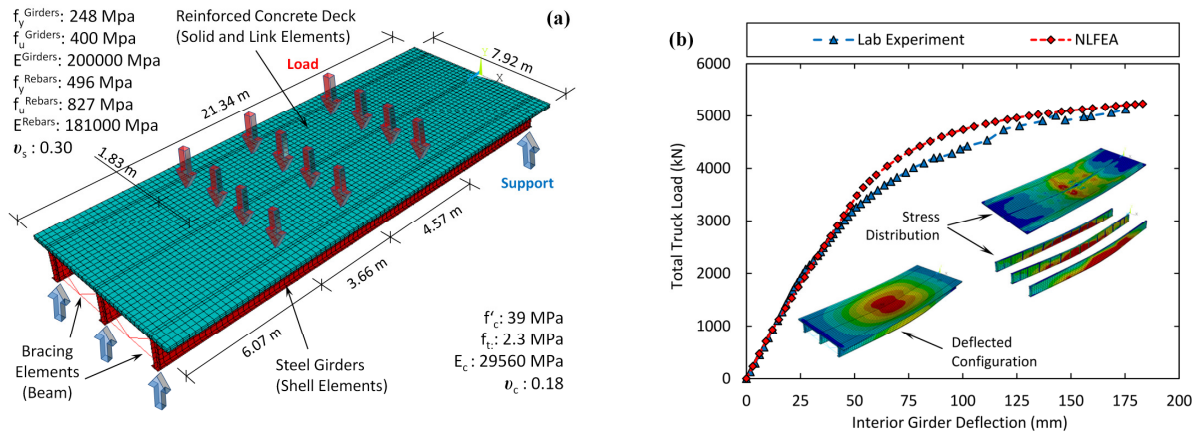


Fig. 3-1: Nebraska laboratory test (a) FE model, (b) validation

The discrepancy between the numerical and experimental results (8% at most) can be attributed to the residual stresses in the steel plate girders which were not included in the model. These stresses could potentially promote the onset of material plasticity in the girders and cause the numerical results to deviate from experimental outcomes. The nonlinear validation of the

proposed modeling approach (Barth and Wu 2006; Bechtel et al. 2011) provided sufficient confidence such that it could be extrapolated to evaluate the inelastic distribution behavior of the selected in-service Michigan bridges. Additional details on the numerical modeling approach and further discussion on the failure characteristics of the composite steel girder bridges are presented elsewhere (Gheitasi and Harris 2014a, c).

Representative Bridges

Two in-service bridge superstructures were selected in this study to investigate the variations in the lateral distribution behavior over the entire loading history up to failure. The selected bridges were titled Stanley Bridge and Huron Bridge, and considered as representative bridges to demonstrate the effect support conditions and loading position on the inelastic distribution behavior. Both bridges were also subjected to non-standard loadings, which provided a basis for evaluating the influence of vehicle configuration on distribution behavior. These bridges were primarily chosen due to available data on the structural details and loading configurations, obtained from a live load test program (Nowak and Eom 2001). Results from the experimental investigation served as the metric to evaluate the results obtained via numerical analysis.

Stanley Bridge

A simply-supported three-span bridge with a total length of 86.8 m operating on Stanley Road over I-75 (S11-25032) in Flint, Michigan, is one of the representative bridges. Only the second span of this bridge superstructure was tested in the field (Nowak and Eom 2001) and selected in this study. As illustrated in Fig. 3-2a, the selected span of the bridge is 41.1 m long with clear span of 38.4 m between pin and hanger connections. It is comprised of a 203.0 mm reinforced concrete deck supported by seven steel girders having uniform transverse spacing of 2.21 m (see Fig. 3-2b). All the structural details regarding the deck reinforcement layout, lateral bracings, and section properties of the girders were derived from the Michigan Department of Transportation (MDOT), see Figs. 3-2c to 3-2f.

In the experimental study, the selected span of the bridge was loaded with measured oversized 11-axle trucks (see Figs. 3-2g and h) in single and two-lane loading scenarios. The loaded span was instrumented at midspan with a series of strain transducers on the bottom flange of each girder to record the longitudinal strain during the field test. Results from static load tests with trucks moving at crawling speed, were used to determine distribution factors for each loading scenario (Nowak and Eom 2001).

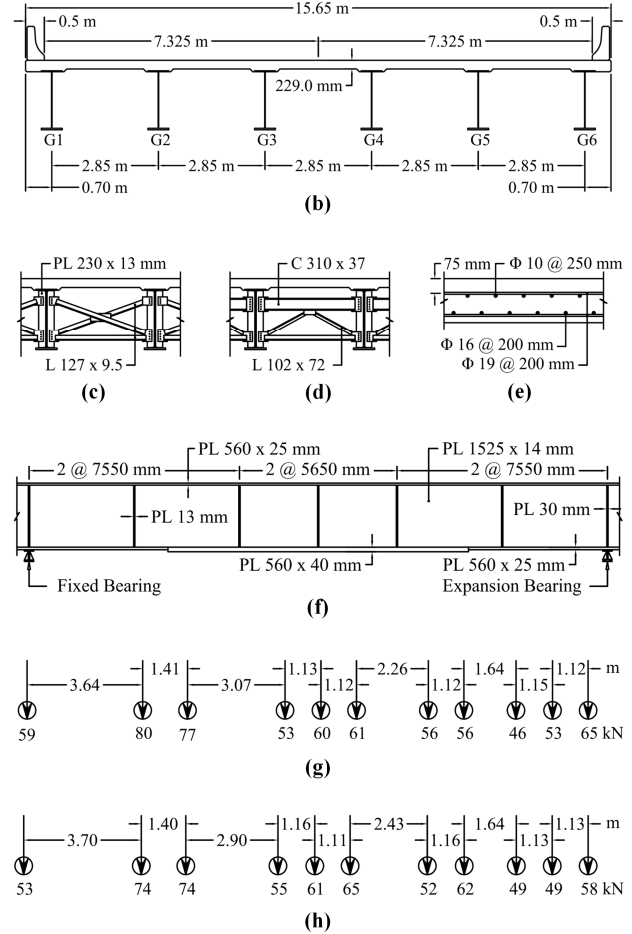
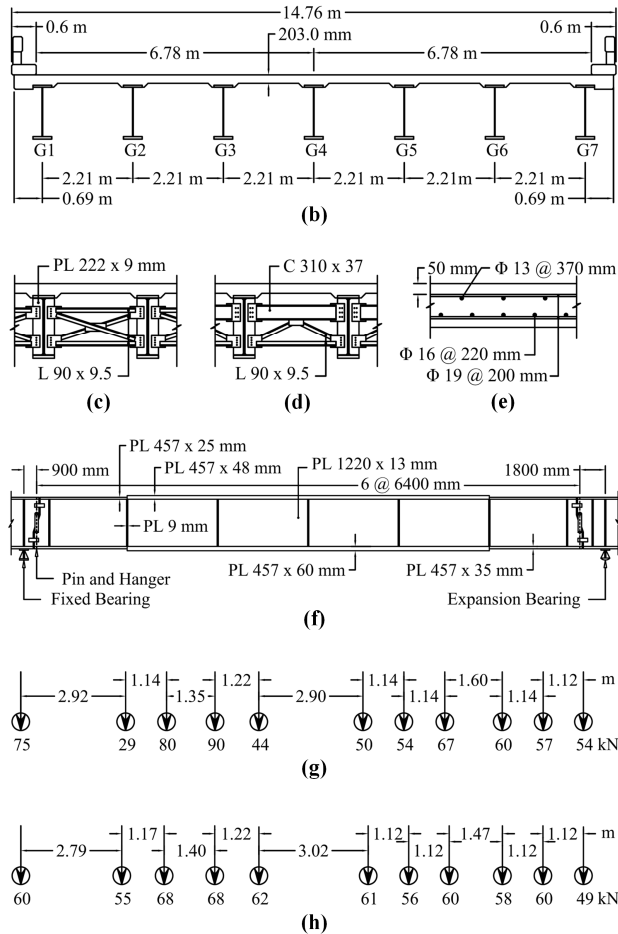
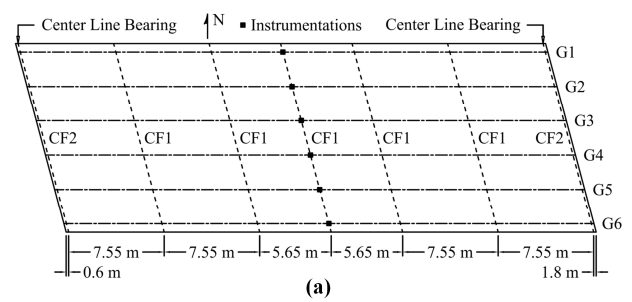
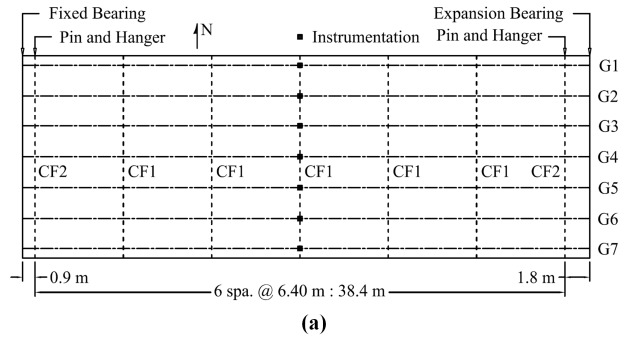


Fig. 3-2: Stanley bridge: (a) plan view of tested span, (b) cross section, (c) deck reinforcement, (d) CF1, (e) CF2, (f) girder elevation, (g) truck S1, (660kN-15.67m wheelbase), (h) truck S2 (657kN-15.55m wheelbase)

Fig. 3-3: Huron bridge: (a) plan view, (b) cross section (non-skewed), (c) CF2, (d) CF, (e) deck reinforcement, (f) girder elevation, (g) truck H1, (666 kN-17.66 m wheelbase), (h) truck H2 (652 kN-17.76 m wheelbase)

Huron Bridge

The second case study selected in this investigation was a single span, 15 ° skew, simply supported bridge serving on M-36 over the Huron River in Livingston County, Michigan

(Nowak and Eom 2001). The bridge superstructure has a total length of 42.6 m, having a 229 mm reinforced concrete slab supported by six identical steel girders spaced at 2.85 m, (see Figs. 3-3a and b), with all structural details given in Figs. 3-3c to f (derived from MDOT plans). Similar to the Stanley Bridge, the live load test was performed with measured oversized 11-axle trucks (see Figs. 3-3g and h) considering both single and double-lane loading scenarios. Strains measured at the midspan of the bridge were used to determine distribution factors (Nowak and Eom 2001).

Investigative Approach

This study aims to evaluate the effects of variations in support conditions, loading position and load configuration on the inelastic load distribution behavior of two representative in-service bridges. For each bridge superstructure, the FE model was developed based on the validated numerical modeling approach. In these models, material properties including compressive strength of the concrete and yield stress of the steel components were extracted from MDOT plans; however, the corresponding constitutive stress-strain relationships were assumed to incorporate the post-yield behavior of material in the analysis (see Fig. 3-4). The developed FE models were loaded with the oversized 11-axle (Figs. 3-2 and 3-3) and standard AASHTO HS20 trucks, applied in three different transverse positions (see Fig. 3-5) in accordance to the field testing program. The longitudinal positions of the applied truck loads were defined using influence line analysis to produce maximum positive moment near the mid-span of each bridge system. Assumed trucks were applied on the models through a series of point loads distributed over 500 x 200 mm (20 x 8 in.) patch areas (Harris and Gheitasi 2013). Geometric nonlinearities and dynamic effects of the moving trucks were not considered in this study.

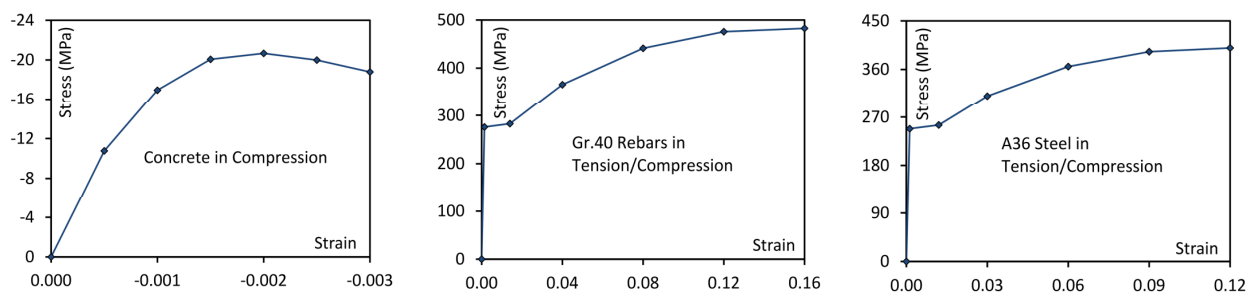


Fig. 3-4: Assumed material properties

The numerical investigation of the simulated bridges was performed in two phases. The first

phase aimed to study the elastic distribution behavior and calibrate the models using existing experimental data (Nowak and Eom 2001). For the second phase, a series of non-linear static analyses were performed on the developed models to investigate the nonlinear response and inelastic load distribution behavior of the selected bridge superstructures, with straight and skewed configuration, as they approach their ultimate capacity.

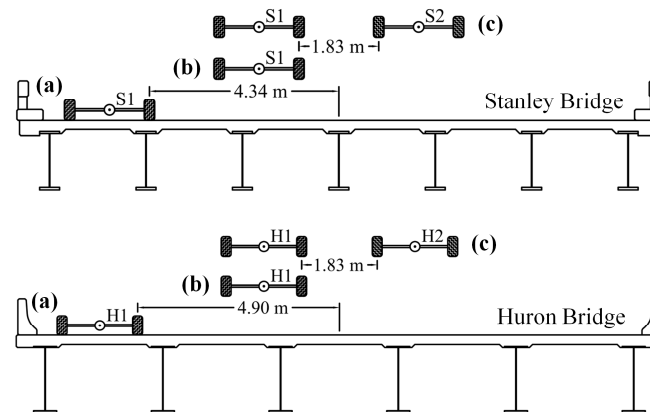


Fig. 3-5: Transverse loading positions: (a) Position 1, one-lane loaded close to the curb; (b) Position 2, one-lane loaded; (c) Position 3, two-lane loaded

Discussion of Results

Linear-Elastic Behavior

Under the effect of identical load configurations applied in the field test program (Figs. 3-2 and 3-3), strain distributions were derived from linear elastic FE analysis of the representative bridges and compared to the test results. Previous investigations of the selected bridges (Nowak and Eom 2001, Harris and Gheitsi 2013) demonstrated that the actual boundary conditions of these structures are somewhere between the ideal pin-pin and pin-roller conditions as a result of partially frozen supports. In-service environmental effects such as corrosion or accumulation of debris may have contributed to the amount of fixity.

Results from this investigation also demonstrate that the models with ideal pin-pin (PP) and pin-roller (PR) conditions serve as lower and upper bounds for the actual behavior of both simulated bridge systems (see Fig. 3-6). In addition to the ideal boundary conditions (PR and PP), a partially frozen (PF) scenario was also considered in this study by adding linear longitudinal springs to the top and bottom flanges of steel girders. The modeling procedure in

updating the boundary condition mimicked the approach employed by Nowak and Eom (2001). The stiffnesses of these springs were calibrated via field test results. Upon calibration, numerical outcomes were in a good agreement with the experimental results. However, there exists a discrepancy between the results, which can be attributed to the fact that same stiffness was assumed for all of the applied springs, while in actual practice the amount of partial fixity would be different for each girder depending on the level of accumulated damage.

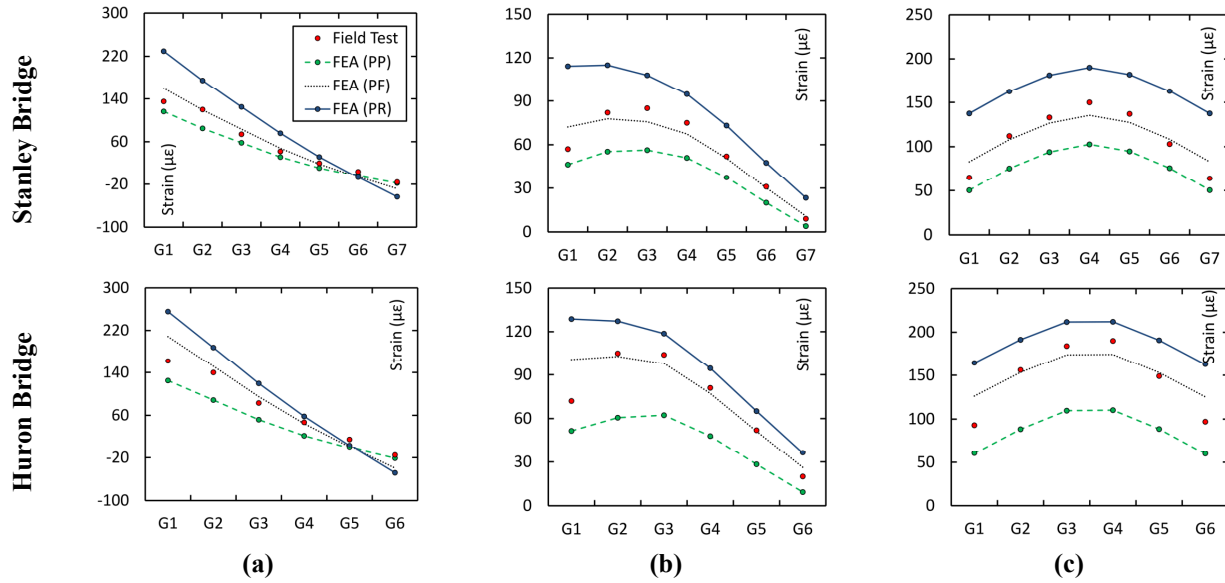


Fig. 3-6: Linear elastic analysis: (a) position 1; (b) position 2; (c) position 3

Nonlinear Characteristics

A sensitivity study with respect to three parameters of boundary condition, loading position and load configuration was conducted to assess the variations in inelastic distribution factors. In the analyses, the selected vehicular loads were incrementally applied to the models. The loads within each axle of the truck were proportionally increased, while the ratio of the axle loads remained unchanged. Crushing on the top surface of the concrete deck and/or plastic hinging in the steel girders were the main failure mechanisms determining the ultimate capacities of the simulated bridge systems.

Effect of Boundary Conditions

To evaluate the influence of the boundary restraint on the nonlinear behavior and inelastic distribution response of the selected bridge superstructures, the developed FE models were

subjected to two side-by-side 11-axle trucks (position 3) identical to those implemented in the field test (Nowak and Eom 2001). The boundary restraints varied from pin-roller (PR) to partial fixity (PF) to pin-pin (PP). Fig. 3-7 illustrates the total applied load versus the maximum deflection in the girders obtained from nonlinear FE analysis for both simulated bridges. Regardless of the applied boundary conditions, the nonlinear responses of the system illustrate significant amount of additional capacity in comparison to the total load applied in the field test program (2 trucks). This would highlight the complexity in understanding the system-level behavior and evaluating the performance of in-service bridge superstructures; the concepts which are not considered in the current load-rating practices of in-service bridge superstructures.

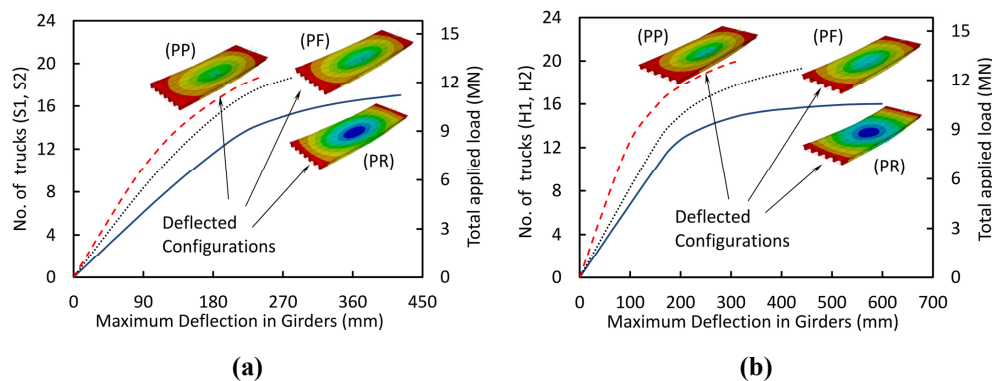


Fig. 3-7: Effect of boundary conditions on nonlinear behavior – position 3: (a) Stanley Bridge, (b) Huron bridge

When comparing the relative responses under the effect of different applied boundary conditions (PR, PF, and PP), it is evident that the ultimate system capacity is significantly influenced by the support stiffness. Under a similar loading scenario, changing the boundary condition from PR to PP allowed a 10% increase in the ultimate load-carrying capacity of the Stanley Bridge, while the capacity of the Huron Bridge increased by 25%. However, stiffening the supports has an adverse effect on the overall system ductility, which can be defined by comparing the maximum deflection of the system to the deflection at the moment of first yield in the girders. The results indicate 43% and 48% reductions in the system ductility of the Stanley and Huron Bridges, respectively; as the boundary conditions were changed from PR to PP in the corresponding developed models.

The evolution of girder distribution factors throughout the loading history of the simulated bridge models was derived for the assumed boundary conditions (PR, PF, and PP) at mid-span of

the selected structures (see Figs. 3-8). In addition, variations in girder distribution behavior within the cross sections of the simulated bridges were captured at four representative stages of applied loading with respect to the ultimate capacity of the system (see Fig. 3-9). As illustrated, the girder distribution behavior in both bridge superstructures remained almost unchanged prior to formation of first flexural cracks in the concrete slabs, which would demonstrate the linear elastic behavior of the bridge systems. Within the elastic range of behavior, the distributing behavior is slightly influenced by the assumed boundary conditions. Stiffening the supports from PR to PP allows the closer girders to the applied loads to absorb more load (G3, G4, and G5 in Stanley bridge, G3 and G4 in Huron bridge). On the other hand, the girders further from the location of the applied trucks contribute less to the load carrying mechanism of the system as the support conditions stiffen.

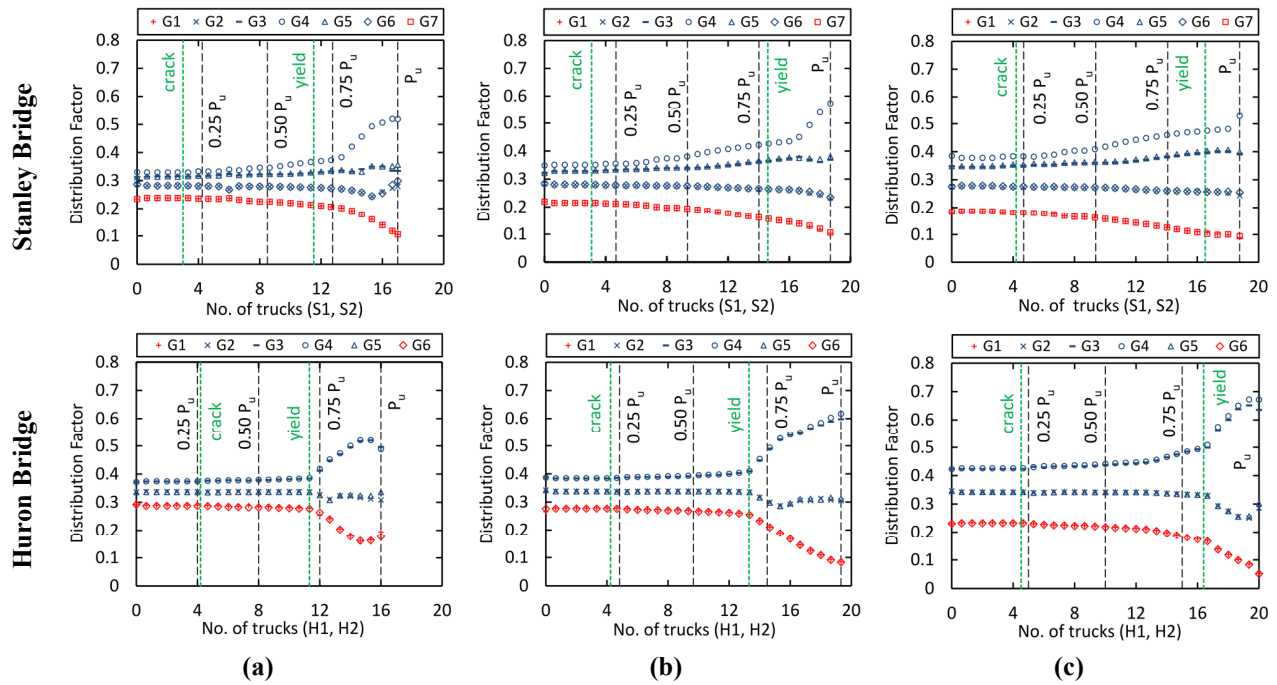


Fig. 3-8: Evolution of distributing behavior throughout loading history of the selected bridges loaded with oversized trucks in position 3: (a) PR, (b) PF, (c) PP

By increasing the loads, flexural cracks start to propagate all over the concrete deck. Initiation and propagation of material nonlinearity in the system causes the distribution factors to deviate from their previous steady state within the elastic range of behavior (see Figs. 3-8 and 3-9). This deviation becomes more critical as material plasticity initiates in steel girders. The

variation in the distribution factors appears to be more gradual in the Stanley bridge as the system undergoes additional loading. In the Huron bridge, however, much of deviation in the lateral distributing behavior occurs after plasticity initiated in the girders. As the bridge systems undergo additional loading, the girders closest to the location of the applied trucks absorb more load (G4 in Stanley bridge, G3 and G4 in Huron bridge); whilst, the participation of exterior girders (G1 and G7 in Stanley bridge, G1 and G6 in Huron bridge) in the load sharing mechanism decreases significantly. Other interior girders have less variation in their level of contribution to the lateral load distribution (G2, G3, G5, and G6 in Stanley bridge, G2 and G5 in Huron bridge). It is worth mentioning that refinement of the support conditions has negligible influence on the initiation of material nonlinearity in the concrete deck (cracking). However, initiation, location and extent level of plasticity in girders are significantly affected by the assumed boundary conditions. In both bridge models with ideal PR supports, plasticity in the girders is mainly concentrated at mid-span of the structure. By stiffening the supports, the plasticity propagates not only at mid-span but also at the vicinity of the supports.

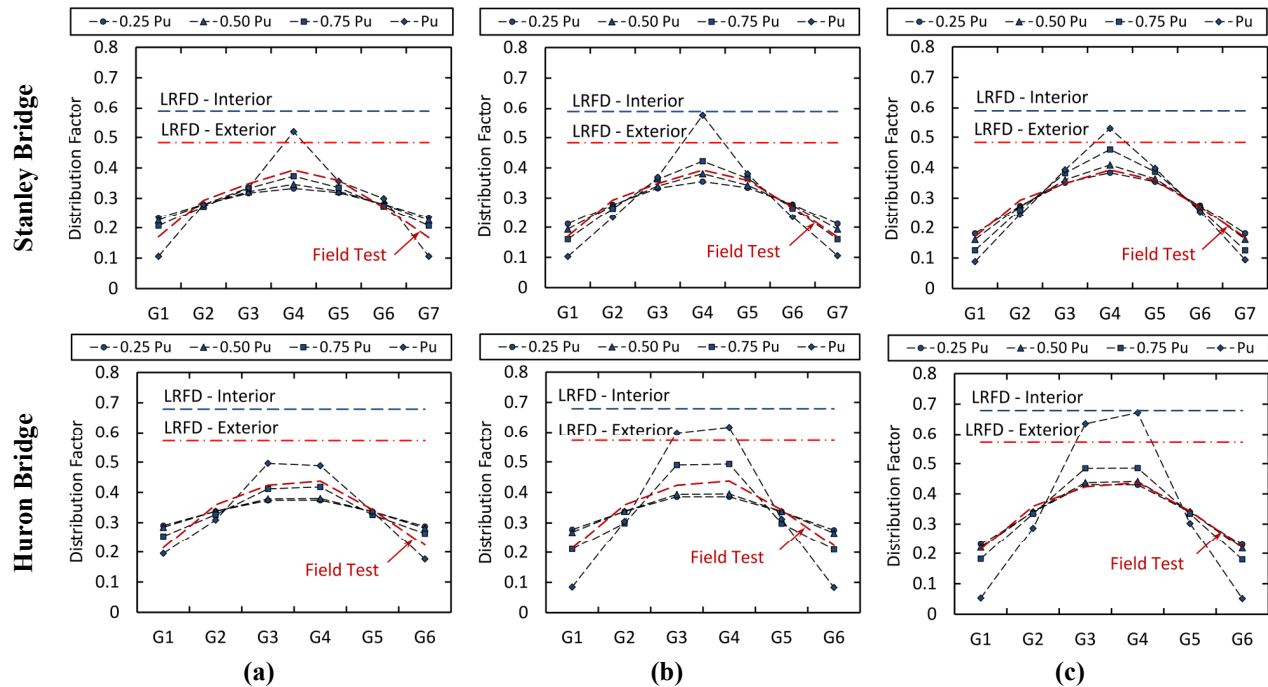


Fig. 3-9: Variation of distributing behavior over cross section of the selected bridges loaded with oversized trucks in position 3: (a) PR, (b) PF, (c) PP

In addition to the numerical analysis, girder distribution factors for selected bridge superstructures were calculated based on AASHTO LRFD specification. When evaluating the system behavior under the effect of oversized 11-axle trucks, it can be observed that the AASHTO LRFD approach is generally conservative in predicting the girder distribution factors for exterior girders, regardless of the assumed boundary conditions. Although the amount of contribution of the interior girders closer to the applied load increased dramatically with supports stiffened, especially when the bridges approach their ultimate capacity, none of the girders violate the limits of the AASHTO LRFD specifications. For the critical scenarios, the simulated bridges were loaded to nearly 18 oversized trucks, which is unlikely to occur during the normal service life of the selected structures. It should be noted that refining the boundary conditions would provide the potential to integrate the effects of end deterioration in steel girders in the load rating practices and performance evaluation of in-service bridge superstructures.

Also illustrated in Fig. 3-9 are the distribution factors obtained from the field test program (Nowak and Eom 2001) for the identical two-lane loading scenario. The lateral load distribution behavior at first two stages of loading ($0.25P_u$, $0.50P_u$) corresponds well with the actual response of these structure in the experimental investigation. This would highlight the negligible influence of material nonlinearity (cracking) in concrete slab on the overall load distributing mechanism of the selected bridges. However, the lateral load distributing mechanisms of both simulated superstructures diverge from the experimental results at higher stages of loading ($0.75P_u$, P_u), when the material nonlinearity (plasticity) propagates through the girders. This would indicate that the inelastic distributing mechanism in the girder-type bridge superstructures is mainly affected by the behavior of their main load-carrying element (i.e. girders).

Effect of Loading Position

In addition to the previous analysis case on the bridges subjected to side-by-side loading scenario (position 3) with PR boundary condition, additional analyses were performed to study the effect of loading position on the nonlinear girder distribution characteristics. Both of the bridge models were supported with PR boundary conditions and subjected to the oversized 11-axle trucks applied in two different single-lane positions (position 1 and 2), identical to two of the single lane configurations used in the field test. Fig. 3-10 illustrates the total applied load versus the maximum deflection in the girders obtained from nonlinear FE analysis for both

simulated bridges. As demonstrated, the load-deflection response of the systems is highly sensitive to the position of the applied loads. Both bridges exhibit the greatest reserve capacity under the effect of two side-by-side truck configuration; however, their reserve capacities reach a minimum value as the truck loading is applied asymmetrically in one lane close to the curb.

In addition, results indicate a significant reduction in the overall system ductility of the simulated bridges as the truck loads are applied in the one-lane loading scenarios. Moving the trucks to the edge of the structure increases the level of compressive stresses on the top surface of the concrete decks, especially close to the curb. Due to low compressive strength of the concrete in the selected structures and also lack of effective deck width beyond exterior girder (short overhang), crushing on the top surface of the concrete decks governs the failure mode of the simulated bridges in the corresponding numerical analysis. This would result in a restriction to the expansion of material plasticity among the steel girders, which in turn reduces the overall ductility of the simulated systems.

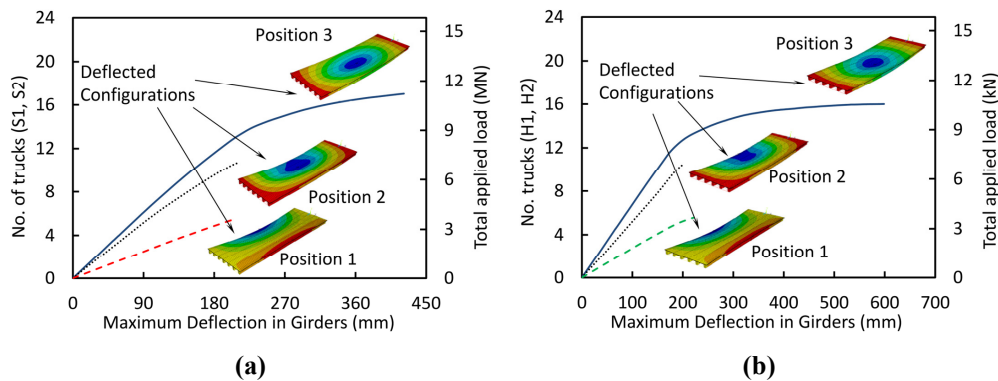


Fig. 3-10: Effect of loading positions on nonlinear behavior with PR boundary conditions: (a) Stanley Bridge, (b) Huron bridge

The evolution of load distribution factors for each girder was monitored throughout the loading history of the analyzed structures and depicted in Figs. 3-11. Comparing the results with those previously illustrated in Fig. 3-8a, it is evident that the girder distribution behavior is highly dependent on the position of the applied loads. In the one-lane loading scenarios, all girders cannot effectively contribute to load sharing mechanism of the bridge superstructures. As expected, the girders closest to the applied loads contribute the most, while the girders furthest from the location of the loads experience a decreased participation. Similar to the side-by-side loading configuration, the girder distribution behavior in both bridge superstructures loaded with

single trucks in position 1 and 2, remained almost unchanged prior to formation of first cracks in the concrete slabs. In contrast to position 3, the girder distributing behavior under the effect of single truck loading scenarios does not deviate significantly with initiation of material nonlinearity in the concrete decks. As the bridge models are subjected to additional loads beyond the first yield, girders closest to the location of the applied trucks (G1 in position 1, G3 in position 2 for both bridge models) absorb more loads; while, participation of other girders to the load sharing mechanism remained almost unchanged, especially for the girders furthest from the location of the applied loads (G5, G6, G7 in Stanley bridge, G5 and G6 in Huron bridge).

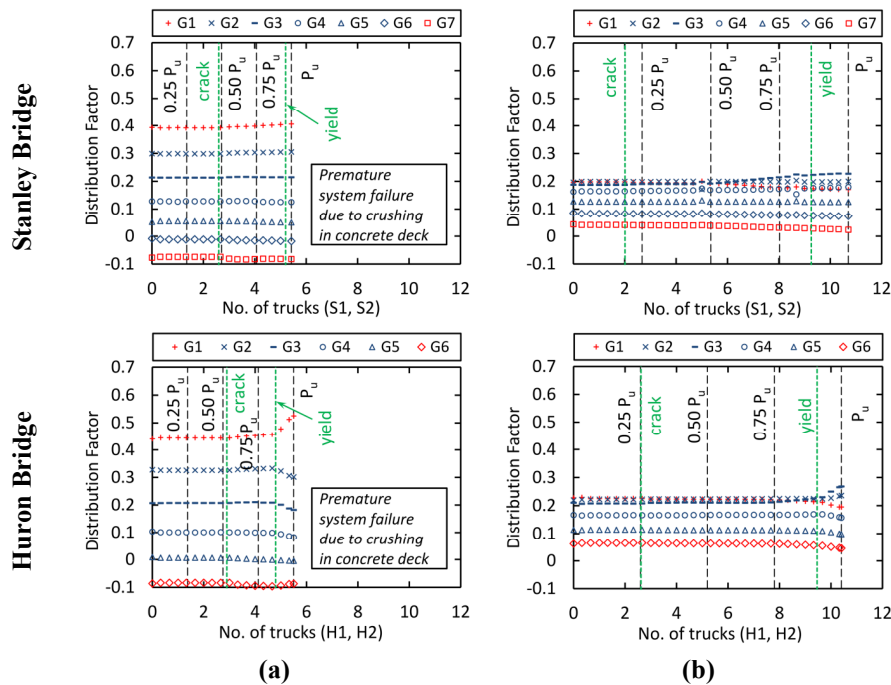


Fig. 3-11: Evolution of distributing behavior throughout loading history of the selected bridges with PR boundary conditions: (a) position 1, (b) position 2

Variations in girder distribution behavior within the cross sections of the simulated bridge superstructures were also captured at four representative stages of loading and depicted in Fig. 3-12. Comparing the results to those obtained under the effect of two side-by-side oversized trucks (Fig. 3-9a) demonstrates less variation in the lateral load distributing behavior of the systems subjected to asymmetric one-lane loading scenarios. This could be attributed to the limited propagation of material plasticity amongst girders as a result of crushing that dictates a premature failure mechanism in the simulated bridges. As illustrated in Fig. 3-12, the values of

distribution factors proposed by the AASHTO LRFD specifications provide a reasonable bound of confidence on the distribution behavior of the critical exterior girders when the bridge models are loaded in position 1; however, in the remaining girders, the distribution factors are highly over-estimated. As the over-sized truck is moved towards the middle of the bridge cross section (position 2), the design distribution factors are generally conservative for both interior and exterior girders. Also demonstrated in Fig. 3-12 are the corresponding test results for each of the applied single-lane loading positions. Results in all load stages are in a good agreement with the actual behavior of the simulated structures. This would also highlight the limited evolution of material nonlinearity in the selected structures, especially in the girders, under the effect of asymmetric loading scenarios.

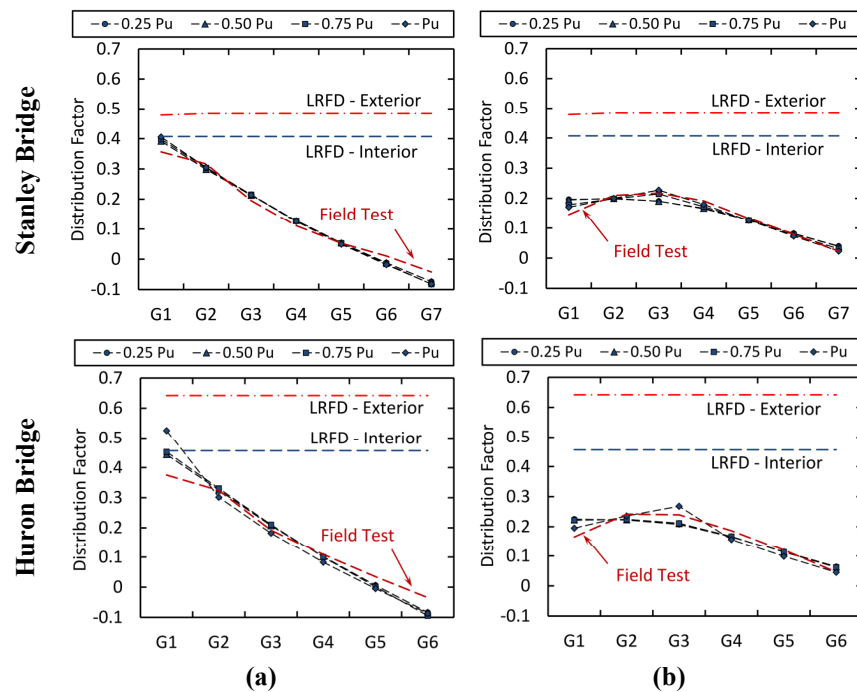


Fig. 3-12: Variation of distributing behavior over cross section of the selected bridges with PR boundary conditions: (a) position 1, (b) position 2

To investigate the effect of boundary restraint on the inelastic distribution behavior under the effect of asymmetric loading configuration, both of the bridge models were analyzed while loaded in position 2 with oversized trucks and supported with PP boundary conditions. Similar to the side-by-side loading scenario, the ultimate capacity of the selected bridges increased as the support conditions were changed from PR to PP (9% in Stanley bridge, 21% in Huron bridge).

However, results illustrated in Fig. 3-13 demonstrate a slight change in the overall distribution behavior of both bridges with PP boundary conditions, comparing to values obtained for the systems with PR supports (see Fig. 3-12b). By changing the supports from PR to PP, the contribution of the closest girder to the applied load (G3) increased by almost 25% in both bridge superstructures with minor change in the participation of the other girders. Regardless of the applied boundary conditions, crushing in the concrete slab generally dictates the premature failure in the systems under the effect of asymmetric single-lane loading scenario. Moreover, the girder distribution factors proposed by AASHTO LRFD specification for one-lane loading scenario, still highly overestimate the actual behavior of the selected bridges, even with the stiffened supports.

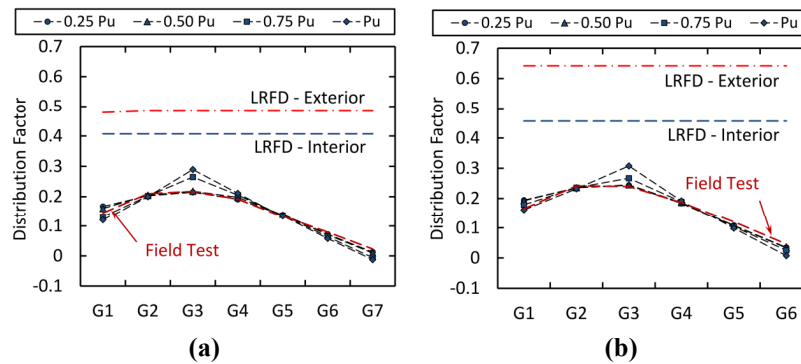


Fig. 3-13: Variation of distributing behavior over cross section of the selected bridges with PP boundary conditions - position 2: (a) Stanley Bridge, (b) Huron bridge

Effect of Truck Configuration

To study the influence of vehicular load configuration on the nonlinear distribution behavior of the selected bridges, the developed FE models with PR boundary conditions were subjected to the standard AASHTO HS20 design trucks in both single-lane and side-by-side loading scenarios (positions 2 and 3). Based on AASHTO LRFD (1994), the HS20 design truck is defined as a three-axle vehicle with weights of 35, 142, 142 kN (8, 32, and 32 kips) on the front, middle, and trailing axles, respectively. The spacing between the front and middle axles is 4.3 m (14 ft.), while the spacing between the middle and trailing axles varies between 4.3 m and 9.1 m (14ft. and 30ft.) to produce extreme force effects. The difference in geometrical configuration of the implemented oversized trucks and the standard AASHTO HS20 trucks provides a basis for

comparing the impact of vehicle type on the load distribution behavior, especially beyond the elastic limit.

Fig. 3-14 illustrates the impact of truck configuration on the load-deflection response of the selected bridge superstructures. When the oversized 11-axle trucks were replaced by HS20 trucks, the ultimate capacities of the simulated systems drop 6% and 14% on average, for the single-lane (position 2) and double-lane (position 3) loading scenarios, respectively. With this reduction in capacity, the bridge systems reach a certain level of deflection at relatively lower levels of the applied load, under the effect of trucks with 3-axle configuration as compared to the oversized 11-axle trucks. This effect can be directly attributed to the length of the wheelbase of the applied trucks, where the HS20 trucks have almost the half wheelbase length of the 11-axle trucks. The more concentrated configuration of the applied loads increases the level of internal stresses at midspan of the structure and facilitates the evolution of material nonlinearity in the main structural component, which in turn results in a global reduction in the system stiffness and a relative increase in the maximum deflection of the system. Moreover, changing the truck configuration also affects the overall ductility of the system. For the side-by-side loading scenario (position 3), the overall system ductility decreases by 17% and 32% in the Stanley and Huron bridges, respectively. This reduction in ductility can also be attributed to the more concentrated wheelbase configuration of the applied HS20 trucks, as it increases the local internal stresses and enhances the potential for crushing on the top surface of the concrete slabs at lower levels of applied loading. However, variations in system ductility under the effect of single-lane loading scenario (position 2) are negligible (see Fig. 3-14).

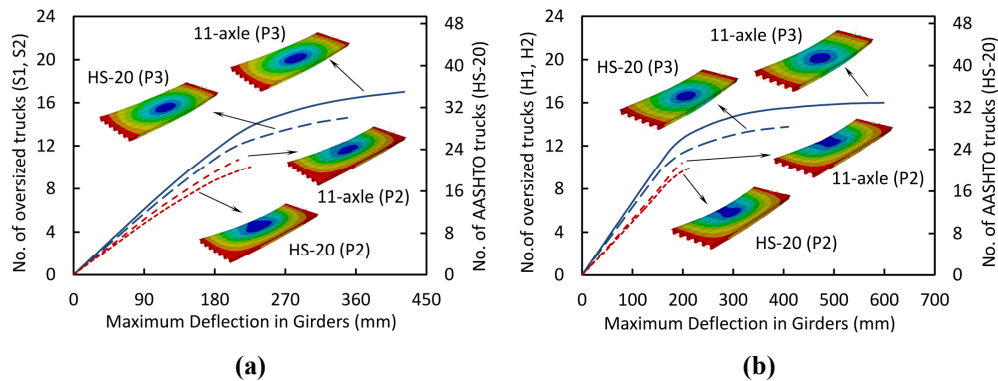


Fig. 3-14: Effect of truck configuration on nonlinear behavior with PR boundary conditions: (a) Stanley Bridge, (b) Huron bridge

The evolution of nonlinear lateral load distribution behavior resulting from the HS20 trucks applied at different locations (position 2 and 3) is illustrated in Fig. 3-15. Similar to the 11-axle oversized trucks, variations in distribution factors are observed once flexural cracks begin to propagate in the concrete deck. With increasing load, additional material nonlinearity (further cracking in concrete deck, plasticity in girders) is initiated, causing a significant change in the lateral load distribution behavior of the simulated bridge systems. Girders closer to the truck load absorb a greater portion of the applied load, while the other girders further from the applied load participate less. Comparing the distribution behavior between different loading configurations, (see Figs. 3-9a, 3-12b, and 3-15), it can be concluded that the evolution of distribution behavior in the selected bridge systems approaching their ultimate capacities obeys similar patterns, regardless of the truck configuration. However, the intensity of variations is more severe for the cases where the bridge models were loaded with HS20 trucks. Comparing the results from numerical analysis of the selected bridges with the values of distribution factors proposed by AASHTO (see Fig. 3-15), it can be observed that the AASHTO LRFD specification may be less conservative in predicting the distribution behavior in the presence of high material nonlinearities, with the degree of conservativeness dictated by load position and configuration.

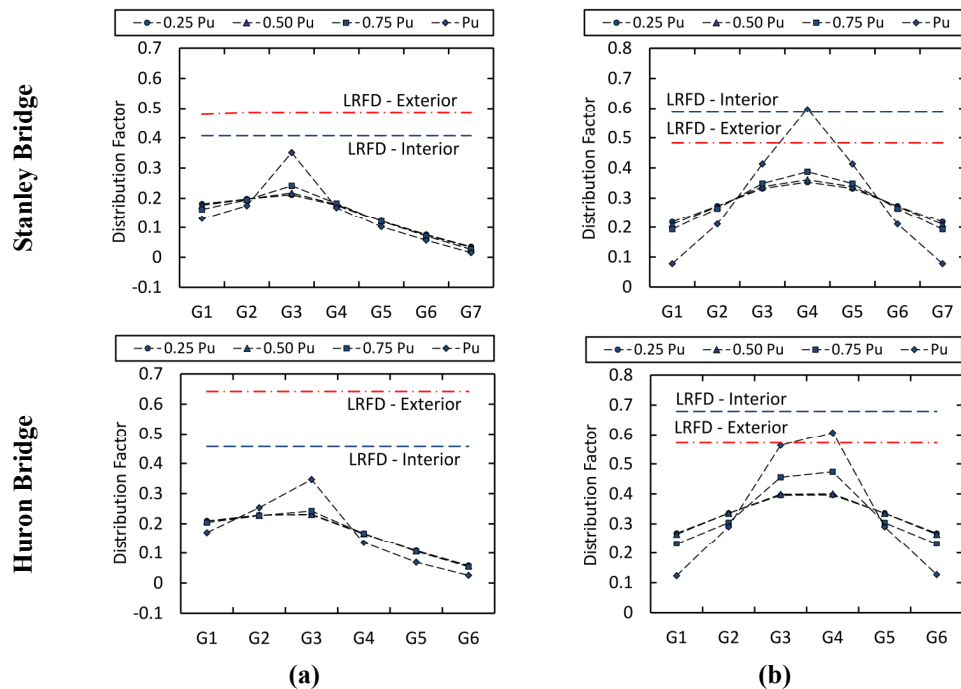


Fig. 3-15: Variation of distributing behavior over cross section of the selected bridges loaded with HS20 trucks with PR boundary conditions: (a) position 2, (b) position 3

Comparison of FE results with AASHTO

Table 3-1 provides a summary of the critical distribution factors, derived from 16 cases of nonlinear FE analyses of the selected bridge superstructures with variations through loading and boundary conditions, together with the corresponding values proposed by the AASHTO LRFD specifications. The ratios of the code-specified distribution factors to the critical numerical values for both interior and exterior girders at the ultimate capacities of the selected bridges indicate the overall conservativeness of the approach provided by the AASHTO LRFD specifications (conservative for values >1 , while unconservative for values <1). Similar trends have been previously reported in a study by Razaqpur et al. (2012), which investigated the influence of geometric and loading parameters on the inelastic load distribution behavior of a series of hypothetical composite steel girder bridges.

In the presence of high material nonlinearities, the distribution factors proposed by the AASHTO LRFD are on average 24% and 33% higher than the numerically derived values for the interior girder of the Stanley and Huron Bridge, respectively. Only in one case of analysis, where the Stanley Bridge was loaded with two side-by-side standard HS20 trucks, the AASHTO-specified distribution factor slightly underestimates (by 2%) the maximum distribution factor of the critical interior girder (G4). For the exterior girders, however, the AASHTO LRFD is significantly conservative in predicting the actual distribution behavior (300% and 365% on average for the Stanley and Huron Bridge, respectively). Comparing the standard deviation derived for the corresponding ratios in both interior and exterior girders, it is evident that the distribution behavior of the exterior girders at the ultimate capacity of the selected bridges is more sensitive to the variations in the loading and boundary conditions than the interior girders.

Table 3-1: Comparison between distribution factors, FE results vs. AASHTO-LRFD

Stanley Bridge (straight configuration)									
Analysis Case	Boundary condition	Loading position	Truck	Critical DF values				Ratios	
				Interior		Exterior		AASHTO/FE	
				FE	AASHTO	FE	AASHTO	Interior	Exterior
1	PR	3	S1/S2	0.52	0.59	0.11	0.48	1.13	4.57
2	PF	3	S1/S2	0.57	0.59	0.11	0.48	1.02	4.57
3	PP	3	S1/S2	0.53	0.59	0.09	0.48	1.11	5.13
4	PR	1	S1	0.31	0.41	0.41	0.48	1.33	1.18
5	PR	2	S1	0.23	0.41	0.17	0.48	1.79	2.80
6	PP	2	S1	0.29	0.41	0.12	0.48	1.41	3.97
7	PR	2	HS-20	0.35	0.41	0.13	0.48	1.16	3.66
8	PR	3	HS-20	0.60	0.59	0.08	0.48	0.98	6.21
Ave.:								1.24	4.01
St. dev.:								0.26	1.53
c.o.v.:								0.21	0.38
Huron Bridge (skewed configuration)									
Analysis Case	Boundary condition	Loading position	Truck	Critical DF values				Ratios	
				Interior		Exterior		AASHTO/FE	
				FE	AASHTO	FE	AASHTO	Interior	Exterior
9	PR	3	H1/H2	0.50	0.68	0.19	0.57	1.37	2.93
10	PF	3	H1/H2	0.62	0.68	0.08	0.57	1.10	6.76
11	PP	3	H1/H2	0.67	0.68	0.05	0.57	1.01	10.76
12	PR	1	H1	0.30	0.46	0.53	0.64	1.51	1.22
13	PR	2	H1	0.27	0.46	0.20	0.64	1.70	3.29
14	PP	2	H1	0.31	0.46	0.16	0.64	1.48	3.96
15	PR	2	HS-20	0.35	0.46	0.17	0.64	1.32	3.77
16	PR	3	HS-20	0.61	0.68	0.13	0.57	1.12	4.50
Ave.:								1.33	4.65
St. dev.:								0.24	2.92
c.o.v.:								0.18	0.63

Conclusions

A comprehensive numerical study was performed on two representative actual in-service bridge superstructures in the State of Michigan, to investigate the impact of variations in boundary condition, loading position, and load configuration on the overall structural response

and girder distribution behavior of bridges approaching their ultimate capacities. Based on the results, the following conclusions can be drawn:

- The ultimate capacities and system ductility of the selected bridge superstructures are highly sensitive to all three investigated parameters. Stiffening the support would result in higher capacity, while reducing the overall ductility of the system. Applying load in an asymmetric pattern significantly reduces the capacity of the system. With same boundary condition and loading position, a bridge system can tolerate higher magnitude of loads in the presence of longer trucks with a larger wheelbase.
- Variations in lateral distribution behavior occur once the structure passes the linear elastic stage of the behavior. Deviation in the girder distribution factors begins with material nonlinearity (cracking) initiating in the concrete slab, and becomes more critical as the plasticity starts to propagate in girders. In the presence of material nonlinearity, all of the selected parameters in this study (loading and boundary conditions) do have an influence on the evolution of girder distribution behavior. For instance, stiffening the supports would increase the level of contribution of the girders closer to the applied loads; while loading the bridge in an asymmetric configuration (single-lane loading scenarios) significantly decreases the load sharing contributions in the girders furthest from the applied loads.
- Girder distribution factors proposed by the AASHTO LRFD specifications are usually conservative in predicting the distributing behavior of the selected bridge superstructures as they approach their ultimate capacities. However, the level of conservativeness highly depends on the loading configuration, which in this study was selected to be consistent with the loading patterns of the corresponding field testing programs. The code-specified values for distribution factors can be violated in the presence of high material nonlinearities and refined loading configuration based on the AASHTO-LRFD specifications. Nevertheless, the amount of applied loads corresponding to this critical stage is much larger than typical service loads, for which the bridge superstructure was designed.
- Although the design philosophy of the LRFD specification is to control the safety of the structure at the ultimate strength limit state, the proposed equations for defining the girder distribution factors were calibrated based on the linear elastic behavior. Within the

inelastic range of behavior, the lateral load distribution factors are governed by the geometry of the structure and the loading configuration. Therefore, any adjustment to the current AASHTO LRFD equations to make them applicable for inelastic behavior and ultimate limit states would need to be validated through a parametric study using nonlinear FE analyses on series of structures with a wide range of geometrical and loading configurations.

Chapter 4:

Redundancy and Operational Safety of Composite Stringer Bridges with Deteriorated Girders

(ASCE, Journal of Performance of Constructed Facilities, under review, 2014)

Summary

As a critical component of the national transportation network, bridges have received a lot of attention regarding their safety and condition state. Similar to the concept of immediate depreciation of a new vehicle purchase, bridge superstructures begin to degrade after they are placed in service, albeit at a lower rate. To combat this issue, owners have begun to utilize a variety of technologies to monitor the behavior and detect different sources of damage in their bridges and generate higher fidelity condition metrics. However, an appropriate maintenance decision making requires knowledge of characterizing the influence of detected damage and deterioration mechanisms on the overall system behavior.

This paper presents a performance-based numerical modeling framework that can be used to characterize the impact of deteriorating conditions on the performance of in-service bridge superstructures. The framework was validated through a sensitivity analysis of two representative in-service composite steel girder bridges under the impact of corrosion in steel girders, with an objective of evaluating the functionality and operational safety. The sensitivity analysis utilized a series of non-linear finite element analyses to assess the system-level performance under a variety of damage scenarios. Results from the analyses demonstrated that the shape of the damage configuration has negligible effect on the capacity reduction in deteriorated structures, while the damage depth can significantly reduce the capacity of the structure up to 60% of the intact system tolerance. It is expected that the proposed framework for evaluating system behavior will provide a first step for establishing a critical linkage between design, maintenance, and rehabilitation of highway bridges, which are uncoupled in current infrastructure decision-making processes.

Introduction

State of Practice

An efficient and well maintained transportation infrastructure is an essential component to the economic health of the United States not only by providing a corridor for the transportation of goods and people (CSI 2008, Kavinsky 2007), but also serves a coast to coast and border to border passageway for the nation's military (GAO 2008). Historically the highway system, which includes both roads and bridges, has flown underneath the radar of the public opinion when compared to other engineering marvels, but is easily recognized as a critical component in the everyday lives of most people. Recent tragic bridge failures (NTSB 2008 and 2013a, b) have brought the challenges associated with existing infrastructure to the forefront of public scrutiny, as they often result in loss of human lives and significant economic hardship to the surrounding communities (MnDOT 2010).

The occurrence of bridge failures is somewhat rare and typically attributed to unforeseen events such as impact, fires or flooding as opposed to general deterioration (Kumalasari and Fabian 2003). Nevertheless, it is the condition states associated with deterioration that represents the greatest challenges for transportation agencies across the country. With a national inventory of more than 600,000 bridges (FHWA 2013), 10 percent of which are classified as structurally deficient while 14 percent are functionally obsolete, strategies and resources for maintenance are a growing challenge for federal, state and local governments, especially considering that many bridges are reaching or exceeding their design service lives of 50 years. While it is not feasible to simultaneously repair all of the deficient bridges, the operating condition does underscore the importance of quality inspection to prioritize the corresponding repair efforts.

Deteriorations in Highway Bridges

Under the premise of a rational structural design, the service lives of highway bridges are governed by the operating environment, load effects and history, and maintenance and preservation practices; with really only the last factor being under the owner's influence. Successful maintenance practices require knowledge of condition state of the bridge system. To some extent, this is accomplished through traditional inspection methods (AASHTO 2011) and novel technologies (Lynch and Loh 2006, Pakzad et al. 2008, Vaghefi et al. 2012 and 2013),

which are employed by most transportation agencies to identify the visible deteriorations and improve the confidence in locating internal degradation mechanisms.

The type of damage and deterioration conditions associated with the bridge systems varies from one structural type to another (FHWA 2012). In composite steel girder bridges for instance, concrete decks typically suffer from a range of damage scenarios spanning from rebar corrosion and subsurface delamination to spalled sections and scaling. In the steel girders, however, degradation often manifests as corrosion, section loss, and fatigue cracking. Other mechanisms such as frozen bearings, over-height vehicular impacts, and bridge settlement, which address the overall system behavior, are also common in this type of bridge superstructures.

Despite the type of the damage and the implemented detection method, the basic question that still needs to be answered is how the collected damage data can be used to correlate the impact of existing deteriorating conditions on the performance of highway bridges. An answer to this question requires a fundamental understanding of system-level behavior of the deteriorated bridges during their varying life stages. A comprehensive investigation performed by Ghosn et al. (NCHRP 1997, 2014) is a representative example of the previous efforts that has been carried out to quantify the impact of a main member removal on the behavior and redundancy of bridge superstructures. Furthermore, a correlation of this behavior to the safety and serviceability of the bridge system has the potential to help transportation officials in developing preservation strategies essential to defining a bridge's life-cycle. Among all types of damage mechanisms associated with steel-concrete composite bridges, the present study exclusively focuses on the impact of corrosion in steel girders, on the overall performance and behavior of composite steel girder bridges. Previous work by the authors has also explored the impact of deck deterioration (rebar corrosion and delamination) on the behavior of steel-concrete composite bridges (Gheitsi and Harris 2014b).

Background of Study

Steel corrosion is an electro-chemical reaction which results in deterioration and eventual destruction of the metallic material. The rate and progress of the corrosion are affected by several factors including type of steel, surface protection, state of stress, and the environmental conditions (i.e. presence of chemicals, temperature, humidity, and airborne pollution). Corrosion in steel bridge superstructures is classified in many forms such as uniform corrosion, crevice corrosion, and deposit attack (Kulicki et al. 1990). Fig. 4-1 illustrates these general

classifications, but it is well recognized in transportation community that girder corrosion is mostly to occur at end span locations due to chemicals such as deicers and water leaking from the deck joints or from salt spray caused by passing vehicles. Moreover, crevice corrosion can occur at any location along the length of the bridge between the concrete deck and steel girder, as a result of moisture penetration through the cracked concrete deck. Deposit attack due to debris accumulation or bird roosting can also occur at the web-flange connection corner. The corresponding deteriorating mechanisms typically consist of section loss or thickness reduction in the flange and web plates. These deteriorating conditions may significantly reduce the load-carrying capacity of the degraded member and eventually the bridge system, due to localized failure mechanisms such as local buckling, web crippling or crushing of the end stiffeners.

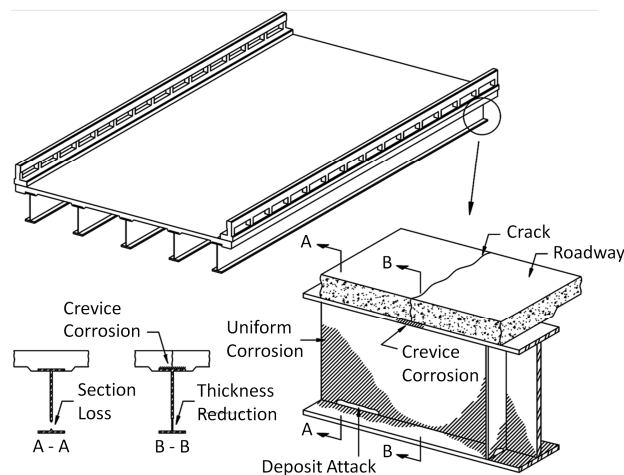


Fig. 4-1: Corrosion-induced damage scenarios

In the last few decades, corrosion has received a lot of attention to understand its detrimental effects on the serviceability of deteriorated structures and accommodate appropriate maintenance practices to reduce the cost imposed to the preservation community. Several research studies were conducted to evaluate the residual capacity of the corroded steel girders (Dunbar et al. 2004, Liu et al. 2011, Rahgozar 2009, Sharifi and Paik 2011, van de Lindt and Ahlborn 2005). In a recent experimental study, Kim et al. (2013) conducted shear failure tests on a series of fabricated stringers with variations in the height, depth, and pattern of the web corrosion, to evaluate the shear buckling behavior and strength of the locally corroded plate girders. Their investigation demonstrated that corrosion would decrease the shear buckling strength by over 10% compared to the intact girder, while the separation in the web-flange connection due to

excessive corrosion would result in about an 80% reduction in shear capacity. Following this experimental investigation, a non-linear FE analysis was performed (Ahn et al. 2013a, b) to study the shear buckling failure modes and post-buckling behavior of the tested web panels with various corrosion patterns and web boundary conditions.

Much of the investigations performed thus far to assess the safety of the corroded bridge superstructures were limited to the individual behavior of the girder with deteriorated web panels, while neglecting the bridge system-level performance and the inherent redundancy. In current preservation practices (AASHTO 2011), there exists a lack of baseline behavior characterization for in-service bridges beyond the component-based behavior assumed in design methodology (AASHTO 2012), especially when the damage is present. An accurate measure of the system safety requires a comprehensive understanding of the concept of redundancy and how it would be influenced by different damage mechanisms.

Research Significance

This paper builds from this foundation of research with an objective of understanding the complex bridge system-level interaction and characterizing the influence of corrosion in steel girders on the system safety, redundancy, and performance of in-service bridge superstructures. This study has been limited to composite steel girder bridges, as they represent one of the most common structure types in service (FHWA 2013), but the proposed approach is generic, allowing for extrapolation across other bridge types in the inventory having a wide variety of structure types, component materials, existing conditions, and operational environments. This investigation proposes a first step in a philosophy change aimed at establishing damage-integrated baseline system performance measures, from which preservation decisions can be made for in-service bridges.

Investigation Approach

With the limited data available on the ultimate capacity testing of in-service bridges with damage present, computational modeling provides a rational alternative to study the performance of intact and damaged bridge superstructures. However, there are certain challenges that must be properly treated to yield comprehensive and representative results. For a robust system-level evaluation, it is necessary to integrate material characteristics, damage models, as well as element and system-level behavior into a composite model that describe their interaction. Given

the lack of quantitative understanding with regards to the system-level behavior of bridge superstructures, this investigation aims to describe a rationale for linking these components together and also provide a quantitative measure for describing the performance of deteriorated bridges.

To accomplish this goal, the investigation approach of this study has been categorized into four different phases; Fig. 4-2 illustrates the schematic of the proposed performance-based numerical modeling framework. Numerical models of the intact and damaged structural components and systems have been developed in the commercial FEA package, ANSYS (2011), based on the existing literature. Model accuracy and validity for the numerical results obtained from each phase were evaluated through a comparison of corresponding experimental data. It should be noted that the results presented here for phases I-III are a representative summary of the analyses performed within the proposed framework. Further details on the selected cases, modeling approach, and validation process are presented in the previous works (Gheitasi and Harris, 2014a and c).

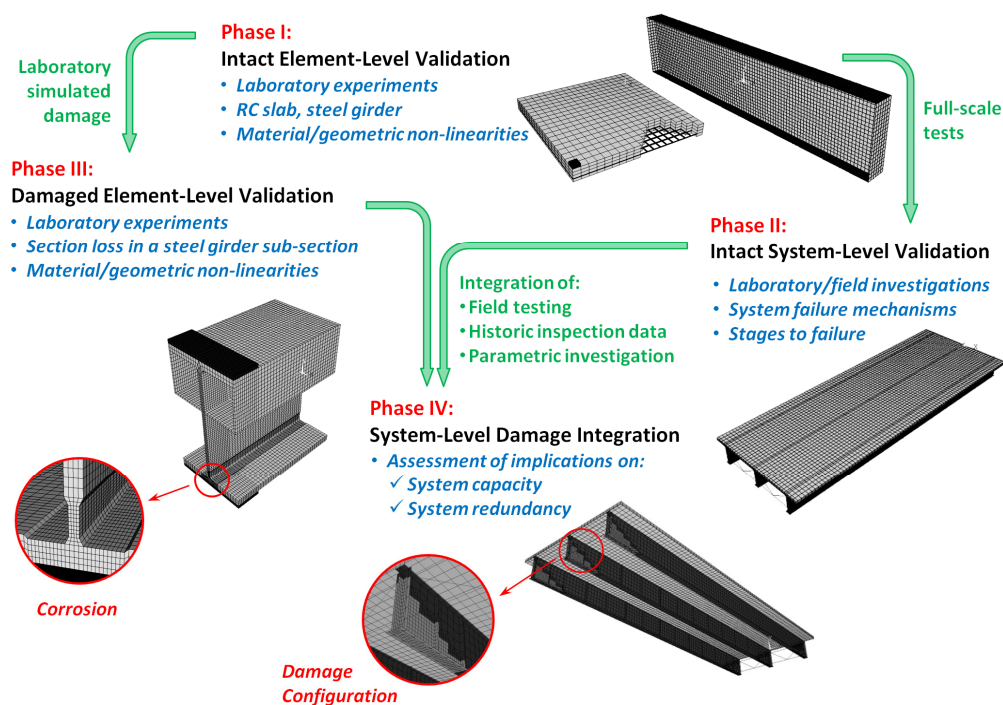


Fig. 4-2: Schematic representation of the proposed framework

Phase I: Intact Element-Level Validation

The first phase focuses on the development of undamaged element-level numerical models representing the main structural components of the bridge system. In the selected genre of bridges, reinforced concrete slabs and steel girders are the main components that comprise in the load-carrying mechanism of the bridge system. Two representative experimental investigations on a corner-supported two-way reinforced concrete slab and a simply-supported steel girder were selected in this study to validate the full non-linear (material and geometric) element modeling approach, thus providing confidence for element integration into the system-level models.

In an experimental study, McNeice (1967) performed a scaled test on a square reinforced concrete slab. The slab was supported at four corners and tested under a central concentrated load. Due to the symmetry of the structure in geometry and loading conditions, only one quarter of the slab was modeled in this study (Fig. 4-3a). In another study (Lagerqvist 1995, Johansson and Lagerqvist 1995), a series of experimental investigations were conducted on simply-supported high strength steel plate girders under lateral patch loading. Among all specimens, a girder with geometrical configurations illustrated in Fig. 4-3b, was chosen in this study for model development and validation. Appropriate material constitutive relationships with suitable failure criteria were included in each model to account for the material non-linearities including inelastic stress-strain relationships, cracking and crushing of the concrete, as well as yielding and strain hardening of the steel component. For the steel girder, geometric non-linearity was also included in the analysis (Tryland et al. 1999) to allow for the development of local instabilities which often dominate the behavior of thin-walled structures (Alinia et al. 2009 and 2011).

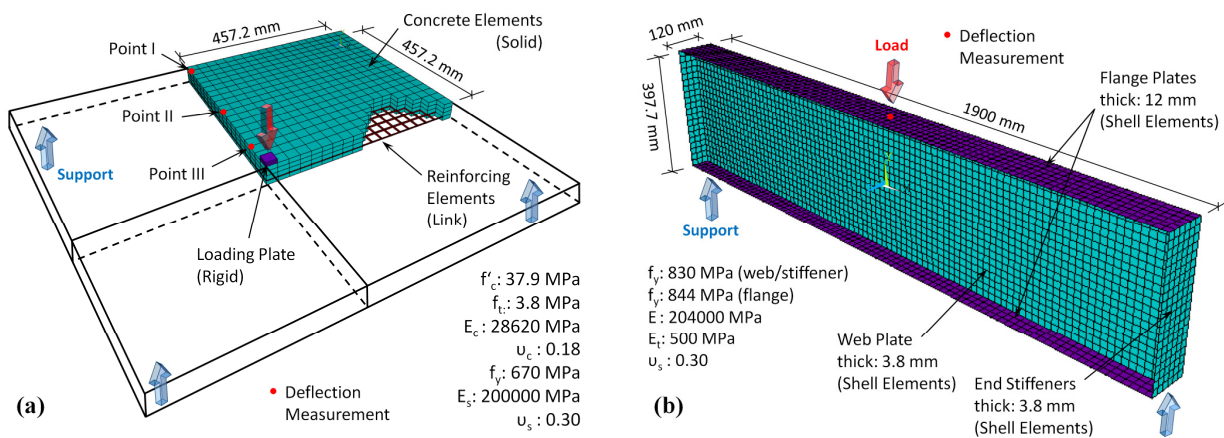


Fig. 4-3: Intact element-level FE model development (a) concrete slab, (b) plate girder

Displacement-controlled static analysis with the Newton-Raphson non-linear solution algorithm was used in the analysis. Load-deflection responses at predefined nodes (see Fig. 4-3) were derived from the numerical analysis and compared to the corresponding experimental outcomes for validation (as illustrated in Fig. 4-4). For the concrete slab, the proposed model was able to predict the first cracking load of 5 kN, compared to the corresponding experimental value of 5.33 kN. Beyond the cracking point, there are some discrepancies between the results; however, the FE model predicts the general reduction in structural stiffness and global behavior. Although the experiment was limited to study the serviceability of the slab, the numerical analysis was expanded to capture the ultimate capacity of this component. For the steel girder, on the other hand, the proposed model was able to capture the ultimate capacity and failure mode (web local buckling) of this structural element. The FE model predicts the ultimate capacity of 310.7 kN, compared to 310 kN obtained in the lab test. Additional details on the numerical modeling approach within the intact element-level domain are presented elsewhere (Gheitasi and Harris 2014a, see Appendix A-C).

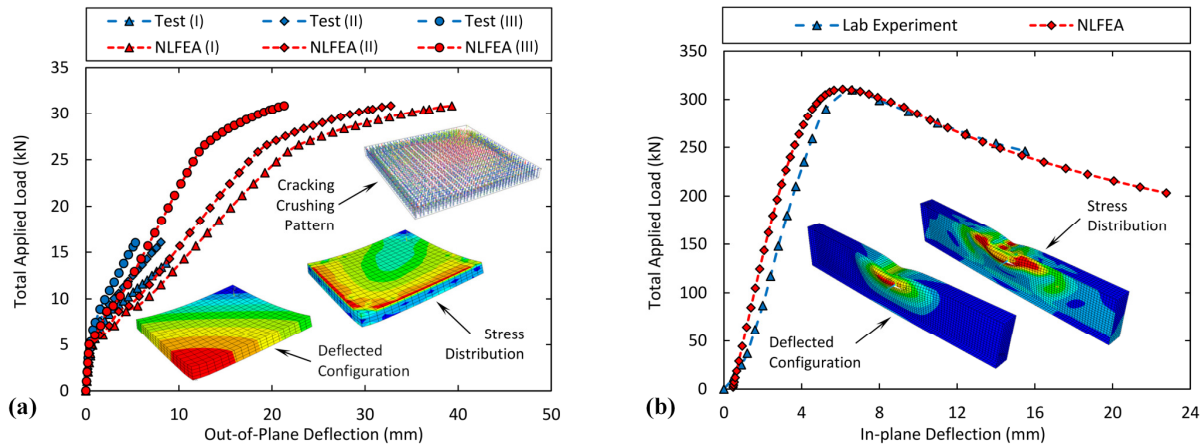


Fig. 4-4: Intact element-level validation (a) concrete slab (b) steel girder

Phase II: Intact System-Level Validation

Phase two focuses on the development of system-level numerical models for intact bridge superstructures to understand their non-linear behavior, failure characteristics, and correlation with the expected element-level response. The primary challenge associated with model validation of bridges is the limited pool of complete experimental datasets available in the literature (e.g. Kathol et al. 1995, Burdette and Goodpature 1971, Bechtel et al. 2011). The

outcome of this phase will be essential to the latter stages of the investigation as it provides a baseline for as-designed behavior from which actual in-service behavior can be referenced to define the influence of damage and deterioration (phase IV).

Results from full scale destructive tests on a simply-supported steel girder bridge (Kathol et al. 1995) and a four-span continuous composite girder bridge (Burdette and Goodpature 1971) were used in this study to accomplish the goal of the second phase. However, only results obtained from numerical investigation of the simply-supported bridge superstructure (Kathol et al. 1995) are presented herein. Fig. 4-5a illustrates the FE model developed for this bridge superstructure. All of the structural components including the concrete deck, flexural reinforcement, steel girders, lateral bracings, composite action between deck and girders were accurately modeled with the material and section properties given in the test. The model was restrained with hinge and roller supports at the ends and loaded with a series of concentrated loads applied over patch areas.

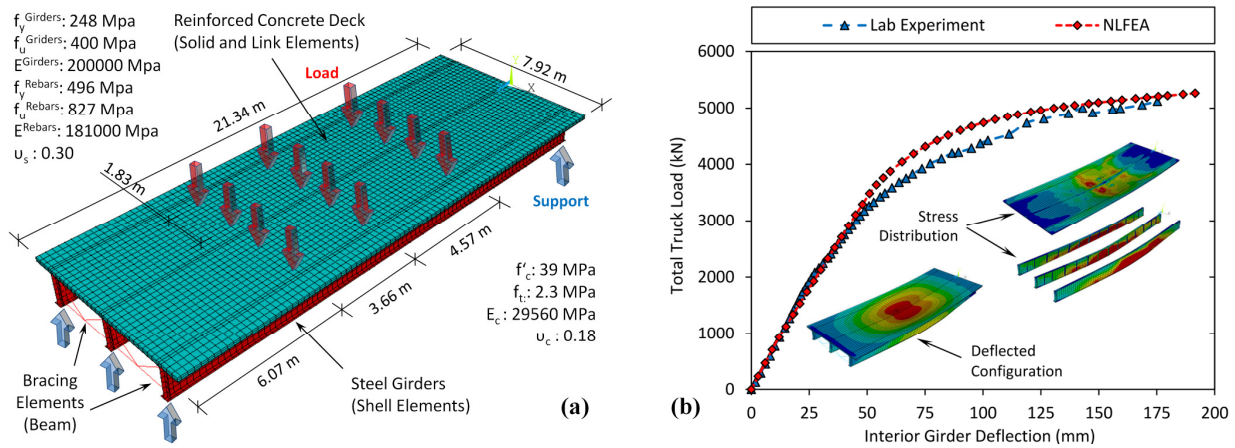


Fig. 4-5: Intact system-level simulation (a) FE model development (b) validation

Load-controlled non-linear static analysis was implemented. Interior girder deflection at mid-span of the bridge was used to validate the proposed numerical model. As illustrated in Fig. 4-5b, results obtained via non-linear FE analysis correlated well (less than 8% error) with the experimental outcome. The proposed FE model captures the punching shear failure mechanism in the system that terminated the corresponding laboratory experiment. The outcome of this phase was a fundamental understanding of the intricacies necessary for a robust modeling and behavioral characterization of this type of bridge superstructures. Further details on the modeling

assumptions and discussion on behavioral characteristics including stages to failure and girder distribution behavior in composite steel girder bridges are presented elsewhere (Gheitasi and Harris 2014c, see Appendix D).

Phase III: Damaged Element-Level Validation

With the limited test data that exists on the behavior of bridge structures with accumulated damage, the development of modeling strategies for integrating damage at the element-level provides a suitable alternative. Despite the variety of sources that may cause each damage scenario, from a mechanics perspective it is their influence on the structural behavior that is of primary concern. As a result, the third phase of the proposed framework aims to establish a fundamental understanding to characterize the impact of damage and deteriorating mechanisms on the individual bridge components. In this study, the validation of the damage was limited to girder corrosion, but the process described can be used for other damage mechanisms.

Results from a comprehensive experimental investigation conducted at Michigan Technological University to characterize the influence of end deterioration on the capacity of degraded sub-sections of wide flange beams (van de Lindt and Ahlborn 2005) was used in this study for model development and validation. Fig. 4-6a illustrates the geometrical configurations in the developed FE model of the selected specimen. In the experimental program, the stiffening plates welded to the top flange and upper portion of the web were attached to simulate the influence of a deck or other mechanisms which provide rotational restraint and force the buckling to occur at the lower portion of the web where damage exists.

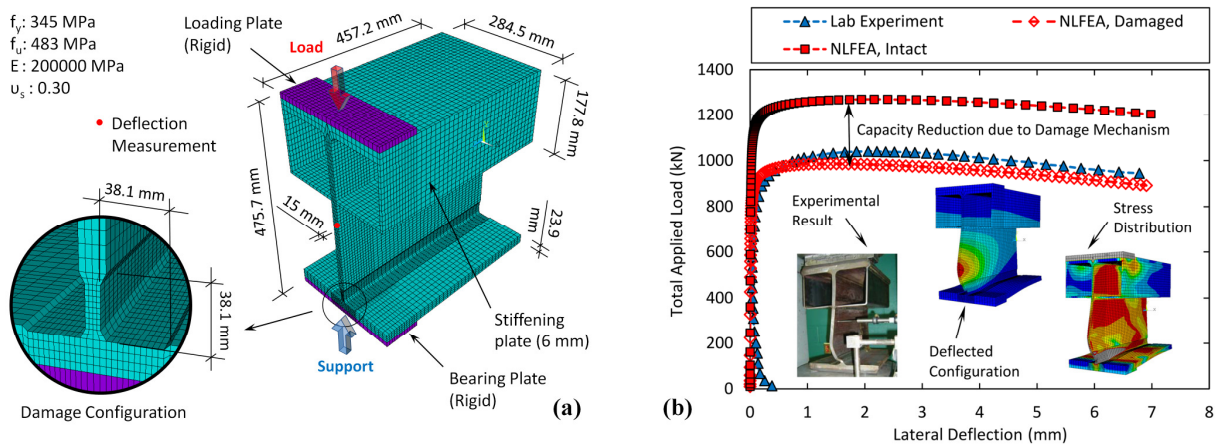


Fig. 4-6: Damaged element-level simulation (a) FE model development (b) validation

Two FE models were created to assess the intact and damaged conditions of the selected specimen. Displacement-controlled non-linear static analysis was implemented considering both material and geometric non-linearities. Out-of-plane deflection at the mid-height of the section was used in this study to validate the proposed damaged model. As illustrated in Fig. 4-6b, the FE model predicts the ultimate capacity at the load level of 986 kN, which is consistent with the experimental value of 1040 kN (5% error). The modeling approach allowed for simulation of combined global-local buckling failure that was observed in the experiment. Moreover, comparing the numerical results of intact and damaged models demonstrated the magnitude of the influence of the section loss damage mechanism on the load-carrying capacity of this element. Additional details on the numerical modeling approach within the damaged element-level domain are presented elsewhere (Gheitsi and Harris 2014a).

Phase IV: System-Level Damage Integration

The first three phases aimed to establish a comprehensive foundation on the model development and damage integration strategies, which were essential to the body of the proposed framework. Upon completion, the damage modeling strategies along with the established understanding of the intact system-level behavior and interaction among sub-components can be integrated into the measure of system performance to characterize the impact of deteriorating conditions on the ultimate capacity, redundancy, and operational safety of any given bridge superstructure.

System Safety Assessment

Current load rating practices of in-service structures are limited to the element-level evaluation, where the overall performance of the deteriorated bridge system is extrapolated from the individual behavior of the main load-carrying members under the influence of specific type of damage. In this approach, however, the interaction between structural components of the bridge system, which causes the inherent redundancy, is embedded in the analysis in terms of distribution factors which is overly simplistic. According to the AASHTO specifications (2012), a structure is classified as non-redundant if failure of a single element results in the collapse of the structure. In other words, bridge redundancy can be defined as the capability of the superstructure system to carry loads and continue its functionality after damage or failure occurred in one of its members. As a result, the level of safety in a given bridge superstructure

has a direct correlation with the concept of system redundancy. The investigation approach presented in NCHRP Reports 406 and 776 (Ghosn et al. 1997 and 2014) is used in this study to evaluate the redundancy in highway bridge superstructures.

Methodology – NCHRP Approach

The direct analysis method proposed by Ghosn et al. (1997 and 2014) has the potential to evaluate the safety of highway bridges and provide a quantitative measure of system redundancy. Based on this study, a bridge system is considered safe if it can satisfy the following criteria: (1) provide a reasonable safety level against first member failure; (2) not to reach its ultimate capacity under extreme loading conditions; (3) not to produce large deformations under expected loading scenarios; and (4) be able to carry some traffic loads after damage occurred to a component. These criteria define the limit states that are required to be checked for safety assessment of any bridge superstructure.

Each limit state must satisfy a target system safety criterion. These target values were calculated using structural reliability analysis of numerous in-service bridges, which according to current practice, are believed to provide adequate level of redundancy. Using incremental non-linear analysis, the capacity of a bridge superstructure to carry live loads before these limit states are reached can be defined as proportional factors that are multiples the weights of the trucks which can be applied on the system. These multipliers are referred herein as the load factors, LF. The following subsections provide a brief summary on the selected limit states and the application of the direct analysis method in evaluating the redundancy of the system.

Member failure

The member failure criterion is defined as the maximum possible truck load that a bridge superstructure can tolerate before first member failure occurs. Bridges that are not redundant may still provide high level of system safety if their main structural members are oversized. The member safety check can be performed by comparing the actual capacity of the bridge component, $R_{provided}$ (nominal capacity), to the capacity required by the design specification, $R_{required}$. The member failure load factors for both nominal and required capacities can be defined using Eqns. 4-1 and 2:

$$LF_1 = \frac{R_{provided} - D}{L} \quad (4-1)$$

$$LF_{1\ required} = \frac{R_{required} - D}{L} \quad (4-2)$$

where D and L are the dead load and live load effects on the most critically loaded member and can be defined using linear elastic analysis of the bridge system. For the live load calculation, the lateral distribution factors shall be derived for different load effects (flexure or shear) using any numerical model that can simulate the system behavior of the bridge superstructure (Hue et al. 2005, Barr and Amin 2005, Harris 2010, Harris and Gheitasi 2013). The member reserve ratio, r_1 , can then be calculated using Eqn. 4-3. Values for r_1 greater than one indicate that the selected member is overdesigned.

$$r_1 = \frac{LF_1}{LF_{1\ required}} = \frac{R_{provided} - D}{R_{required} - D} \quad (4-3)$$

Ultimate Limit State

The ultimate capacity of the intact system is defined as the maximum possible truck load that a bridge superstructure can tolerate before it collapses. In composite steel girder bridges, plastic hinging in the girders and crushing in the concrete deck can be identified as the primary failure mechanism (Ghosn and Moses 1997). The load factor that corresponds to this limit state is referred to LF_u , which can be defined using non-linear static analysis of the intact bridge superstructure considering all sources of material non-linearities (see Fig. 4-7).

Functionality Limit State

Under the effect of excessive live loading, the bridge superstructure may undergo permanent deformations that does not necessarily cause the structure to collapse, but may significantly reduce the serviceability of the system for the regular traffic. Controlling the permanent deformations in a bridge superstructure can be achieved by applying specific criteria over the maximum deflection or hinge rotation that occurs in the system. Many research studies have

been conducted to provide limits on the level of displacement that can be handled by the bridge before the regular traffic condition is violated (Galambos et al. 1992, Ghosn and Moses 1997).

A review of these investigations found that the maximum inelastic displacement is usually restricted to a value on the order of span length/100 to span length/300. These proposed displacement limits are based on engineering judgments and are consistent with experimental data obtained from destructive testing of bridge superstructures under flexural loading. However, there has been less attention to developing such criterion to describe functionality limit state under shear loading configuration, which is envisioned to be governed by out-of-plane displacement and large rotation of the girders at end span locations, as opposed to large deflection at midspan of the structure. Therefore in this study, load factor that corresponds to functionality limit state, LF_f , is defined as the maximum possible truck load that initiates material non-linearity and permanent deformation in the steel girders (see Fig. 4-7). Performing non-linear structural analysis, this approach has the potential to control the functionality of the intact system irrespective of the applied loading scenarios and assumed boundary conditions.

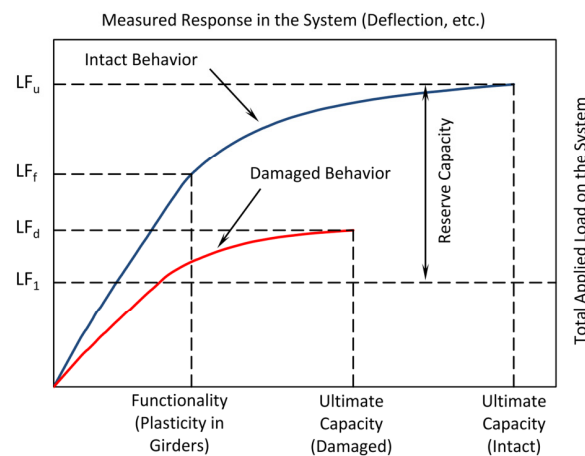


Fig. 4-7: Measure of system performance

Damaged Condition Limit State

The existence of damage mechanisms could significantly reduce the load-carrying capacity of a bridge superstructure and as a result, decrease the level of operational safety. The damaged condition limit state is defined as the maximum possible truck load that a deteriorated bridge superstructure can tolerate before it collapses. Possible damage scenarios in composite steel

girder bridges can range from localized conditions such as corrosion and section loss in steel girders or delamination in concrete deck, to complete removal of a main load-carrying element due to truck/ship collision. The load factor that corresponds to this limit state is referred to LF_d , which can be defined using non-linear static analysis on the damaged bridge superstructure considering both material and geometric non-linearities, as applicable (see Fig. 4-7).

Redundancy Factors

As the concept of redundancy relates to the capability of the structure to serve its function after damage occurs to one of its main components, a comparison of LF_1 , LF_u , LF_f , and LF_d would provide a measure of the level of redundancy. The system reserve ratios can be defined for ultimate, functionality, and damaged condition limit states as summarized in Eqns. 4-4 to 4-6:

$$R_u = \frac{LF_u}{LF_1} \quad (4-4)$$

$$R_f = \frac{LF_f}{LF_1} \quad (4-5)$$

$$R_d = \frac{LF_d}{LF_1} \quad (4-6)$$

These ratios provide deterministic measures of bridge system redundancy. To check the adequacy of the level of redundancy in a given bridge superstructure, it is required to compare the calculated system reserve ratios to a series of minimum acceptable values (target values). These values were previously defined based on examining the results of a series of in-service bridges that are clearly redundant according to the current engineering practices (Ghosn and Moses 1997). Moreover, the reliability analysis approach that was implemented to derive these minimum acceptable values would account for the uncertainties associated with determining the loads and the resistance of the bridge superstructures. Based on the performed analysis, the bridge system is considered adequately redundant if:

$$R_u \geq 1.3 \quad (4-7)$$

$$R_f \geq 1.1 \quad (4-8)$$

$$R_d \geq 0.5 \quad (4-9)$$

It is expected that the level of system redundancy for each bridge superstructure highly depends on the bridge type (material, design, geometry), but also on the existing condition states. Using the proposed approach, the redundancy factor, ϕ_{red} , for any given bridge superstructure can be defined as:

$$\phi_{red} = \min \{ r_1 \times r_u, r_1 \times r_f, r_1 \times r_d \} \quad (4-10)$$

in which r_1 is the member reserve ratio defined in Eqn. 4-3, while r_u , r_f , and r_d are the redundancy ratios for ultimate, functionality, and damaged condition limit states, respectively and can be defined as:

$$r_u = \frac{R_u}{1.3} \quad (4-11)$$

$$r_f = \frac{R_f}{1.1} \quad (4-12)$$

$$r_d = \frac{R_d}{0.5} \quad (4-13)$$

A ϕ_{red} greater than one indicates adequate level of system redundancy for the bridge superstructure under consideration, while ϕ_{red} less than one is the indication of insufficient level of redundancy for the system. The bridge superstructures that fail to satisfy this criterion are no longer safe to operate. As a result, appropriate repair strategies could be applied to strengthen the main structural components of the deteriorated bridge system until an overall satisfaction of the system reliability target is achieved (Ghosn and Moses 1997).

Application to In-service Structures

Using the described methodology together with the validation numerical modeling framework, a sensitivity analysis was performed in this study on two selected in-service bridge superstructures within the Commonwealth of Virginia to evaluate their level of redundancy and

operational safety. A detailed summary of the modeling assumptions with regards to the geometrical characteristics of the selected structures, assumed damage scenarios, and applied loading and boundary conditions is provided in the following subsections.

Selected Structures

According to the Virginia Department of Transportation (VDOT) database, there are more than 13,700 bridges in-service in the Commonwealth of Virginia, with almost 25% (~3600) of them are classified as composite steel girder bridges. Only 16% of these stringer bridges are single-span structures, while majority of them have three spans or more. Regardless of the number of spans, more than 70% of all in-service composite stringer bridges are simply-supported structures. Almost 75% of these bridges have a total length 90m (300ft) or less, while the maximum span length for more than 60% of them varies from 12 to 30 m (40 to 100 ft). For more than 75% of these bridges, the total deck width varies from 6 to 15 m (20 to 50 ft), while the skew angle is limited to 5 degrees for more than 40 % of them. Based on the common geometrical features of these in-service structures, two representative bridges were selected to perform the sensitivity study. The selected bridges were titled Aylett Bridge and Creek Bridge, and considered as representative structures to demonstrate the effect of corrosion in steel girders on the performance of the system.

The first selected bridge, Aylett bridge, is a simply-supported five-span structure with the total length of 112.8 m (370 ft) operating on Mattaponi river in King and Queen county, Virginia. Only the first span of the superstructure was selected for the numerical investigation. The selected span is 39.6 m (130 ft) long and comprised of a 216 mm (8.5 in) reinforced concrete deck supported by five steel plate girders having a uniform transverse spacing of 2.8 m (9 ft). The second selected bridge, Creek bridge, is a simply-supported three-span structure with a total length of 36.6 m (120 ft) serving over the Piscataway Creek in Essex county, Virginia. Only the second span of the superstructure was selected for the numerical investigation. The selected span is 12.2 m (40 ft) long with and comprised of a 216 mm (8.5 in) reinforced concrete deck supported by six rolled steel girders having a uniform transverse spacing of 2.2 m (7 ft – 2 in). All the structural details for the selected structures regarding the deck reinforcement layout, lateral bracings, and section properties were derived from the Virginia Department of Transportation plans and are illustrated in Fig. 4-8.

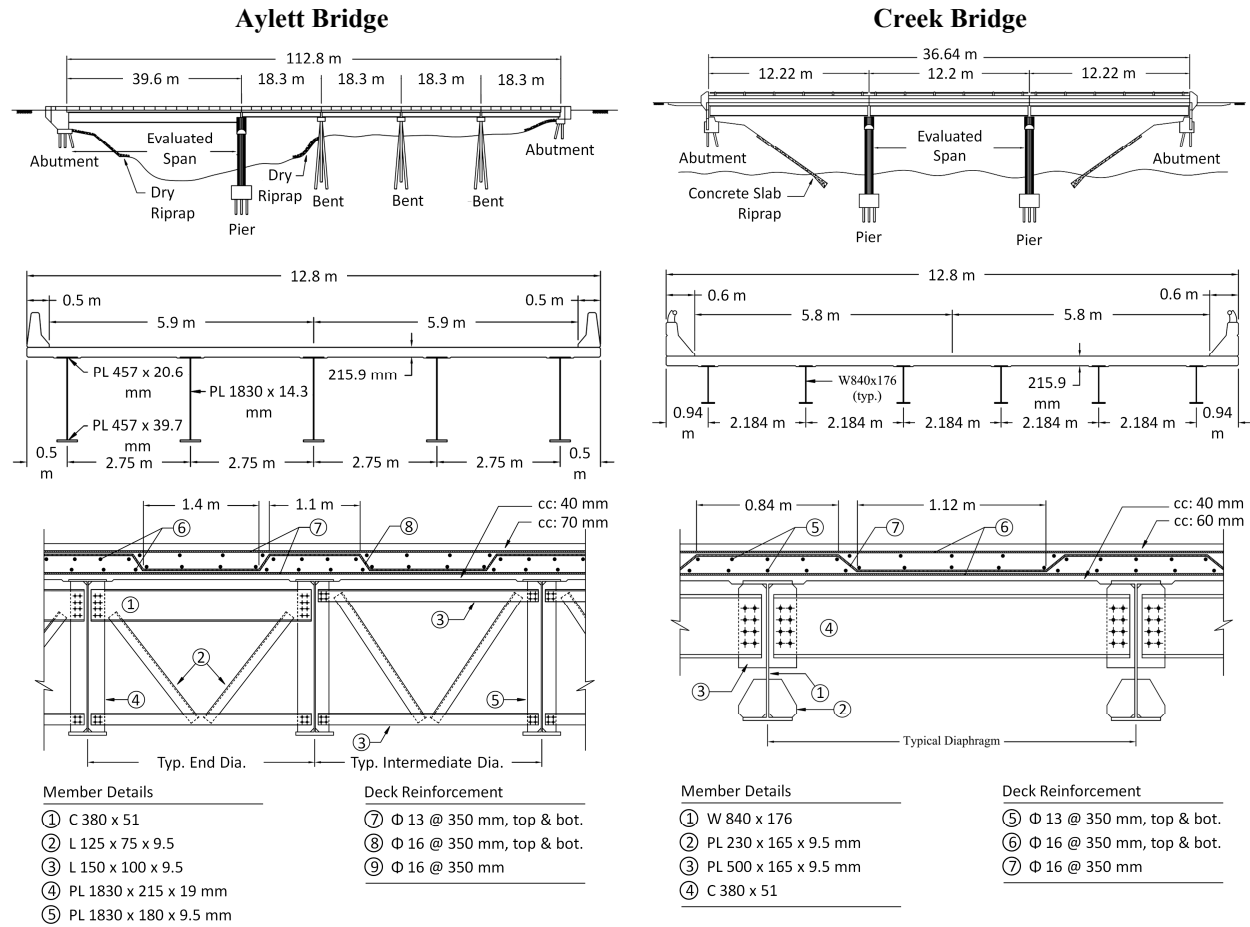


Fig. 4-8: Geometrical characteristics of the selected bridges

Damage Scenarios

Current NBI inspection methods (FHWA 2012) evaluate the average condition of bridge components based on a qualitative rating. This rating ranges from 0 to 9 with 0 being the worst and 9 being the best for the entire element. However, accurate assessment of overall bridge system behavior requires more specific data regarding damage conditions and a qualitative measure of their extension. In this study, a series of damage scenarios were selected based on a questionnaire submitted to the VDOT engineers to collect more details on the existing corrosion damage mechanisms of in-service structures in nine different districts across the state. Fig. 4-9 illustrates the damage cases used in this study, which were derived from the synthesis of the questionnaire. As illustrated, the selected damage scenarios have the potential to integrate the effect of variations in the shape, extent level, and depth of corrosion in girders on the performance of the system. The corresponding range of variation was assumed based on the

minimum, maximum, average of the damage level observed and reported by VDOT inspection professional and engineers. In all cases, it was assumed that the corrosion would occur in the support regions (either end of the girders), as many of the corrosion problems in steel girders of composite stringer bridges have been exclusively reported in these areas due to leaking joints, chemical exposure, high moisture level, poor air circulations, and accumulation of sediments and deposits.

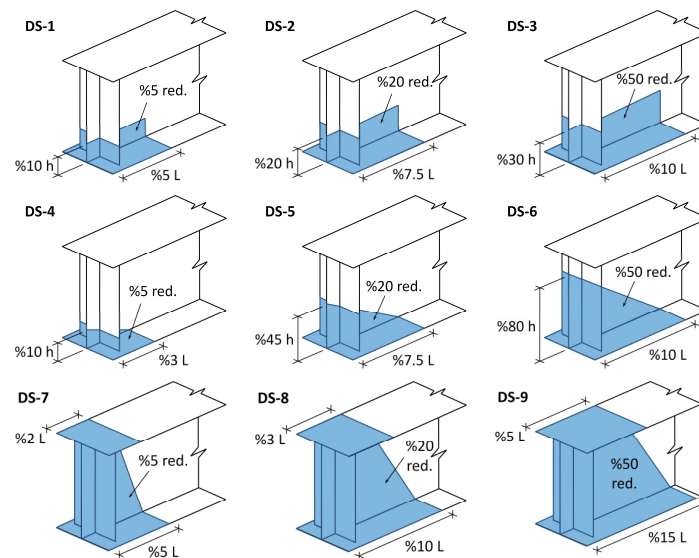


Fig. 4-9: Selected damage scenarios

Model Development and Updating

With the modeling approach validated in phase II, FE models were generated for the selected structures. In these models, material properties including the compressive strength of the concrete as well as the yield stress and ultimate strength of the steel components were extracted from VDOT plans. To update these models with the assumed damage mechanisms, the mesh of the girders in the vicinity of the supports was refined to allow for the accurate simulation of the corrosion pattern (see Fig. 4-10). As validated in phase III, the assumed damage scenarios were integrated in the models by reducing the thickness of the corroded regions in the web, flanges, and stiffener plates.

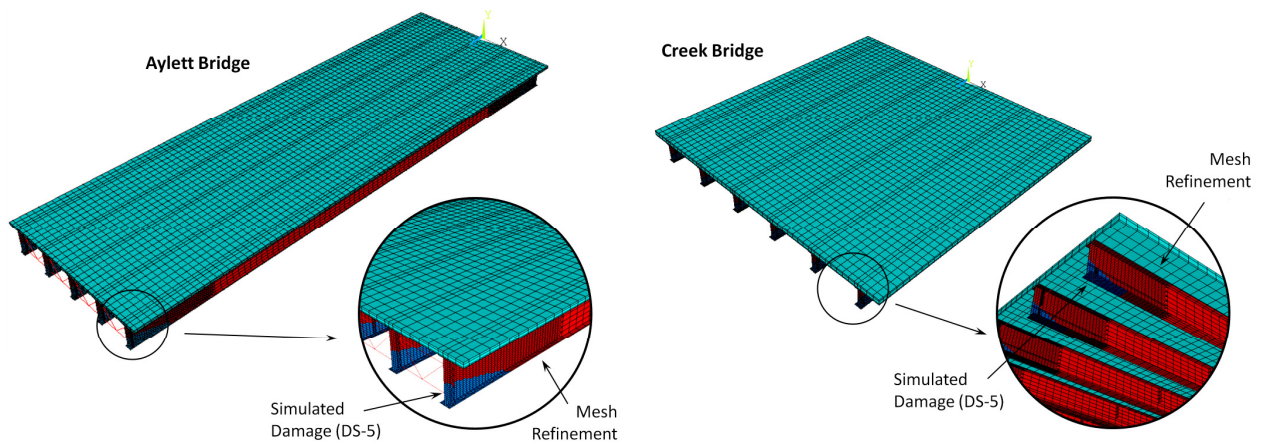


Fig. 4-10: Developed FE models with integrated damage for the selected structures

Although in actual practices the amount of corrosion could vary from one girder to another, identical states of damage were assumed for all of the girders at both ends in this investigation. It should be noted that the corresponding damage configurations are ideal representations of actual quantities and were selected to demonstrate the applicability of the proposed modeling framework. With improvement in the non-destructive inspection techniques, more refined values with regards to the damage parameters can be provided and integrated in the corresponding models, but this was beyond the scope of this investigation.

Both of the developed models were restrained with pin and roller supports at either ends to mimic the actual boundary conditions of the simulated spans of the representative structures. Although accumulation of corrosion product would likely change the support behavior from the ideal as-designed conditions and add partial fixity, the refinement of the boundary conditions was not considered in this investigation due to lack of sufficient data on the amount of fixity that would be provided under each cases of the assumed damage scenarios. Additional discussion on the impact of variations in boundary conditions on the non-linear behavior and load-carrying capacity of composite steel girder bridges are provided elsewhere (Gheitasi and Harris 2014d).

Regarding the loading conditions, two side-by-side AASHTO HS-20 trucks were considered in this study. This loading configuration is believed to be the governing condition for simple span bridges based on the assembled loading scenarios during the calibration of AASHTO LRFD specifications (Ghosn and Moses 1997). The bridge models with both intact and damaged conditions were loaded in shear and flexural configurations, in which the trucks are positioned at mid-span and close to the supports to cause maximum flexural moment and reaction forces,

respectively. In the transverse direction, however, trucks were assumed to be centered within the traffic lanes of the selected superstructures as they are serving. All sources of material non-linearities in both concrete and steel components were included in the analysis. With the refined mesh of the girders at both ends, the geometric non-linearity was also included in the analysis to account for any possible lateral instability of the girders in the corroded regions that may influence the performance and capacity of the selected structures.

Results and Discussion

The selected structures with both intact and damaged configuration were analyzed using the validated numerical modeling approach, presented within the proposed framework. Tables 4-1 (Aylett Bridge) and 4-2 (Creek Bridge) summarize the system reserve and redundancy ratios for these bridge superstructures considering flexural and shear loading scenarios. For each case, the corresponding ratios for member failure, ultimate capacity, and functionality limit states were derived using AASHTO LRFD specifications together with non-linear analysis of the intact systems. For the damaged condition limit state, the reserve and redundancy ratios were calculated separately for each individual damage scenario. Comparing results obtained from the non-linear (material and geometric) analysis demonstrates that the shape of assumed damaged conditions (i.e. rectangular, triangular, and trapezoidal) has negligible impact on the ultimate capacity of the system. However, the extent level of the corrosion attack and the amount of thickness reduction in the girders dominate the behavior and capacity of the selected deteriorated structures.

It should be highlighted that reduction in the load-carrying capacity of the system has a direct correlation with not only the integrated damage conditions, but also with the geometry of the structure and the assumed loading scenarios. As a case in point, variations in the damage configuration have negligible impact on the capacity of the Aylett bridge under the flexural loading. As it was demonstrated in phase III, the capacity of deteriorated thin-walled structures are usually governed by local failure mechanisms, which could be a combination of geometrical instability and material non-linearity. When compared to the shear loading scenario, the applied loads are further from the location of the deterioration when the Aylett bridge is subjected to the flexural loading. This distance between load and damage locations minimizes the local effects and justifies the lower sensitivity of the system behavior to the variations in damage configuration. In Creek bridge, however, the system capacity is significantly affected by

assumed damage conditions under the both loading scenarios due to shorter span length and relative location of the applied loads to the corroded region.

Table 4-1: Redundancy ratios for the Aylett bridge

Shear Loading						Flexural Loading					
Intact System		Damaged System				Intact System		Damaged System			
$V_{required}$	316 k	Case	LF _d	R _d	r _d	$M_{required}$	8504 k.ft	Case	LF _d	R _d	r _d
$V_{provided}$	902 k	DS-1	18.34	2.26	4.52	$M_{provided}$	12701 k.ft	DS-1	13.45	2.65	5.31
r _l	3.58	DS-2	15.34	1.89	3.78	r _l	1.74	DS-2	13.42	2.65	5.29
LF _l	8.12	DS-3	9.62	1.18	2.37	LF _l	5.07	DS-3	13.37	2.64	5.27
LF _u	18.97	DS-4	18.36	2.26	4.52	LF _u	14.42	DS-4	13.44	2.65	5.30
R _u	2.34	DS-5	15.26	1.88	3.76	R _u	2.84	DS-5	13.43	2.65	5.30
r _u	1.80	DS-6	8.92	1.10	2.20	r _u	2.19	DS-6	13.39	2.64	5.28
LF _f	12.14	DS-7	18.10	2.23	4.46	LF _f	10.00	DS-7	13.44	2.65	5.30
R _f	1.50	DS-8	15.16	1.87	3.73	R _f	1.97	DS-8	13.41	2.64	5.29
r _f	1.36	DS-9	8.82	1.09	2.17	r _f	1.79	DS-9	13.30	2.62	5.25

Table 4-2: Redundancy ratios for the Creek bridge

Shear Loading						Flexural Loading					
Intact System		Damaged System				Intact System		Damaged System			
$V_{required}$	144 k	Case	LF _d	R _d	r _d	$M_{required}$	1054 k.ft	Case	LF _d	R _d	r _d
$V_{provided}$	361 k	DS-1	8.66	1.80	3.59	$M_{provided}$	2479 k.ft	DS-1	13.51	2.37	4.75
r _l	2.80	DS-2	7.48	1.55	3.10	r _l	2.72	DS-2	12.63	2.22	4.44
LF _l	4.82	DS-3	4.46	0.93	1.85	LF _l	5.69	DS-3	7.78	1.37	2.73
LF _u	8.92	DS-4	8.70	1.80	3.61	LF _u	13.90	DS-4	13.23	2.33	4.65
R _u	1.85	DS-5	7.06	1.46	2.93	R _u	2.44	DS-5	10.94	1.92	3.85
r _u	1.42	DS-6	4.17	0.87	1.73	r _u	1.88	DS-6	5.71	1.00	2.01
LF _f	5.32	DS-7	8.42	1.75	3.49	LF _f	9.36	DS-7	13.40	2.36	4.71
R _f	1.10	DS-8	7.02	1.46	2.91	R _f	1.64	DS-8	11.01	1.93	3.87
r _f	1.00	DS-9	4.19	0.87	1.74	r _f	1.50	DS-9	5.73	1.01	2.01

Table 4-3 summarizes the redundancy factors defined for the selected structures based on the methodology proposed by Ghosn et al. (NCHRP 1997, 2014). In both bridge systems, the minimum redundancy factor obtained from flexural and shear loading scenarios are greater than one. This would indicate the overall safety of the selected structures for continuous operation under the assumed damaged conditions. It should be however noted that these factors are exclusively attributed to the assumed loading scenarios and damage conditions. Nevertheless, the

procedure is applicable for any other loading scenario with regards to the number of trucks, truck location, and even truck configuration (Gheitasi and Harris 2014d). Moreover, damage scenarios with different extent levels as well as other types of deteriorating conditions associated with this type of bridge superstructures can be integrated into the proposed numerical modeling framework to evaluate the safety of the selected structures (Gheitasi and Harris 2014d).

Table 4-3: Redundancy factors for the selected structures

Bridge	Loading Scenario	Redundancy Factor (ϕ_{red})
Aylett	Shear	4.87
	Flexural	3.13
Creek	Shear	2.81
	Flexural	4.07

Conclusions

This study aimed at representing a conceptual schematic of a computational modeling strategy for evaluating the operational safety of in-service bridge superstructures in the presence of common deteriorating mechanisms. The finite element method was selected as the primary tool for studying these phenomena with numerical models generated from the basic levels of intact bridge components to more complicated stages with deteriorated bridge systems. Extensive experimental data in literature, along with rational modeling assumptions were included in the study to validate the accuracy and consistency of the numerical modeling approach.

Upon validation, a direct analysis approach was implemented to study the behavior of two representative in-service bridge structures within the Commonwealth of Virginia under the impact of corrosion in steel girders. Results obtained from a sensitivity study of over forty cases demonstrated that the selected structures provide adequate amount of system safety in the presence of assumed damage mechanisms. Moreover, it was highlighted that the shape of the corrosion damage has less influence on the behavior of the structure, while the extent level of the damage mechanism would significantly reduce the load-carrying capacity of the structure.

The numerical modeling approach implemented in the proposed framework also has the potential to explore the implication of advances in material, design methodologies and construction practices on the performance of in-service bridges with different structural systems

and deteriorating conditions. By updating the developed numerical model based on biennial inspection data, degradations in the structural performance can be monitored and evaluated over time. Extrapolating the degradation trend through the design life of the structure would help the bridge owners to estimate remaining service life of the bridge system. Given the condition state of the in-service bridges nationwide along with the shrinking budgets of the transportation agencies to maintain and repair all the deficient structures, the proposed framework has the potential to complement the recent efforts in developing appropriate repair techniques (Ahn et al. 2013c, Fam et al. 2009, Narmashiri et al. 2012) to increase the functionality and service lives of deteriorated in-service structures.

Chapter 5:

Performance Assessment of Steel-Concrete Composite Bridges with Subsurface Deck Delamination

(Elsevier, Structures, under review, 2014)

Summary

In-service composite steel girder bridges typically experience a variety of deterioration mechanisms during their service lives, ranging from cracking, spalls, and delaminations in the reinforced concrete deck to corrosion in the steel girders. To date, several innovative inspection techniques and novel technologies are widely being implemented to identify and measure different sources of defects associated with bridge systems, especially within the concrete deck. Despite successful implementation of these evaluation methodologies, what is lacking is a fundamental understanding of the system-level behavior and the potential impact of the identified deterioration conditions on the overall performance of the bridge superstructures.

In this paper, the impact of corrosion-induced subsurface deck delamination on the overall behavior and performance of steel-concrete composite bridges was investigated. Using the commercial FE package, ANSYS, a sensitivity study was performed to investigate the influence of variations in different damage parameters on the nonlinear behavior, ultimate capacity and overall ductility of the bridge system. The accuracy and validity of the implemented modeling approach was also assessed via comparing the numerical results with available experimental data in the literature. Results obtained from the performed nonlinear FE analyses demonstrated that the deck delamination has negligible influence on the nonlinear behavior of the system and evolution of material nonlinearities. However, loss in composite action between the concrete and reinforcing rebars would cause local crushing on the deck surface, which dictates premature failure and reduction in ultimate capacity and overall ductility of the system.

Introduction

State of Practice

Bridges represent one of the most critical components within the U.S. transportation network. Generally, the occurrence of bridge failures is somewhat rare, and most often it is related to

unforeseen natural and man-made hazards such as impacts, fire or flooding (Kumalasari and Fabian (2003). However, it is the condition states of aging in-service bridges that plague the health of the national infrastructure in the United States. Considering the various operational conditions, in-service bridges are subjected to temporal damage and deterioration mechanisms once they are put into service. According to the national bridge inventory (FHWA 2013), almost 10% of over 600,000 bridges in-service in the United States are categorized as structurally deficient. While it is not feasible to immediately repair all of the deficient in-service bridges, this deteriorating condition does underscore the importance of quality inspection and performance assessment mechanisms to prioritize the repair efforts.

Challenges for Composite Steel Girder Bridges

The main types of deterioration that composite steel girder bridges experience have been well documented in recent years (FHWA 2012) with challenges observed in both the primary load-bearing girders and the deck. Much of the degradation in the steel girders manifests as corrosion and section loss, which is often caused by exposure to chemical-laden solutions resulting from leaking expansion joints or roadway spray. Furthermore, reinforced concrete decks suffer from a variety of deteriorating conditions associated with cracking due to the low tensile resistance of the concrete material. These cracks would provide direct pathway for chloride and moisture penetration and allow for accelerated exposure, which eventually leads to corrosion in the reinforcement. Once initiated, the corrosion by-products can occupy up to 10 times the volume that it replaces (FHWA 2012), and create internal pressures resulting in longitudinal surface cracks, delaminations, and spalls (see Fig. 5-1).

Several recent studies have focused on developing applicable methodologies to measure different sources of defects associated with bridge structures, especially within the deck system which suffers the most from deteriorating conditions. Among those, are the innovative inspection techniques and novel technologies (Lynch and Loh 2006, Pakzad et al. 2008, Vaghefi et al. 2012 and 2013), which are widely being implemented to identify the visible deteriorations and improve the confidence in locating internal degradation mechanisms. However, a challenge that remains is a rational use of this collected data for decision-making regarding long-term preservation strategies of the deteriorated structures. In fact, what is still lacking is a fundamental understanding of the potential impact of these identified deterioration mechanisms on the system-level behavioral characteristics, functionality and overall performance of in-service

bridges. The development of this correlation would provide transportation officials with a rational mechanism to estimate the safety and a remaining service life of the in-service structure. Among all types of damage mechanisms associated with steel-concrete composite bridges, the present study focuses on the impact of deck deteriorations, specifically delamination, on the overall performance of composite steel girder bridges.

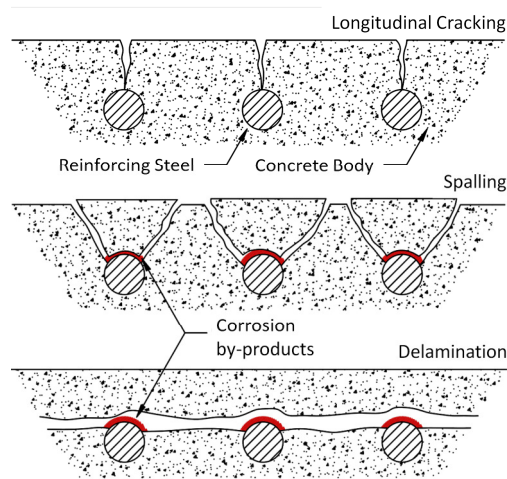


Fig. 5-1: Corrosion-induced damage scenarios

Delamination in Reinforced Concrete Decks

Within concrete bridge decks, delamination usually occurs as a result of separation in the concrete layers parallel and close to the surface at or near the outermost layer of rebars (ACI 2003). Separation of the concrete layers occurs when corrosion induced cracks join together to form a fracture plane. With a random and irregular pattern, delamination is historically considered one of the most complicated issues associated with in-service concrete structures. The location and extent level of the delaminated area not only depend on the environmental conditions, which directly dictates the corrosion rate, but are also related to the geometrical configuration of the concrete member such as cover thickness, rebar spacing and diameter. Once the delaminated area reaches the surface and completely separates from the concrete member, the resulting deteriorating mechanism is called spalling. Delamination and spalling can occur on both the top surface and underside of an operating reinforced concrete slab (FHWA 2012). Although these damage mechanisms may not cause the structure to collapse, in most cases they do have a major impact on the serviceability and functionality, while also marring the

appearance of the structure.

Background

Much of the early research on corrosion induced degradation in reinforced concrete structures focused on the development of mathematical models to represent the process of corrosion in the embedded steel rebars (Beaton and Stratfull 1973, Bažant 1979). Based on these theoretical models, several analytical studies were then performed to investigate the effect of corrosion-product buildup around rebars on the mechanical characteristics of the deteriorated RC structures (Pantazopoulou and Papoulia 2001, Li et al. 2007).

With evolution of numerical methods, several researchers focused their efforts to investigate the behavior of concrete structures considering mechanical deteriorations due to time-dependent characteristics including creep, shrinkage, fatigue, and thermal effects (Bažant 1982, Onate 1994). In addition, chemical-physical attacks on the cementitious material and steel rebars as well as their coupling effects with mechanical damage were also investigated using continuum damage mechanics (Kachanov 1986). Numerous damage models (Farja and Oliver 1993 and 1998, Saetta et al. 1998 and 1999, Berto et al. 2007) were proposed to update the stress-strain constitutive relationship of the concrete material subjected to chemical and mechanical defects.

In recent years, numerical investigations have been widely implemented to study the mechanism of corrosion induced cracking and delamination in concrete structures. Molina et al. (Molina et al. 1993) proposed a finite element (FE) model to simulate cracking in concrete specimens when subjected to corrosion of their reinforcement. In another study, Zhou et al. (2005) presented a two-dimensional FE model to predict damage propagation and corresponding failure modes (longitudinal cracking, spalling, and delamination) in the concrete cover of the bridge decks caused by corroding reinforcing bars. Chloride-induced degradation of reinforced concrete structures was also assessed by Chen and Mahadevan (2007) considering three phases of deterioration process including chloride penetration, rust expansion, and cracking in their finite element-based model. In these models, initiation and propagation of the corrosion-induced cracks in concrete material were captured using different failure criteria (e.g. smeared-cracking, damaged plasticity, William-Warnke).

In addition to the phenomenological studies, several research studies have focused on assessing the behavior and performance of corroded RC structural members (Coronelli and Gambarova 2004, Kallias and Rafiq 2010). In these investigations, nonlinear FE analyses were

implemented to model the effects of corrosion by reducing the geometry of the elements, while modifying the constitutive laws of the materials and the interface bond behavior between rebars and concrete. These modifications were generally performed based on the experimental investigations of representative specimens subjected to accelerated corrosion processes.

While the proposed numerical modeling approaches proved adequate in predicting the behavior of deteriorated RC members, their applicability in evaluating the behavior of real in-service structures is still not fully understood. Moreover, it is not possible to accurately quantify all the damage parameters required in the proposed numerical models representing the reduction in geometrical configurations and material properties. The majority of previous numerical investigations have concentrated on studying the mechanism of corrosion, crack initiation and material degradation in structural components; while in practice, most of the collected data on the location, shape, and extent level of different damage mechanisms are qualitative and usually provided through biennial inspection programs (FHWA 2012, Vaghefi et al. 2012). As a result, transportation officials are seeking to assess the overall performance and serviceability of in-service structures under the reported deterioration conditions.

This study aims to provide a fundamental understanding on the impact of subsurface deck delamination on the system behavior including both the ultimate load-carrying capacity and serviceability of composite steel girder bridge superstructures. Using this numerical analysis framework, an efficient and practical modeling approach is presented in this study, which is expected to help the preservation community evaluate the condition of in-service structures with deteriorated deck systems. The proposed approach also has the potential to determine the system-level characteristics of the girder-type bridge superstructures with both intact and deteriorated configurations. These characteristics are considered neither in the traditional design approach of girder-type bridge structures, nor in the current load rating practices (AASHTO 2011 and 2012).

Method of Study

The investigation approach used in this study was initiated with the development of a numerical model for a representative intact bridge superstructure. The intended outcome of this modeling effort was to establish a fundamental understanding of the system-level behavior, nonlinear characteristics, and the corresponding failure mechanism of the simulated bridge system. Due to the limited experimental data that exists on the behavior and ultimate capacity of bridge superstructures with accumulated damages, the development of modeling strategies for

integrating damage at the element-level domain provides a suitable alternative. Thus, the second goal of this study was aimed at establishing a numerical modeling approach to study the impact of deck delamination on the behavior of a representative reinforced concrete slab.

The commercial finite element (FE) computer package, ANSYS (2011), was used to generate the numerical models within both element-level and system-level domains. The accuracy and validity of the FE simulation and analysis were investigated through comparison of the results to available experimental data. Once the damage modeling approach was validated, it could be integrated into the validated bridge model to investigate the influence of delamination in RC slabs on the overall bridge system-level behavior. Accordingly, a sensitivity study was performed to determine the impact of variations in different geometrical and material characteristics of the damage configuration on the overall behavior of the selected system and its susceptibility to failure. Upon calibration, the proposed modeling approach was implemented to study the behavior of an actual in-service structure under the effect of deck deterioration.

FE Modeling and Analysis

The finite element method provides an efficient tool to simulate and predict the behavior of different structural systems. However, there are certain challenges with the modeling approach that must be properly treated to yield realistic results. Within the framework of this study, appropriate simulation assumptions, selection of material constitutive models, interpretation of complex system-level interaction and behavior, and damage modeling approach are some of the main challenges that were considered. The following sub-sections provide a detailed summary of the numerical simulation process implemented in this study.

Modeling of Bridge Superstructure – System Behavior

A full-scale destructive laboratory investigation of a simply-supported steel girder bridge model, performed at the University of Nebraska (Kathol et al.1995), was selected to study the system-level behavior of an intact composite steel girder bridge. Fig. 5-2a illustrates the geometrical properties of the selected bridge system. In the model (see Fig. 5-2b), the concrete slab was simulated using solid elements and discretely reinforced by link elements in two layers. Shell elements were used to model the steel girders, which were laterally braced with beam elements at the supports. Multi point constraint (MPC) elements were implemented to model the interaction between top flange of the girders and the bottom surface of the deck. Appropriate

material constitutive relationships with suitable failure criteria were included in the model. Inelastic stress-strain relationships, cracking and crushing of the concrete, as well as yielding and plasticity of the steel components (i.e. girders, rebars, and bracings) are the main sources of material non-linearities incorporated in the analysis (see Fig. 5-2c and Fig. 5-3).

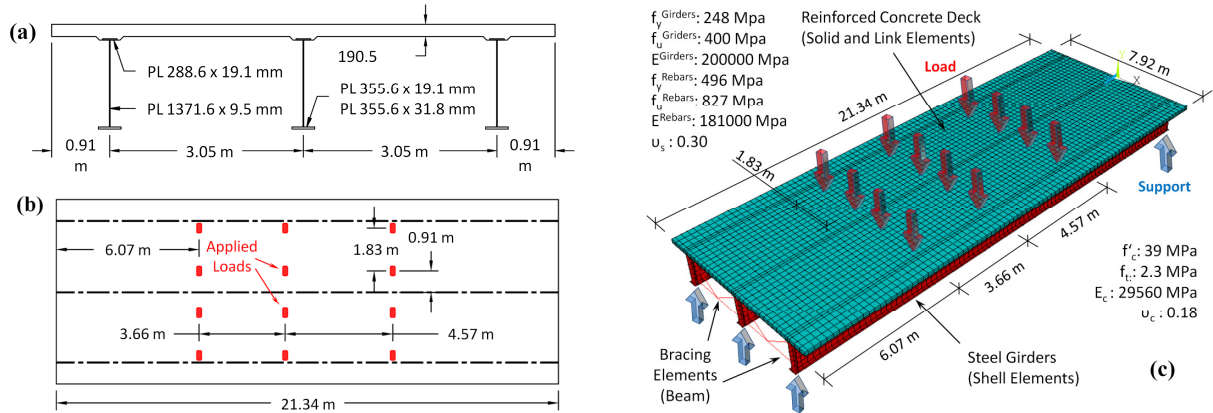


Fig. 5-2: Nebraska laboratory test (a) bridge cross section, (b) bridge plan, (c) proposed FE model

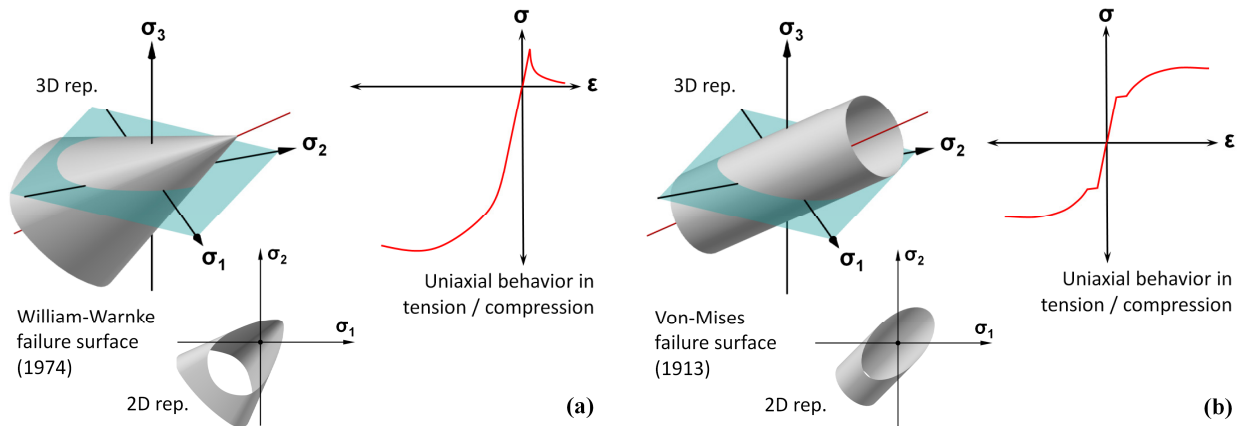


Fig. 5-3: Assumed material behavior and corresponding failure criteria: (a) concrete, (b) steel

According to the test setup, the model was restrained with hinge and roller supports at the ends and loaded with a series of concentrated loads applied over 500 x 200 mm patch areas (Harris and Gheitasi 2013) to mimic two side-by-side HS-20 trucks with modified axle spacing. The proposed FE model was analyzed using static analysis with the Newton-Raphson non-linear solution algorithm. Interior girder deflection at mid-span of the bridge is presented to demonstrate the validation of the applied modeling approach. As illustrated in Fig. 5-4, result obtained via nonlinear FE analysis correlates well with the experimental outcome within both

elastic and inelastic ranges of the behavior. The laboratory experiment on this bridge model was terminated due to a punching shear failure that occurred under one of the patch loadings. In the analysis, the model was loaded until it reached the level of nominal punching shear capacity calculated based on AASHTO LRFD specifications (AASHTO 2012). Additional details on the correlated behavior and stages to failure are presented elsewhere (Gheitasi and Harris 2014c).

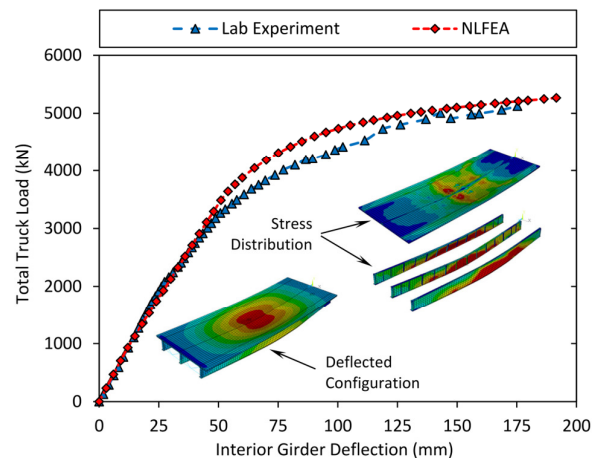


Fig. 5-4: FE model validation - Nebraska lab test

Damage Modeling – Element Behavior

Results from an experimental investigation on the behavior of overlaid bridge decks, conducted at the University of California, San Diego (Seible et al. 1998), was used in this study to develop a numerical damage model representing delamination in reinforced concrete slabs. In the experimental program, a series of simply-supported one-way two-layer RC slab panels, representing an effective portion of a bridge deck spanning between longitudinal girders, were designed, cast, and tested to failure to study their interlayer behavior. A range of contact surface preparation methods (namely lubrication, roughening, and scarification) between the two layers were used to provide a basis for comparison. Among all of the specimens, the one that had been lubricated with bond breaking agents was selected in this study to develop the FE damage model. With no chemical and mechanical bonding provided between the layers of the reinforced concrete slab and its overlay, this specimen represents the worst case scenario with respect to the magnitude of delamination that could exist in reinforced concrete decks. Figs. 5-5a and 5-5b illustrate the geometrical configurations of selected slab panel. According to the test setup, the slab was supported by polished and greased steel slip plates to allow horizontal translation and

elastomeric bearing pads to allow rotation. A concentrated load was applied at the center of the span through a MTS actuator reacted against a structural steel load frame.

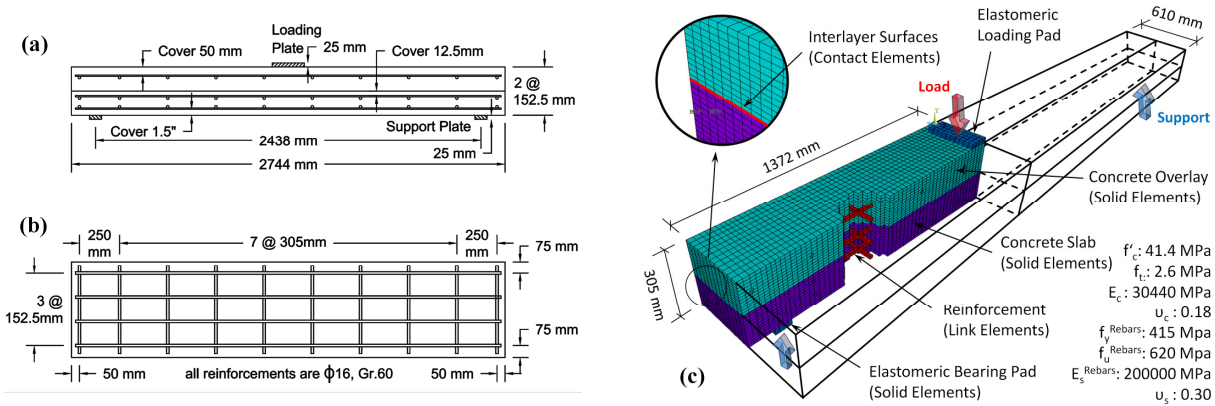


Fig. 5-5: Reinforced concrete slab with overlay: (a) elevation, (b) plan, (c) proposed FE model

Two FE models were created to assess the intact and delaminated conditions of the selected overlaid RC panel. Both models were generated only for one-quarter of the actual specimen to take the advantage of symmetry in geometry and loading conditions (see Fig. 5-5c). In the numerical model of the intact slab, the concrete layers were assumed to be fully bonded at the interlayer surface, forming a monolithic configuration. For the model representing damage, standard surface-to-surface contact elements with the augmented Lagrangian algorithm (ANSYS 2011) were implemented at the interlayer surfaces to simulate the state of ideal delamination. In modeling, the upper surface of the RC slab was selected as the target surface, while the contact surface was attributed to the lower surface of the overlay. In general, the contact elements are constrained against penetration into target surface at their integration points (see Fig. 5-6). Thus, they would allow for internal compression to be transferred with no tensile restraint against separation. Moreover, the surfaces in contact can carry shear stresses based on a Coulomb friction model. In the proposed model, however, the interlayer shear stresses were released at the interface to mimic the ideal situation of lubricated surfaces in the experiment. In addition to all sources of material nonlinearities integrated into the model (see Fig. 5-5c), the implementation of contact elements incorporates a changing-status type of nonlinearity in the numerical analysis.

The load-deflection behavior at the mid-span of the slab were derived from the nonlinear FE analysis and compared to the corresponding experimental result for validation. Fig. 5-7 illustrates this comparison for both the intact and delaminated numerical models. The observed

discrepancies exist between the results can be mainly attributed to the unknown material properties of the elastomeric loading pads used in the experiment. Nevertheless, the proposed FE models were able to predict the general nonlinear behavior of the selected overlaid RC slab with both intact and damaged (delaminated) configurations. Moreover, comparing the results of intact and damaged models demonstrated the influence of delamination in reducing the load-carrying capacity of the selected slab. This would highlight the capability of the proposed numerical modeling approach in simulating the interlayer slip which represents the ideal extreme state of delamination in reinforced concrete structures.

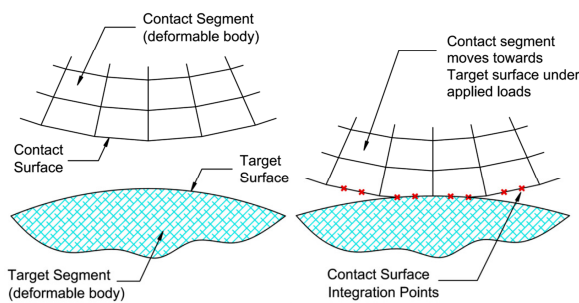


Fig. 5-6: Contact/target element behavior

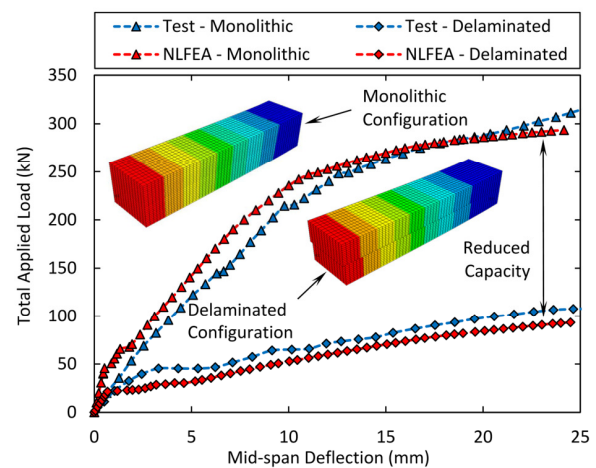


Fig. 5-7: FE model validation - UCSD lab test

Damage Integration – Damaged System Behavior

The validated damage modeling approach, which was used to simulate the interlayer behavior of the reinforced concrete slab overlay, could then be integrated into the calibrated numerical model of the intact bridge system to investigate the effects of corrosion induced delamination on the system-level behavior of the selected superstructure. To accurately integrate the effect of delamination into the proposed numerical model of the bridge system, it is essential to understand the details of the corresponding damage mechanism and its effects on the material properties and geometrical characteristics within the damaged area of the deck.

According to the data provided through implementation of different inspection and nondestructive evaluation methods (SHRP2 2013), delaminations in concrete decks do not usually occur in concentrated areas, but instead they are distributed randomly across the bridge deck (see Fig. 5-8a). Depending on the severity of the corrosion attack, the deterioration process

may initiate on one side of the affected layer of reinforcement or propagate all the way around to the other side of the attacked layer. Accumulation and expansion of the corrosion products would degrade the structural integrity and result in the development of fracture planes (delamination) on upper, lower, or even both sides of the corroded rebars. Fig. 5-8b illustrates a modeling approach to integrate these fracture surfaces into the numerical model of the bridge deck. Similar to the model proposed for the concrete slab overlay, the interlayer separation can be modeled using surface-to-surface contact elements. In the case of asymmetric delamination where the fracture plane only propagates through one side of the rebar, the reinforcing elements are assumed to be in perfect bond with the concrete element on the intact side, while the bond behavior on the corroded side is dictated by the shear transfer behavior of the contact elements.

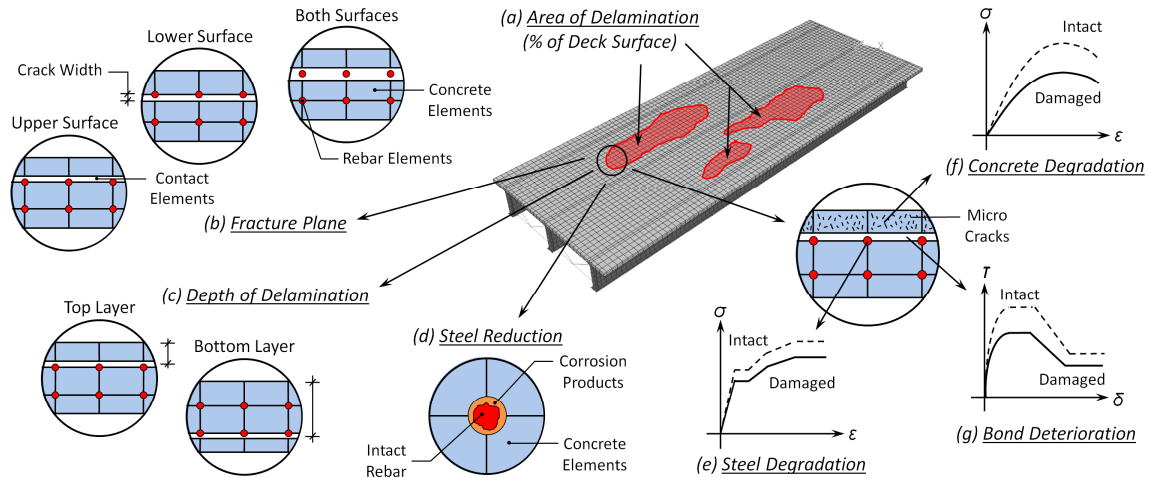


Fig. 5-8: Effects of deck delamination on material properties and geometrical characteristics

In the case of fully symmetric delamination with the corrosion products propagating all around the rebars, a similar contact algorithm was implemented to model the interaction between separated concrete layers, while debonding between the corroded rebars and the surrounding concrete elements was simulated using node-to-surface contact elements. With no tensile restraint against separation, the node-to-surface contact algorithm would restrain the nodes of the crossing corroded rebars from penetrating into the adjacent concrete elements by transferring compressive stresses (ANSYS 2011). The level of debonding can also be controlled through variations in the shear transfer coefficient of the implemented contact elements.

Moreover, delamination can happen at various depths through the thickness of the deck,

resulting from the corrosion in the top or bottom layers of reinforcement and can be modeled as depicted in Fig. 5-8c. Irrespective of the location, depth and relative position of the fracture plane, corrosion induced delamination would cause alterations in the material and geometrical characteristics of the damaged elements. Several parameters have been proposed in the literature to quantify these alterations and provide more accurate measurement of the extent level of delamination and its corresponding damage mechanisms in the reinforced concrete members. The most dominant effects which were considered in this numerical study are the crack width (Fig. 5-8b), reduction in the cross section and yield stress of the corroded rebars (Figs. 5-8d and e), change in the compressive strength of the concrete cover (Fig. 5-8f) due to micro cracking induced by rebar rust expansion, and concrete-rebar bond deterioration (Fig. 5-8g).

Sensitivity Analysis

Using the proposed numerical modeling approach for damage integration, a sensitivity analysis was performed to investigate the influence of variations in different damage parameters, including geometrical and material characteristics, on the non-linear behavior, ultimate capacity and system ductility of the selected bridge superstructure. It should be noted that the corresponding values for the selected damage parameters are ideal representations of actual quantities and were selected to demonstrate the applicability of the proposed modeling approach. With improvement in the non-destructive inspection techniques, more accurate values for these parameters can be provided and integrated in the corresponding numerical analysis, but this was beyond the scope of this investigation.

Area of Delamination

Cases (1) through (4) were selected to investigate the effect of damage shape and its extent level on the overall system behavior. As illustrated in Fig. 5-9, four different generic delamination patterns were selected to update the intact bridge model. With the maximum positive flexural moment induced at midspan of the selected simply-supported structure under the applied loads, the chosen delamination patterns would cause the worst case damage effects on the performance of the system. In all of these cases, it was assumed that the delamination occurred at the depth of 75 mm (3 in.) from the top surface of the slab, as a result of corrosion in the top layer of the deck reinforcement, and the corresponding fracture planes were asymmetrically modeled on the upper surface of the corroded rebars.

Fracture Plane/ Depth of Delamination

Variations in the relative location of the fracture planes with respect to the corroded rebars, were also included in the analysis by updating the damaged model in case (2) with interlayer separation applied on the lower surface and both surfaces of the corroded rebars (cases (5) and (6), respectively). Moreover, the bridge model was updated in the analysis cases (7) to (9) to study the effect of damage depth on the system behavior, assuming that the corrosion-induced delamination occurred at the bottom layer of the deck reinforcement (150mm (6 in.) from the top surface). Fracture planes were applied on the upper, lower and both surfaces of the bottom layers of the deck reinforcement.

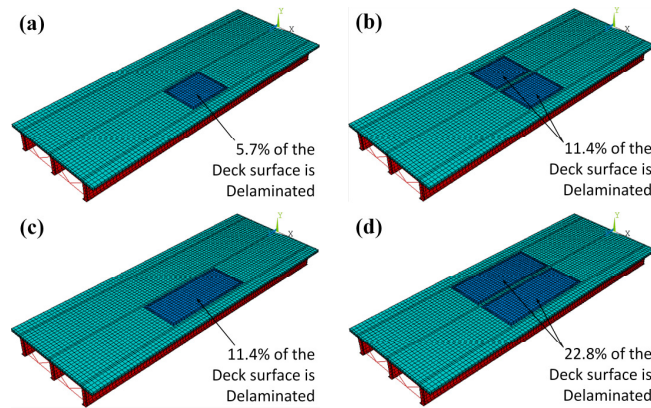


Fig. 5-9: Integrated delamination patterns

Steel Reduction

According to the literature, numerous experimental studies have been conducted to provide a quantitative measure of reduction in the rebar cross section. Broomfield (1997) and Alonso et al. (1998) suggested that a radius loss of 100 μm to 150 μm is necessary for concrete to crack and spall. In an experimental study performed on corrosion impaired RC structures, Roberts et al. (2000) proposed a threshold of 6 mm loss in rebar cross section to cause delamination, which corresponds to 50 μm of radius loss assuming uniform corrosion. As a result, case (10) was created to investigate the effect of section loss in the rebars on the behavior of degraded bridge model. In this case, a 5% uniform reduction in the rebar cross section was assumed, which is equivalent to 150 μm radius loss in the simulated rebars ($\Phi 13$, #4).

Steel Material Degradation

Depending on the severity of the environmental-chemical attack, material properties of the corroded rebars can also be degraded. For actual in-service structures where uniform corrosion dominates the state of subsurface delamination in the RC decks, the stress-strain properties of the corroded rebars are not significantly affected by the corrosion damage. However, in the laboratory experimentations on the corroded RC member, the implemented corrosion process is usually accelerated which can result in pitting. The presence of pitting would significantly degrade the mechanical properties of the corroded rebars due to localized stress concentrations (Cairns et al. 2005). Steel material degradation can be included in the numerical model (see Fig. 5-8e) by reducing the yield stress of the corroded rebars using Eqn. 5-1 (Stewart 2009).

$$f_y^D = \left[1.0 - 0.5 \left(\frac{A_{pit}}{A_{stnom}} \right) \right] f_y \quad (5-1)$$

where f_y^D and f_y are the rebar yield stresses with damaged and intact configurations, A_{pit} is the area of the pit, and A_{stnom} is the nominal cross section area of the intact rebar. Although occurrence of pitting corrosion is not common in the actual in-service structures, in this study analysis cases 11 and 12 were attributed to investigate the impact rebar material degradation on the behavior of the selected bridge superstructure with a delaminated deck. Corresponding pit areas were assumed as 10% and 50% of the intact rebar cross section, which result in 5% and 25% reduction in the yield stress of the corroded rebar, respectively.

Concrete Material Degradation

Internal pressure developed from the expansion of the corrosion products would result in the formation of cracks in the surrounding concrete. Cracks can be developed at the top or bottom layers of concrete; however, the top cover of the deck would most likely exhibit a reduction in performance compared to undamaged concrete as it is subjected to the compressive stresses under the externally applied loads. A reduction in the compressive strength of the cracked concrete depends on the average tensile strains induced by internal pressure and can be ideally integrated into the numerical model (see Fig.8f) of the damaged concrete using Eqn. 5-2 (Coronelli and Gambarova 2004).

$$f_c^D = \frac{f_c}{\left[1.0 - 0.1 \left(\frac{\varepsilon_1}{\varepsilon_0} \right) \right]} \quad (5-2)$$

where f_c^D and f_c are the concrete compressive strengths with damaged and intact configurations, ε_0 is the intact concrete strain at the peak strength, and ε_1 is corrosion-induced tensile strain in transverse direction which is a function of number of corroded rebars, volumetric expansion of the rust products, and average corrosion attack penetration. The proposed equation was calibrated for a series of artificially corroded beams tested in the lab (Kallias and Rafiq 2010), where an exact measure of the transverse tensile strains was available. However, this measurement is not common in current field inspection practices of in-service bridges. Therefore, results from the experimental investigation were used in this study to incorporate the effect of concrete material degradation on the behavior of damaged bridge system. Accordingly, the bridge model was updated with 30%, 50%, and 65% reduction in the compressive strength of the top concrete cover (cases (13-15)), representing the lower bound, average, and upper bound values of material degradation in the corresponding experimental study.

Bond Deterioration

The mechanical bond behavior between concrete and reinforcement is significantly affected by the corrosion products growing at the rebar-concrete interface. Prior to cracking in concrete, a limited amount of corrosion increases the bond strength. With expansion of the rust products, the bond strength starts to deteriorate as a result of corrosion-induced cracking in the concrete. In the presence of severe corrosion attack, bond failure may eventually occur by splitting (Coronelli and Gambarova 2004). Several experimental and numerical studies were performed to propose theoretical models predicting the bond strength and bond-slip relationship in damaged RC members (Rodriguez et al. 1994, Harajli et al. 2004, Maaddawy et al. 2005). Most of the proposed equations were derived through curve-fitting of various bond-test data, with empirical constants which define the corrosion rate as a function of the current used in the corresponding accelerated lab experiment. Given the insufficient data provided through field inspections, there is no accurate measure on the amount of bond deterioration in the bridge slabs with subsurface delamination. As a result, the ideal case of severe debonding was considered in this study with

no shear stress being transferred amongst the delaminated layers of concrete. This assumption would provide a lower bound on the behavior of in-service bridges with delaminated slabs.

4.7. Crack Width / Opening

Crack opening is an important parameter that is widely being used to measure the concrete delamination due to rebar corrosion. Vu and Stewart (2002) assumed a limit between 0.5 and 1.0 mm for the crack width to cause concrete delamination and spalling. Similarly, Torres-Acosta and Martinez-Madrid (2003) found that if the crack width in the concrete slab reaches a limit within the range of 0.1-1.0 mm, delamination can occur. Based on the suggested values, the crack opening was assumed to be 0.75 mm wide in all of the developed models.

Results and Discussion

Under the same loading and boundary conditions applied to the intact bridge system, the updated models with integrated damage were numerically analyzed to evaluate the effect of variations in different geometrical and material characteristics associated with subsurface corrosion-induced delamination on the overall system behavior of the representative composite steel girder bridge. Fig. 5-10 demonstrates the variations in the system-level response of the damaged bridges based on the interior girder deflection at mid-span of the structure. As illustrated, the assumed damage scenarios have negligible effects on the nonlinear behavior of the system, in which behavior is defined as the path of the load deflection response. Moreover, the evolution of material nonlinearities, including formation of flexural cracks in the deck and growth of plasticity in steel girders, appears to be unchanged in presence of damage as the structure was loaded to failure.

By assuming perfect debonding between the delaminated layers of concrete, interlayer shear stresses cannot be transferred through the fracture plane. This would cause a loss in composite action between the layers of the concrete deck, which in turn results in localized failure mechanism (i.e. crushing) on the top surface of the deck at the margins of the delaminated areas. This premature failure mechanism adversely affects the ultimate capacity and overall ductility (ratio of maximum deflection to the deflection at first yield in the girders) of the system.

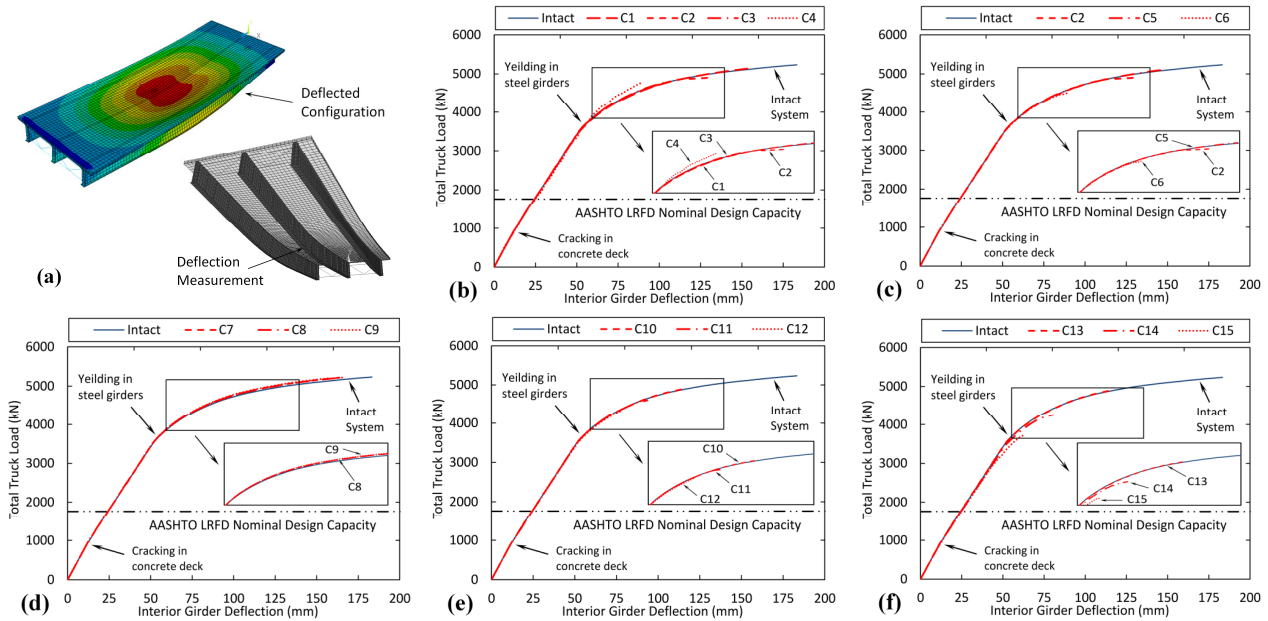


Fig. 5-10: Effect of damage on system behavior: (a) measured behavior (b) damage pattern, (c) fracture plane, (d) damage depth, (e) steel material degradation (f) concrete material degradation

Table 5-1 summarizes the relative reduction caused by these simulated damage mechanisms with respect to the corresponding values of the intact system. The ultimate capacity of the system decreases as the area of delamination increases over the surface of the slab (cases 1-4). This increase also significantly reduces the overall ductility of the system. For the top layer of reinforcement, modeling the fracture plane in an asymmetric fashion (cases 2 and 5) has less impact on both the capacity and ductility of the system compared to the symmetric modeling (case 6). However, the system capacity and ductility are less sensitive to the relative location of the fracture plane when the delamination was modeled as a result of corrosion in the bottom layer of reinforcements (cases 7-9). Uniform corrosion in the steel rebars with no effect on the material yield stress (case 10) has low and moderate impacts on the system capacity and ductility, respectively. Under more severe corrosive attack (cases 11 and 12), pitting would degrade not only the material resistance of the rebars, but also significantly decrease the capacity and ductility of the system. Material degradation in the cracked concrete cover due to the rust expansion (cases 13-15) would have a major impact on the ultimate capacity and also dramatically decreases the overall system ductility.

All of the numerical models including the intact system demonstrated additional reserve capacity over the AASHTO LRFD element-level nominal design capacity. This would confirm high levels of inherent redundancy, which can be attributed to the complex interaction between

structural members in the simulated bridge superstructure. It would also demonstrate a margin of safety for the serviceability of the selected structure, considering the facts that the service loads are usually below the design capacity; and the integrated damage scenarios have negligible effect of the behavior of the system within this limit of the applied loads.

Table 5-1: Effect of material and geometrical refinements on the behavior of damaged models

Model	Damage Pattern	Fracture Plane	Depth (mm)	Steel		Conc.	Capacity (kN)	Ductility ($\Delta u/\Delta y$)	Relative reduction	
				f_y^1	area ²	f'_c^3			Capacity	Ductility
Intact	-	-	-	-	-	-	5235	3.6	-	-
Case (1)	(a)	asym./top	75	-	-	-	5144	3.0	1.7%	16.2%
Case (2)	(b)	asym./top	75	-	-	-	4915	2.6	6.1%	27.4%
Case (3)	(c)	asym./top	75	-	-	-	4806	2.1	8.2%	41.3%
Case (4)	(d)	asym./top	75	-	-	-	4774	1.7	8.8%	52.5%
Case (5)	(b)	asym./bot	75	-	-	-	5113	3.0	2.3%	16.2%
Case (6)	(b)	sym.	75	-	-	-	4522	1.8	13.6%	50.8%
Case (7)	(b)	asym./top	150	-	-	-	5218	3.2	0.3%	10.6%
Case (8)	(b)	asym./bot	150	-	-	-	5229	3.3	0.1%	7.8%
Case (9)	(b)	sym.	150	-	-	-	5207	3.1	0.5%	13.4%
Case (10)	(b)	asym./top	75	-	5%	-	4911	2.3	6.2%	35.8%
Case (11)	(b)	asym./top	75	5%	10%	-	4605	1.9	12.0%	46.9%
Case (12)	(b)	asym./top	75	25%	50%	-	4341	1.6	17.1%	55.3%
Case (13)	(b)	asym./top	75	-	-	30%	4838	2.3	7.6%	35.8%
Case (14)	(b)	asym./top	75	-	-	50%	4257	1.6	18.7%	55.3%
Case (15)	(b)	asym./top	75	-	-	65%	3732	1.3	28.7%	63.7%

¹ reduction in rebar yield stress

² reduction in rebar x-section area

³ reduction in concrete compressive strength

Comparing the behavior of damaged and intact systems (see Fig. 5-10) demonstrates the fact that the overall performance of the bridge system is governed by the behavior of the main load-carrying elements (i.e. girders); while the concrete deck is primarily responsible for proportionally distributing the applied loads amongst girders. To further study this phenomenon, the effect of subsurface delamination on the transverse load distribution mechanism was investigated through studying the state of stresses in the deck at high levels of the applied loads. Fig. 5-11 illustrates the principal stress vectors at the mid-span of the structure for the intact system and two damaged scenarios where delamination was modeled at top and bottom layers of

reinforcements (cases (2) and (7)). The stress vectors in all three cases demonstrate high concentrations under the applied loads (top layer of the deck) and in the vicinity of the girders, while they are significantly decreased in the bottom layer of the deck. This would confirm the existence of an arching action that governs the transverse load distribution mechanism (Fang et al. 1990, Hewitt and deV Batchelor 1975). The minimal effect of the integrated damage scenarios on the distribution mechanism would justify the low impact of deck delamination on the overall performance of the system. This can be attributed to the fact that the fracture planes under the applied external loads is subjected to compressive stresses, which are able to be transferred among the implemented contact elements.

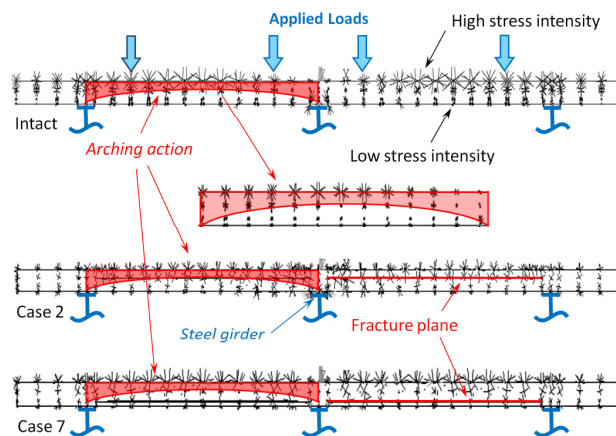


Fig. 5-11: Lateral load distribution mechanism

Deck Behavior and Design

Due to the high correlation between the system-level response and behavior of the girders, the direct impact of subsurface delamination on the deck independent behavior is still under the question. The last part of this study aims to characterize this impact and assess the implication on the current design methodologies of the reinforced concrete decks. According to the AASHTO LRFD bridge design specifications (AASHTO 2012), the concrete decks can be designed using either empirical or traditional (strip) methods. In these methods, the external applied loads are assumed to be transferred among girders via arching action or flexural behavior of the deck, respectively. From the design perspective, it is assumed that the slab is vertically supported at the location of the girders; hence the vertical deflections in the girders are neglected. To reflect this assumption in this study, the steel girders were extracted from a series of the developed

numerical models. Instead, the slab was supported at the location of girders through the length of structure, as depicted in Fig. 5-12.

The variation in the deck behavior due to integration of subsurface delamination was studied with respect to three parameters of damage pattern, damage depth, and relative location of the fracture plane. Under the same loading configuration, the representative deck models were analyzed and the corresponding load-deflection curves were derived at the mid lateral span of the decks (see Fig. 5-13). The deck systems with integrated damage from the developed bridge models in cases (1-4) were considered to investigate the effect of delamination pattern on the behavior of the deck system. As it is illustrated in Fig.13a, the capacity of the deck decreased consistently with expansion of the delaminated area from 5.7% to almost 23% of the total deck surface. The effect of damage depth was also studied through nonlinear analysis of the deck systems extracted from bridge models in cases (2) and (7). When comparing the behavior of damaged deck with intact model (see Fig.13b), it is evident that delamination due to corrosion in bottom layer of rebars have much less effect on the overall behavior of the deck system compared to the case where delamination occurs around the top layer of reinforcement. Similarly, deck systems were extracted from developed bridge models in cases (5) and (6) to evaluate the impact of fracture plane modeling (with respect to its relative location) on the behavior of damaged decks. As illustrated in Fig. 13c, variations over the relative location of the fracture plane demonstrates almost the same impact on the behavior of the damage deck system; nevertheless, the symmetric modeling of the delaminated surface on both sides of the corroded rebars has the most deteriorating effect on the behavior of the deck system.

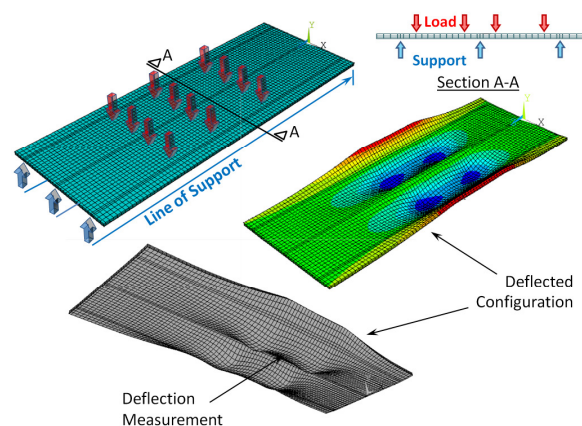


Fig. 5-12: Refined model for deck (no girders)

The deck system in the corresponding lab experimentation of the intact bridge (Kathol et al. 1995) was originally designed using the empirical method. The nominal capacity of the deck system with the existing reinforcement as well as its flexural capacity based on the traditional (strip) method were calculated according to the AASHTO LRFD and plotted on the same graphs (see Fig. 5-13). Regardless of the design methodology, it is clear that the actual capacity of the deck system is significantly higher than the assumed nominal design capacities. This can be related to the two-way action of the deck plate in transferring loads to the supports and the post-cracking behavior of concrete material, which are not considered in the current design practices.

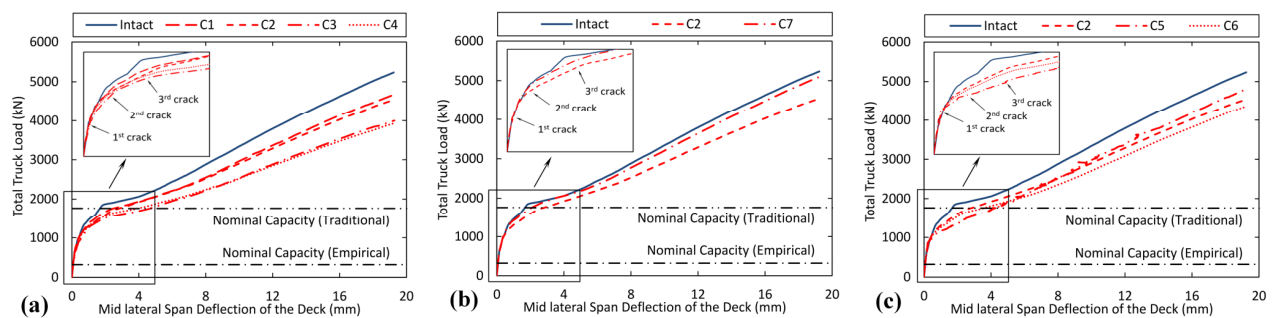


Fig. 5-13: Impact of damage on deck behavior: (a) damage pattern, (b) damage depth, (c) fracture plane

Application to In-service Structures

The modeling approach presented herein was implemented to study the behavior of a laboratory bridge model under the effect of deck deterioration; however, the applicability of the proposed methodology in actual practices is still under the question. In order to fulfill this transition, the behavior of an in-service bridge superstructure and its corresponding deck system with subsurface delamination was also investigated and included in this study. The selected structure was a simply-supported five-span bridge operating on the Richmond Highway over Mattaponi River in Aylett, Virginia. Only the first span of this bridge superstructure was selected for numerical study. As illustrated in Fig. 5-14a, the selected span is 39.6 m long and comprised of 215.9 mm reinforced concrete deck supported by five identical girders with uniform transverse spacing of 2.75 m. This structure was selected as its geometrical characteristics represent common features of composite steel-concrete girder bridges within the Commonwealth of Virginia. All of the structural details required for model generation were derived from Virginia Department of Transportation (VDOT) plans. Fig. 5-14b demonstrates the FE model

that was generated for this bridge superstructure.

According to the inspection reports, the deck of the selected structure is in a good condition with no major deteriorations. However, a series of damage scenarios were chosen in this study to investigate the potential impact of deck delamination on the behavior of this bridge system (see Figs. 5-15a-c). The geometrical characteristics of the deteriorated areas (percentage and pattern) were assumed based on a questionnaire which collected qualitative visual inspection data from the VDOT engineers in nine different districts across the Commonwealth. In the numerical models with integrated damage, it was assumed that the delamination occurred as a result of uniform corrosion in the top layer of reinforcement. The corresponding fracture planes were modeled at the upper surface of the corroded rebars with a uniform crack width of 0.7 mm. Given the lack of quantitative inspection data, rebar cross section and its material properties were assumed intact. However, the compressive strength of the concrete cover in the delaminated areas was reduced by 30% to capture deterioration in the concrete material due to existence of micro cracks resulted from expansion of the corrosion products. An ideal case of debonding between delaminated layers of concrete deck was also assumed in the analysis.

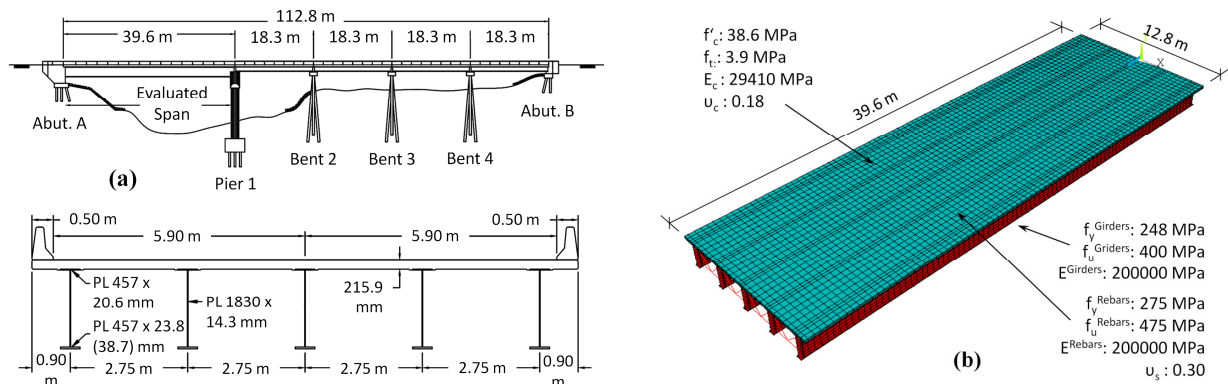


Fig. 5-14: Selected in-service bridge: (a) superstructure geometry, (b) generated FE model

Pin-roller boundary conditions were assumed for the simulated bridge model with both intact and damaged configurations. Similar to the lab test bridge, the steel girders were extracted from the numerical model of the selected actual structure to study the impact of deck deterioration on the individual behavior of the deck system. All the models were loaded with two side-by-side AASHTO HS-20 trucks located in a specific longitudinal position to cause maximum flexural moment at the mid-span of the structure. The total load vs. maximum deflection response (see

Fig. 5-15d) was collected from the performed nonlinear analysis of the both bridge and deck models. As depicted in Fig. 5-15e, the assumed damage scenarios have negligible effects on the nonlinear behavior of the system and evolution of material nonlinearities. However, the premature crushing failure in concrete cover would adversely affect the ultimate capacity and overall ductility of the system.

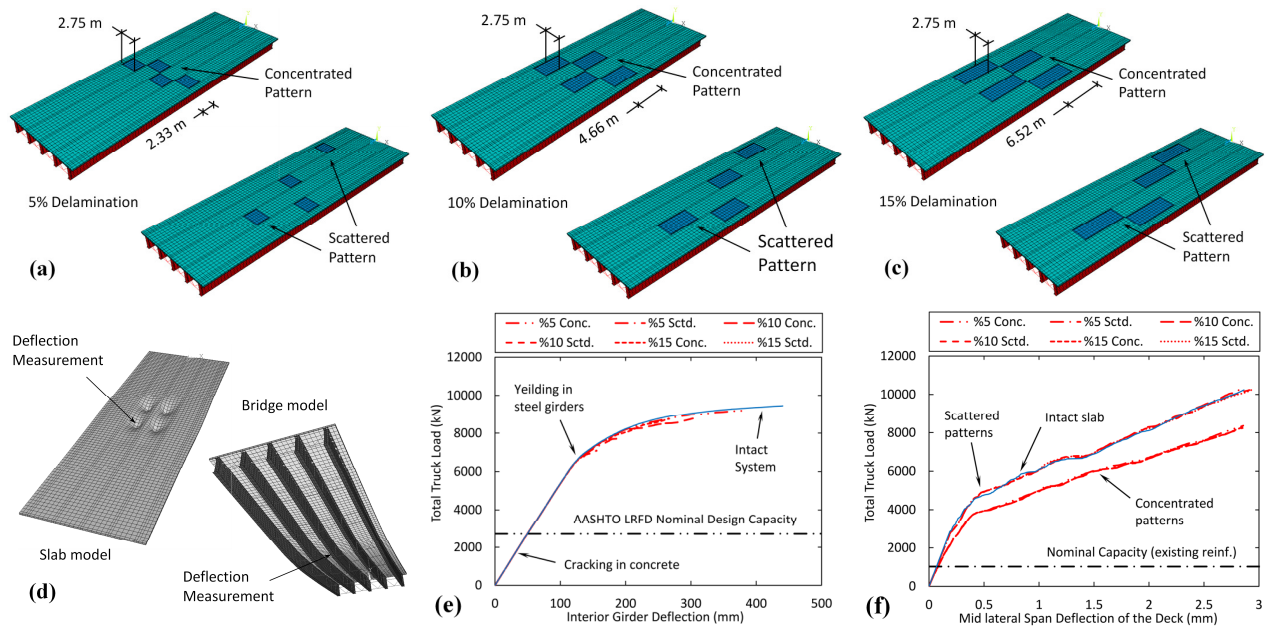


Fig. 5-15: Damage integration: (a-c) damage scenarios, (d) measured behavior, (e) impact on system behavior, (f) Impact on deck behavior

Table 5-2 summarized the relative reduction of these parameters with respect to the corresponding values of the intact system. As given, detrimental effects of the deck delamination on both system capacity and system ductility are elevated by increases in the damage area. With the same area of damage, scattered patterns would result in more severe degradation in the overall performance of the system. For the slab models, on the other hand, only damage scenarios with the concentrated patterns would influence the behavior of the deck system under the assumed loading scenario (see Fig. 5-15f). Results of this investigation would demonstrate that the implemented methodology can be extrapolated to assess the safety and functionality of other in-service bridges with different geometrical and damage characteristics (Gheitasi and Harris 2014a).

Table 5-2: Impact of delamination on the behavior of the selected in-service structure

Model	Capacity (kN)	Ductility ($\Delta u/\Delta y$)	Relative reduction	
			Capacity	Ductility
Intact	9472	3.8	-	-
5% *	9215	3.3	2.7%	13.2%
5% **	7727	1.7	18.4%	55.3%
10% *	8763	2.7	7.5%	28.9%
10% **	7088	1.4	25.2%	63.2%
15% *	8746	2.3	7.7%	39.5%
15% **	7050	1.3	25.6%	65.8%

* concentrated pattern

** scattered pattern

Conclusions

The main objective of this investigation was to characterize the impact of subsurface deck delamination on the behavior and overall performance of steel-concrete composite bridge superstructures. Upon validation of the numerical modeling approach via available experimental data in the literature, the proposed methodology was implemented to study the behavior of a laboratory bridge model and an actual in-service structure. Based on the results obtained from the corresponding sensitivity study, it can be concluded that:

- The assumed damage scenarios had negligible effects on the nonlinear system behavior and evolution of material nonlinearities in the selected bridge structures. However, loss of composite action between layers of concrete within the delaminated areas causes significant reduction in the capacity and ductility of the system, due to local premature crushing failures occurred in the reinforced concrete deck.
- The nonlinear behavior of the selected bridges and their corresponding deck systems demonstrated the existence of an additional reserve capacity over the nominal capacities defined based on the AASHTO LRFD design methodology. This can be attributed to high levels of inherent redundancy, system-level interaction and two-way action of the slab, which are generally neglected in current design practices.
- Given the fact that significant resources are being invested each year to maintain and repair the aging infrastructure within the U.S., the proposed approach has the potential to

help the preservation community to reinforce their maintenance decisions such as repair, rehabilitation and replacement alternatives or even a risk-based do nothing alternative.

Chapter 6:

Summary and Future Work

The overall objective of this research project was to establish a framework to evaluate the in-service condition of bridge superstructures in the presence of common deteriorating conditions and provide a measure of system performance by characterizing the impact of damage mechanisms on the ultimate capacity, redundancy, and operational safety of the bridge system. The investigation presented herein was limited to composite steel girder bridges and aimed at illustrating a conceptual schematic of a computational modeling strategy for describing the in-service performance of these structures under the influence of corrosion in steel girders and subsurface delamination in concrete decks. Based on the results obtained via numerical analyses, the following conclusions can be drawn:

- Concrete slab on steel stringer bridges usually demonstrate additional reserve capacity over the theoretical nominal design capacity according to the AASHTO LRFD specifications, which could be attributed to the high level of redundancy and complex interaction that exists among structural components in this type bridge superstructures.
- Crushing in the concrete deck and plastic hinging in the steel girders are the main failure mechanisms associated with intact girder-type composite structures. The stages to failure, which demonstrate the evolution of material non-linearity in the bridge system, are highly dependent on the geometrical characteristics, material properties, support conditions, girder-deck bond properties, and even loading scenarios and are subjected to change for variations in the bridge system.
- The lateral distribution behavior in composite steel girder bridges varies once the structure passes the linear elastic stage of behavior. These variations usually begin with cracking in concrete slab and become more critical as the plasticity starts to propagate in girders. The distribution factors proposed by AASHTO LRFD specifications are generally conservative; nevertheless, the code-specified values can be violated in the presence of high material non-linearities, although the amount of applied loads corresponding to this critical scenario is much larger than typical service loads.
- Corrosion in steel girder may significantly influence the performance of the composite steel bridge superstructures. However, the operational safety of the system is mainly

governed by the geometrical characteristics (shape and extent level) of the accumulated damage scenario. It should be highlighted that the damage pattern has less influence on the behavior of the system, while the amount of thickness reduction in the steel members would highly influence the ultimate load-carrying capacity of the structure.

- Subsurface delamination in reinforced concrete slabs of the steel-concrete composite bridges has negligible effects on the non-linear system behavior and evolution of material non-linearities. However, loss of composite action between layers in concrete within the delaminated areas would cause significant reduction in the capacity and ductility of the system, due to local premature crushing failures occurred in the reinforced concrete deck.
- The proposed framework could be beneficial to the preservation community as a mechanism to make decisions based on in-service conditions, but also has implications in the design community where a system-level design strategy would have a major impact on design economy as compared to current element-level design strategies. Moreover, results obtained from this investigation highlight the ability of the proposed framework to provide a critical linkage between the design and preservation communities by correlating the element-level behavior to the system-level response under the influence of existing damage and deteriorating conditions.

On the basis of the performed investigation, the following future work is recommended to enhance the knowledge regarding the condition assessment and evaluation of the national bridge infrastructure network:

- Using the same numerical modeling framework, this investigation can be extrapolated to study the impact of other damage mechanisms associated with composite steel girder bridges including fire and vehicle/ship collision. Critical to this extrapolation is the validation of the damage modeling approach within the element-level domain (Phase III) and establish a modeling strategy to integrate these damage effects into the measure of system performance.
- As it was demonstrated, the assumed individual damage scenarios (corrosion, delamination) did not have major impacts on the overall safety and functionality of the selected structures and the types of loads that are common in practice. For future research, it is worth to study the impact of coupled damage mechanisms (two or more) on

the performance of in-service structures. Moreover, the performed sensitivity study can be extended to identify the critical stage of the damage scenario(s) under which, the structure is no longer safe to be in service. Accurate evaluation of this criterion requires a parametric set of bridges that includes variations over geometrical and material characteristics, as well as loading and boundary conditions in the analyses.

- The proposed numerical modeling approach can be used to evaluate other types of bridge superstructures under the effect existing conditions. Concrete girder and prestressed girder bridges are the closest scenarios to extrapolate. Appropriate damage scenarios shall be selected based on the recognized common deteriorations associated with each type of the selected structures.
- The proposed performance-based evaluation framework can be upgraded by integrating the sub-structure and foundation into the numerical models. This would provide the opportunity to address damage scenarios associated with these parts of the bridge structure (e.g. scour and flooding) and study their impacts on the overall safety and functionality of the bridge system. The upgraded modeling framework also has the potential to include soil-water-structure and vehicle-structure interactions to include seismic load effects and investigate the impact of dynamic amplification on the performance of the in-service bridges.

Appendices

Numerical models of intact systems were developed in this study for representative bridge components (element level), including concrete beam, concrete deck, steel girder, and a full-scale bridge test (system level) based on existing literature. Each of the models was developed in ANSYS (2011), a commercially available general purpose finite element software program. The main objective of this section is to clarify how to incorporate the material and geometrical nonlinearities in the numerical simulation and analysis of the selected structures and their sub-components. Results presented here are based on the preliminary investigation of the numerical modeling approach and were updated in the later stages of the project as necessary.

Appendix A:

Numerical Analysis of a Simply Supported Concrete Beam

A.1. Experimental Investigation

Results obtained from an experimental testing of a reinforced concrete beam performed by Buckhouse (1997), depicted in Fig. A.1, were utilized in this study to calibrate the proposed finite element model. The cross sectional dimensions of the tested beam were 10 in width by 18 in height. The length of the beam was 15 ft - 6 in with supports located 75 mm 3 in from each end of the beam, allowing a simply supported span of 15 ft (Wolanski 2004). As illustrated in Fig. A.2, the concrete beam was reinforced with 3-#5 mild steel bars, located at the tension side of the cross section, to satisfy the flexural demand; while #3 U-stirrups implemented as vertical shear reinforcement. Cover for the rebars was also set to 2 in for both longitudinal and lateral reinforcements.



Fig. A.1: Experimental setup, Buckhouse (Buckhouse 1977)

For loading scenario, two 50-kip capacity load cells were placed at third points, or 5ft from each support, on steel bearing plates. Data acquisition equipment was utilized in the experiment to record applied loading, beam deflection at the midspan, and strain in the internal flexural reinforcements. The beam was loaded to capture flexural failure. Vertical cracks first formed in the constant moment region, extended upward, and then out towards the constant shear region with eventual crushing of the concrete in the constant moment region. The corresponding

ultimate load for the beam was determined to be 16310 lbs, associated with the midspan deflection of 3.65 in.

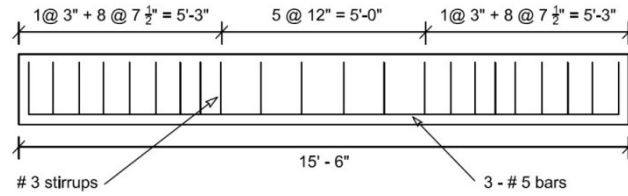


Fig. A.2: Reinforcing details for tested beam, Buckhouse (1977)

A.2. Finite Element Characterization

For validation study, the ANSYS (2011) finite element package was implemented to simulate the reinforced concrete beam. Due to the symmetry of the structure in geometry and loading conditions, only one quarter of the beam was modeled for numerical simulation, see Fig. A.3. The general trend in the modeling of the reinforced concrete beam is categorized in different stages and is going to be discussed in details in the next following sections.

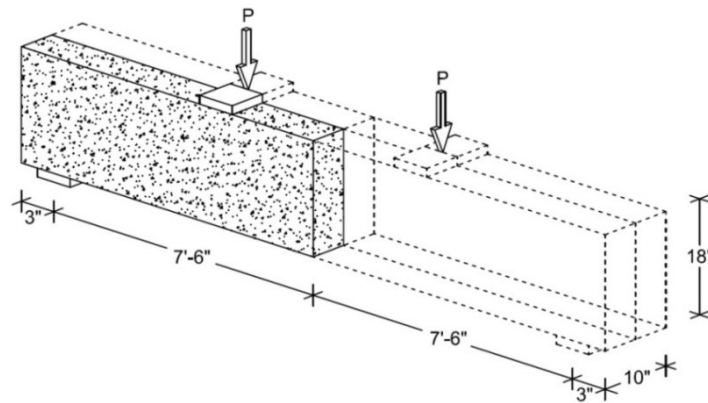


Fig. A.3: Application of symmetry in FE modeling

Three types of elements were utilized in the FE modeling of different parts of reinforced concrete beam. Solid65 element was used for the 3D modeling of the concrete body, with or without reinforcing bars. This element is defined by eight nodes, each of which has three translational degrees of freedom in the x, y, and z directions; see Fig. A.4(a). The concrete element is similar to a 3-D structural solid element (brick element) but with the addition of special cracking and crushing capabilities in three principal directions. For 3D modeling of steel

plates at the supports and loading points of the concrete beam, Solid185 element, as given in Fig. A.4(b), with its three translational degrees of freedom at each node, was implemented in FE simulation. This element is, however, capable in modeling plasticity, hyperelasticity, stress stiffening, creep, large deflection, and large strain.

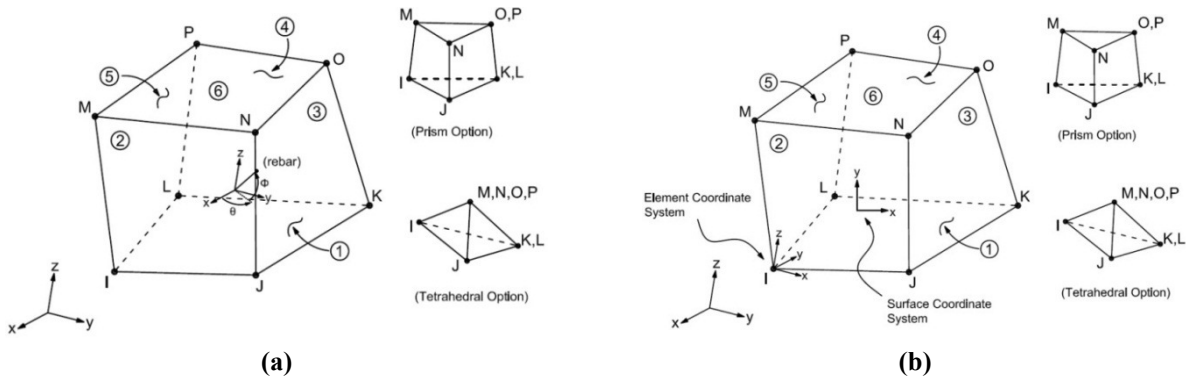


Fig. A.4: Implemented volumetric elements: (a) Solid65, (b) Solid 185

As it is given in Fig. A.5, Link180 element was finally utilized for modeling of the steel reinforcements. This 3D spar element is a uniaxial tension-compression element with three translational degrees of freedom at each node. Plasticity, creep, rotation, large deflection, and large strain capabilities are included within the element domain, while no bending is considered.

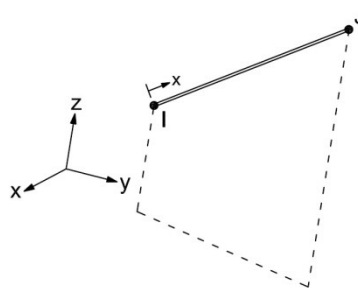


Fig. A.5: Link180 element

In FE modeling of reinforced concrete structures, real constants shall be defined for steel rebars to characterize their geometrical properties. Generally there are three different techniques (Tavarez 2001) that can be utilized for the numerical simulation of reinforcing steels in the concrete members: (1) discrete model, (2) embedded model, (3) smeared model; as depicted in Fig. A.6. In discrete model, the reinforcing bars are simulated as link or beam elements in the 3-D finite element model, sharing the nodes with the adjacent concrete elements. This would

ensure the state of full bonding effect between steel and concrete domain. In this model, however, the mesh generation is restricted to the rebar configuration. The restriction can be resolved in the embedded model by satisfying the compatibility between the rebar nodes and the surrounding concrete elements by adding new nodes at the intersection. Nevertheless, this model will be computationally deficient due to additional degree of freedoms added to the model in order to satisfy the compatibility. Finally in the smeared model the reinforcing steel is uniformly distributed all over the volume of the concrete element, providing the opportunity to simulate reinforced concrete members with more complicated rebar patterns. The smeared model for reinforcing rebar is actually a feature of the Solid65 provided by ANSYS and can be activated by introducing the volume ratio, material properties and the orientation of the smeared rebars in three different directions. However in this study, rebars was chosen to be simulated using discrete model and therefore a value of zero was entered for all corresponding real constants.

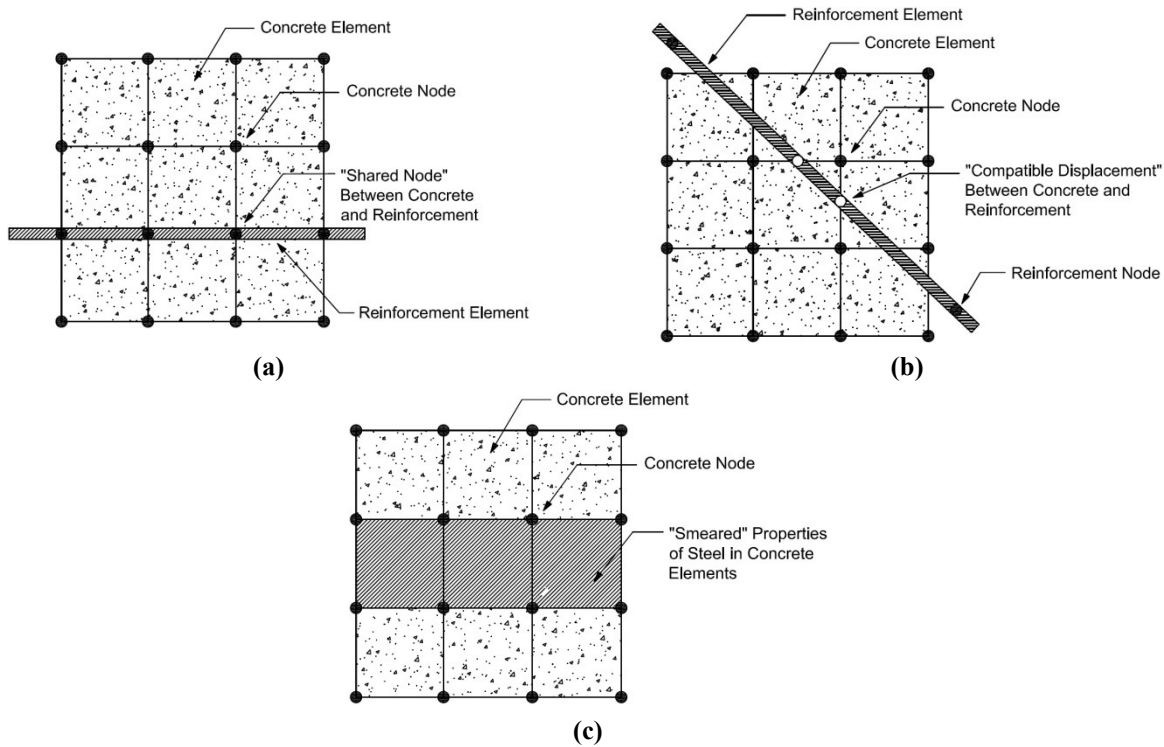


Fig. A.6: Modeling techniques for reinforcing bars: (a) discrete, (b) embedded, (c) Smeared model

As given in Table A.1, four additional real constants were defined for the link180 element, representing the reinforcing bars using discrete model approach. Real constants 2 and 3 referred

to the longitudinal (#5) bars located on the tension side of the control beam as the main flexural reinforcements, whilst, real constants 4 and 5 were dedicated to the stirrups (#3 bars).

Table A.1: Real constants for proposed FE model of concrete beam

Real Constant	Element Type	Constants		
		Rebar 1	Rebar 2	Rebar 3
Set 1	Solid65	Material Number	0	0
		Volume Ratio	0	0
		Orientation Angle (θ)	0	0
		Orientation Angle (ϕ)	0	0
		Rebar		
Set 2	Link180	Cross Section (in ²)	0.31	-
Set 3		Cross Section (in ²)	0.155	-
Set 4		Cross Section (in ²)	0.11	-
Set 5		Cross Section (in ²)	0.055	-

Since the advantage of the symmetry was utilized in the FE modeling, the real constants 3 and 5 were assigned to the intermediate longitudinal rebar and midspan stirrup, respectively, with half the sectional area of real constants 2 and 4 attributed to other flexural and shear reinforcements. It should be finally noted that the no real constant was considered for the Solid185 element (Wolanski 2004).

For the proposed FE model, the material properties were defined separately for each element type, regarding the corresponding material characteristics. Development of a model to represent the nonlinear behavior of concrete is a challenging task in FE simulations. Concrete is a quasi-brittle material with different behavior in compression and tension. Although concrete behaves ideally as an isotropic material in compression, propagating cracks dominate the response of the concrete member under the application of tensile stresses. In compression, the stress-strain curve is linearly elastic up to about 30 percent of the maximum compressive strength, σ_{cu} . Above this point, the stress increases gradually up to the maximum strength and consequently descends into a softening branch. The crushing failure eventually occurs at an ultimate strain of ϵ_{cu} . In tension, however, the stress-strain curve is approximately linearly elastic up to the maximum tensile strength, σ_{tu} , where concrete cracks and the strength decreases gradually to zero, as illustrated in Fig. A.7.

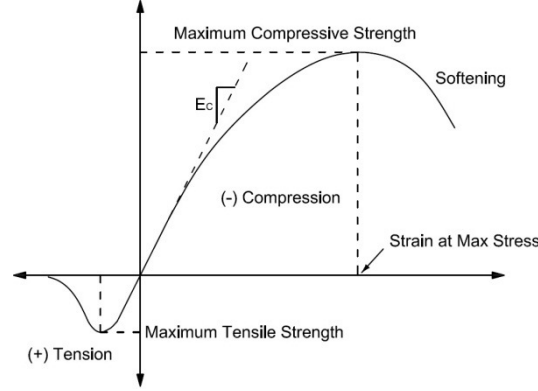


Fig. A.7: Actual uniaxial stress-strain curve for concrete both in tension and compression

The elastic modulus of 3949.08 ksi with respect to uniaxial compressive strength of 4.8 ksi was used in this study to characterize the nonlinear isotropic material properties of the concrete based on equation (A.1), (ACI 2011). In addition, the Poisson's ratio for proposed FE model was assumed to be 0.18 for validation purposes.

$$E_c = 57000\sqrt{f'_c} \quad (A.1)$$

Two different constitutive material models were considered in the numerical investigation, to represent the behavior of concrete under compression, see Fig. A.8. In model C1, the softening region of the concrete material beyond the maximum compressive strength, was neglected and idealized as an inelastic-perfectly plastic material. However, full nonlinear behavior of concrete was considered in model C2, where descending branch of stress-strain relationship was incorporated in the simulation and restricted to the codified crushing strain of 0.003.

It should be also mentioned that the nonlinear stress-strain relationship for both material models was defined based on equation (A.2) (Macgregor 1992); however, the multilinear material model was implemented in ANSYS to represent the corresponding nonlinear constitutive laws.

$$\sigma = \frac{E_c \varepsilon}{1 + \left(\frac{\varepsilon}{\varepsilon_0}\right)^2} \quad \text{where} \quad \varepsilon_0 = \frac{2f'_c}{E_c} \quad (A.2)$$

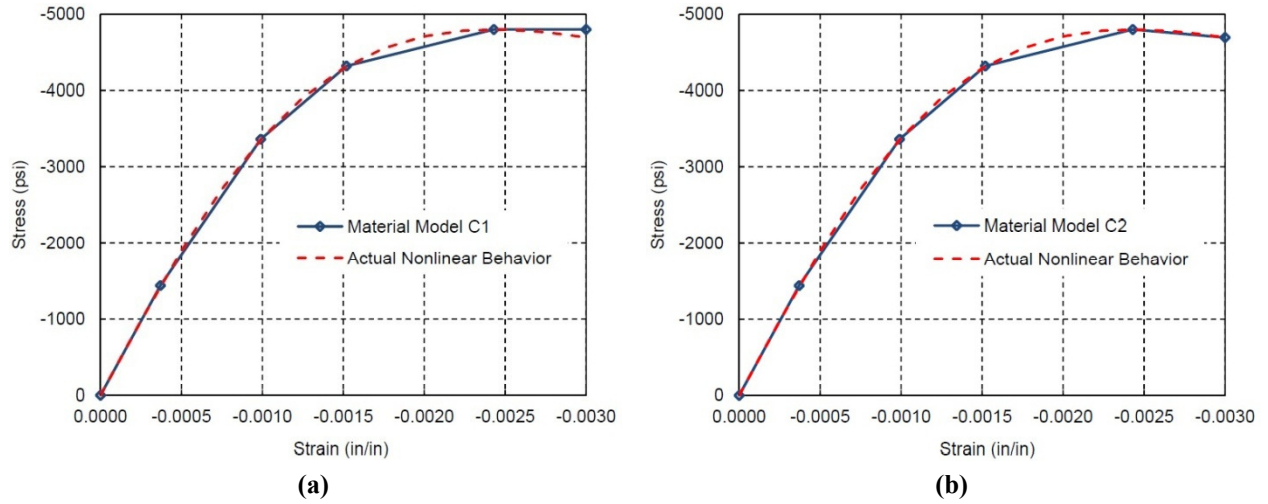


Fig. A.8: Idealized uniaxial stress-strain curve for concrete in compression: (a) model C1, (b) model C2

The William and Warnke (1974) model was also implemented in the analysis to define the triaxial failure surface of the plain concrete. In order for ANSYS to simulate the corresponding failure surface, specific constants, such as shear transfer coefficient as well as uniaxial cracking and crushing stresses, shall be introduced by user. In this study, the shear transfer coefficients were set to 0.3 and 1 (no loss of shear transfer) for open and close cracks, respectively. Moreover, the uniaxial cracking stress was defined as the modulus of rupture based on the ACI Code (2011), which was set to 0.52 ksi in this study. In order to overcome the convergence problems, the crushing capacity of the implemented failure model was turned off by setting the uniaxial crushing stress equal to -1. Both 3D and 2D (projection on the σ_{xp} - σ_{yp} plane) representations of the William and Warnke failure surface in the principal stress space are depicted in Fig. A.9.

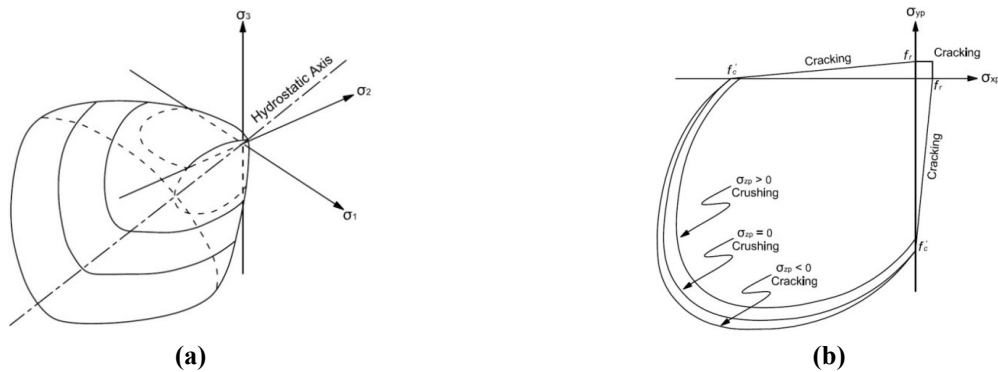


Fig. A.9: William and Warnke failure surface: (a) 3D representation, (b) 2D representation

As depicted in Fig. A.9 (b), cracking occurs in a concrete element when the principal tensile stress in any direction lies outside the failure surface. After cracking, the elastic modulus of the concrete is set to zero in the direction parallel to the principal tensile stress direction. On the other hand, crushing occurs when all principal stresses are compressive and lie outside the failure surface; subsequently, the elastic modulus is set to zero in all directions (ANSYS 2011). Similar to concrete, two different constitutive material models were considered in this investigation to simulate the actual nonlinear behavior (William and Warnke 1974) of Gr.60 steel rebars. As depicted in Fig. A.10, an elastic-perfectly plastic idealization as well as full nonlinear stress-strain relationship were identified to represent the S1 and S2 material models, respectively.

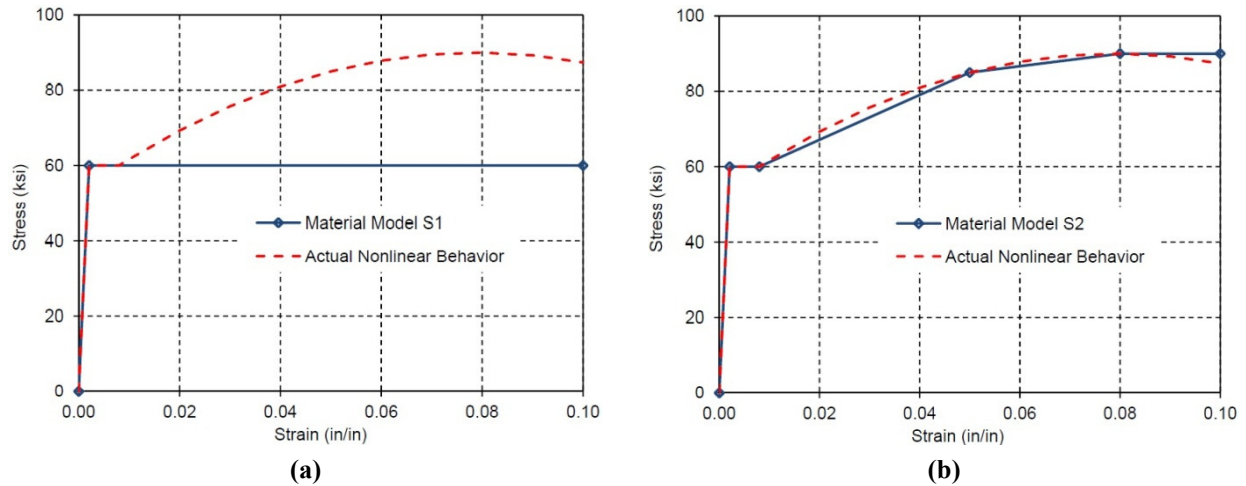


Fig. A.10: Idealized uniaxial stress-strain curve for steel in tension/compression: (a) model S1, (b) model S2

For both proposed idealized material models, the elastic modulus of 29000 ksi with the Poisson's ratio of 0.3 were introduced to characterize the behavior of the steel reinforcements prior to the yield point. However, the bilinear and multilinear isotropic material models were implemented in ANSYS to define the proposed material constitutive laws. It should be mentioned that Von-Mises yield criteria was also associated in the numerical analysis to simulate the triaxial failure surface for steel rebars. Both 3D and 2D representations of the Von-Mises failure surface in the principal stress space are depicted in Fig. A.11. Finally, in order to have a realistic FE simulation, the steel plates added to the numerical model at the supports as well as the loading points. The material properties for these steel plates assumed to be linear elastic with the elastic modulus of 29000 ksi and Poisson's ratio of 0.3.

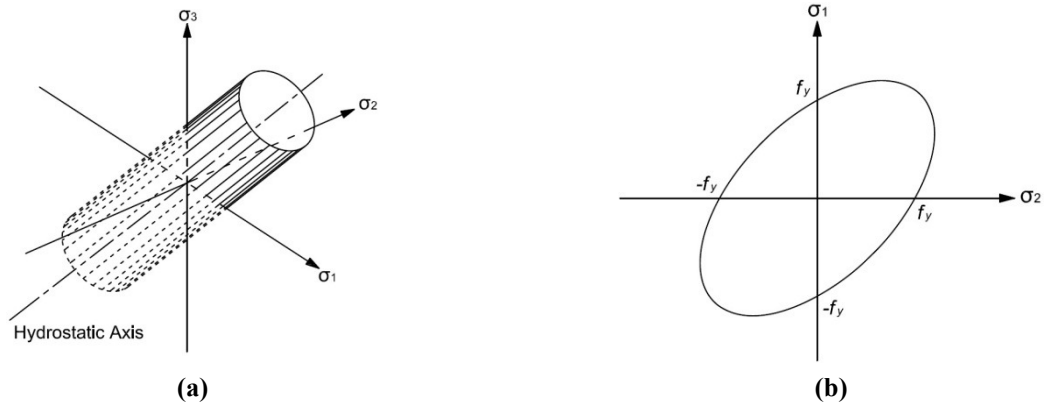


Fig. A.11: Von-Mises failure surface: (a) 3D representation, (b) 2D representation

A.3. Modeling

The corresponding FE mesh generation for the proposed numerical model, representing the simulated elements of concrete body, steel reinforcements, and loading plates, is illustrated in Fig. A.12. To provide the perfect bond between the concrete and steel reinforcement, link elements were connected to the adjacent nodes of neighboring concrete solid element. In order to validate the proposed numerical model with the experimental investigation, an appropriate loading and boundary conditions shall be assigned to FE model. The corresponding boundary conditions were applied at the planes of symmetry as well as a single centerline of the support plate to simulate a roller condition. On the other hand, the lateral loading was applied across the entire centerline of the loading plate, evenly distributed between the nodes.

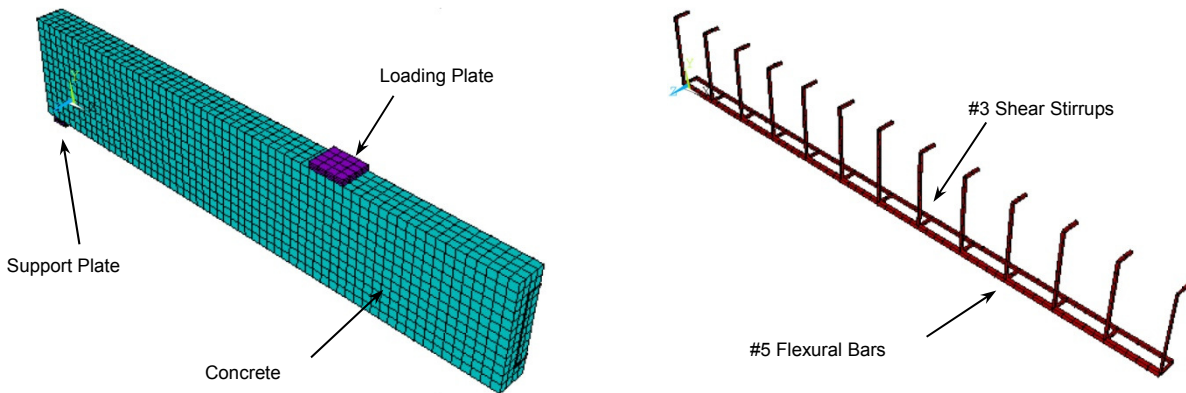


Fig. A.12: FE modeling of reinforced concrete beam

A.4. Analysis

Nonlinear static analysis with small displacements was selected for the numerical investigation of the experimental beam. Two analysis cases were also considered to evaluate the effect of material properties on the behavior of concrete structures. In other words, a sensitivity analysis has been done to define how global nonlinear response of a concrete structure can be influenced by implementing different idealizations for constitutive material models within the element domain. Consequently, the idealized material models of C1 and S1 were used for analysis case 1; while full nonlinear representation of material behavior was considered in analysis case 2, utilizing C2 and S2 constitutive models for concrete and steel elements, respectively.

The lateral load was applied on the simulated concrete beam incrementally using different load steps. The restart option was then implemented to initiate the new load step after the convergence occurred for a given load increment. The automatic time stepping was also turned on to facilitate the convergence at the end of each substep and precisely trace the nonlinear response of the structure. A detailed list of load steps with the corresponding number of substeps and the incremental applied loads, for both analysis cases, are given in Table A.2.

The load increments vary during the nonlinear analysis, based on the response of the structure. Prior to initial cracking, the load steps were chosen to be large enough since the structure was expected to behave linearly elastic within this region. After the first cracks formed in the concrete body, the load was applied in smaller portions on the beam to fully trace the nonlinear behavior upon cracking. The load increment was raised slightly until the steel reinforcements in the beam began to yield. After yielding of the steel, the stiffness of the structure was dramatically decreased which cause the corresponding displacements to increase rapidly. As a result, the load increment was reduced again to the smaller values in order to capture the ultimate capacity and failure of the beam.

All the corresponding parameters to define the nonlinear algorithm for the numerical analysis were set to their default values except for the convergence criteria, which are mostly categorized into force and displacement based methods. For the numerical analysis of reinforced concrete structures, force criteria usually fail to converge once cracking occurs in concrete. Therefore, only displacement criterion was implemented in this study with the reference value of 5 and the tolerance value of 0.05. However, the program was set to terminate the analysis, if the nonlinear

solution does not converge upon a given load increment. In this case, analysis shall be resubmitted under smaller load increment to overcome local instabilities and corresponding convergence issues.

Table A.2: Load steps for the FE analysis: (a) analysis case 1, (b) analysis case 2

(a)				(b)			
Load Step	Beginning Time	End Time	# of Sub-steps	Load Step	Beginning Time	End Time	# of Sub-steps
1	0	2500	15	1	0	2500	15
2	2500	2600	105	2	2500	2600	105
3	2600	2700	105	3	2600	2700	105
4	2700	2800	105	4	2700	2800	105
5	2800	2900	105	5	2800	2900	105
6	2900	3000	105	6	2900	3000	105
7	3000	3500	105	7	3000	3500	105
8	3500	4500	105	8	3500	4500	105
9	4500	5500	105	9	4500	5500	105
10	5500	6500	105	10	5500	6500	105
11	6500	7000	105	11	6500	7000	105
12	7000	7200	105	12	7000	7200	105
13	7200	7300	105	13	7200	7300	105
14	7300	7400	105	14	7300	7400	105
15	7400	7500	105	15	7400	7500	105
16	7500	7600	105	16	7500	7600	105
17	7600	7700	105	17	7600	7700	105
18	7700	7800	105	18	7700	7800	105
19	7800	7850	105	19	7800	7900	105
20	7850	7900	105	20	7900	8000	105
21	7900	7950	105	21	8000	8100	105
22	7950	8000	105	22	8100	8200	105
23	8000	8050	112	23	8200	8300	105
24	8050	8100	132	24	8300	8400	105

A.5. Discussion of Results

In order to assess the validity and accuracy of the proposed numerical model, the load-deflection curve at mid span of the beam derived from full nonlinear FE analysis, was compared to the corresponding experimental result provided by Buckhouse (1977). As depicted in Fig. A.13, the load deflection curves were derived numerically for both analysis cases 1 and 2 to

investigate the effect of material nonlinearity on the behavior of the reinforced concrete beam. Comparison of the outcomes demonstrated that there is a bifurcation point at which the results obtained from two analysis cases deviate from each other. As long as the loading and boundary conditions are identical for both analysis cases, this discrepancy would be definitely related to the idealization of the constitutive material models associated with the numerical simulation.

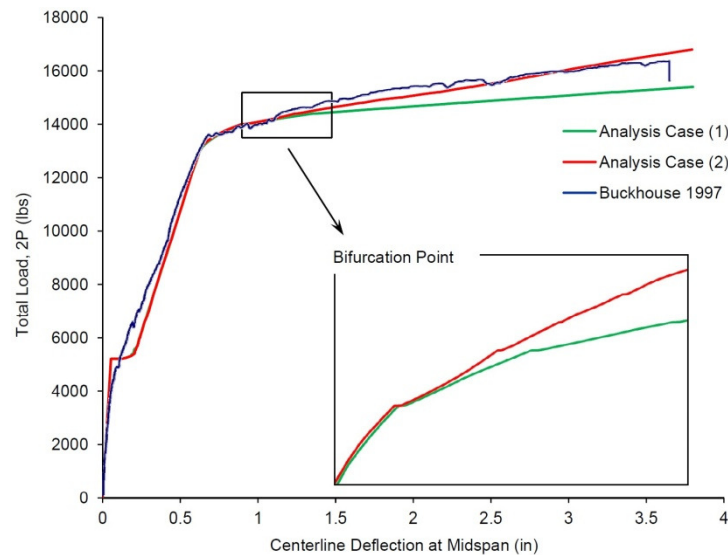


Fig. A.13: Load deflection curves at the midspan of the beam

Fig. A.14 illustrates the longitudinal stress distribution in concrete elements for both analysis cases, at the load step corresponds to the bifurcation point. Based on the similarities observed, it can be assumed that the modification of stress-strain relationship for concrete material, from inelastic-perfectly plastic idealization to full nonlinear behavior, does not have significant effect on the general response of the reinforced concrete beam. Therefore, the discrepancy between the results can mostly be attributed to the material properties of steel rebars.

As it was previously discussed, the stress-strain relationship for reinforcing steel has been modified by adding strain hardening region to the material properties assumed for model S1. Accordingly, it is expected that the structural stiffness of the simulated beam might be affected by this modification. Beyond the bifurcation point, however, the gradual increment in the slope of the load deflection curve corresponds to the analysis case 2, can justify this phenomenon. In contrary with the stress distribution in concrete body, the differences between axial stress

distribution in the flexural rebars, obtained from both analysis cases, ensure the effect of post-yield material hardening on the global system performance (see Fig. A.15).

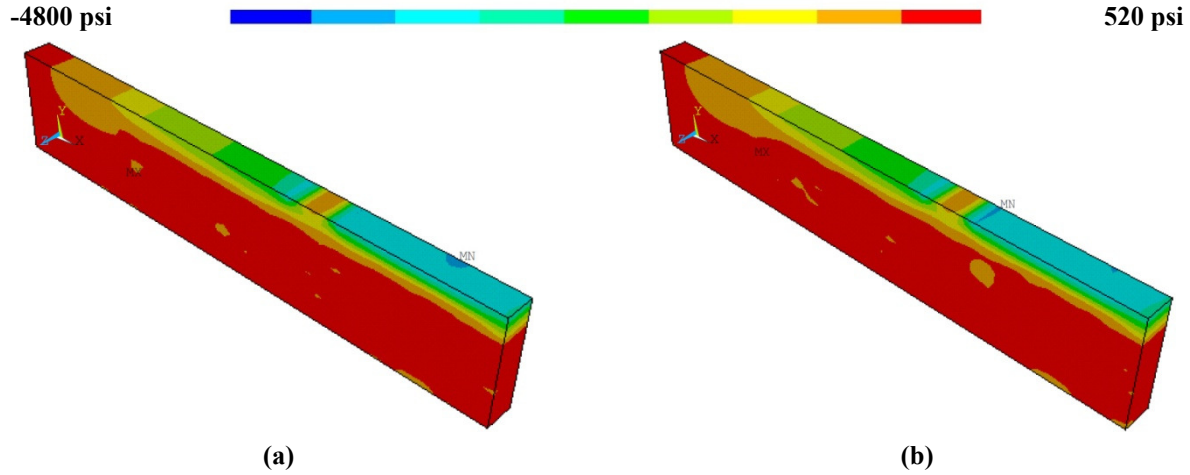


Fig. A.14: Longitudinal stress distribution in concrete at bifurcation: (a) analysis case 1, (b) analysis case 2

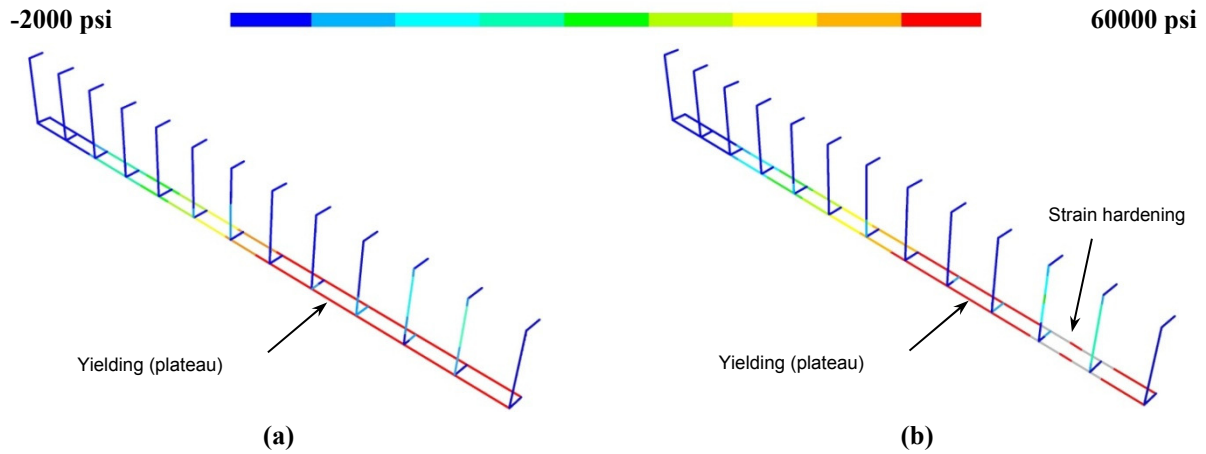


Fig. A.15: Longitudinal stress distribution in concrete at bifurcation: (a) analysis case 1, (b) analysis case 2

Fig. A.16 illustrates different behavioral stages throughout the loading history of the simulated R/C beam. As it is depicted, the response of the system can be generally classified into two main categories: (a) linear elastic behavior and (2) nonlinear behavior. The simulated reinforced concrete beam behaves linearly elastic prior to formation of flexural cracks (see Fig. A.17(a)). The state of strains in concrete, depicted in Fig. A.18(a), also demonstrated that the concrete beam keeps on its elastic response, even with the occurrence of the first flexural crack on the tension side of the beam. After crack initiation, the stress distribution is altered in both

concrete and reinforcing steel materials, which cause the structure to behave in a nonlinear fashion. By increasing applied load, flexural cracks propagate all the way through the concrete body, as depicted in Fig. A.17(b). Concrete nonlinearity also spread over the volumetric elements being affected by the crack propagation (see Fig. A.18(b)).

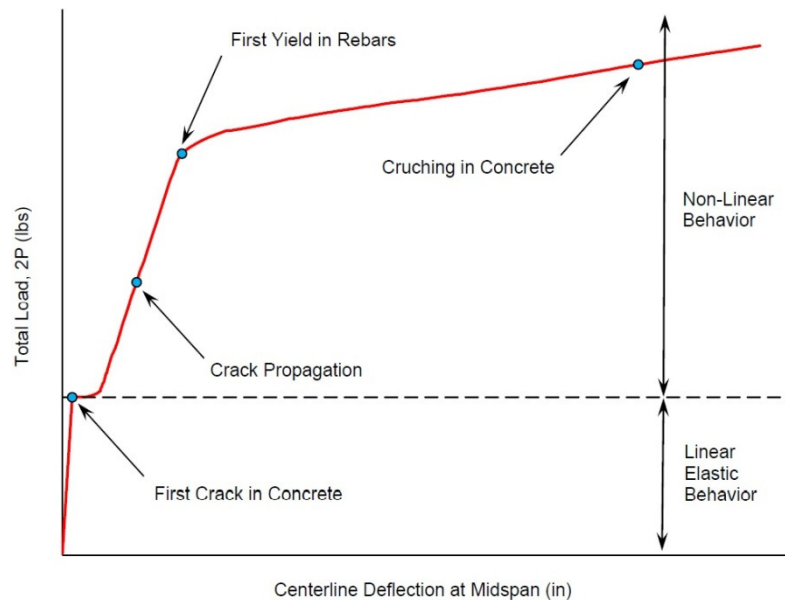


Fig. A.16: Behavioral stages throughout the loading history

Upon cracking, the load deflection curve moves up with a constant slope, due to linear behavior of reinforcing rebars prior to their yield point. Once the steel reinforcements yield, the global structural stiffness of the system decrease significantly and the slope of the load deflection curve drops off. Respectively, the mid span deflection of the beam increases rapidly under any further incremental load. At this point, not only the flexural cracks dominate all over the constant-moment region of the beam, but also diagonal tension cracks propagate near the supports, as given in Fig. A.17(c). This would represent the arc action mechanism of the load redistribution within the cracked concrete structure. The nonlinear distribution of longitudinal strain in concrete elements at the corresponding moment is also depicted in Fig. A.18(c).

By further increment in loading, cracks propagate through the height of cross section, until they reach the compression side of the beam, as given in Fig. A.17(d). These cracks are formed in a series of planes parallel to the longitudinal axis. Furthermore, they can simply be separated from ordinary flexural crack dominated on the planes perpendicular to the longitudinal direction.

Although the crushing capacity of the proposed concrete model has been turned off to overcome the convergence problems during nonlinear analysis, the formation of these horizontally oriented cracks on the compression side of the beam can be represented as the occurrence of crushing in concrete for the proposed simulated model. In addition, this assumption can be justified by simultaneous investigation on the longitudinal strain distribution in corresponding degraded elements that exceed the crushing limit of 0.003, as illustrated in Fig. A.18(d).

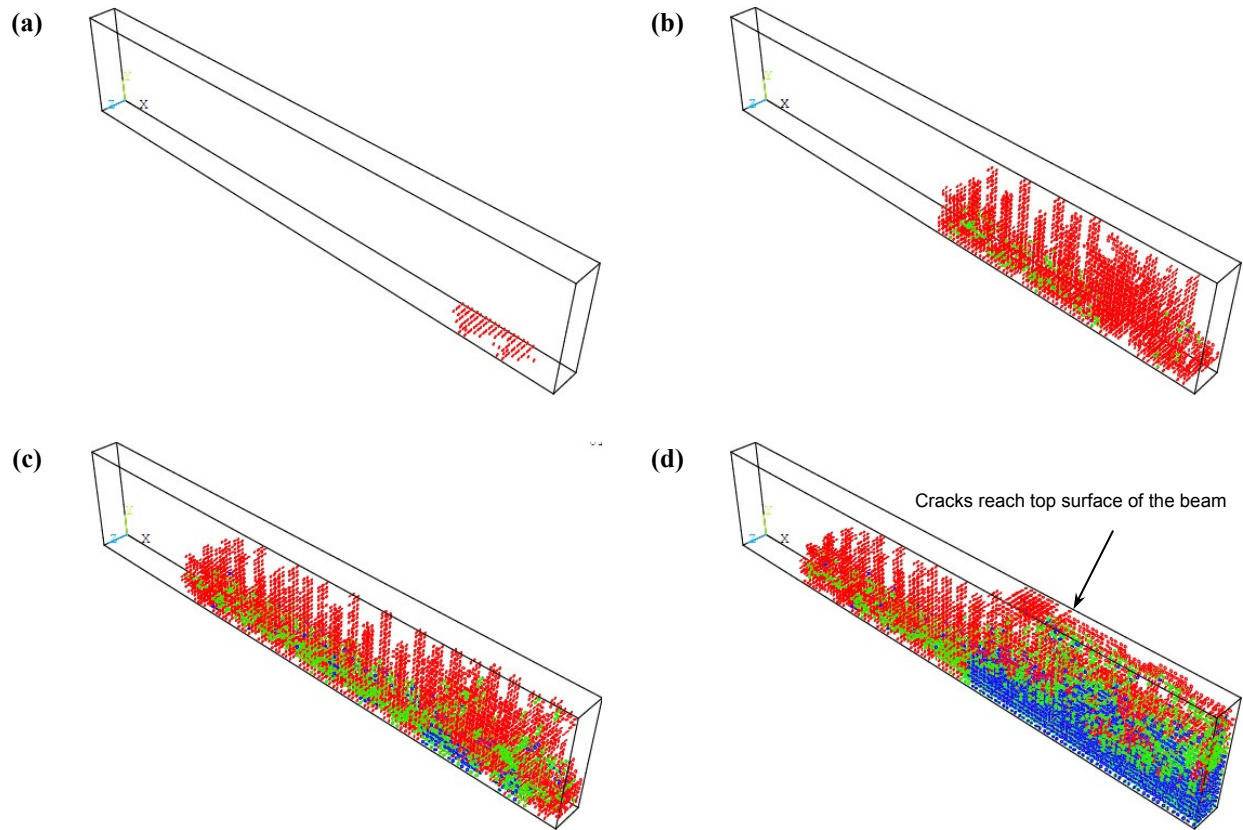


Fig. A.17: Cracking pattern at different stages of loading: (a) first crack in concrete, (b) crack propagation, (c) first yield in rebars, (d) crushing in concrete.

Nonlinear FE analysis of the simulated beam can be continued with smaller load increments until the rest of concrete elements are degraded by crack propagation. In actual practice, however, the failure of the reinforced concrete beam occurs once the crushing zone on the compression side is large enough to create a local instability and cause the beam to reach its ultimate capacity. In this study, the propagation of horizontally oriented cracks within a finite strip on the compression side is introduced as the failure criteria.

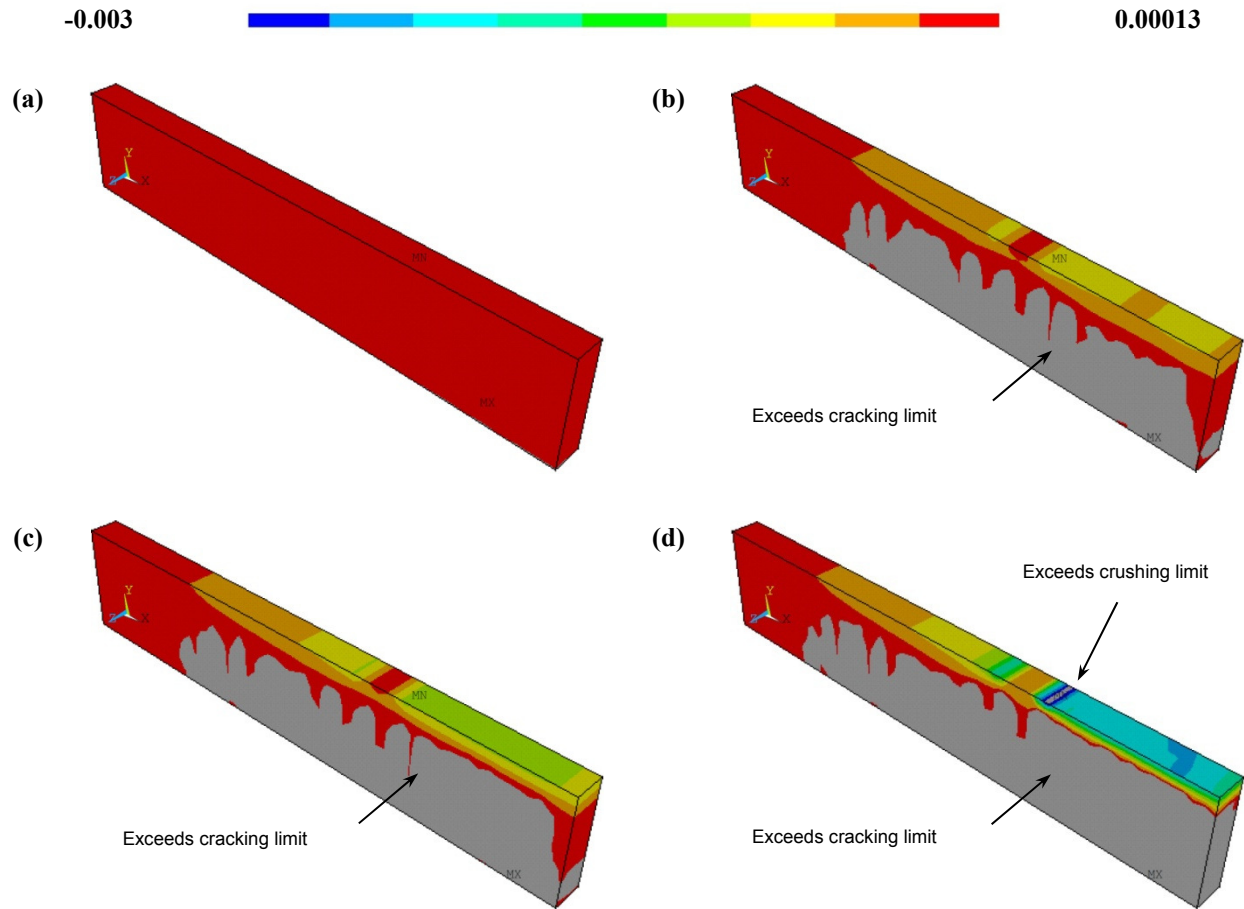


Fig. A.18: Axial strain distribution in concrete body at different stages of loading: (a) first crack in concrete, (b) crack propagation, (c) first yield in rebars, (d) crushing in concrete.

By implementing proposed failure criteria, the ultimate capacities and the corresponding centerline deflections of the reinforced concrete beam derived from experimental investigation and numerical study, associated with analysis case 2, are summarized in Table A.3. It can be concluded that the proposed numerical model is capable enough in predicting the nonlinear behavior of reinforced concrete beam under lateral loading.

Table A.3: Comparison of the results

	Test	FEA
	Buckhouse 1997	Analysis case 2
Ultimate capacity (lbs)	16310	16180.4
Centerline deflection (in)	3.65	3.13

Appendix B:

Numerical Analysis of a Corner Supported Two-Way Concrete Slab

B.1. Experimental Investigation

Results obtained from an experimental testing of a corner-supported two-way reinforced concrete slab performed by McNeice (1967) were utilized in this study to calibrate the proposed finite element model.

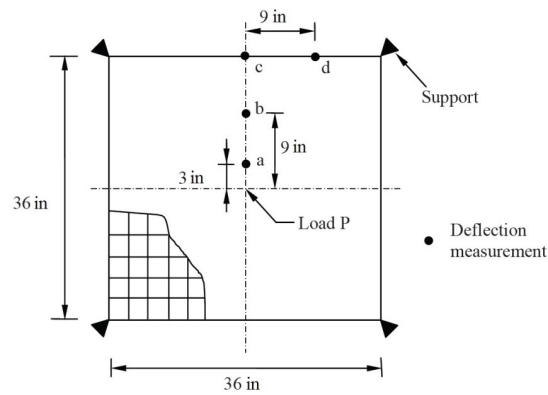


Fig. B.1: Configuration of two-way slab tested by McNeice (1967)

The tested slab was 36 in square by 1.75 in thick with an isotropic mesh of 0.85% placed at a depth of 1.31 in. Moreover, the experimental specimen was supported at four corners and tested under a central load applied at the middle of the span. Deflections measured at several points at the edge of the slab as well as close to the center of the slab, were implemented to derive the corresponding load deflection curve for validation purposes (Ferrand 2005), see Fig. B.1.

B.2. Finite Element Characterization

For validation study, the ANSYS finite element package was implemented to simulate the reinforced concrete slab. Due to the symmetry of the structure in geometry and loading conditions, only one quarter of the slab was modeled for numerical simulation and analysis, see Fig. B.2. The general trend in the modeling of the reinforced concrete slab is categorized in different stages and is going to be discussed in details in the next following sections.

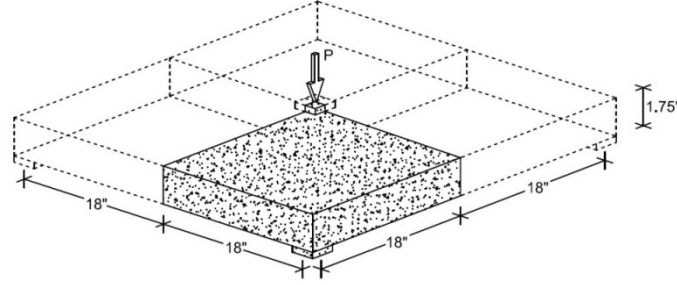


Fig. B.2: Application of symmetry in FE modeling

Similar to calibrated reinforced concrete beam, three types of elements were utilized in the FE modeling of reinforced concrete slab. Solid65, Solid185, and Link180 elements were implemented to simulate concrete body, loading plates, and reinforcing rebars, respectively. Moreover, the rebars was chosen to be simulated using discrete model, having common nodes with adjacent concrete element to ensure the full bonding effect. The corresponding real constants for the proposed model of concrete slab are summarized in Table B.1.

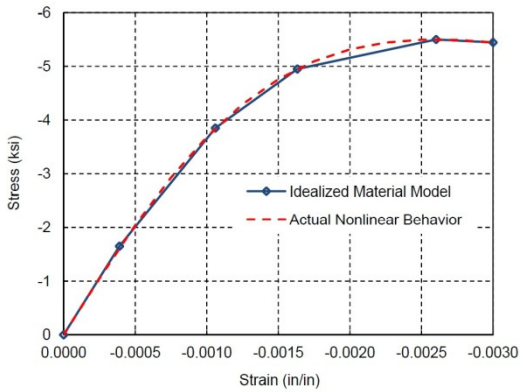
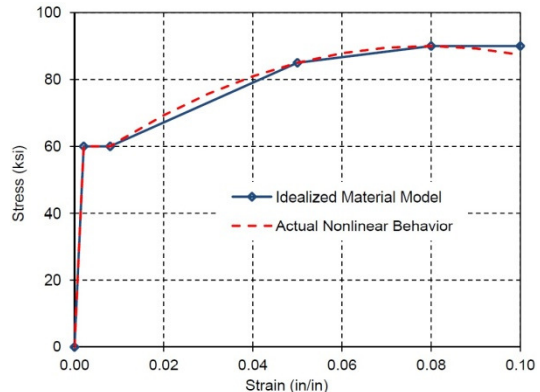
Table B.1: Real constants for proposed FE model of concrete slab

Real Constant	Element Type	Constants		
		Rebar 1	Rebar 2	Rebar 3
Set 1	Solid65	Material Number	0	0
		Volume Ratio	0	0
		Orientation Angle (θ)	0	0
		Orientation Angle (ϕ)	0	0
Set 2	Link180	Rebar		
		Cross Section (in ²)	0.31	-

The material properties were also defined for each element type, regarding the corresponding material characteristics, as summarized in Table B.2. The elastic modulus of 4227.2 ksi with respect to uniaxial compressive strength of 5.5 ksi along with the Poisson's ratio of 0.15 were used to characterize the nonlinear material behavior of the concrete. To define the triaxial failure surface, the William and Warnke (1974) model was also implemented with the same shear transfer coefficients introduced for the concrete beam and the uniaxial cracking stress of 0.56 ksi. For Gr.60 steel rebars, full nonlinear stress-strain relationship with the elastic modulus of 29000 ksi and Poisson's ratio of 0.3 were introduced, associated with Von-Mises yield criteria to simulate the triaxial failure surface for steel rebars. Finally, the material properties for loading

steel plates assumed to be linear elastic with the elastic modulus of 29000 ksi and Poisson's ratio of 0.3.

Table B.2: Material properties for FE model of reinforced concrete slab

Material Model	Element Type	Material Properties		Material Nonlinear Constitutive Laws
1	Solid65	Linear isotropic		
		Elastic Modulus (ksi)	4227.2	
		Poisson's Ratio	0.15	
		Multilinear isotropic (comp.)		
		Stress (ksi)	Strain	
		1.65	0.00039	
		3.85	0.00106	
		4.95	0.00163	
		5.50	0.00260	
		5.44	0.0030	
		Concrete		
		ShrCf-Op	0.3	
		ShrCf-Cl	1	
		UnTensSt (ksi)	0.56	
		UnCompSt (ksi)	-1	
2	Link180	Linear isotropic		
		Elastic Modulus (ksi)	29000	
		Poisson's Ratio	0.3	
		Multilinear isotropic		
		Stress (ksi)	Strain	
		0	0.00000	
		60	0.00138	
		60	0.01400	
		85	0.04000	
		90	0.08000	

B.3. Modeling

The corresponding FE mesh generation for the proposed numerical model, representing the simulated elements of concrete body, steel reinforcements, and loading plates, is illustrated in Fig. B.3. To eliminate stress concentration at corner supports, an additional row of elements was

added to the external sides of the simulated slab. In order to validate the proposed numerical model with the experimental investigation, an appropriate loading and boundary conditions shall be assigned to FE model. The corresponding boundary conditions were applied at the planes of symmetry as well as a single node of the support plate to simulate a roller condition. Besides, the central load was applied over the loading plate, evenly distributed between the nodes.

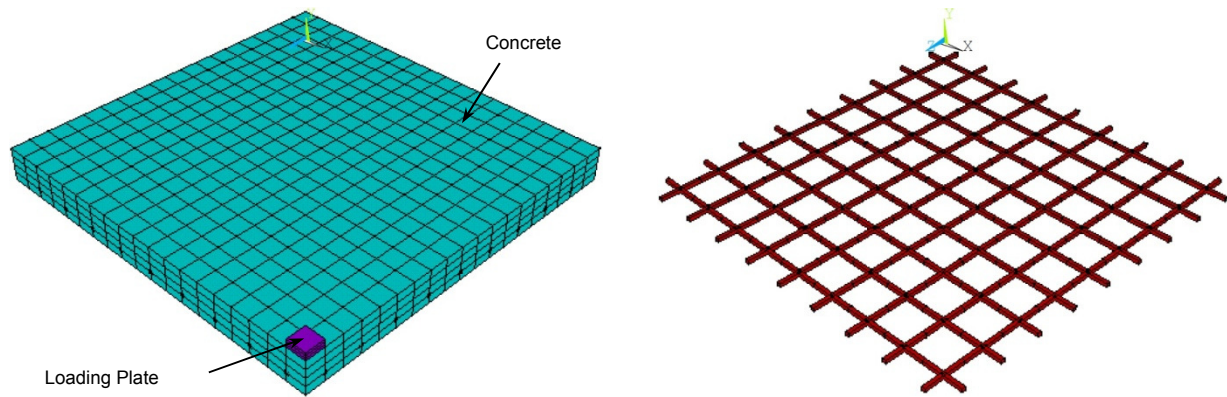


Fig. B.3: FE modeling of reinforced concrete slab

B.4. Analysis

Nonlinear static analysis with small displacements was selected for the numerical investigation of the experimental slab. The lateral load was applied on the simulated concrete slab incrementally using different load steps. The restart option was then implemented to initiate the new load step after the convergence occurred for a given load increment. A detailed list of load steps with the corresponding number of the sub-steps and the incremental applied loads, for both analysis cases, are given in Table B.3. All the corresponding parameters to define the nonlinear algorithm for the numerical analysis were set to their default values except for the convergence criteria. Similar to the calibrated concrete beam, only displacement criterion was implemented with the reference value of 5 and the tolerance value of 0.05.

B.5. Discussion of Results

The general configuration of the deformed reinforced concrete slab under central loading, obtained from numerical FE analysis is illustrated in Fig. B.4. In order to evaluate the accuracy of the proposed numerical model, load-deflection curves at the predefined selected nodes, derived from full nonlinear FE analysis, was compared to the corresponding experimental results (McNeice 1967), as depicted in Fig. B.5. Despite the experimental investigation, complete

nonlinear behavior of the reinforced concrete slab was captured using corresponding FE analysis on the proposed numerical model.

Table B.3: Load steps for the FE analysis of concrete slab

Load Step	Beginning Time	End Time	# of sub-steps
1	0	100	105
2	100	200	105
3	200	300	105
4	300	400	105
5	400	500	105
6	500	600	105
7	600	700	105
8	700	800	105
9	800	900	105
10	900	1000	105
11	1000	1100	105
12	1100	1200	105
13	1200	1300	105
14	1300	1400	105
15	1400	1500	105

Based on the load deflection curves obtained from experimental study, it can be concluded that the applied load was only capable to cause cracks in the concrete slab; whilst, the flexural reinforcements remained elastic.

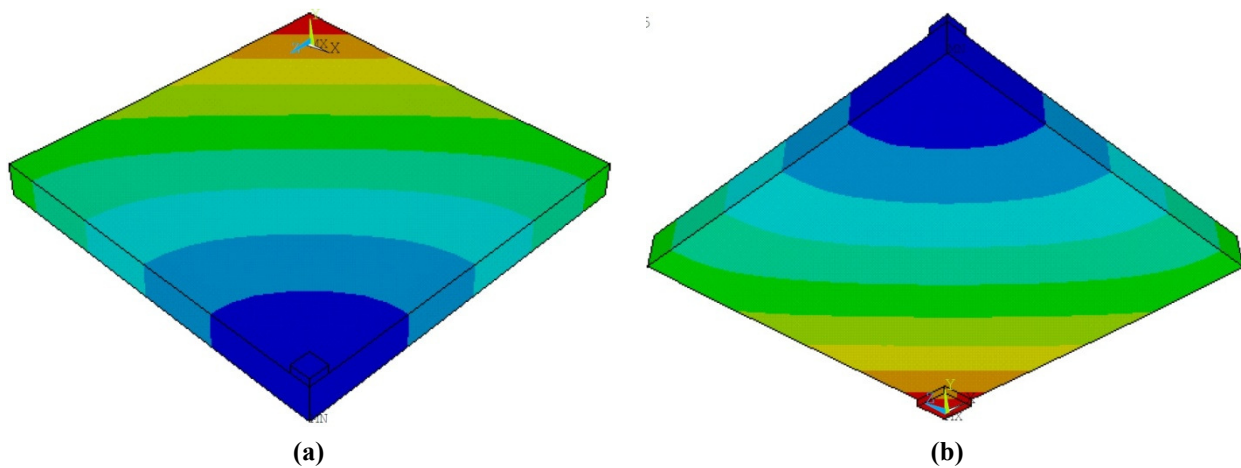


Fig. B.4: Deflection pattern of the proposed FE model: (a) top view, (b) bottom view

This can be strongly justified by comparing the results with those obtained from numerical analysis. As it can be seen in Fig. B.5, the proposed numerical model is capable enough in predicting the response of the structure within the elastic region. Once first crack occurs in concrete body, the global structural stiffness of the system decreases dramatically. In other words, the load carrying mechanism of the slab was altered from an intact composite system to a cracked concrete section associated with flexural reinforcements. Nevertheless, the numerical results are still in good agreement with the experimental data, even after the initiation of nonlinear behavior. Moreover, it seems that the discrepancy between the results is going to be diminished with further load increment. Same trend was also observed in the analytical load deflection behavior of the reinforced concrete beam, (see Fig. A.13).

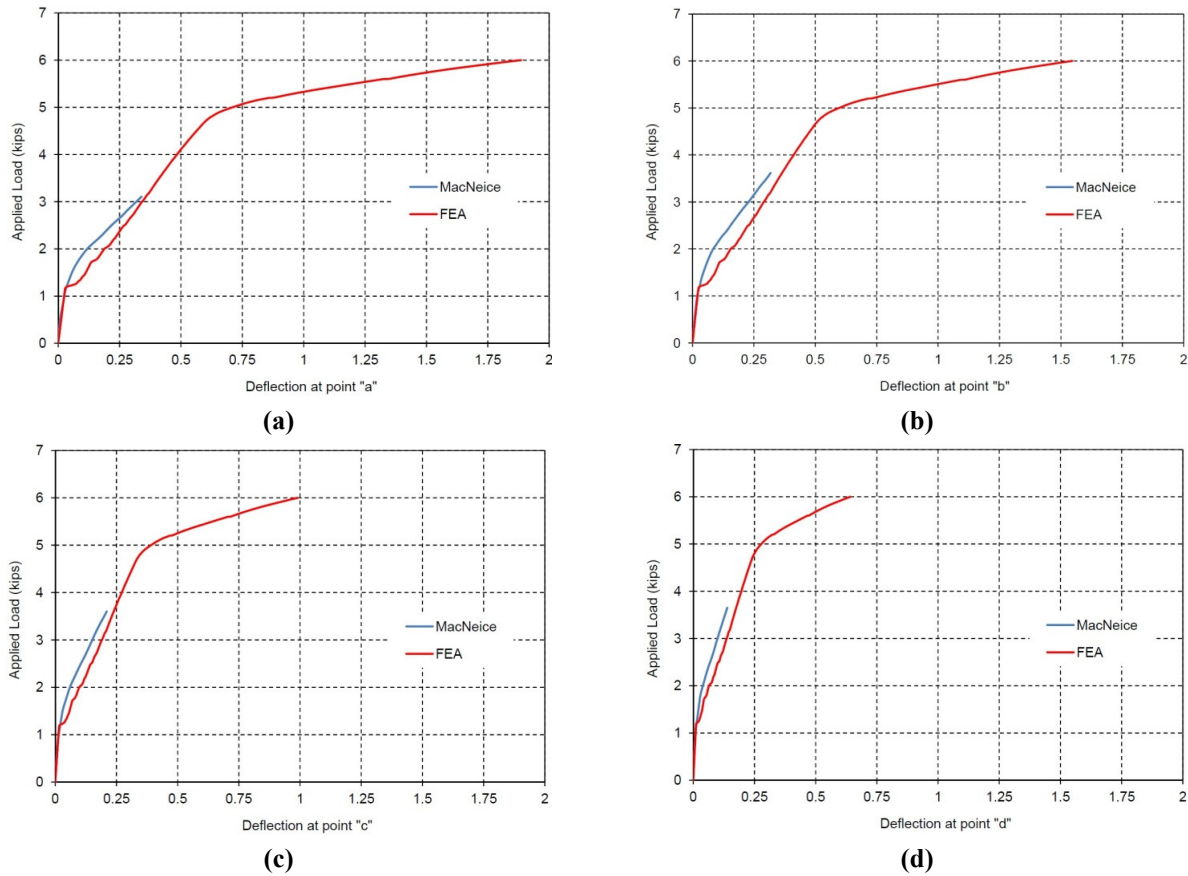


Fig. B.5: Load deflection curves at: (a) point "a", (b) point "b", (c) point "c", (d) point "d"

The behavioral stages of the simulated reinforced concrete slab throughout the loading history, is almost the same as that previously illustrated in Fig. A.13 for reinforced concrete beam. The proposed model for the concrete slab behaves linearly elastic prior to formation of

flexural cracks (see Fig. B.6(a)). The state of strains in concrete (only along x direction due to symmetry in loading conditions and geometry), depicted in Fig. B.7(a), also demonstrated that crack propagation initiates from the bottom surface of the slab.

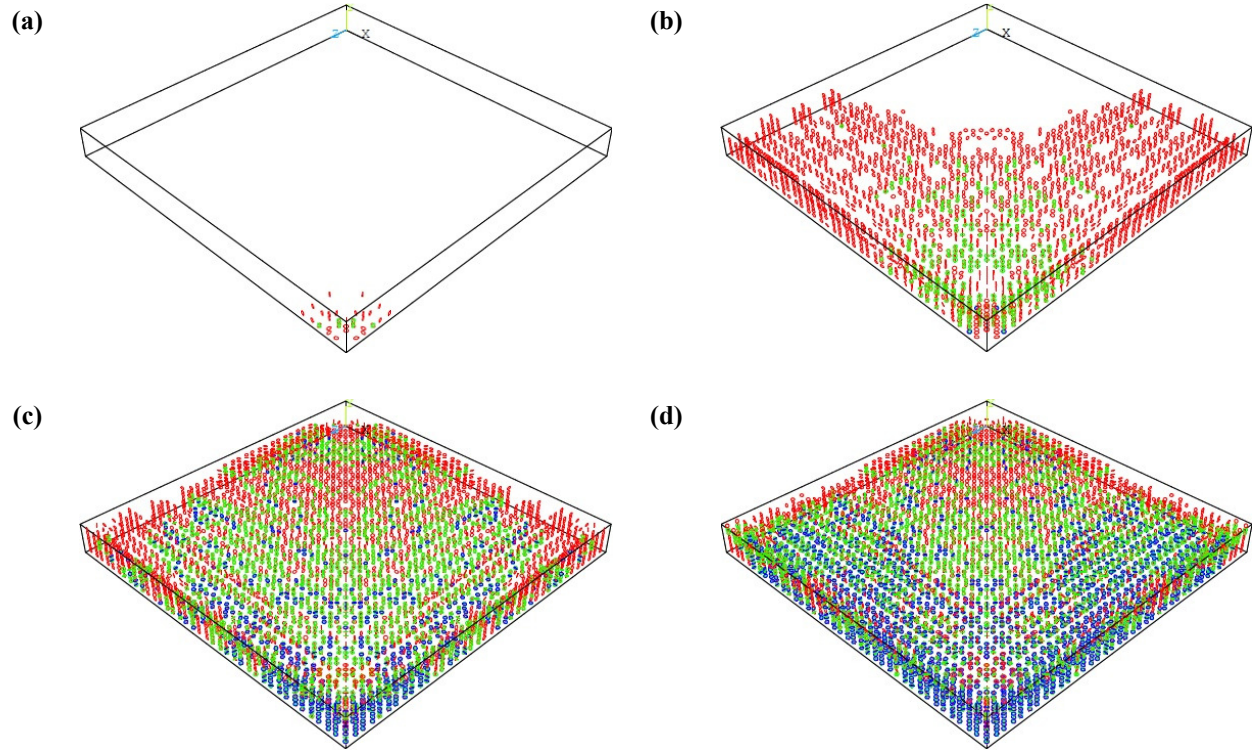


Fig. B.6: Cracking pattern at different stages of loading: (a) first crack in concrete, (b) crack propagation, (c) first yield in rebars, (d) crushing in concrete.

After crack initiated, the stress distribution is altered in both concrete and reinforcing steel materials, which cause the structure to behave in a nonlinear fashion. By increasing applied load, flexural cracks propagate all the way through the concrete body, as depicted in Fig. B.6(b). Concrete nonlinearity also spread over the volumetric elements being affected by the crack propagation (see Fig. B.7(b)). Upon cracking, the load deflection curve moves up with a constant slope, due to linear behavior of reinforcing rebars prior to their yield point. Once the steel reinforcements yield, the global structural stiffness of the system decrease significantly and the slope of the load deflection curve drops off. Respectively, the vertical deflection of the slab increases rapidly under any further incremental load. At this point, the first and second flexural cracks dominate almost all over the slab in two principal directions, as given in Fig. B.6(c).

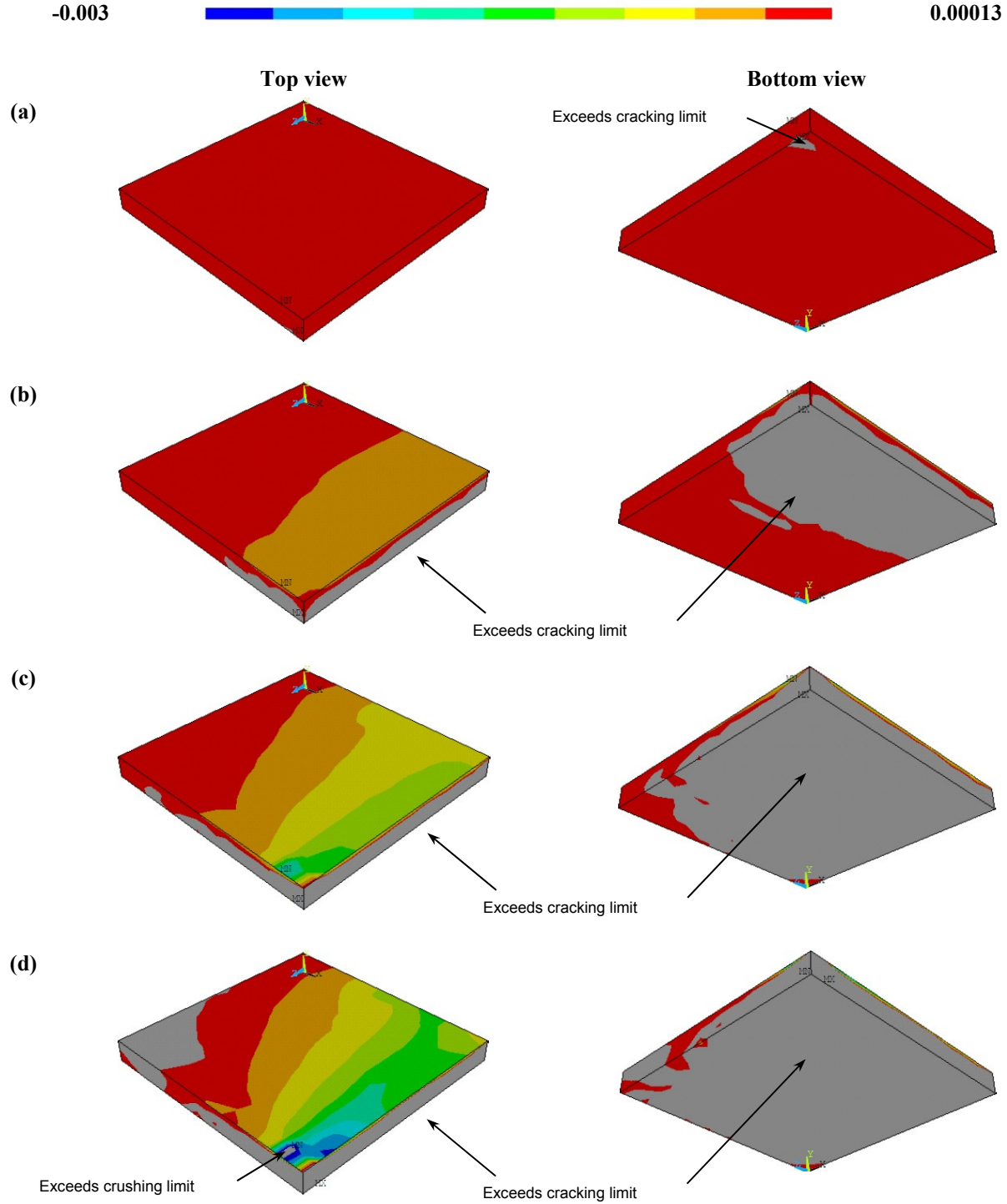


Fig. B.7: Strain distribution (along x direction) in concrete body at different stages of loading: (a) first crack in concrete, (b) crack propagation, (c) first yield in rebars, (d) crushing in concrete.

The nonlinear distribution of strain in concrete elements at the corresponding moment is also depicted in Fig. B.7(c). By further increment in loading, third flexural cracks also propagate

through the concrete body of the slab, as given in Fig. B.6(d). Although the crushing capacity of the proposed FE model has been turned off to overcome the convergence problems during nonlinear analysis, ultimate capacity and failure of the reinforced concrete slab can be predicted numerically by monitoring the strain distribution close to the applied load, that exceed the crushing limit of 0.003, as illustrated in Fig. B.7(d). To sum up, it can be concluded that the proposed numerical model is capable enough in predicting the nonlinear behavior of corner-supported RC slab under central loading.

Appendix C:

Numerical Analysis of a Simply Supported Steel Plate Girder

C.1. Experimental Investigation

Results obtained from a series of experimental investigations on simply supported high strength steel plate girders under lateral patch loading by Lagerqvist and colleagues (1995), were utilized in this study to calibrate the proposed finite element model. The selected plate girder for validation study has the overall length (L) of 1900 mm, having geometrical characteristics as illustrated in Fig. C.1. Vertical deformation under loading plate was implemented to derive the load-deflection response of the girder for validation purposes.

C.2. Finite Element Characterization

For validation study, the ANSYS finite element package was implemented to simulate the selected steel plate girder. Although the loading and boundary conditions are almost symmetric in this case, a full scale model shall be created numerically to capture the effect of geometrical instabilities associated with the behavior of steel plate girders. As usual in thin-walled structures, the geometrical nonlinearities dominate the nonlinear behavior of the system. Moreover, the structure may experience material nonlinearities at higher levels of loading, due to excessive large deformations caused by local instabilities. The general trend in the modeling of the high strength steel plate girder is categorized in different stages and is going to be discussed in details in the next following sections.

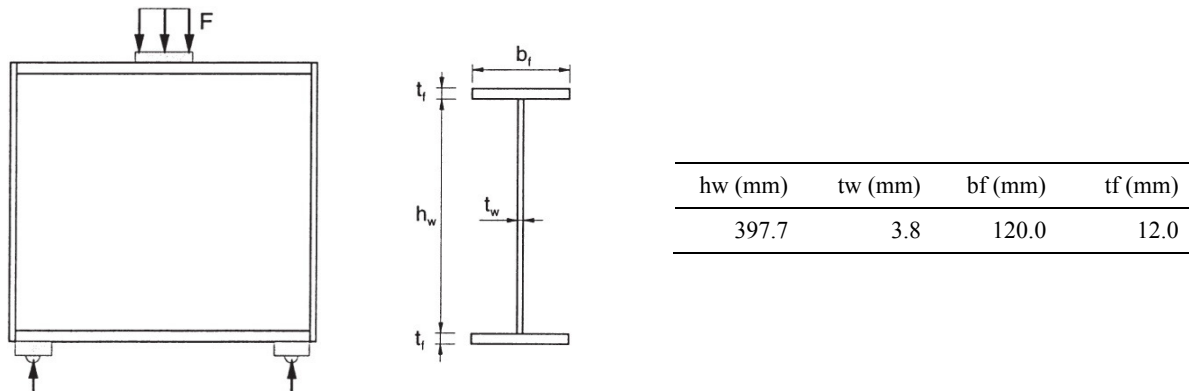


Fig. C.1: Geometrical configuration of selected plate girder for validation study

A Solid185 element was implemented to simulate loading and support plates, as previously discussed for the concrete beam and slab. Moreover, 4-node shell element, Shell181, with three translational and three rotational degrees of freedom at each node, was utilized to model the steel plate girder in the FE simulation.

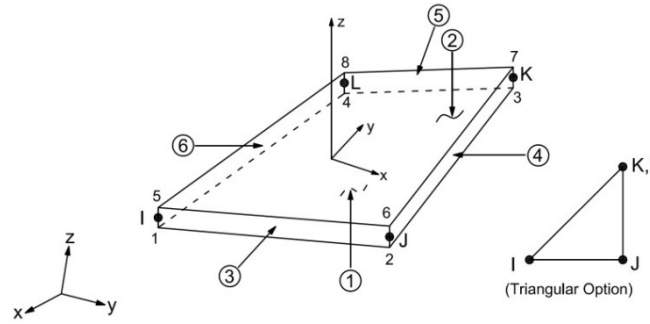
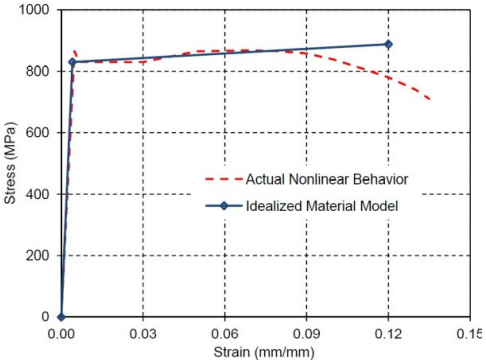
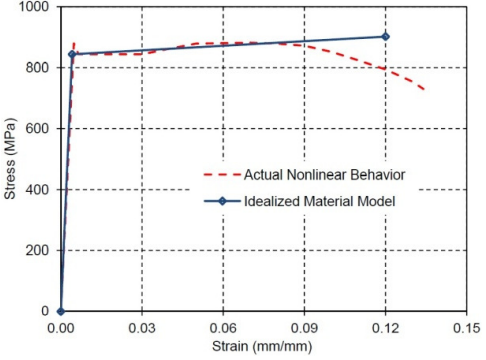


Fig. C.2: Shell181 element

The element is well-suited for linear, large rotation, and large strain nonlinear applications. Moreover, both full and reduced integration schemes are supported as an option within the element domain. Fig. C.2 shows the geometry, node locations, and the element coordinate system for this element. The selected girder cross section was divided into three parts including top flange, web, and bottom flange. Each part was then simulated using shell elements which were characterized with the corresponding thickness and material properties. Moreover, to facilitate the modeling process, the girder section was simplified by setting the web height in the numerical model equal to $h_w + t_f$. The number of integration points through the thickness of shell was set to the default value of 5 presumed by ANSYS (2011).

Two different material properties were considered for different parts of the simulated plate girder, including flanges and web. The stress-strain curve for both materials assumed to have bilinear relationship, based on the approximation of the actual behavior made by Lagerqvist (1995). As summarized in Table C.1, the elastic modulus of 204 GPa, tangent modulus of 0.5 GPa and Poisson's ratio of 0.3 were introduced both material properties; whilst yield stresses were set to 830 and 844 MPa for the web and flange plates, respectively. A von-Mises yield criterion was also utilized to simulate the three dimensional failure surface of the steel material. It should be finally noted that the loading plates and supports was assumed to be rigid in numerical analysis with the elastic modulus of 204000 GPa and Poisson's ratio of 0.3.

Table C.1: Material properties for FE model of steel plate girder

Material Model	Element Type	Material Properties	Material Nonlinear Constitutive Laws
1	Shell181 (web)	Linear isotropic	
		Elastic Modulus (GPa)	
		Poisson's Ratio	
		Bilinear isotropic	
		Tangent Modulus (GPa)	
2	Shell181 (flange)	Linear isotropic	
		Elastic Modulus (GPa)	
		Poisson's Ratio	
		Bilinear isotropic	
		Tangent Modulus (GPa)	

C.3. Modeling

Fig. C.3 illustrates the corresponding FE mesh generation for the proposed numerical model, representing the simulated elements of steel plate girder as well as loading and support plates. In order to validate the model with the experimental investigation, an appropriate loading and boundary conditions shall be assigned to FE model. The corresponding boundary conditions were applied on centerline of the support plates to simulate roller condition. Moreover, common node between the web and flange plates, right in the mid-span of the girder, was also restrained in longitudinal direction, to ensure the state of symmetry in deformed configuration and stress distribution of the FE model, even after it undergoes large deformations (Alinia et al. 2011). On the other hand, the lateral loading was applied as a uniform pressure all over the loading plate.

In order to capture the nonlinear response of the simulated plate girder associated with geometrical instabilities during FE analysis, initial imperfections shall be assigned to the proposed numerical model to agitate the occurrence of buckling phenomenon. The numerically induced imperfection pattern must also be consistent with actual out-of-flatness of tested plate

girders due to the manufacturing process. These imperfections may govern the mode of deformation, and therefore influence the response of the structural members. However, it is probable that the inherent distortions may vary along the length of the girder. In this study, the out-of-flatness of the web were approximated by almost circular buckles, whereas twisting represented the imperfections of the flange subjected to the concentrated loading. As shown in Fig. C.4, the web distortion was modeled as sinusoidal waves over the web height, and the number of waves along the length of the girder was chosen such that the imperfection had maximum amplitude below the concentrated load (Tryland 1999).

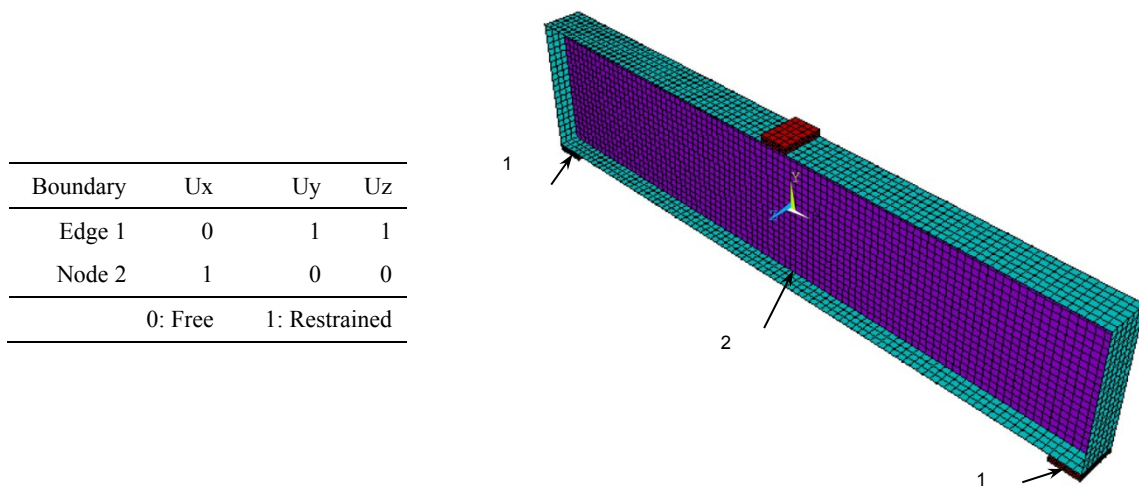


Fig. C.3: FE modeling of steel plate girder and applied boundary conditions

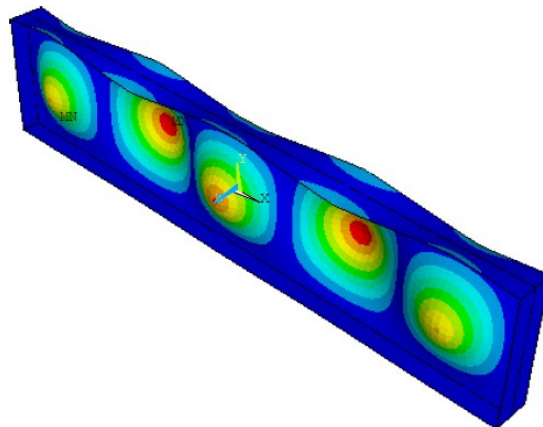


Fig. C.4: Geometrical imperfection applied to FE model of plate girder

C.4. Analysis

Nonlinear static analysis with large displacements was selected for the numerical investigation of the experimental girder. The lateral patch loading was applied incrementally on the simulated plate girder previously deformed by initial imperfections. The Arc-length method was also activated as solution method, in order to capture the softening behavior of the proposed FE model after its ultimate capacity. All the corresponding parameters regarding nonlinear algorithm for the analysis were set to their default values including the convergence criteria.

C.5. Discussion of Results

In order to evaluate the accuracy and validity of the proposed numerical model, the load-deflection response of the girder was derived from full nonlinear FE analysis for the common node between the web and top flange located under the loading plate. As it is depicted in Fig. C.5, the obtained load-deflection behavior is in a good agreement with the corresponding experimental results. For comparison purposes, results obtained from both numerical and experimental investigations are summarized in Table C.2.

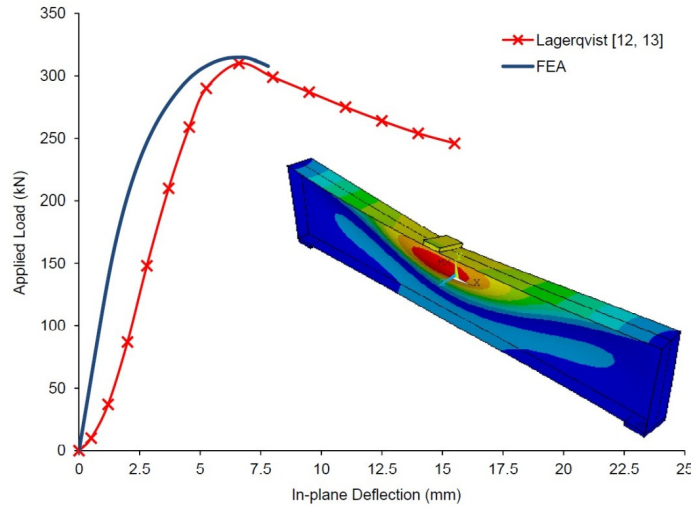


Fig. C.5: Nonlinear response of slender plate girder subjected to patch loading

Furthermore, deformed configuration of the steel plate girder under lateral patch loading, also depicted in the Fig. C.5, demonstrated that the performed FE analysis associated with geometrical and material nonlinearities is capable enough in predicting the large deformations of the girder, represented as buckling of the web in this problem.

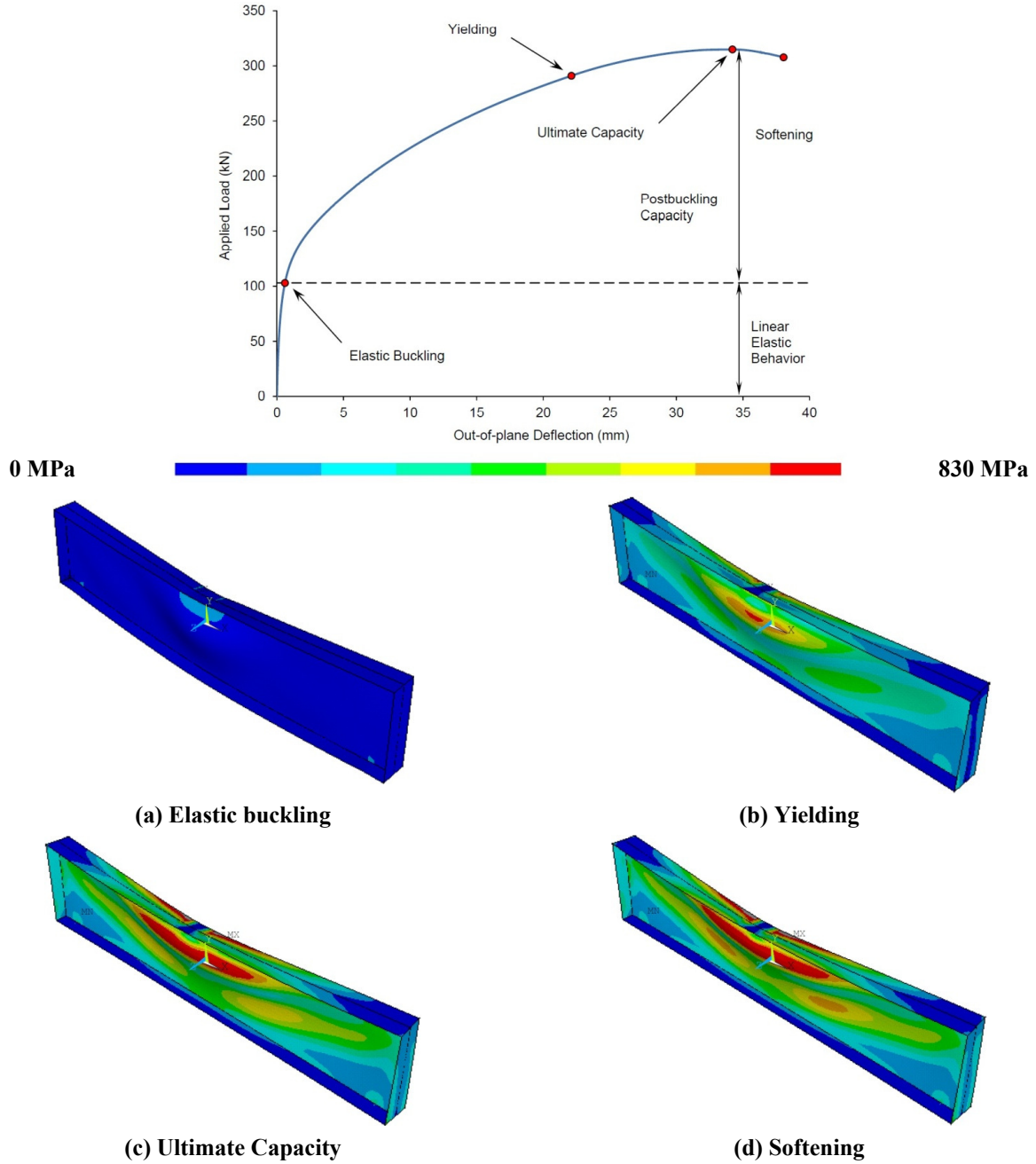


Fig. C.6: Behavioral stages and state of stresses in simulated plate girder

As it can be seen, the applied loading history for the proposed FE model can be divided into four stages. The simulated plate girder with slender web experienced elastic buckling and continued to absorb more loads beyond the buckling capacity up to its ultimate load. In fact, the elastic buckling stage is followed by the elastic postbuckling capacity (due to the formation of diagonal tension field) up to material yielding and ultimate capacity which in turn is followed by the softening stage. The corresponding Von-Mises stress distributions within the simulated plate

girder are also depicted in Fig. C.6 in order to provide a visual representation of different behavioral stages (Alinia et al. 2009 and 2011).

Table C.2: Comparison of the results

	Test	FEA
	Lagerqvist (1995)	ANSYS
Ultimate capacity (kN)	310.0	314.7
Deflection (mm)	6.60	6.53

Appendix D:

Numerical Analysis of a Full Scale Composite Bridge

D.1. Experimental Investigation

A field testing of a 4-span continuous composite steel bridge has been done by Burdette et al. (1971), to capture the nonlinear response of the bridge structure and determine the ultimate load capacity of the composite system under the excessive loading. The bridge superstructure covers the total distance of 320 ft with 4 spans, having lengths of 70, 90, 90, and 70 ft, respectively. A seven in concrete deck constructed on four W36x170 steel girders, provides the driving surface for the passing traffic and guarantees the integrity of the bridge superstructure. As illustrated in Fig. D.1, the girders are evenly placed with a uniform spacing of 8 ft and 4 in. Moreover, two symmetrical overhangs of 4 ft and 9 in on each side of the deck makes the overall bridge width roughly equal to 34 ft and 6 in (Barth et al. 2006).

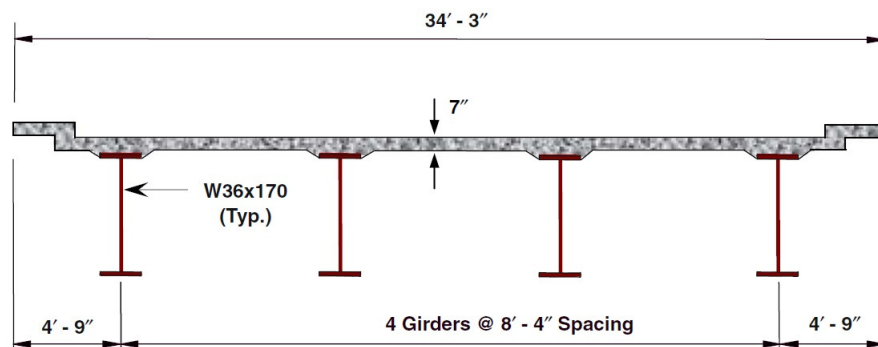


Fig. D.1: Cross section of Tennessee 4-span continuous bridge

The corresponding loading pattern associated with the full scale test of the bridge superstructure is depicted in Fig. D.2. The spacing and magnitude of the applied loads were chosen to mimic the rear wheels of regular HS-20 trucks in each lane. Furthermore, the loads are applied at specific longitudinal positions to create the maximum positive moment approximately near the midspan. The loads were evenly applied at each of the eight points through a rock anchor system with a 200 kips capacity center hold jack resting on a bearing grill (Barth et al. 2006).

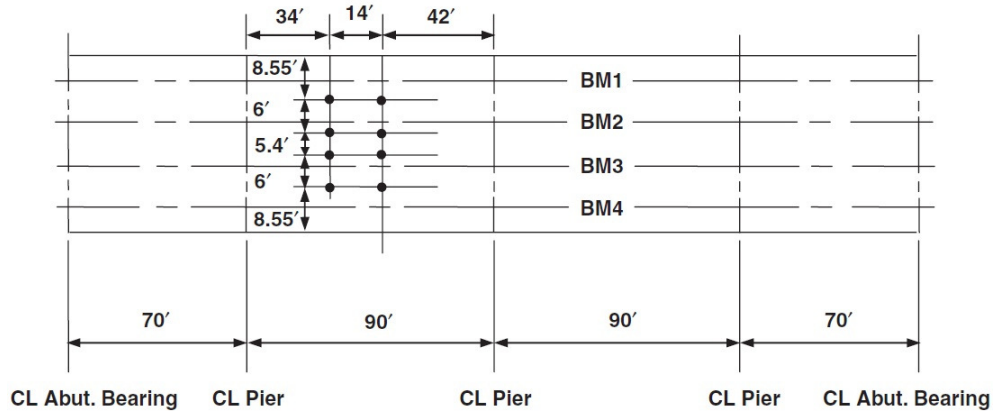


Fig. D.2: Loading configuration of a 4-span continuous bridge

D.2. Finite Element Characterization

In this study, however, the ANSYS FE computer package was utilized for validation of the nonlinear response of the corresponding composite bridge structure. The modeling techniques of the 4-span actual bridge including element characteristics, material models, mesh generation, loading and boundary conditions are categorized in different stages and going to be discussed in the next following sections.

Five different types of elements were utilized in the FE analysis to simulate different parts of composite steel bridge, including concrete deck, reinforcing rebars, steel girders, cross frame bracings and the shear studs. SOLID65 element was used for 3D modeling of the concrete deck. As it was previously mentioned, nonlinear behavior of concrete material can be fully characterized by the features embedded in the element, such as cracking, crushing, plastic deformation, and creep. An uniaxial tension-compression 3D spar element, Link180, was implemented to simulate the rebars reinforcing the concrete deck of the bridge superstructure. Similar to the pervious case of validation Shell181, was utilized to model the steel plate girders in the FE simulation.

The lateral bracing of the steel girders in the given bridge superstructure are provided by the cross frames. In the FE model, these cross frames were modeled with Beam188 element. The element is linear, quadratic 2-node beam element defined in 3D space, as shown in Fig. D.3(a). It has three translational and three rotational degrees of freedom at each node. This element is based on Timoshenko beam theory which includes shear-deformation effects and is well-suited

for linear, large rotation, and/or large strain nonlinear applications. Elasticity, plasticity, creep and other nonlinear material models are all supported by the element.

In practice, the full composite action between steel girders and the reinforced concrete deck is provided by shear stud. For numerical model, however, the multiple-point constraint rigid beam element, MPC184, is utilized to mimic the composite action. The MPC184 rigid beam element can be used to model a rigid constraint between two deformable bodies or as a rigid component used to transmit forces and moments in engineering applications. This element is well suited for linear, large rotation, and/or large strain nonlinear applications. Fig. D.3(b) shows the geometry, node locations, and the coordinate system for this element.

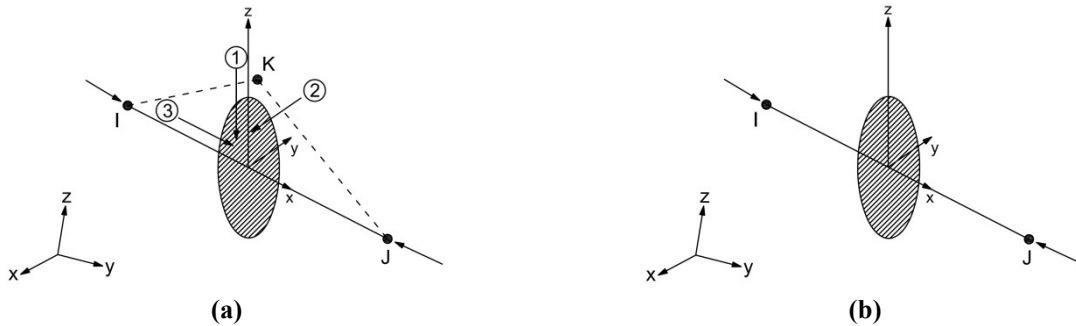


Fig. D.3: Implemented elements in numerical simulation: (a) Beam188, (b) MPC184 rigid beam

As it was mentioned in the previous section, Solid65 element is capable of modeling concrete material with or without embedded reinforcements. Since the rebars was chosen to be modeled using discrete method, a value of zero was entered for all real constant 1 which turned the smeared reinforcement capability of the Solid65 element off. On the other hand, there was limited information on the concrete deck reinforcement of the actual bridge, in the corresponding report provided by Burdette et al. (1971). Therefore, reasonable assumptions based on practical design values were made by Karl E. Barth (2006). Specifically, #4 was used at a spacing of 8 in both the longitudinal and transverse directions. Additionally, the top reinforcement cover was assumed to be 2 in and the bottom cover was chosen to be 1 in.

In this study, however, the reinforcing rebar pattern was adjusted based on the mesh generation of the FE model. Furthermore, only one layer of reinforcement at an effective distance (3 in) from the bottom surface of the deck was considered in the analysis for the sake of simplicity in modeling. As a result, the cross sectional area of the new reinforcing pattern in both the longitudinal and transverse directions has been modified to 1.00 in², refers to #9 rebar, based

on the new mesh-dependent spacing of the rebar pattern in one effective layer. The real constants for the proposed FE model in ANSYS are summarized in Table D.1. It should be finally noted that no real constant was considered for the elements representing the concrete deck, steel girders, cross frames, and shear studs.

Table D.1: Real constants for FE model of girder type bridge superstructure

Real Constant	Element Type	Constants		
		Rebar 1	Rebar 2	Rebar 3
Set 1	Solid65	Material Number	0	0
		Volume Ratio	0	0
		Orientation Angle (θ)	0	0
		Orientation Angle (ϕ)	0	0
Set 2	Link180	Rebar		
		Cross Section (in ²)	1.00	-

In the current FE model, there are two main components to which, cross sections shall be assigned: steel girders and cross frame bracings. In order to model the steel girders, the girder cross section was divided into three parts including top flange, web, and bottom flange. Each part was then simulated using shell elements which were characterized with the corresponding thickness and material properties. The section offset was also set for all three separated parts of the girder to eliminate the area overlapping at the connection node between the web and flanges. Moreover, the number of integration points through the thickness of shell was set to the default value of 5 presumed by ANSYS. For the beam elements utilized to simulate the cross frames, it is also essential to be associated with a cross section to define the axial and bending stiffness of the bracing members. Therefore, standard L4x4x0.5 angle was introduced as the cross section of the bracing elements in this study, based on the assumption made by Karl E. Barth (2006). The cross sections introduced for the proposed FE model are summarized in Table D.2.

For the proposed FE model, the material properties including linear and nonlinear characteristics are defined separately for each type of elements, and summarized in Table D.3. The elastic modulus of 4725 ksi with respect to uniaxial compressive strength of 6.87 ksi was defined to characterize the linear isotropic material properties of the concrete. In addition, the Poisson's ratio of the proposed FE model was assumed to be 0.18. Moreover, the multilinear stress-strain relationship (Macgregor 1992) with full nonlinear representation of material

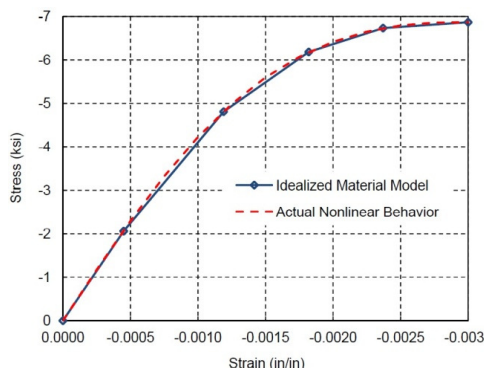
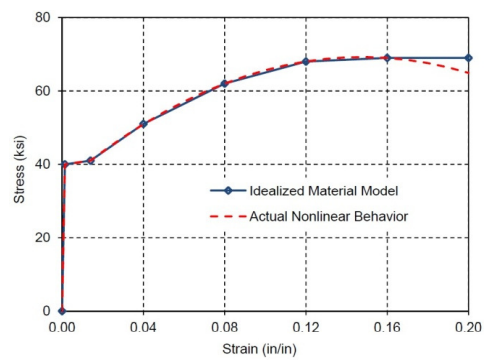
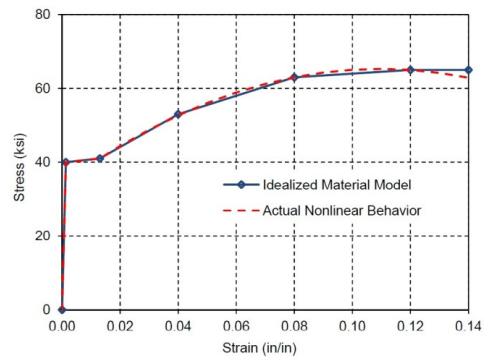
behavior was introduced in the concrete material model, as given in Table D.3. In addition, the Willam and Warnke (1974) model was implemented to define the triaxial failure surface of the concrete. The shear transfer coefficients were set to 0.3 and 1 for open and close cracks, respectively and the uniaxial cracking stress was set to 0.3 ksi. Similar to previous validation problems, the uniaxial crushing stress was chosen as -1 to turn off the crushing capability of failure model, in order to overcome the convergence problems.

Table D.2: Cross sections for FE model of girder type bridge superstructure

Element Type	Section ID	Constants	
Shell181	1 (Top Flange)	Thickness (in)	1.1
		Material Model	3
		Section Offset	Bottom Plane
	2 (Web)	Thickness (in)	0.68
		Material Model	3
		Section Offset	Middle Plane
	3 (Bot Flange)	Thickness (in)	1.1
		Material Model	3
		Section Offset	Top Plane
Beam188	4 (Angle)	Flange length (in)	4
		Flange Thickness (in)	0.5
		Section Offset	Centroid

The nonlinear behavior of the Gr.40 reinforcing rebars was modeled using the isotropic multilinear material model. The elastic modulus of 29000 ksi with the Poisson's ratio of 0.3 was introduced to model the material behavior of the steel reinforcement. ASTM A36 with the assumed (Barth et al. 2006) yield stress of 40 ksi and maximum tensile strength of 65 ksi, was also implemented in this study to capture full nonlinear material behavior of steel girders and cross frame. The elastic modulus of 30750 ksi with the Poisson's ratio of 0.3 was introduced respectively to simulate the material behavior of the steel materials prior to the yield point. After yielding, the nonlinear behavior was defined using multilinear isotropic material model associated with Von-Mises yield criteria. Since the MPC184 elements model rigid component of the composite bridge system, material properties are not required for these type of element in the proposed FE model.

Table D.3: Material properties for FE model of girder type bridge superstructure

Material Model	Element Type	Material Properties		Material Nonlinear Constitutive Laws	
1	Solid65	Multilinear isotropic (comp.)		Linear isotropic	
		Stress (ksi)	Strain	Elastic Modulus (ksi)	4724.5
		2.061	0.00045	Poisson's Ratio	0.18
		4.809	0.00119		
		6.183	0.00182		
		6.733	0.00237		
		6.87	0.00300		
		Concrete			
		ShrCf-Op	0.3		
		ShrCf-CI	1		
		UnTensSt (ksi)	0.3		
		UnCompSt (ksi)	-1		
Linear isotropic					
Elastic Modulus (ksi)	29000				
Poisson's Ratio	0.3				
Multilinear isotropic					
Stress (ksi)	Strain				
40	0.00138				
41	0.01400				
51	0.04000				
62	0.08000				
68	0.12000				
69	0.16000				
Linear isotropic					
Elastic Modulus (ksi)	30750				
Poisson's Ratio	0.3				
Multilinear isotropic					
Stress (ksi)	Strain				
40	0.0013				
41	0.0130				
53	0.0400				
63	0.0800				
65	0.1200				

D.3. Modeling

The numerical FE model of the 4-span composite steel bridge was created in ANSYS computer package. The representative mesh generation of the proposed model is also depicted in Fig. D.4(a) only for one end span. As it is illustrated in Fig. D.4(b), the concrete deck is simulated with 8-node volumetric solid elements and reinforced with one equivalent layer of steel rebars (see Fig. D.4(c)). In this study, perfect bond between concrete elements and the reinforcing steel rebars was considered and provided by connecting the shared nodes of the adjacent elements. Steel girders were then modeled using quadratic 4-node shell elements and laterally braced with the cross frames of standard 4x4x0.5 angels, spaced 280 in. for two end spans and 270 in for two intermediate spans (see Fig. D.4(d)). Full composite action was also provided between the top flange of the steel girders and the bottom surface of the concrete deck, using MPC beam elements between directly matched nodes to mimic the shear studs.

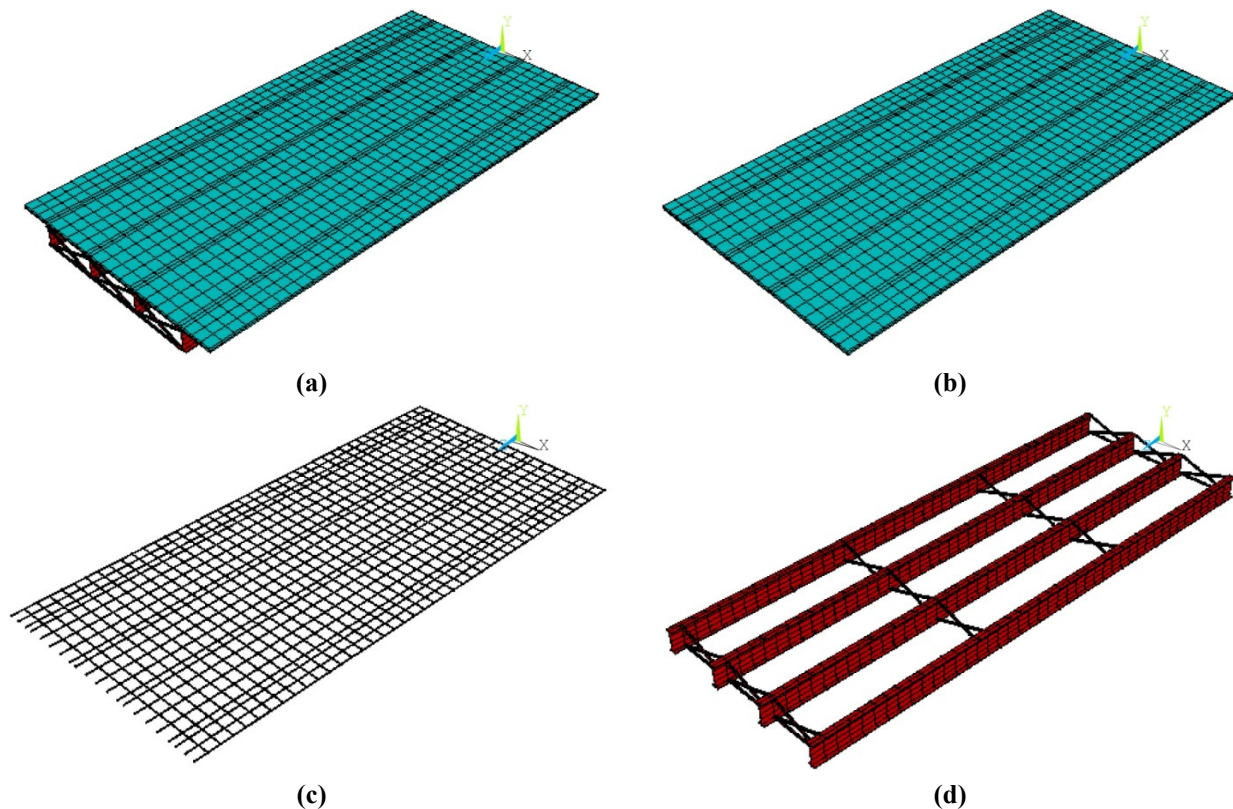


Fig. D.4: FE model for a 4-span continuous bridge superstructure (only end span of model shown): (a) 3D representation of mesh generation, (b) concrete deck elements, (c) reinforcing rebar elements, (d) Steel girders and cross frame (bracing) elements.

The boundary conditions for the continuous 4-span bridge include a hinge support with the three translation degrees of freedom constrained for all nodes along the bottom flanges of one end of the girders and roller constraints preventing vertical displacement for all nodes along the bottom flanges at the pier locations as well as the other end of the girders. The point loads were also applied over the patch area of 1 in by 2 in, representing tire area of the actual HS-20 truck, and distributed to the corner nodes of the affected elements via element shape function. This approach allows for the loading to be uncoupled from the mesh and yields a statically equivalent loading scenario (Harris et al. 2010 and 2013).

D.4. Analysis

The static analysis with small displacements was selected for the numerical investigation of the 4-span composite steel bridge. The point loads were applied on the simulated concrete deck elements incrementally using different load steps. The restart option was then implemented to initiate the new load step after the convergence occurred for a given load increment. The automatic time stepping was also turned on to facilitate the convergence at the end of each substep and precisely trace the nonlinear response of the structure. A detailed list of load steps with the corresponding number of the sub-steps and the incremental applied loads are given in Table D.4.

The load increments vary during the nonlinear analysis, based on the response of the structure. Prior to initial yielding of the steel girders, large load steps were chosen to reduce time and computational costs. Once the yielding initiated in the bottom flange of the girders, the stiffness of the structure was dramatically decreased and loads were applied in smaller portions on the model to fully trace the nonlinear behavior upon yielding. The load increment was raised slightly until the formation of plastic hinges the steel girders, the cross section of which was fully yielded. Consequently, the load increment was reduced again to the smaller values in order to capture the ultimate capacity and failure of the bridge superstructure.

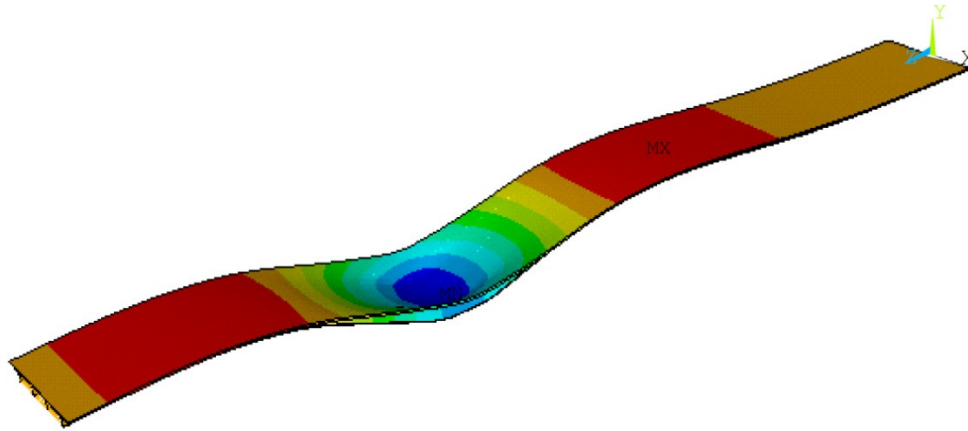
The Newton-Raphson method was chosen as the nonlinear solver for the analysis. All the corresponding parameters to define the nonlinear algorithm were set to their default values except for the convergence criteria. Only displacement criterion was implemented in this study with the reference value of 5 and the tolerance value of 0.05.

Table D.4: Load steps for the FE analysis of composite girder type bridge

Load Step	Beginning Time	End Time	# of sub-steps
1	0	20	24
2	20	40	24
3	40	60	24
4	60	80	24
5	80	100	52
6	100	110	24
7	110	120	24
8	120	130	24
9	130	140	14
10	140	145	14
11	145	150	14
12	150	155	14
13	155	160	14
14	160	162.5	9
15	162.5	165	6
16	165	167.5	6
17	167.5	170	7

D.5. Discussion of Results

Based on the numerical analysis, the FE model of the composite bridge superstructure deflects under the applied concentrated loads, in the fashion depicted in Fig. D.5. As it was expected, the maximum deflection occurred at the third span affected by the lateral simulated truck loading.

**Fig. D.5: Deflection in the proposed FE model of composite bridge**

For validation purposes, the total applied load versus the average vertical deflection of the steel girders at critical section, was derived from full nonlinear FE analysis, and compared to the corresponding experimental result proposed by Burdett et al. (1971). As it is illustrated in Fig. D.6(a), the proposed FE model is capable enough in predicting the nonlinear behavior of the composite steel bridge superstructure as well as ultimate load capacity and maximum deflection under truck loading. Furthermore, the validation study of the 4-span bridge has been previously investigated by Barth et al. (2006) at the West Virginia University, utilizing ABAQUS finite element simulation package. In their study, the Von-Mises yield criteria associated with the isotropic hardening rule was implemented to capture the nonlinear behavior of reinforcing rebars and steel girders; while they used two alternative material models: smeared crack concrete as well as concrete damaged plasticity, to simulate the nonlinear behavior of the concrete deck in their FE model. Consequently, they compared the load-deflection curves obtained from their numerical analysis to the field-test result to validate their proposed model, see Fig. D.6 (b).

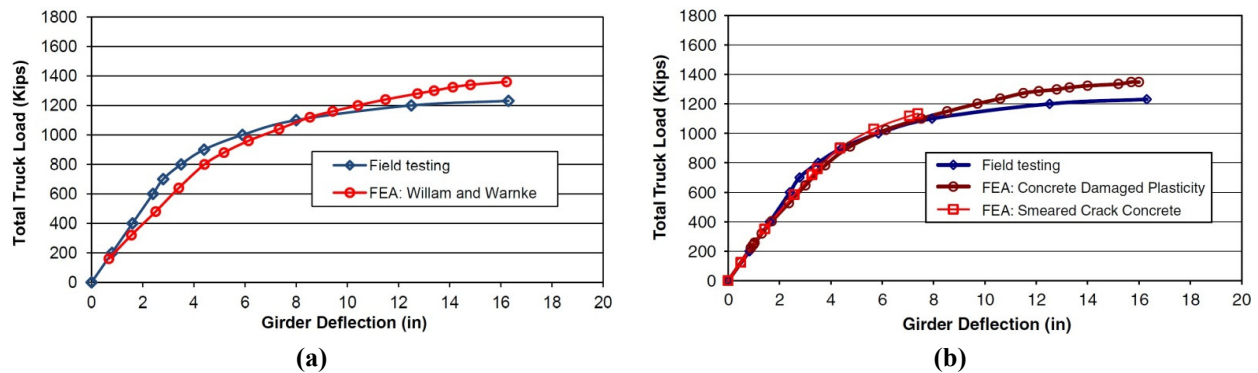


Fig. D.6: Comparison of load-deflection responses: (a) ANSYS, University of Virginia, (b) ABAQUS, West Virginia University

By comparing the results obtained from numerical analysis using ANSYS (at University of Virginia) and ABAQUS (at West Virginia University), it can be concluded that both FE packages predict the nonlinear response of the composite bridge superstructure in a same fashion. Moreover, this would ensure the validity of the numerical modeling procedure in this study, including the selection of the element types, real constant, cross sectional properties, material characteristics (especially the Willam and Warnke model representing the failure criteria for deck elements having concrete material), nonlinear algorithm and the convergence criteria. However, the discrepancies between numerical and field test results can be attributed to

the assumed boundary conditions which might be different from the actual state of the bridge superstructure. Fig. D.7 also illustrates the different behavioral stages throughout the loading history of the bridge proposed FE model.

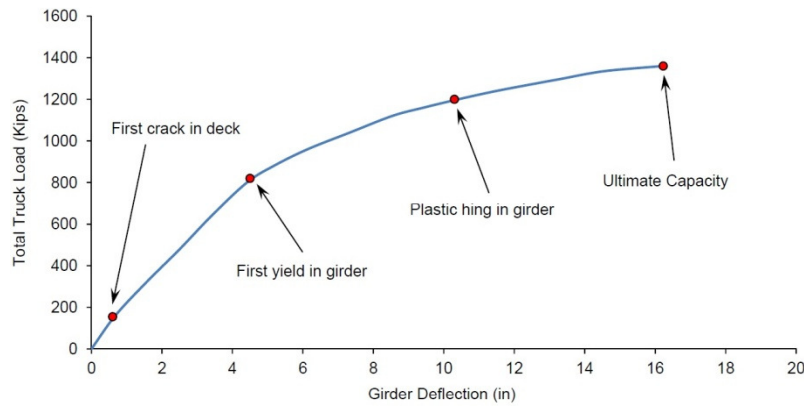


Fig. D.7: Structural behavior at different stages of loading

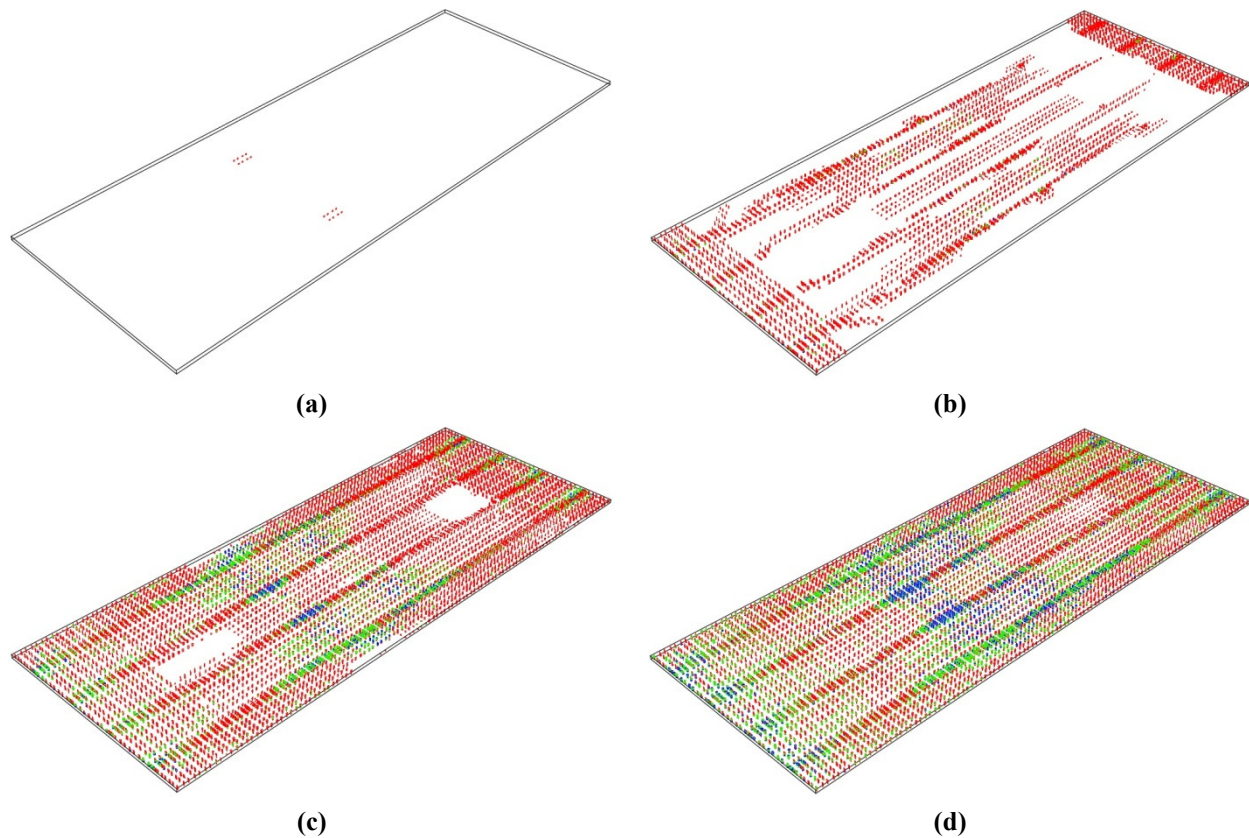


Fig. D.8: Cracking pattern in concrete deck of the loaded span, at different stages of loading: (a) first crack in deck, (b) first yield in girder, (c) plastic hinge in girder, (d) ultimate capacity

The bridge superstructure behaves linearly elastic prior to the cracking of the concrete deck. Once the first crack forms on the tension side of the deck, the stress and strain distributions completely change and the nonlinear behavior of the structure initiates. The first cracking pattern initiated in the concrete deck as well as the corresponding longitudinal strain distribution are depicted in Fig. D.8(a) and D.9(a), respectively. Moreover, the equivalent Von-Mises stress distribution in the steel girders at this moment is also depicted in Fig. D.10(a).

By increasing the applied load beyond the first cracking of the deck, flexural cracks propagate (Fig. D.8(b)). Moreover, the longitudinal compressive strains on the top surface of the deck increase near the mid span, as shown in Fig. D.9(b). However, the load deflection curve continues its trend with a constant slope, due to linear behavior of steel girders prior to the yield point. Once the steel girders yield (Fig. D.10 (b)) under the increasing load, the stiffness of the system decrease significantly and the load deflection slope drops off.

However, due to post yield reserve of steel material, the load bearing capacity of the bridge superstructure continues until the plastic hinges form in the steel girders (Fig. D.10(c)), with the flexural cracks dominate most parts of the loaded span (Fig. D.8(c)). Consequently, the structure reaches the ultimate capacity with the moderate plasticity region expanded within the steel girders, as given in Fig. D.10(d). At this moment, the flexural cracks propagate almost all over the loaded span, while the longitudinal strain on the bottom surface of the deck exceeds the cracking limit all across the deck width (right beneath the loading truck), as depicted in Fig. D.8(d) and D.9(d) respectively. It should be finally mentioned that the flexural reinforcements of the deck system yield right under the applied load as well as the adjacent supports of the loaded span, once the bridge superstructure reaches its ultimate capacity.

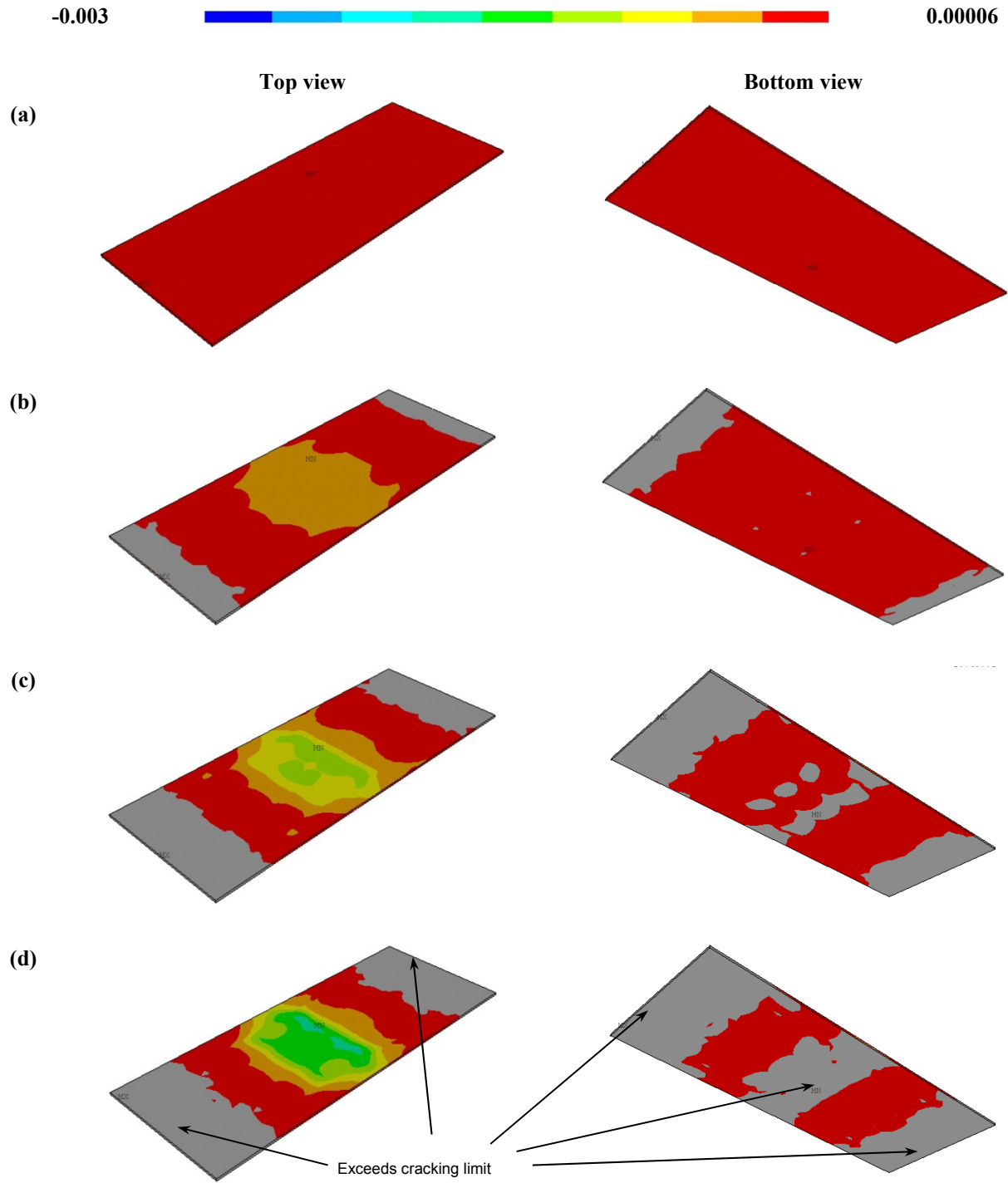


Fig. D.9: Longitudinal strain distribution in concrete deck of the loaded span, at different stages of loading:
 (a) first crack in deck, (b) first yield in girder, (c) plastic hinge in girder, (d) ultimate capacity

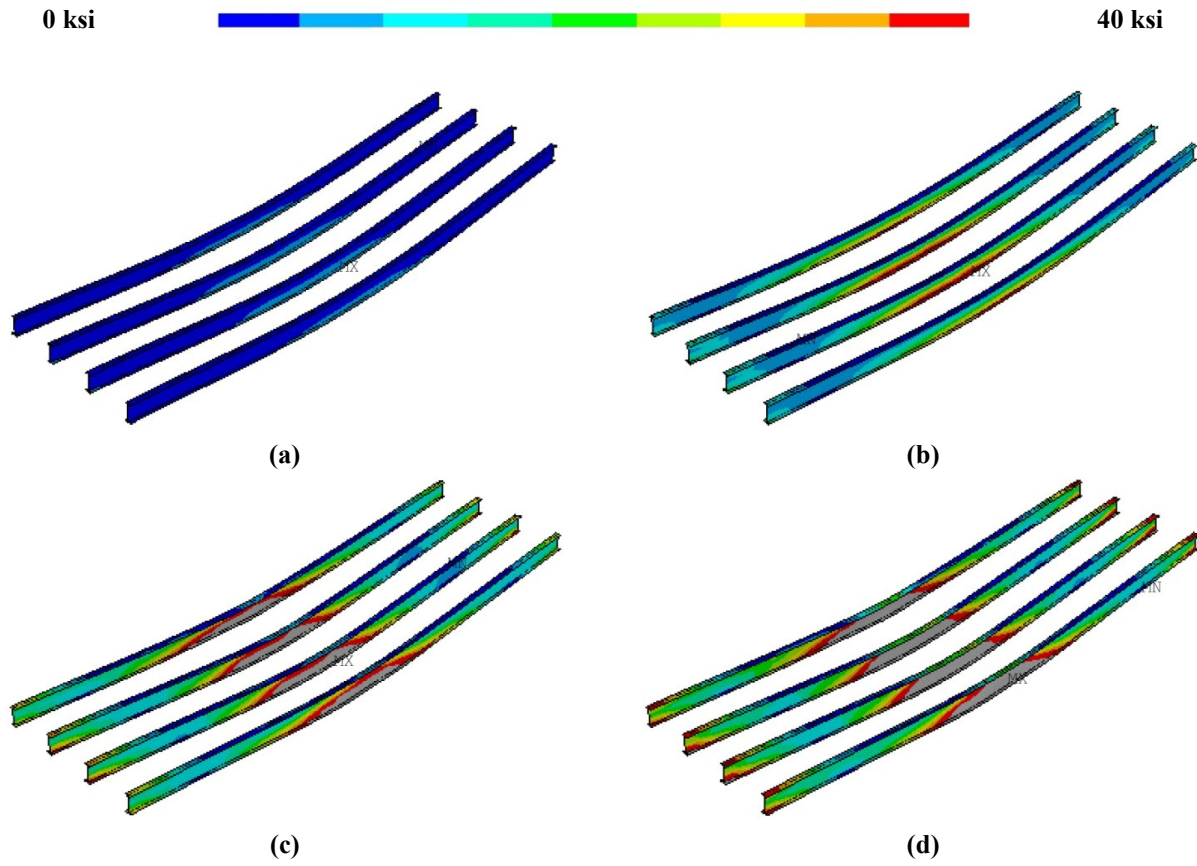


Fig. D.10: Distribution of Von-Mises stresses in steel girders of the loaded span, at different stages of loading:
 (a) first crack in deck, (b) first yield in girder, (c) plastic hinge in girder, (d) ultimate capacity

References

- Ahn, J.H., Kim, I.T., Kainuma, S., and Lee, M.J. (2013a). "Residual shear strength of steel plate girder due to web local corrosion." *Journal of Constructional Steel Research*, 89: 198-212.
- Ahn, J.H., Kainuma, S., and Kim, I.T. (2013b). "Shear failure behaviors of a web panel with local corrosion depending on web boundary conditions." *Thin-Walled Structures*, 73: 302-317.
- Ahn, J.H., Kainuma, S., Yasuo, F., and Takehiro, I. (2013c). "Repair method and residual bearing strength evaluation of a locally corroded plate girder at support." *Engineering Failure Analysis*, 33: 398-418.
- Alinia, M.M., Shakiba, M., and Habashi, H.R. (2009). "Shear failure characteristics of steel plate girders." *Thin-Walled Structures*, 47(12): 1498-1506.
- Alinia, M.M., Gheitasi, A., and Shakiba, M. (2011). "Postbuckling and ultimate state of stresses in steel plate girders." *Thin-Walled Structures*, 49(4): 455-464.
- Alonso, C., Andrade, C., Rodriguez, J., and Diez, J. M. (1998). "Factors controlling cracking of concrete affected by reinforcement corrosion." *Materials and Structures*, 31(211): 435-441.
- American Association of State Highway and Transportation Officials (1994). *AASHTO LRFD bridge design specifications*, 1st ed. American Association of State Highway and Transportation Officials, Washington, D.C.
- American Association of State Highway and Transportation Officials (2012). "AASHTO LRFD bridge design specifications." 6th ed., American Association of State Highway and Transportation Officials, Washington, D.C.
- American Association of State and Highway Transportation Officials (2008). "Bridging the gap: restoring and rebuilding the nation's bridges." Washington, D.C.
- American Association of State Highway Transportation Officials (1992). *Standard specifications for highway bridges*, 15th edition, Washington, D.C.
- American Association of State Highway and Transportation Officials (2002). "Standard specifications for highway bridges." 17th ed., American Association of State Highway and Transportation Officials, Washington, D.C.
- American Association of State Highway and Transportation Officials, AASHTO (2011). "The manual for bridge evaluation." 2nd ed., American Association of State Highway and Transportation Officials, Washington, D.C.
- American Concrete Institute (2011). *Building Code Requirements for Structural Concrete and Commentary*, ACI committee 318, Farmington Hills, MI.
- American Concrete Institute (2003). *Cement and Concrete Terminology, Manual of Concrete Practice*, Part1. Committee 116R-00, American Concrete Institute, Farmington Hills, MI.
- ANSYS Software (2011). "ANSYS User's Manual v. 14.0." Canonsburg, PA.
- Bae, H.U., and Oliva M.G. (2012). "Moment and shear load distribution factors for multi-girder bridges subjected to overloads." *ASCE Journal of Bridge Engineering*, 17(3): 519-527.
- Bakht, B., and Jaeger, L.G. (1992). "Ultimate load test of slab-on-girder bridge." *ASCE Journal of Structural Engineering*, 118(6): 1608-1624.
- Barker, R.M., and Puckett, J.A. (2007). "Design of highway bridges, an LRFD approach." 2nd ed., John Wiley & Sons, Inc., Hoboken, NJ.
- Barth, K.E., Wu, H. (2006). "Efficient nonlinear finite element modeling of slab on steel stringer bridges." *Finite Elements in Analysis and Design*, 42, 1304-1313.
- Barr, P.J., and Amin, N. (2006). "Shear live-load distribution factors for I-girder bridges." *ASCE Journal of Bridge Engineering*, 11(2): 197-204.
- Bazant, Z. P. (1979). "Physical model for steel corrosion in concrete sea structures – theory and application." *ASCE Journal of the Structural Division*, 105(6): 1137-1166.
- Bazant, Z. P. (1982). "Mathematical modeling of creep and shrinkage in concrete. Creep and shrinkage in concrete."

- John Wiley & Sons, Inc., New York, N.Y., 163-256.
- Bazant, Z.P., and Oh, B.H. (1982). "Strain-rate effect in rapid triaxial loading of concrete." *ASCE Journal of Engineering Mechanics*, 108, 764-782.
- Baskar, K., Shanmugam, N.E., and Thevendran, V. (2002). "Finite-element analysis of steel-concrete composite plate girder." *ASCE Journal of Structural Engineering*, 128: 1158-1168.
- Beaton, J. L., and Stratfull, R. F. (1973). "Environmental influence on the corrosion of reinforcing steel in concrete bridge substructures." California Department of Highways, Sacramento, CA.
- Bechtel, A., McConnell, J., and Chajes, M. (2011). "Ultimate capacity destructive testing and finite-element analysis of steel I-girder bridges." *ASCE Journal of Bridge Engineering*, 16(2): 197-206.
- Berto, L., Simioni, P., and Satta, A. (2007). "Numerical modelling of bond behaviour in RC structures affected by reinforcement corrosion." *Engineering Structures*, 30(5): 1375-1385.
- Bishara, A.G., Liu, M.C., and Elali, N.D. (1993). "Wheel load distribution on simply supported skew I-beam composite bridges." *ASCE Journal of structural Engineering*, 119(2): 399-419.
- Broomfield, J. (1997). "Corrosion of steel in concrete, understanding, investigating, and repair." E & FN Spon, London.
- Buckhouse, E.R. (1997), "External Flexural Reinforcement of Existing Reinforced Concrete Beams Using Bolted Steel Channels", Master's Thesis, Marquette University, Milwaukee, WI.
- Burdette, E.G. and Goodpature, D.W. (1971). "Full scale bridge testing - an evaluation of bridge design criteria." University of Tennessee, Knoxville, TN.
- Cai, C.S. (2005). "Discussion of AASHTO LRFD load distribution factors for slab on girder bridges." *ASCE Practice Periodical on Structural Design and Construction* 10(3): 171-176.
- Cairns J, Plizzari GA, Du Y, Law DW, Franzoni C. (2005). "Mechanical properties of corrosion-damaged reinforcement." *ACI Material Journal*, 102(4): 256-64.
- Cambridge Systematics Inc. (2008). "The transportation challenge: Moving the U.S. economy." National Chamber Foundation, U.S. Chamber of Commerce, Washington, D.C.
- Canadian Standards Association, CSA (2010). "Canadian Highway Bridge Design Code." CSA 56-00, Rexdale, Ontario, CA.
- Chan, T.H.T., and Chan, J.H.F. (1999). "Use of eccentric beam elements in the analysis of slab-on-girder bridges." *Structural Engineering & Mechanics*, 8(1): 85-102.
- Chen, D. and Mahadevan, S. (2007). "Chloride-induced reinforcement corrosion and concrete cracking simulation." *Cement and Concrete Composites*, 30: 227-238.
- Cheung, M.S., Gardner, N.J., and Ng S.F. (1986). "Load distribution characteristics of slab-on-girder bridges at ultimate." *Proceedings of 2nd international conference on short and medium span bridges*, Canadian Society for CE, Montreal, 461-485.
- Chung, W., Liu, J., and Sotelino, E.D. (2006). "Influence of secondary elements and deck cracking on the lateral load distribution of steel girder bridges." *ASCE Journal of Bridge Engineering*, 11(2):178-187.
- Chung, W., and Sotelino, E.D. (2006). "Three-dimensional finite element modeling of composite girder bridges." *Engineering Structures*, 28(1): 63-71.
- Constable, G., and Somerville, B. (2000). "Greatest engineering achievements of the 20th century." National Academy of Engineering of the National Academies, www.greatachievements.org.
- Corner, S., and Huo, X.S. (2006). "Influence of parapets an aspect ratio on live-load distribution." *ASCE Journal of Bridge Engineering*, 11(2): 188-196.
- Coronelli, D. (2002). "Corrosion cracking and bond strength modeling for corroded bars in reinforced concrete." *ACI Structural Journal*, 99 (3):267-276.

- Coronelli, D. and Gambarova, P. (2004). "Structural assessment of corroded reinforced concrete beams: modeling guidelines." *ASCE Journal of Structural Engineering*, 130(8):1214-24.
- Coulomb, C.A. (1776). "Essai sur une application des regles des maximis et minimis a quelques problemes de statique relatifs, a la architecture." *Mem. Acad. Roy. Div. Sav.*, 7, 343–387.
- Dagher, H. J., and Kulendran, S. Finite element modeling of corrosion damage in concrete structures. *ACI Structural Journal*, 89(6):699-708, 1992.
- Domingo, S., Ignacio, C., Ravindra, G., and Guillermo, E. (2002). "Study of the behavior of concrete under triaxial compression." *ASCE Journal of Engineering Mechanics*, 128, 156-163.
- Drucker, D.C. and Prager, W. (1952). "Soil mechanics and plastic analysis for limit design." *Quarterly of Applied Mathematics*, 10(2), 157–165.
- Dunbar, T.E., Pegg, N., Taheri, F., and Jiang, L. (2004) "A computational investigation of the effects of localized corrosion on plates and stiffened panels." *Marine Structures*, 17(5): 385-402.
- Ebeido, T., and Kennedy, J.B. (1995). "Shear distribution in simply supported skew composite bridges." *Canadian Journal of Civil Engineering* 22(6): 1143-1154.
- Ebeido, T., Kennedy, J.B. (1996). "Girder moments in continuous skew composite bridges." *ASCE Journal of Bridge Engineering* 1(1): 37-45.
- Ellobody, E. and Young, B. (2006). "Performance of shear connection in composite beams with profiled steel sheeting." *ASCE Journal of Constructional Steel research*, 62: 682.
- Eom, J., and Nowak, A.S., (2001). "Live load distribution for steel girder bridges." *ASCE Journal of Bridge Engineering*, 6(6): 489-497.
- Fam, A., MacDougall, C., and Shaat, A. (2009). "Upgrading steel-concrete composite girders and repair of damaged steel beams using bonded CFRP laminates." *Thin-Walled Structures*, 47(10): 1122-1135.
- Fang, K.I.J., Worley, N.H., and klinger, R.E. (1990). "Behavior of isotropic reinforced concrete bridge decks on steel girders." *ASCE Journal of Structural Engineering*, 116(3): 659-678
- Farja, R., and Oliver, J. (1993). "A rate dependent plastic-damage constitutive model for large scale computation in concrete structures." *Monograph No. 17, Centro Internacional de Me'todos Numericos en Ingeniero, Barcelona, Spain.*
- Farja, R., and Oliver, J. (1998). "A strain-based viscous-plastic-damage model for massive concrete structures." *International Journal of Solids and Structures*, 35(14): 1533–1558.
- Federal Highway Administration, FHWA (2001). "Reliability of visual inspection for highway bridges, volume I: final report." *Publication No. FHWA-RD-01-020*, Washington D.C.
- Federal Highway Administration, FHWA (2006). "Bridge inspector's reference manual – BIRM." *Publication No. FHWA-NHI-03-001/002*, Washington D.C.
- Federal Highway Administration, (2011). "Steel bridge design handbook - design for fatigue." *Publication No. FHWA-IF-12-052*, Washington D.C.
- Federal Highway Administration, FHWA (2012). *Bridge Inspector's Reference Manual (BIRM)*. Washington, D.C.
- Federal Highway Administration, FHWA (2013). "National Bridge Inventory Database." *Federal Highway Administration, Washington, D.C.*
- Ferrand, D. (2005), "Reliability Analysis of a Reinforced Concrete Deck Slab Supported on Steel Girders", A dissertation submitted to the University of Michigan, MI, USA, in partial fulfillment of the requirements for the degree of Doctor of Philosophy.
- Fu, G., and Hag-Elsafi, O. (1996a). "A bridge live load model including overloads. Probabilistic mechanics and structural and geotechnical reliability." *Proc., of the 7th Specialty Conf., ASCE, Reston, VA*, 34–37.
- Fu, G., and Hag-Elsafi, O. (1996b). "New safety-based checking procedure for overloads on highway bridges."

- Transportation Research Record N1541, Transportation Research Board, Washington, DC, 22–28.
- Fu, K.C., and Lu, F. (2003). “Nonlinear finite-element analysis for highway bridge superstructures.” *ASCE Journal of Bridge Engineering*, 8(3): 173-179.
- Galambos, T.V., Leon, T.R., and French, C.W. (1992). “Inelastic rating procedures for steel beam and girder bridges.” NCHRP project 12-28(12), Transportation Research Board, Washington, D.C.
- Gerstle, K.H. (1981). “Simple formulation of biaxial concrete behavior.” *ACI Journal*, 78, 62-68.
- Gheitis, A. and Harris, D.K. (2014a). “A performance-based framework for bridge preservation based on damage-integrated system-level behavior.” Transportation Research Board (TRB), 93rd Annual Meeting, Transportation Research Board, Washington, D.C.
- Gheitis, A. and Harris, D.K. (2014b). “Effect of deck deterioration on overall system behavior, resilience, and remaining life of composite steel girder bridges.” *ASCE Structures Congress*, 623-634.
- Gheitis, A. and Harris, D.K. (2014c). “Case Study: Failure Characteristics and Ultimate Load-Carrying Capacity of Redundant Composite Steel Girder Bridges.” *ASCE Journal of Bridge Engineering*, In press.
- Gheitis, A., and Harris, D.K. (2014d) “Overload Flexural Distribution Behavior in Composite Steel Girder Bridges.” *ASCE, Journal of Bridge Engineering*, In press.
- Ghosn, M., and Moses, F. (1997). “Redundancy in highway bridge superstructures.” Final report prepared for National Cooperative Highway Research Program (NCHRP), Report 406, Department of Civil Engineering, City University of New York, NY.
- Ghosn, M., and Yang, J. (2014). “Bridge System Safety and Redundancy.” National Cooperative Highway Research Program (NCHRP), Report 776, Transportation research Board, Washington D.C.
- Government Accountability Office, GAO (2008). “Defense critical infrastructure: adherence to guidance would improve DOD's approach to identifying and assuring the availability of critical transportation assets.” *Defense Capabilities and Management*, Washington, D.C.
- Green, T., Yazdani, N., and Spainhour, L. (2004). “Contribution of intermediate diaphragms in enhancing precast bridge girder performance.” *ASCE Journal of Performance of Constructed Facility*, 18(3): 142-146.
- Hall, J.C., and Kostem, C.N. (1981). “Inelastic overload analysis of continuous steel multi-girder highway bridges by the finite element method.” Fritz Engineering Lab Report No. 432.6, Lehigh University, PA.
- Harajli, M.H., Hamad, B.S., and Rteil, A.A. (2004). “Effect of confinement on bond strength between steel bars and concrete.” *ACI Structural Journal*, 101(5): 595-603.
- Harris, D.K., Cousins, T., Murray, T.M., and Ferro, A. (2006). “Live load test of a SPS bridge” *International Conference on Short & Medium Span Bridges*. Montreal, QC.
- Harris, D.K., Cousins, T., Murray, T.M., and Sotelino, E.D. (2008). “Field Investigation of a Sandwich Plate System bridge deck.” *ASCE Journal of Performance of Constructed Facilities*, 22(5): 1-11.
- Harris, D.K. (2010). “Assessment of flexural lateral load distribution methodologies for stringer bridges.” *Engineering Structures*, 32(11): 3443-3451.
- Harris, D.K., Gheitis, A. (2013). “Implementation of an energy-based stiffened plate formulation for lateral load distribution characteristics of girder-type bridges.” *Engineering Structures*, 54: 168-179.
- Hays, C. O. (1984). “Evaluating bridge overloads using the finite element method.” *Official Proc., Int. Bridge Conf., Engineer's Society of Western Pennsylvania*, Pittsburgh, 232–238.
- Heins, J.C.P., and Kuo, I.T.C. (1975). “Ultimate live load distribution factor for bridges.” *ASCE Journal of Structural Engineering*, 101(7): 1481-1496.
- Hewitt, B.E., and deV Batchelor, B. (1975). “Punching shear strength of restraint slabs.” *ASCE Journal of Structural Division*, 101(ST9): 1837-1853.
- Huang, H., Shenton, H.W., and Chajes, M.J. (2004). “Load Distribution for a Highly Skewed Bridge: Testing and

- Analysis." ASCE Journal of Bridge Engineering, 9(6): 558-562.
- Huo, X.S., Wasserman, E.P., and Iqbal, R.A. (2005). "Simplified Method for Calculating Lateral Distribution Factors for Live Load Shear." ASCE Journal of Bridge Engineering, 10(5): 544-554.
- Johansson, B., and Lagerqvist, O. (1995). "Resistance of plate edges to concentrated forces." Journal of Constructional Steel Research, 32: 69-105.
- Kathol, S. Azizinamini, A. and Luedke, J. (1995). "Final report: strength capacity of steel girder bridges." Nebraska Department of Roads (NDOR), RES1(0099) P469.
- Kachanov, L. M. (1986). Introduction to continuum damage mechanics. Martinus Nijhoff Publishers, The Netherlands.
- Kallias, A.N., and Rafiq, M.I. (2010). "Finite element investigation of the structural response of corroded RC beams." Engineering Structures, 32(9): 2984-2994.
- Khaloo, A.R., and Mirzabozorg, H. (2003). "Load Distribution Factors in Simply Supported Skew Bridges." ASCE Journal of Bridge Engineering, 8(4): 241-244.
- Kavinoky, J. F. (2007). "The importance of transportation infrastructure to the american business community." U.S. House of Representatives Committee on Transportation and Infrastructure, U.S. Chamber of Commerce, Washington, D.C.
- Kim, I.T., Lee, M.J., Ahn, J.H., and Kainuma, S. (2013). "Experimental evaluation of shear buckling behaviors and strength of locally corroded web." Journal of Constructional Steel Research, 83, 75-89.
- Kukreti, A.R., and Cheraghi, E. (1993). "Analysis procedure for stiffened plate systems using an energy approach. Computers & Structures, 46(4): 649-657.
- Kukreti, A.R., and Rajapaksa, Y. (1990). "Analysis procedure for ribbed and grid plate systems used for bridge decks. ASCE Journal of Structural Engineering, 116(2): 372-391.
- Kulicki J.M., Prucz, Z., Sorgenfrei, D.F., Mertz, D.R., and Young, W.T. (1990). "Guidelines for Evaluating Corrosion Effects In Existing Steel Bridges." National Cooperative Highway Research Program Report 333, NCHRP.
- Kumalasari, W., and Fabian, C. H. (2003). "Analysis of recent bridge failures in the United States." ASCE Journal of Performance of Constructed Facilities, 17(3), 144-150.
- Lagerqvist, O. (1995). "Patch loading-resistance of steel girders subjected to concentrated forces. PhD thesis, Division of Steel Structures, Luleå University of Technology.
- Li, C.Q.; Zheng, J.J.; Lawanwisut, W.; and Melchers, R.E. (2007). "Concrete delamination caused by steel reinforcement corrosion." Journal of Materials in Civil Engineering, 19(7): 591-600
- Lin, J.J., Fafard, M., Beaulieu, D., and Massicotte, B. (1991). "Nonlinear analysis of composite bridges by the finite element method." Computers and Structures, 40(5): 1151-1167.
- Liu, C., Miyashita, T., and Nagai, M. (2011). "Analytical Study on Shear Capacity of Steel I-Girders with Local Corrosion nearby Supports." Procedia Engineering, 14, 2276-2284.
- Lynch, J. P., and Loh, K. J. (2006). "A summary review of wireless sensors and sensor networks for structural health monitoring." Shock and Vibration Digest, 38(2): 91-128.
- Maaddawy, T.E., Soudki, K., and Topper T. (2005). "Analytical model to predict nonlinear flexural behavior of corroded reinforced concrete beams." ACI Structural Journal, 102(4): 550-9.
- Mabsout, M.E., Tarhini K.M., Frederick G.R., and Kobrosly M., (1997). "Influence of sidewalks and railings on wheel load distribution in steel girder bridges." ASCE Journal of Bridge Engineering, 2(3): 88-96.
- Mabsout, M.E., Tarhini K.M., Frederick G.R., and Kesserwan A. (1998). "Effect of Continuity on wheel load distribution in steel girder bridges." ASCE Journal of bridge Engineering, 3(3): 103-110.
- MacGregor, J.G. (1992), "Reinforced Concrete Mechanics and Design", Prentice-Hall, Inc., Englewood Cliffs, NJ.

- Mathematica software (2008). "Wolfram Research Inc. v. 7.0.1.0." Champaign, IL.
- McNeice, G.M. (1967). "Elastic-Plastic Bending of Plates and Slabs by Finite Element Method." PhD thesis, University of London, London, England.
- Michigan Department of Transportation (2013). "Michigan's truck-weight law and truck-user fees." MDOT Intermodal Policy Division, http://www.michigan.gov/documents/mdot/MDOT_013-4-16TruckWeightsMichigan_418609_7.pdf, Accessed September 3, 2013.
- Minnesota Department of Transportation, MnDOT (2010). "Economic Impacts of the I-35W Bridge Collapse." <http://www.dot.state.mn.us/i35wbridge/rebuild/municipal-consent/economic-impact.pdf>.
- Molina, F. J., Alonso, C., and Andrade, C. (1993). "Cover cracking as a function of rebar corrosion: part 2 - numerical model." *Materials and Structures*, 26(163): 532-548.
- Moses, J.P., Harries, K.A., Earls, C.J., and Yulismama, W. (2006). "Evaluation of effective width and distribution factors for GFRP bridge decks supported on steel girders." *ASCE Journal of Bridge Engineering*, 11(4): 401-409.
- Narmashiri, K., Ramli Sulong, N.H., and Jumaat, M.Z. (2012). "Failure analysis and structural behaviour of CFRP strengthened steel I-beams." *Construction and Building Materials*, 30: 1-9.
- National Transportation Safety Board (2008). "Collapse of I-35W Highway Bridge, Minneapolis, Minnesota, August 1, 2007." Accident report, NTSB/HAR-08/03, PB2008-916203, Washington, D.C.
- National Transportation Safety Board (2013a). "Washington State I-5 Bridge Collapse Investigation." Preliminary report, HWY13MH012, Washington, D.C.
- National Transportation Safety Board (2013b). "Railroad Train Collision, Resulting in Highway Bridge Collapse." Preliminary report, DCA13MR004, Washington, D.C.
- Newmark, N.M. (1948). "Design of I-beam bridges." *ASCE Journal of the Structural Division*, 74(1): 305-330
- Nowak, A.S., Eom, J., Sanli, A., and Till, R. (1999). "Verification of girder-distribution factors for short-span steel girder bridges by field testing." *Transportation Research Record* (1688): 62-67.
- Nowak, A.S., and Eom, J. (2001). "Verification of girder distribution factors for steel girder bridges." University of Michigan, Michigan Department of Transportation, Report# Report RC-1393, Lansing, MI.
- Onate, E. (1994). Reliability analysis of concrete structures. Numerical and experimental studies. Seminar CIAS (Centro Internazionale di Aggiornamento Sperimentale e Scientifico), Evoluzione nella sperimentazione per le costruzioni, Merano, Italy, 125-146.
- Pakzad, S.N., Fenves, G.L., Kim, S., Culler, D.E. (2008). "Design and implementation of scalable wireless sensor network for structural monitoring." *Journal of Infrastructure Systems*, 14(1): 89-101.
- Pantazopoulou, S. J., and Papoulia, K. D. (2001). Modeling cover-cracking due to reinforcement corrosion in RC structures. *Journal of Engineering mechanics*, 127(4): 342-351.
- Queiroz, F.D., Queiroz, G., and Nethercot, D.A. (2009). "Two-dimensional FE model for evaluation of composite beams, I: formulation and validation." *ASCE Journal of Constructional Steel Research*, 65: 1055-1062.
- Queiroz, F.D., Vellasco, P.C.G.S., and Nethercot, D.A. (2006). "Finite element modeling of composite beams with full and partial shear connection." *ASCE Journal of Constructional Steel Research*, 63: 505-521.
- Qureshi, J., Lam, D., and Ye, J. (2011). "Effect of shear connector spacing and layout on shear connector capacity in composite beams." *ASCE Journal of Constructional Steel research*, 67:706-719.
- Rahgozar, R. (2009). "Remaining capacity assessment of corrosion damaged beams using minimum curves." *Journal of Constructional Steel Research*, 65(2), 299-307.
- Rajapaksa, Y. (1985). "Formulation of analysis and design procedure for ribbed and grid plate systems used for highway bridges." M.S. thesis, University of Oklahoma, Norman, OK.
- Razaqpur, A.G., and Nofal, M. (1990). "Analytical model of nonlinear behavior of composite bridges." *ASCE*

- Journal of Structural Engineering, 116(6): 1715-1733.
- Razaqpur, A.G., Shedid, M., Nofal, M. (2012). "Inelastic load distribution in multi-girder composite bridges." *Engineering Structures*, 44: 234-247.
- Roberts, M. B., Atkins, C., Hogg, V., and Middleton, C. (2000). "A proposed empirical corrosion model for reinforced concrete." *Proc. Inst. Civ. Eng., Struct. Build.*, 140(1): 1-11.
- Robitaille, P. and Girard, R. (2013). "Super-sized, 780-tonne oil sands vessel hits Highway 63." *Alberta Oil*, <http://www.albertaoilmagazine.com/2013/04/oilsands-megamodules-fort-mac>, Accessed August 29, 2013.
- Rodriguez, J., Ortega, L., and Garcia, A. (1994). "Corrosion of reinforcing bars and service life of R/C structures: Corrosion and bond deterioration." *Proc., Int. Conf. on Concrete across Borders*, 2, 315-326.
- Saetta, A., Scotta, R., and Vitaliani, R. (1998). "Mechanical behavior of concrete under physical-chemical attacks." *ASCE Journal of Engineering Mechanics*, 124(10): 1100-1109.
- Saetta, A., Scotta, R. and Vitaliani, R. (1999). "Coupled environmental-mechanical damage model of RC structures." *ASCE Journal of Engineering Mechanics*, 125(8): 930-940.
- Sapountzakis, E.J., and Katsikadelis, J.T. (2000). "Analysis of plates reinforced with beams." *Computational Mechanics*, 26(1): 66-74.
- Sapountzakis, E.J., and Katsikadelis, J.T. (2002). "A new model for slab and beam structures - Comparison with other models." *Computers & Structure*, 80(5-6): 459-470.
- Sebastian, W. M., and McConnel, R. E. (2000). "Nonlinear FE analysis of steel-concrete composite structures." *ASCE Journal of Bridge Engineering*, 126(6): 662-674.
- Seible, F., Latham, C., and Krishnan, K. (1998). "Structural concrete overlays in bridge deck rehabilitations – experimental program." Department of Applied Mechanics and Engineering Sciences, University of California, San Diego, La Jolla, CA.
- Sharifi, Y. and Paik, J.K. (2011). "Ultimate strength reliability analysis of corroded steel-box girder bridges." *Thin-Walled Structures*, 49(1), 157-166.
- Sotelino, E.D., Liu, J., Chung, W., and Phuvoravan, K. (2004). "Simplified load distribution factor for use in LRFD design." Publication FHWA/IN/JTRP-2004/20. Joint Transportation Research Program, Indiana Department of Transportation and Purdue University, West Lafayette, IN.
- Strategic Highway Research Program, SHRP2 (2012). "Nondestructive testing technologies for rapid renewal; reduce traffic distributions, improve efficiency." Transportation Research Board (TRB), Washington D.C.
- Stewart, M.G. (2009). Mechanical behaviour of pitting corrosion of flexural and shear reinforcement and its effect on structural reliability of corroding RC beams. *Struct Saf.*, 31(1):19-30.
- Tabsh, S.W., and Tabatabai, M. (2001). "Live load distribution in girder bridges subject to oversized trucks." *ASCE Journal of Bridge Engineering*, 6(1): 9-16.
- Tahmasebinia, F., Ranzi, G., and Zona, A. (2013). "Probabilistic three-dimensional finite element study on composite beams with steel trapezoidal decking." *ASCE Journal of Constructional Steel Research*, 80: 394-411.
- Tavarez, F.A. (2001). "Simulation of behavior of composite grid reinforced concrete beams using explicit finite element methods." Master's Thesis, University of Wisconsin-Madison, Madison, WI.
- Taylor, M.A., Jain, A.K., and Ramey, M.R. (1972). "Path dependent biaxial compressive testing of an all light weight concrete." *ACI Journal*, 69, 758-764.
- Thevendran, V., Chen, S. Shanmugam, and N.E., Liew, J.Y.R. (1999). "Nonlinear analysis of steel-concrete composite beams curved in plan." *Finite Elements in Analysis and Design*, 32: 125-139.
- Timoshenko, S., and Woinowsky-Krieger, S. (1959). "Theory of Plates and Shells." McGraw-Hill, New York, NY.
- Torres-Acosta, A. A., and Martinez-Madrid, M. M. (2003). "Residual life of corroding reinforced concrete structures in marine environment." *J. Mater. Civ. Eng.*, 15(4): 344-353.

- Tryland, T., Hopperstad, O.S., Langseth, M. (1999). "Steel girders subjected to concentrated loading-Validation of numerical simulations." *Journal of Constructional Steel Research*, 50: 199-216.
- Tsai, W.T. (1988). "Uniaxial compressional stress-strain relation of concrete." *ASCE Journal of Engineering Mechanics*, 114, 2133-2136.
- Ugural, A.C. (1999). "Stresses in Plates and Shells." WCB/McGraw Hill, Boston, MA.
- Vaghefi, K., Oats, R., Harris, D., Ahlborn, T., Brooks, C., Endsley, K., Roussi, C., Shuchman, R., Burns, J., and Dobson, R. (2012). "Evaluation of commercially available remote sensors for highway bridge condition assessment." *ASCE Journal of Bridge Engineering*, 17(6): 886-895.
- Vaghefi, K., Ahlborn, T., Harris, D., and Brooks, C. (2013). "Combined imaging technologies for concrete bridge deck condition assessment." *Journal of Performance of Constructed Facilities*, In Press.
- Van de Lindt, J. W., and Ahlborn, T. M. (2005). "Development of Steel Beam End Deterioration Guidelines." Michigan Tech Transportation Institute, Center for Structural Durability, MDOT Research Report RC-1454.
- Ventsel, E., and Krauthammer, T. (2001). "Thin Plates and Shells: Theory, Analysis, and Applications." Marcel Dekker, New York, NY.
- Vinson, J.R. (1999). "The Behavior of Sandwich Structures of Isotropic and Composite Materials." Technomic Pub. Co., Lancaster, PA.
- Von Mises, R. (1913) "Mechanik der festen Körper im plastisch deformablen Zustand" *Göttin. Nachr. Math. Phys.*, 1, 582-592.
- Vu, K. A. T., and Stewart, M. G. (2002). "Spatial variability of structural deterioration and service life prediction of reinforced concrete bridges." *Proc., Int. Conf. on Bridge Maintenance, Safety, and Management*, Barcelona, Spain.
- Waldron, C.J., Cousins, T.E., Nassar, A.J., and Gomez, J.P. (2005). "Demonstration of use of high-performance lightweight concrete in bridge superstructure in Virginia." *ASCE Journal of Performance of Constructed Facilities*, 19(2): 146-154.
- Wang, P.T., Shah, S.P., and Naaman, A.E. (1978). "Stress-strain curves of normal and lightweight concrete in compression." *ACI Journal*, 75, 603-611.
- Westergaard, H.M. (1930). "Computation of stresses in bridge slabs due to wheel loads." *Public Roads*, 11(1): 1-23.
- Willam, K.J., and Warnke, E.P. (1974). "Constitutive model for triaxial behavior of concrete. Concrete structures subjected to triaxial stresses." *International Association for Bridges and Structural Engineering*, Bergamo, Italy.
- Wolanski, A.J. (2004). "Flexural behavior of reinforced concrete beams using finite element analysis." Master's thesis, Marquette University, Milwaukee, WI.
- Yam, L. C. P., and Chapman, J. C. (1972). "The inelastic behavior of continuous composite beams of steel and concrete." *J. Instit. Civ. Engrs.*, 53(12): 487-501.
- Yam, L. C. P., and Chapman, J. C. (1968). "The inelastic behavior of simply supported composite beams of steel and concrete." *J. Instit. Civ. Engrs.*, 41(1): 651-683.
- Zhou, K., Martin-Perez, B., and Lounis, Z. (2005). "Finite element analysis of corrosion-induced cracking, spalling and delamination of RC bridge decks." *1st Canadian Conference on Effective Design of Structures*, Hamilton, Ont., July 10-13, 187-196.
- Zokaie T. (2000). "AASHTO-LRFD live load distribution specifications." *ASCE Journal of Bridge Engineering*, 5(2): 131-138.
- Zokaie T. (1992). "Distribution of wheel loads on highway bridges." *NCHRP, Research Results Digest*, 1-31.
- Zokaie T., Osterkamp, T.A., and Imbsen, R.A. (1991). "Distribution of wheel loads on highway bridges." *NCHRP 12-26/1 Final Rep*, National Cooperative Highway Research Program (NCHRP), Washington, D.C.
- Zona, A. and Ranzi, G. (2011). "Finite element models for nonlinear analysis of steel-concrete composite beams

with partial interaction in combined bending and shear.” *Finite Elements in Analysis and Design*, 47: 98-118.